NOTE TO USERS

Page(s) not included in the original manuscript and are unavailable from the author or university. The manuscript was scanned as received.

vi, x

This reproduction is the best copy available.

UMI®

uOttawa

L'Université canadienne
Canada's university

FACULTÉ DES ÉTUDES SUPÉRIEURES ET POSTOCTORALES

uOttawa

L'Université canadienne
Canada's university

FACULTY OF GRADUATE AND POSDOCTORAL STUDIES

Patrick Crewdson

AUTEUR DE LA THÈSE / AUTHOR OF THESIS

Ph.D.(Chemistry)

GRADE / DEGREE

Department of Chemistry

FACULTÉ, ÉCOLE, DÉPARTEMENT / FACULTY, SCHOOL, DEPARTMENT

Basic Research and Practical Applications of Manganese and Chromium Complexes

TITRE DE LA THÈSE / TITLE OF THESIS

Sandro Gambarotta

DIRECTEUR (DIRECTRICE) DE LA THÈSE / THESIS SUPERVISOR

CO-DIRECTEUR (CO-DIRECTRICE) DE LA THÈSE / THESIS CO-SUPERVISOR

EXAMINATEURS (EXAMINATRICES) DE LA THÈSE / THESIS EXAMINERS

S. Barry

D. Stephan

C. Detellier

D. Richeson (absent)

Gary W. Slater

Le Doyen de la Faculté des études supérieures et postdoctorales / Dean of the Faculty of Graduate and Postdoctoral Studies

Basic Research and Practical Applications of Manganese and Chromium Complexes

Patrick Crewdson

Thesis Submitted to the
Faculty of Graduate & Postdoctoral Studies
University of Ottawa
in partial fulfillment of the requirements for the
Ph.D. degree in the

Ottawa-Carleton Chemistry Institute

Thesè soumise à la
Faculté d'études supérieures et postdoctorales
de l'Université d'Ottawa
en vue de l'obtention de la maîtrise des sciences à
Ph.D. degré de

L'Institut de chimie d'Ottawa-Carleton

Your file Votre référence
ISBN: 978-0-494-34124-7
Our file Notre référence
ISBN: 978-0-494-34124-7

I would like to dedicate this work in memory
of my good friend Robert Inglis
who is no longer here to witness me finally graduating

Blue skys wherever you are buddy.

Acknowledgements

So many people have helped me along with during my many years of study in Ottawa that I couldn't possibly thank them all, however I will make my best effort. If I don't specifically mention you by name it's not because I don't love you, but rather due to space limitations; seriously. My first thanks must of course be reserved for my wife Jessica, who has suffered many a delayed night due to my constantly needing "30 more minutes for this reaction" which, of course, always took significantly longer. How she managed to keep from throttling me, I'll never know, but I'm eternally grateful for her support.

From within my group I'd like to thank Sandro for his years of guidance and giving me the opportunity to work in Europe, I will definitely miss his home baked bread. Ilia Korobkov was a constant source of encylopedic chemistry knowledge and techniques, his guidance over the years most certainly has earned him the nickname "Lab-Daddy" and aided my own research greatly. I especially need to thank him for teaching me the very useful skill of X-ray Crystallography and for introducing me to Zubrowka. Jenny Scott was both my best friend and chief rival for all of these years and I will miss her easy laughter and conversation. I would also like to thank Indu, Terri, Harminder and Claire for being such great co-workers and helping me so much as well as putting up with my occasional grumpiness.

Rob Duchateau, took time out of his busy schedule to have me come to the University of Eindhoven not once but three times, for which I am very grateful. These invaluable opportunities allowed me to accomplish much of my catalyst testing, which makes up a large part of this thesis. I'd like to thank Cheryl and Glenn for always taking the time to help me with my NMR "issues".

Perhaps the group I will miss the most is my fellow grad students. Through the CGSA, and Acadia House/Nostalgica nights I met so many great people who also helped me out with my chemistry: Jay, Heather, Ken, Seb, Mark, Rich, Katherine, Johanna, Nat, Liz, Dave, all of the Matt's, LC and Pat; I already miss you all. On a final note I would like to thank the University of Ottawa for providing the tuition waivers which allowed me to afford to attend school and eat three meals a day at the same time during my final three years.

Abstract

This thesis was aimed at exploring a few selected aspects of manganese chemistry with a particular emphasis on the unconventional reactivity for this metal. Firstly, appropriate organomanganese complexes have been prepared and fully characterized. The majority of these species stemmed from our development of the effective reagent $[Mn(CH_2SiMe_3)_2(THF)]_2$ which was used as starting material in ligand metathesis reactions with protic organic ligands. Two such ligands specifically designed for this purpose were the hemi-labile N-MeDipyrrole and N-MeTripyrrole ligands. These ligand systems, and various others, allowed for the synthesis of several model systems to mimic the water oxidation reaction of the OEC in Photosystem II. One such ligand (tartaric acid) formed the complex $[Mn(\mu_3,\eta_2\text{-}O_2CCH(O)CH(O)CO_2)(H_2O)_{0.5}]\cdot H_2O_{1.5}$ which evolves oxygen upon addition of a strong oxidizing agent, thus indicating the oxidation of water.

In another practical application for $Mn^{(II)}$ complexes we probed the analogy between the high spin d^5 electronic configuration with the d^{10} electron configuration of Zn by finding for the first time Mn complexes capable of acting as catalysts in the co-polymerization of CO_2 with an epoxide, producing nearly perfectly alternating polycarbonate. These findings prove that Mn is capable of catalyzing a reaction which is normally only performed by the late transition metal Zn. Similarly, we probed the behavior of Mn complexes of the bis-iminato pyridine ligand system which so effectively supports ethylene polymerization with a variety of metals. Our research into the reduction of $Mn^{(II)}$ complexes has led to the formation of the formally monovalent [(BisImine)MnCl(THF)] complex.

At the end of the thesis we have taken advantage of the synthesis of the novel hemi-labile pyrrolide ligands for the preparation of chromium catalysts for selective ethylene trimerization reaction. The main task was to elucidate the factors which determine selectivity in the oligomerization process. At this preliminary stage we targeted the issue of metal oxidation state. It was found that both $Cr^{(II)}$ and $Cr^{(III)}$ complexes of this ligand were highly active for the production of 1-hexene, but yielded a Shultz-Flory distribution of α-olefins. In addition, various imine-based ligands in

conjunction with $Cr^{(II)}$ were also found to produce statistical distributions of α-olefins. This work led us to revisit the selective processes published in the literature with known SNS and PNP-based compounds of both $Cr^{(II)}$ and $Cr^{(III)}$. Overall, we were unable to unequivocally identify which oxidation state led to the selective formation of 1-hexene, our results instead indicated that selectivity might be entirely ligand-based and independent of the actual oxidation state.

List of Publications

1) Crewdon, P.; Gambarotta, S.; Korobkov, I. *Inorg. Chem.* **2007**, *submitted.*

2) Vidyaratne, I.; Crewdson, P.; Lefebvre, E.; Gambarotta, S. *Inorg. Chem.* **2007**, *accepted.*

3) Nikiforov, G. B.; Crewdson, P.; Gambarotta, S.; Korobkov, I.; Budzelaar, P. H. M. *Organometallics* **2007**, *26*, 48.

4) Temple, C.; Jabri, A.; Crewdson, P.; Gambarotta, S.; Korobkov, I.; Duchateau, R. *Angew. Chem. Int. Ed.* **2006**, *45*, 7050.

5) Arunachalampillai, A. ; Crewdson, P.; Gambarotta, S. ; Korobkov, I. *Organometallics* **2006**, *25*, 3856.

6) Jabri, A.; Temple, C.; Crewdson, P.; Gambarotta, S.; Korobkov, I.; Duchateau, R. *J. Am. Chem. Soc.* **2006**, *128*, 9238.

7) Jabri, A.; Crewdson, P.; Gambarotta, S.; Korobkov, I.; Duchateau, R. *Organometallics*; **2006**, *25*, 715.

8) Wang, B.; Yang, Z.; Wang, Q.; Cai, T.; Crewdson, P. *Bioorg. Med. Chem.* **2006**, *14*, 1880.

9) Crewdson, P.; Gambarotta, S.; Djoman, M.; Korobkov, I.; Duchateau, R. *Organometallics* **2005**, *24*, 5214.

10) Crewdson, P.; Gambarotta, S.; Yap, G. P. A.; Thompson, L. K. *Inorg. Chem.* **2003**, *42*, 8579.

Table of Contents

List of Figures

Chapter 1

Chapter 2

Chapter 3

Chapter 4

Chapter 5

Chapter 6

Chapter 7

Chapter 8

List of Schemes

Chapter 2

Chapter 3

Chapter 4

Chapter 5

Chapter 6

Chapter 7

Chapter 8

List of Tables

Chapter 2

Chapter 3

Chapter 4

Chapter 5

Chapter 6

Chapter 7

List of Common Abbreviations

ADP	Adenosine Diphosphate
ATP	Adenosine Triphosphate
BisImine	[2,6-(2,6-{^{i}Pr}$_2$PhN=C{CH$_3$})$_2$(C$_5$H$_3$N)]
^{t}Bu	Tert-Butyl
calcd	Calculated
CHO	Cyclohexene epoxide
Cp	Cyclopentadienyl Ligand
Cp*	1,2,3,4,5 – Pentamethyl-cyclopentadienyl Ligand
Cy	Cyclohexyl
d^n	Denotes d-orbital electrons where n = 0-10
DMF	Dimethylformamide
DMSO	Dimethylsulfoxide
e^-	Electron
EI	Electron Impact
EPR	Electron Paramagnetic Resonance
Et	Ethyl
EtOH	Ethanol
Et_2O	Diethyl ether
EXAFS	Extended X-ray Absorbance Fine Structure
GPC	Gel Permeation Chromatography
IBAO	Tetraisobutylaluminoxane
LLDPE	Linear Low-Density PolyEthylene
M^+	Molecular Ion
M_w	Weight Average Molecular Mass
M_n	Number Average Molecular Mass
MAO	Methylaluminoxane
Me	Methyl
MeOH	Methanol
MTT	Manganese Tricarbonyl Transfer (reagents)

NADPH	Nicotinamide Adenine Dinucleotide Phosphate
NacNac	N,N'-(pent-2-ene-2-yl-4-ylidene)bis(2,6-diisopropyl-methylaniline)
NMR	Nuclear Magnetic Resonance
N-MeDipyr	2-(diphenyl(1H-pyrrol-2-yl)methyl)-1-methyl-1H-pyrrole
N-MeTripyr	2,5-bis(diphenyl(1H-pyrrol-2-yl)methyl)-1-methyl-1H-pyrrole
OEC	Oxygen Evolving Complex
OAc	Acetate
Oxone	$2\ KHSO_5 \cdot KHSO_4 \cdot K_2SO_4$
PCy_3	Tricyclohexyl Phosphine
PDI	Polydispersity Indice [M_w/M_n]
PE	Polyethylene
Ph	Phenyl
PNP	Bis-(diisopropylphosphino)cyclohexylamine
PO	Proplyene oxide
ppm	Parts Per Million
R	Alkyl Group
R_f	Retention Factor
S^n	Nuclear Spin State
SEC	Size Exclusion Chromatography
THF	Tetrahydrofuran
TLC	Thin Layer Chromatography
TMEDA	NNN'N'-Tetramethylethylenediamine
TOF	Turn Over Frequency
SNS	Bis-(2-(alkylthio)ethyl)amine
XANES	X-ray Absorbance Near Edge Structure

Chapter

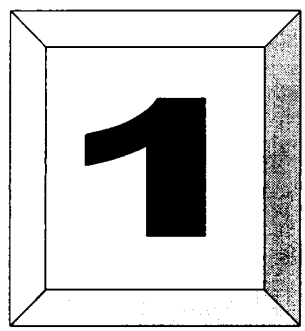

Introduction

Manganese is the twelfth most abundant element and comprises ~0.1% of the earth's crust.[1] All living creatures have been found to contain traces of the metal, and its removal or deficiency results in diminished growth or even death.[2] Of course, excessive amounts of Mn may also lead to problems. In humans the first signs of Mn poisoning are often psychotic fits of laughter or crying[3] (please note that these symptoms shouldn't be confused with graduate students writing their theses). Perhaps the most famous example of Mn in classical 1st year chemistry is the strong oxidizing agent $KMnO_4$ ($Mn^{(VII)}$), which is commonly used in organic syntheses to oxidize various functional groups.[4] The only naturally occurring isotope is ^{55}Mn and the most stable oxidation state is +2, which invariably has the high-field d^5 electronic configuration. Though $Mn^{(II)}$ is the most stable oxidation state, complexes exist for all possible intermediate oxidation states: zero-seven. The quadrupolar nature of the Mn nuclei (S = 5/2) coupled with the five unpaired electrons of its most common oxidation state invariably renders most Mn complexes un-analyzable via NMR. This is not to say that the NMR properties of Mn are

completely useless as they have been used to probe biomechanics and biomacromolecules via magnetic relaxation techniques.[5] Thus, the only incontrovertible evidence for the structural assignments of Mn complexes is often single crystal X-ray diffraction coupled with magnetic moment measurements to clarify the oxidation state. The concomitant problems associated with this method of analysis severely hindered early exploration of Mn chemistry, though these problems have started to be overcome in the past 15 years. An even greater challenge to Mn chemistry is the tendency of the metal towards oxidation by atmospheric O_2 to produce the ubiquitous MnO_2.[6] Traditionally the chemistry of Mn was readily divided into the two fields of organometallic chemistry (for $Mn^{(-I)}$, $Mn^{(0)}$ and $Mn^{(I)}$) and coordination chemistry for $Mn^{(II)}$ and higher with very little overlap.[6] However, our current understanding of inorganic chemistry has blurred these two distinctions and for the purpose of this thesis I will refer to both collectively as "organometallic" chemistry. By far the major driving force behind the exploration of Mn chemistry has been the discovery that the metal Mn is an integral part of many bio-inorganic catalysts. In general these systems contain one to four Mn atoms and are usually found in the oxidation states 2-5 ($Mn^{(II)}$ usually being the resting state).[7] Some important examples are: Superoxide Dismutase,[8] Glucosyltransferase,[9] and Manganese Peroxidase.[10] By far the most important Mn-containing biological system is known as the Oxygen Evolving Complex (OEC), which is found in all plants and is responsible for the conversion of H_2O to O_2, protons, and electrons.[6] This process is light driven and is responsible for all photosynthesis on the planet, making it the object of intense scientific scrutiny. In order to provide the reader with a fuller understanding of Mn chemistry, each oxidation state will be briefly discussed below along with the most common characteristics and uses of each oxidation state.

<u>$Mn^{(0)}$ Chemistry:</u>

Since $Mn^{(0)}$ has a d^7 electronic configuration, stable monomeric species are almost unknown. The chemistry of this oxidation state, not surprisingly, is dominated by octahedral carbonyl compounds.[11] The dimeric complex $[Mn_2(CO)_{10}]$ was first prepared in 1949[3] and is commercially available. Like most pure carbonyl compounds $[Mn_2(CO)_{10}]$ has been well explored photochemically.[12] The radical character which is

generated by the splitting of the Mn-Mn bond allows the complex to catalyze the ring opening of α-propiothiolactones.[13] The carbonyls can be substituted for other Group V (P, As, Sb) or Group VI (S, Se, Te) donor ligands, but generally only a maximum of two carbonyls may be replaced.[11] The phosphine derivatives are able to catalyze homogeneous hydrogenation reactions.[14] Other than these notable examples the chemistry of $Mn^{(0)}$ remains largely undeveloped.

$Mn^{(I)}$ Chemistry:

The chemistry of $Mn^{(I)}$ is much richer than that of the zero valent state for two main reasons. Firstly, the d^6 electronic configuration is inherently more stable, and secondly low-spin octahedral compounds allow the use of NMR for characterization purposes for bound ligand systems. Once again the chemistry is dominated by carbonyl complexes, but the well-known cyclopentadienyl ligand (Cp) is also found ubiquitously.[11] The most readily available Mn^{I} material is $[Mn(CO)_5Br]$ on which ligand exchange can be performed. However, the oxidation state is also accessible via reduction of $Mn^{(II)}$, though only in the presence of strong ligands (eg. CO, ^{-}CN). There is quite a rich amount of carbene and carbyne chemistry,[15] as well as attempts to make coordinatively unsaturated compounds,[16] however very few practical applications have been realized to date. Perhaps the most practical application of $Mn^{(I)}$ compounds is the Manganese tricarbonyl transfer (MTT) reagents. MTT complexes can be used to synthesize hetero and homo- bimetallic compounds as well as desulfurizing benzothiophenes or assembling supra-molecular quinonoid structures.[17] As in the case of the zero-valent oxidation state Mn^{I} compounds are sensitive to oxidation, however disproportionation does not appear to be a common decomposition pathway.

$Mn^{(II)}$ Chemistry:

The vast majority of Mn chemistry has been performed at the +2 oxidation state (high-spin d^5) as the half-filled d-orbitals provides extra electronic stability. $Mn^{(II)}$ is considered to be a "hard" metal,[18] and as such becomes the first oxidation state where carbonyl compounds are the exception and not the rule. In general, $MnX_2 \cdot 6H_2O$ (X = F, Cl, Br, I) is the most common starting material. Aqueous and electrochemical studies

abound for this metal, which quite often serves as a starting material for oxidation to higher valencies.[6,19] The +2 oxidation state has no strong preference for coordination geometry, the complexes that do arise are generally ligand and stericly dependant and complexes are known for the coordination numbers 2 up to 8.[6] In general, octahedral and tetrahedral geometries are the most prevalent. The hardness of the metal means that oxygen donor ligands are normally favoured over nitrogen donor ligands, which can obviously lead to problems in aqueous solutions. Nitrogen based ligand systems (amines, pyridines, etc.) are used extensively, and are often coupled with carboxylate or phenolate moieties to yield robust complexes. The five unpaired electrons of the common high-spin state make the use of EPR spectroscopy (Electron Paramagnetic Resonance) relevant for attempting structural characterization when a crystal structure is not forthcoming.[20] As previously mentioned it is not uncommon to oxidize $Mn^{(II)}$ to yield higher valent complexes. Another commonly employed route to higher valent complexes is the comproportionation of $Mn^{(II)}$ with $Mn^{(VII)}$ sources, generating mixed oxidation state complexes.[21] The mixed oxidation state $Mn^{(IV,V)}$ is important for several metalloenzymes, thus driving this type of research. Cluster compounds containing mixed valent Mn (+2 and higher) are also very important for understanding the photosynthetic coupled OEC complex. A further discussion of the specifics of this will be presented later in this thesis.

<u>$Mn^{(III)}$ Chemistry:</u>

The chemistry of $Mn^{(III)}$ is rather limited due to the propensity of $Mn^{(III)}$ to disproportionate, especially in aqueous solutions, to the stable MnO_2 and $Mn^{(II)}$.[6] That is not to say however, that $Mn^{(III)}$ is completely unstable, as $[Mn(OAc)_3 \cdot 4H_2O]$ is a quite versatile starting material for synthesis. $Mn^{(III)}$ has a d^4 electronic configuration; therefore the octahedral compounds it commonly forms exhibit Jahn-Teller distortions. These distortions, along with the concomitant loss of an EPR signal are often tell-tale signs for the presence of this oxidation state in mixed-valent complexes. The most common coordination numbers found for this oxidation state are five or six.[6] Once again, one of the main driving forces behind the chemistry of this valency is the elucidation of biological mechanisms which either start in, or pass through this oxidation state. The

stereo-selective epoxidation reaction,[22] along with oxidations,[23] and nitrogen transfer[24] reactions are all performed by a $Mn^{(III)}$ starting material coupled with the Schiff-base Salen ligand (see Figure 1.1).

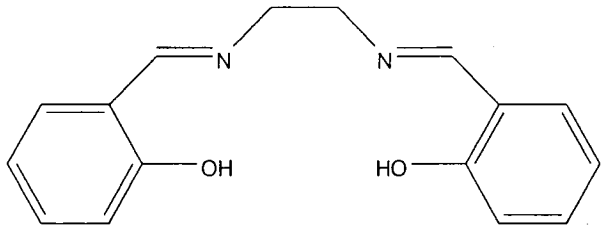

Figure 1.1 Basic Salen Ligand Framework.

The $Mn^{(III)}$Salen system is the exception to the disproportionation rule, as it is able to generate a $Mn^{(V)}$ compound which then performs the previously mentioned catalytic transformations.

$Mn^{(IV)}$ Chemistry:

Unfortunately the most readily available $Mn^{(IV)}$ compound is the insoluble MnO_2, which forms quite readily from a variety of complexes and oxidation states. When useful compounds of this oxidation state do form, their d^3 electronic state is responsible for the commonly found octahedral geometry and high-spin configurations. Remarkably, the tetra-alkyl [$MnMe_4$(dmpe)] has been found to be reasonably stable, though it is actually generated from the disproportionation of a $Mn^{(III)}$.[25] Other ligand systems which are able to, at least temporarily, stabilize $Mn^{(IV)}$ are porphyrins,[26] Salen,[27] and 1,4,7-triazacyclononanes.[28] The triazacyclononane complexes have been used as oxidation,[29] and asymmetric epoxidation catalysts.[30] When cluster compounds are assembled containing the mixed-oxidation states $Mn^{(III,IV)}$, unique superparamagnetic properties can result. These complexes then act like miniature magnets; this property has attracted the interest of researchers for their potential uses as data storage devices.[31]

$Mn^{(V\text{-}VII)}$ Chemistry:

The later oxidation states are all very strongly oxidizing and are dominated by oxo- compounds, with their chemistry being very poorly developed. The exception to this are bulky imido ligands (ie. N^tBu^{2-}). These ligands are able to generate

characterizable compounds for $Mn^{(V\text{-}VII)}$.[32] The oxo- species $Mn^{(V)}O_4^{3-}$, and $Mn^{(VI)}O_4^{2-}$ have generated some interest for their properties as near-IR lasers and represents the main body of interest in the higher oxidation states to date.[33]

Thesis Overview:

The above overview of the coordination chemistry of manganese, in spite of its brevity, gives a convincing impression of the unique versatility of this metal. By spanning a large range of oxidation states, and in combination with its abundance, non-toxicity and prevalence in biological systems, this element provides a great potential for important applications including: solid state chemistry, bio-inorganic, catalysis. We were particularly attracted to the OEC enzyme and trying to understand how such a relatively simple tetranuclear cluster core could perform such a remarkable transformation with only the energy input of sunlight. Besides the possibility of obtaining critical information which in turn may provide the basis for the potential development of photocatalysts for renewable sources of energy, we also found it fascinating that one of the strongest oxidants in nature, di-oxygen, is evolved during a reaction forming a relatively low–oxidation state (Mn^{II}). In turn, this suggested to us that this metal has, indeed, the potential for supporting oxygen-resistant, low-cost alternatives to water-soluble organometallic catalysts. Obviously we are not alone in this interest. As a result of a remarkable wealth of activity in this field, our understanding of this absolutely unique metal has substantially advanced. The state of the art in this field is reviewed in the introductory part of Chapter 4. Thus, by using the available information about oxidation state, coordination geometry, ligand donor atoms and cluster nuclearity, we are in the fortunate position of being able to explore Mn chemistry in a variety of directions.

It should be noted that the type of research performed is not dictated by the transition metal, but rather the goals of the scientist performing the investigation. The field of organometallic chemistry[34] is quite diverse and hosts an entire spectrum of research possibilities. At the practical end of this continuum is the work centred on producing catalysts for the manufacture of commodities (e.g. polyethylene),[35] or for organic transformations.[36] On the more esoteric side of things, there is basic research which explores the fundamental ways in which transition metals interact with one another

or with various organic molecules, be it the formation of cluster compounds,[37] multiple metal-metal bonds,[38] or even unique spin-states.[39] Between these two extremes is the investigation and attempts at mimicry of natural systems which contain transition metals that catalyze various processes. From this field stems research such as di-nitrogen activation/reduction[40] and water oxidation.[41] When we selected the first-row transition metal Mn for this doctoral work, it became readily apparent that the metal could support both practical chemistry as well as basic research. From the practical point of view, creating catalysts from Mn offers cost benefits as it is relatively simples and inexpensive to obtain in a variety of oxidation states. Polymers produced for food packaging purposes by using non-toxic manganese would obviously avoid the health concerns arising from catalysts leaching as recently trumpeted by the media. Most of all we were motivated by understanding the factors (ligand features, coordination geometry, oxidation state and presence of reactive functions) which determine the richness and diversity of the Mn chemical transformations.

As each chapter contains its own unique introductory section, with a review of the relevant literature, only a brief overview of each will be outlined below.

Chapter 2 details the organic synthesis of several novel ligand systems along with a discussion of the accompanying synthetic pitfalls which were encountered during their preparation.

In Chapter 3, the preparation of several $Mn^{(II)}$ di-alkyls which were used extensively in most of the following chapters was explored. The Mn di-alkyl was prepared to act as a starting material for metathesis reactions with ligand systems, including those designed in the second chapter. The first two chapters represent basic research as they were not done for a specific commercial purpose, but rather to create a platform from which more science could be developed.

The fourth chapter, details our preliminary efforts in modelling studies that attempted to mimic the Oxygen Evolving Complex (OEC). This chapter built upon work from previous chapters as the Mn di-alkyls were used extensively, along with some of the ligand systems developed in Chapter 2.

The fifth chapter details our investigations of $Mn^{(II)}$ for the co-polymerization of CO_2 and epoxides. This was the first practical exploration using the Mn di-alkyl materials developed in the third chapter.

Chapter 6 contains a continuation of previous work in our lab, as well as a collaboration of work performed by Jennifer Scott and Indu Vidyaratne in generating extremely low-valent metal-Brookhart ligand complexes. The work was on a less practical level and more along the lines of basic research. However, once again the di-alkyls generated in Chapter 3 were used as starting materials. The resulting complexes are unique as they represent some of the only examples of non-Cp or carbonyl containing $Mn^{(I)}$ complexes.

Continuing the trend started in chapter 5 of examining practical applications of organometallic complexes, Chapter 7 explores the use of the ligands developed in the second chapter for the selective oligomerization of ethylene using $Cr^{(II)}$ and $Cr^{(III)}$ as the inorganic precursors. The reason for switching our interest from Mn to Cr chemistry was dictated by an observation obtained from our work in Mn chemistry that convinced us that the ligand system developed for Mn chemistry could also be used in combination with Cr to provide important answers for an industrially relevant problem. The fundamental aim of this part of the project was to attempt to identify which oxidation state of Cr was closer to that of the actual active catalyst.

Overall this thesis explores both practical applications and a range of basic research into the mid first-row transition metals. Though not strictly related, the chapters of this thesis do knit together to depict a well-rounded investigation of the applications of the transition metals Cr and Mn in both a basic and practical sense.

References:

1) Fortey, R. A. *The Earth: an Intimate History*, Harper Perennial: London, **2005**.
2) Cotzias, G. C. *The Encyclopedia of Biochemistry* Reinhold: New York, **1967**. b) Cotzias, G. C. *Manganese in Mineral Metabolism: An Advanced Treatise* Academic Press: New York, **1962**.
3) Bailar, J. C.; Emeleus, H. J.; Nyholm, R.; Trotman-Dickenson, A. F. *Comprehensive Inorganic Chemistry, vol. 3* Pergamon Press: Toronto, **1973**.
4) Clayden, J.; Warren, S.; Greeves, N.; Wothers, P. *Organic Chemistry*, Oxford University Press: London, **2000**.
5) Niccolai, N.; Tiezzi, E.; Valensin, G. *Chem. Rev.* **1992**, *82*, 359.

6) McCleverty, J. A. *Comprehensive Coordination Chemistry: Volume 5* Oxford Press: London, **2003**.
7) Messerschmidt, A.; Huber, R.; Poulos, T.; Wieghardt, K. *Handbook of Metalloproteins* Wiley: New York, **2001**. b) Bertini, I.; Sigel, A.; Sigel, H. *Handbook on Metalloproteins* Marcel Dekker; New York, **2001**. c) Sigel, A; Sigel, H. *Manganese and its Role in Biological Processes* Marcel Dekker: New York, **2000**. d) Sigel, A.; Sigel H. *Metals Ions in Biological Systems vol. 37* Marcel Dekker: New York, **2000**. e) Yocum, C. F.; Pecoraro, V. L. *Curr. Opin. Chem. Biol.* **1999**, *3*, 182. f) Law, N. A.; Caudle, M. T.; Pecoraro, V. L. *Adv. Inorg. Chem.* **1999**, *46*, 305.
8) Sigel, A.; Sigel H. *Metals Ions in Biological Systems vol. 37* Marcel Dekker: New York, **2000**. b) Raha, S.; Robinson, B. H. *Trends Biochem. Sci.* **2000**, *25*, 502. c) Miller, A. F.; Sorkin, D. L. *Comm. Mol. Cell. Biophys.* **1997**, *9*, 1.
9) Unligil, U. M.; Rini, J. M. *Curr. Opin. Struct. Biol.* **2000**, *10*, 510.
10) Sigel, A.; Sigel H. *Metals Ions in Biological Systems vol. 37* Marcel Dekker: New York, **2000**. b) Leonoqicz, A. *et. al. Fungal Gen. Biol.* **1999**, *27*, 175. c) Banci, L. *J. Biotechnol.* **1997**, *53*, 253.
11) Abel, E. W.; Stone, F. G. A.; Wilkinson, G. *Comprehensive Organometallic Chemistry II, vol 6* Pergamon Press: Toronto, **1995**.
12) Geoffroy, G. L.; Wrighton, M. S. *Organometallic Photochemistry* Academic Press: New York, **1979**. b) Geoffroy, G. L. *J. Chem. Educ.* **1983**, *60*, 861.
13) Adams, R. D.; Huang, M.; Huang, W. *Organometallics* **1997**, *16*, 4479.
14) Giordano, R.; Sappa, E.; Tiripicchio, A.; Tiripicchio Camellini, M.; Mays, M. J.; Brown, M. P. *Polyhedron* **1989**, *8*, 1855.
15) Chen, J.; Wang, R. *Coord. Chem. Rev.* **2002**, *231*, 109.
16) Hartl, F.; Rosa, P.; Ricard, L.; Le Floch, P.; Zalis, S. *Coord. Chem. Rev.* **2007**, *251*, 557.
17) Oh, M.; Reingold, J. A.; Carpenter, G. A.; Sweigart, D. A. *Coord. Chem. Rev.* **2004**, *248*, 561.
18) Arhland, S.; Chatt, J.; Davies, N. R. *Q. Rev., Chem. Soc.* **1958**, *12*, 265.
19) Wilkinson, G.; Gillard, R. D.; McCleverty, J. A. *Comprehensive Coordination Chemistry, vol 4* Pergamon Press: Toronto, **1987**.
20) Duliu, O. G.; Velter-Stefanescu, M. *J. Optoelectro. Adv. Mat.* **2006**, *8*, 1557. b) Mazur, M.; Kleinova, M.; Moncol, J.; Stachova, P.; Valko, M.; Telser, J. *J. Non-Cryst. Sol.* **2006**, *352*, 3158. c) Copik, A. J.; Nocek, B. P.; Swierczek, S. I.; Ruebush, S.; Jang, S. B.; Lu, M.; D'Souza, V. M.; Peters, J. W.; Bennett, B.; Holz, R. C. *Biochem.* **2005**, *44*, 121.
21) Bhaduri, S.; Pink, M.; Christou, G. *Chem. Commun.* **2002**, 2352. b) Dube, C. E.; Wright, D. W.; Bonitatebus, P.J.; Armstrong, W. H. *J. Am. Chem. Soc.* **1998**, *120*, 3704. c) Pal, S.; Chan, M. K.; Armstrong, W. H. *J. Am. Chem. Soc.* **1992**, *114*, 6398. d) Lis, T. *Acta Crystallogr. B* **1980**, *36*, 2042.
22) Das, D.; Cheng, C. P. *J. Chem. Soc. Dalton Trans.* **2000**, *7*, 1081. b) Zhang, W.; Jacobsen, E. N. *J. Org. Chem.* **1991**, *56*, 2296.
23) Kumbhat, V.; Sharma, P. K.; Banerji, K. K. J. Chem. Res. Synop. **2001**, *5*, 562. b) Bansal, V.; Sharma, P. K.; Banerji, K. K. *J. Chem. Res.* **1999**, 480.
24) Du Bois, J.; Tomooka, C. S.; Carreira, E. M. *Acc. Chem. Res.* **1997**, *20*, 364.
25) Dey, K.; De, R. L. *J. Inorg. Nucl. Chem.* **1977**, *39*, 153.

26) Groves, J. T.; Stern, M. L. *J. Am. Chem. Soc.* **1988**, *110*, 8628.
27) Palucki, M.; Finney, N. S.; Pospisil, P. J.; Guler, M. L.; Ishida, T.; Jacobsen, E. N. *J. Am. Chem. Soc.* **1998**, *120*, 948. b) Srinivasan, K.; Michaud, P.; Kochi, J. K. *J. Am. Chem. Soc.* **1986**, *108*, 2309.
28) Zhang, L. *et. al. J. Chem. Cryst.* **2000**, *30*, 251.
29) Hage, R.; Kerschner, J. *Trends Inorg. Chem.* **1998**, *5*, 145.
30) Argouarch, G.; Gibson, C. L.; Stones, G.; Sherrington, D. C. *Tetrahedron Lett.* **2002**, *43*, 3795.
31) Cornia, A.; Affronter, M.; Jansen, A. G. M.; Gatteschi, D.; Caneschi, A.; Sessoli, R. *Chem. Phys. Lett.* **2000**, *322*, 477. b) Sessoli, R. et. al. *J. Am. Chem. Soc.* **1993**, *115*, 1804. c) Sessoli, R.; Gatteschi, D.; Caneschi, A.; Novak, M. A. *Nature* **1993**, *365*, 141.
32) Danopoulos, A. A.; Green, J. C.; Hursthouse, M. B. *J. Organomet. Chem.* **1999**, *591*, 36.
33) Gudel, H. U.; Brunold, T.; Hazenkamp, M.; Herren, M.; Oetliker, U.; Schenker, R. *Proc. Electrochem. Soc.* **1998**, 225. b) Hazenkamp, M. F.; Brunold, T. C.; Gudel, H. U. *J. Luminesc.* **1997**, 675. c) Moncorge, R.; Manaa, H. *Ann. Chimie (Paris)* **1995**, *20*, 241.
34) Crabtree, R. H. *The Organometallic Chemistry of the Transition Metals* John Wiley & Sons LTD: Hobokon, **2005**.
35) Carraher, C. E. *Introduction to Polymer Chemistry* CRC: Boca Raton, **2007**. b) Buchmeiser, M. R. *Metathesis polymerization* Spring: New York, **2005**. c) Odian, G. G. *Principles of polymerization* Wiley: Hoboken, **2004**.
36) Evans, P. A. *Modern Rhodium Catalyzed Organic Reactions* Wiley-VCH: Weinheim, **2005**. b) Blaser, H. U.; Schmidt, E. *Asymetric Catalysis on Industrial Scale* Wiley-VCH: Weinheim, **2003**. c) Coates, R. M.; Denmark, S. E. *Handbook of Reagents for Organic Sythesis: Reagents, Auxiliaries and Catalysts for C-C bonds* John Wiley & Sons LTD: Toronto, **1999**.
37) Macintosh, A. M.; Chisholm, M. H. *Chem. Rev.* **2005**, *105*, 2949. b) Henderson, R. A. *Chem. Rev.* **2005**, *105*, 2365. c) Lombardi, J. R.; Davis, B. *Chem. Rev.* **2002**, *102*, 2431.
38) Macintosh, A. M.; Chisholm, M. H. *Chem. Rev.* **2005**, *105*, 2949. b) Schnepf, A.; Himmel, H.-J. *Angew. Chem. Int. Ed.* **2005**, *44*, 3006. c) Modec, B.; Brencic, J. V. *J. Clust. Sci.* **2002**, *13*, 279.
39) Weiss, R.; Gold, A.; Terner, J. *Chem. Rev.* **2006**, *106*, 2550. b) Dronskowski, R. Adv. Sol. Stat. Phys. **2002**, *42*, 433. c) Poli, R. *Chem. Rev.* **1996**, *96*, 2135.
40) Smythe, N. C.; Schrock, R. R.; Muller, P.; Weare, W. W. *Inorg. Chem.* **2006**, *45*, 9197. b) Vidyaratne, I.; Gambarotta, S.; Korobkov, I. *Inorg. Chem.* **2005**, *44*, 1187. c) Lee, S. C.; Holm, R. H. *Chem. Rev.* **2004**, *104*, 1135. d) Bates, W. M. E.; Clentsmith, G. K. B.; Clock, F. G. N.; Grenn, J. C.; Jenkin, H. D. L. *Chem. Commun.* **2000**, 927. e) Ferguson, R.; Solari, E.; Floriani, C.; Osella, D.; Ravera, M.; Re, N.; Chiesi-Villa, A.; Rizzoli, C. *J. Am. Chem. Soc.* **1997**, *119*, 10104.
41) Mukhopadhyay, S.; Mandal, S. K.; Bhaduri, S.; Armstrong, W. H. *Chem. Rev.* **2004**, *104*, 3981.

Chapter

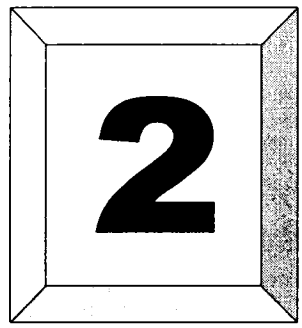

Pyrrole-Based σ, π – Donating Ligand Design and Syntheses

Table of Contents:

2.1 Introduction:

The richness of organometallic chemistry is mediated by two main factors. Foremost is the selection of the transition metal which will imbue a system with its own unique characteristics and reactivity. Secondly, but no less importantly, is the selection of the ligand system that will accompany the metal centre, which can be used to tailor the reactivity of the metal. This can be accomplished through myriad different routes, but the

main goals are always the same. The ligand can be used to alter: the electronic density; the sterics/symmetry; and the coordination geometry about the metal centre. As a ligand system is employed, trends are often noted which can then be used to retool and improve the ligand system in order to explore new directions.

Essentially a ligand, in terms of organometallic chemistry, is any organic molecule which binds to a metal centre through either a neutral lone-pair of electrons or an anionic electron pair. A single ligand can bind to a metal from more than one position on the molecule which leads to the so-called multi-dentate ligand systems.[1] As well as donating electrons to a transition metal, many ligands are also able to accept electron density from a metal centre in a process known as back-bonding.[1]

Perhaps one of the most well-known and widely explored ligand systems to date is the cyclopentadienyl (Cp) or its more sterically bulky derivative; 1,2,3,4,5-pentamethyl-cyclopentadienyl (Cp*) (see Figure 2.1.1) as well as an endless number of alternate variations.

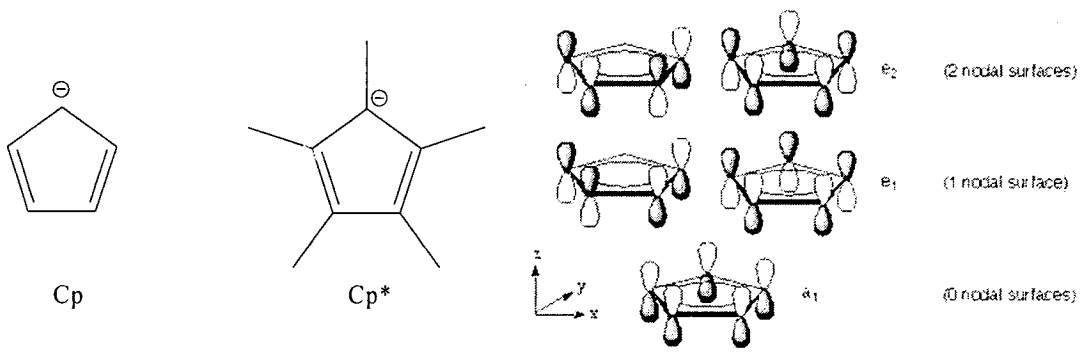

Figure 2.1.1 Cyclopentadienyl Ligand Systems.

What makes this ligand system unique is that it coordinates in an η^5 fashion, composed of one anionic electron pair and two double bonds which, through resonance, allows the ligand to bind strongly to a metal in an orthogonal orientation. Specifically, the molecular orbitals formed upon complexation of Cp to a metal centre allow it to form one σ-bond, two π-bonds, and allows for metal-ligand back donation through a δ-bonding interaction if necessary.

The utility of this ligand, and the richness of chemistry which resulted from its inception, stemmed from the work of Geoffrey Wilkinson and his correct formulation of

the sandwich structure of ferrocene. This seminal discovery, and the realization of the ability of π-systems to bind to transition metals, marked a true milestone in the development of organometallic chemistry and was acknowledged with the award of the Nobel Prize in 1973.

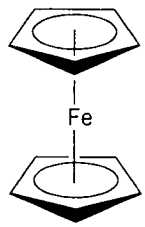

Figure 2.1.2 Structure of Ferrocene.

Today, Cp-based organometallic complexes have been used for almost every chemistry application including among the most famous: coordination chemistry,[2] polyethylene production,[3] electrochemistry,[4] metal promoted organic syntheses[5] and even di-nitrogen activation.[6] The ligand system is capable of supporting a vast array of molecular activation processes and catalytic transformations for several reasons. Foremost is the ligands electronic flexibility. The interaction with the π-system results in the donation of up to 6 electrons when the ligand is centred over the metal. However, crystallographic studies have determined that Cp is also capable of partially slipping from the metal which results in less electron donation.[7] In addition, the π^* orbitals of the Cp rings are capable of receiving excess electron density from the metal centre through δ-bonding, which allows even more electronic flexibility. Also, the steric protection of the Cp ring, positioned perpendicularly with respect to the metal-ligand vector limits the approach of other molecules to well-defined areas around the metal. This effect is even more pronounced in the case of the Cp* ligand, or any substituted Cp, with their larger steric bulk.

The versatility of the Cp–based ligand systems has of course spawned a substantial amount of interest in generating "alternate" ligands which would be able to fulfill or even surpass the usefulness of the Cp system. It was thought that generating a 6 e^- donating ligand with a massive steric bulk or a cone angle comparable to the Cp derivatives would be the best substitute for the Cp ligand. Following this rationale, Wolczanski published extensive studies on bulky alkoxide ligands (see Scheme 2.1.3).[8]

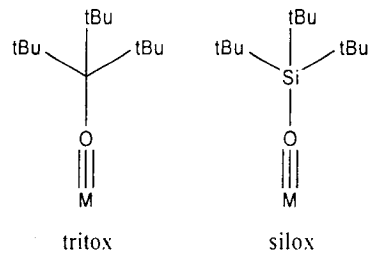

Figure 2.1.3 Cp Alternative Ligands.

Although these ligand systems produced,[9] and continue to produce interesting chemistry, especially in atom transfer reactions,[10] they did not exhibit the same broad chemical reactivity of the Cp organometallic complexes. The reduced reactivity of the tritox and silox organometallic complexes could perhaps be attributed to the inability of the ligands to partake in efficient back-bonding interactions with electronically saturated metal centres.

The simplest ligand system with the potential to mimic the electronic and steric features of Cp is the deprotonated pyrrole molecule. Once deprotonated, the pyrrolide ligand can bind to a metal in one of two fashions. If the anionic charge is localized on the nitrogen a two electron σ–bond can be formed. If, however, the anionic charge is delocalized over the five-membered ring an η^5–bond similar to the traditional Cp ligand (up to six electrons donated) may be formed (see Figure 2.1.4).

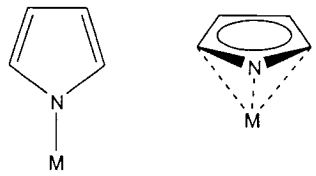

Figure 2.1.4 Bonding Modes of Pyrrolide Ligands.

These two bonding modes create a certain level of flexibility, allowing the ligand systems to accommodate a variety of metals and oxidation states. However, a search of the Cambridge Crystallographic Database demonstrates that the simple pyrrolide ligand always binds to the metal in the σ-bonding fashion, precluding its ability to mimic Cp. When the pyrrolide moiety is incorporated into a larger ligand framework (See Figure 2.1.5), however, the π-bonding orientation becomes much more prevalent.

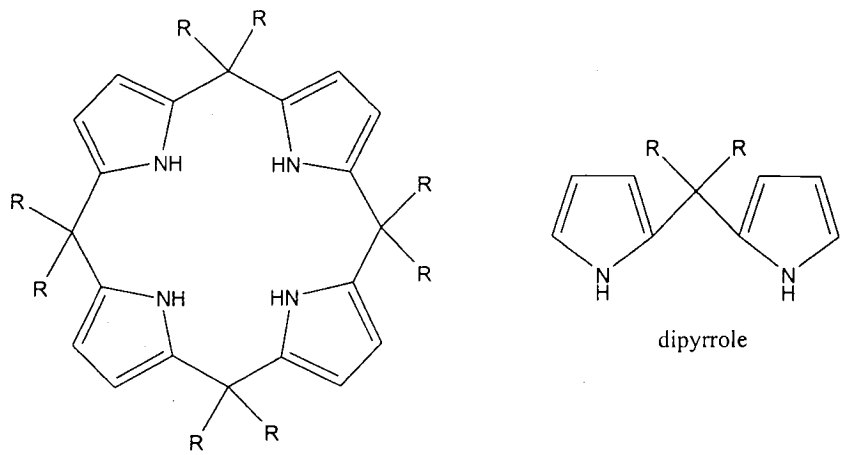

Figure 2.1.5 Basic Structure of Pyrrole Ligands.

These pyrrolide-derived ligand systems have produced a wealth of high-impact chemistry, making them an attractive target for further improvement.

2.2 Pyrrolide Chemistry:

The coordination chemistry of the pyrrolide anions has focused mainly upon the preparation of complexes for small molecule binding and activation; however, pyrrolides do also form potent catalysts.[11] When $SmCl_3(THF)_3$ was treated with the lithium salt of octaethyl-porphyrinogen and then subsequently reduced with metallic Li, a dinuclear complex with a reduced N_2 molecule linking them together resulted.[12] This is in striking contrast to the reactivity of $[Cp^*_2Sm]$ with N_2 which leads to the side-on bound, labile coordination of the molecule with no reduction. Therefore, in this case the pyrrolide-based ligand system shows an increased reactivity over Cp. Within the dinuclear complex, each Sm unit was σ-bound by two pyrrolides, and π-bound by two more (See Figure 2.2.1). The lithium alkali cations were also retained in the dimeric structure in order to balance the overall charge of the tetra-anionic octaethylporphyrinogen ligands.

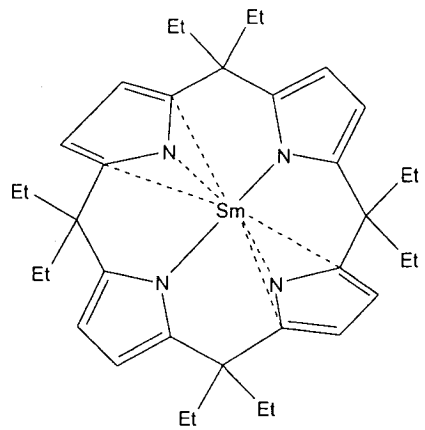

Figure 2.2.1 Simplified Porphyrinogen Structure Showing σ and π Bonding.

Since the porphyrinogen ligand systems always require the presence of alkali cations to balance the overall complex charge in low oxidation state metals, the dipyrrole ligand systems were explored in an attempt to avoid the presence of the alkali metal, by forming neutral divalent complexes. One of the first reported reactions utilizing a dipyrrolide ligand also involved the $Sm^{(II)}$-mediated partial reduction of di-nitrogen.[13] The diphenyldipyrrolide ligand formed a tetra-nuclear cluster complex with each Sm centre being both σ– and π -bound to the pyrrolides. It was also found that the nature of the halogen used in the complex (I vs. Cl) led to either partial N_2 reduction, or no N_2 binding respectively. Di-nitrogen and ethylene[14] coordination and reduction reactions were extensively explored using a variety of different metals and ligand back-bones. However, the common motif of the σ, π-bonding pyrrolides was always present.[15]

Perhaps one of the most striking results was the propensity of the pyrrolide ligands to allow both σ and π-bonding in the formation of cluster compounds (up to octameric).[16] What is even more remarkable is that in some cases it appears that the nuclearity is controlled by an accompanying alkali metal. When diphenyldipyrrole was reacted with $YbCl_3(THF)_3$ a noteworthy observation was made.[17] If the lithium salt of the ligand was used, an octameric cluster resulted. However, if the sodium salt was used a monomeric compound was formed. These results indicated that the nature of the alkali metal and how it interacted with the pyrrolide rings influenced the overall cluster assembly. This is not a general trend, however, and is unique to this and a few other reactions.

In general, the σ, π-donating ability of the pyrrolide ligand systems led to some very rich chemistry. That said, controlling the reactions proved quite difficult as the nature of the metal, the alkali cation, backbone groups, and even solvent influenced the reactivity.

2.3 Hemi-Labile Ligands:

Hemi-labile ligands are defined as multi-dentate ligands which bind strongly to a metal centre at one ligand site, while at the same time having the ability to loosely coordinate to the metal from at least one other position on the ligand.[18] The propensity for labile coordination to the metal from a second position allows the ligand to provide electronic and coordinative stability, while at the same time allowing other substrates access to the metal. Ether moieties[19] and sulfone[20] groups are prime examples of functional groups which can serve to generate hemi-labile ligand systems.

A particularly successfully example of the employment of this class of ligands was recently reported by Hessen *et. al.* who documented the switching of a Ti catalyst system from ethylene polymerization to trimerization via the use of a hemi-labile Cp-based ligand system (see Figure 2.3.1).[21]

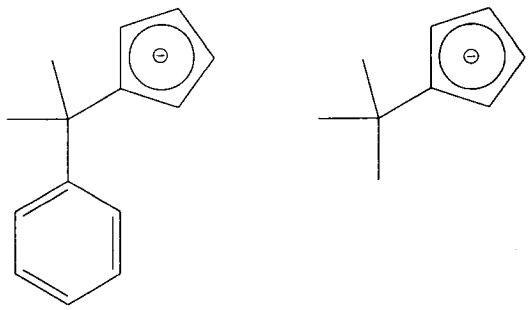

Figure 2.3.1 Ligand Modifications for Trimerization Selectivity.

It was argued that the hemi-labile ligand system is able to stabilize a transient low-valent $Ti^{(II)}$ species (top left Scheme 2.3.2) which in turn feeds the trimerization catalytic cycle. This behaviour was ascribed to the lability of the arene group which, via de-coordination, provides empty metal orbitals for a β-hydride elimination to occur, thus allowing a subsequent reductive elimination to proceed yielding a "$Ti^{(II)}$" species. A $Ti^{(II)}$ species

can indeed provide the two electron redox couple which is believed to be necessary for ethylene trimerization.

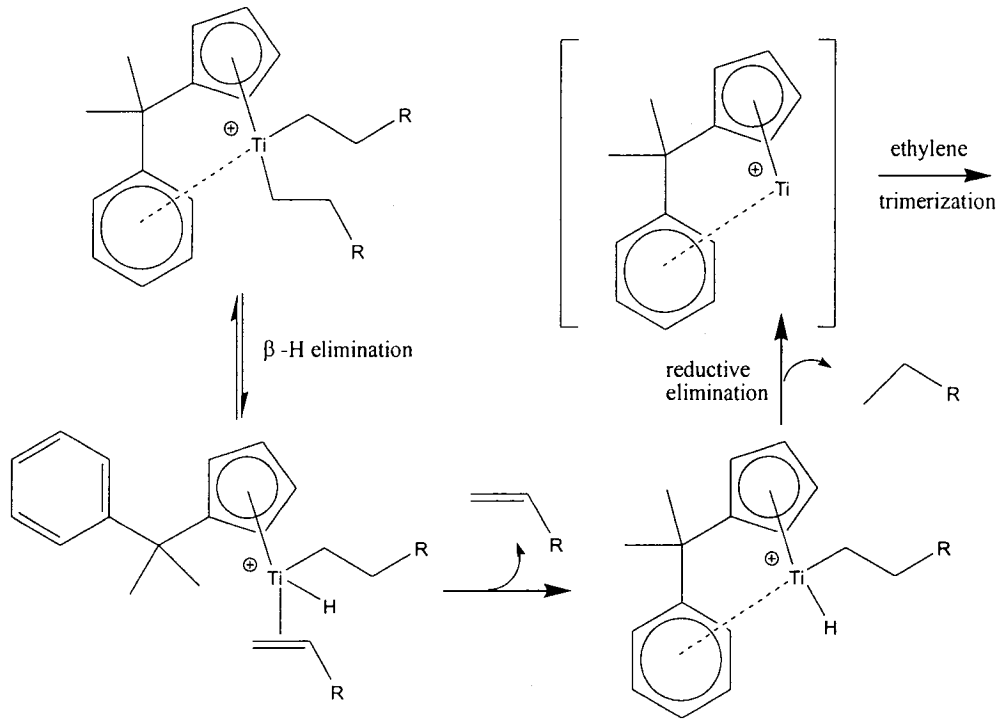

Scheme 2.3.2 Proposed Mechanism for Entrance Into Trimerization Pathway.

The hemi-labile coordination of the arene ring of this remarkable catalytic system made us re-examine the pyrrolide chemistry in a new light. Since it has already been demonstrated that the pyrrolide ring is capable of π–coordination, it seemed logical to explore ways of altering the ligand system to enhance π–ligation. In order to accomplish this goal, one of the N-H bonds must be substituted by an R group in order to ensure that the pyrrole ring can not be deprotonated, thus remaining neutral and incapable of anionic σ-bond donation. Given the above rationale we have targeted the dipyrrole molecule (see Scheme 2.1.5) for a simple modification; such as the alkylation of one of the two nitrogen atoms. We anticipated that such a modification would lead to a hemi-labile ligand, which should be quite useful for a variety of purposes including the catalytic trimerization of ethylene.

2.4 Synthetic Strategies:

Although the pyrrole moiety can be found in many systems, very little comprehensive synthetic chemistry has been published,[22] none of which describes the condensation of an N-R pyrrole. The two literature examples that report N-R pyrrolides are based on the porphyrinogen backbone and provide such dismal yields as to be synthetically useless.[23] Thus, the traditional dipyrrole synthesis[24] seemed to be the best starting point in order to generate the N-R substituted product. It was hypothesized that this could be done in one of several ways. The first route would attempt to condense an N-Me pyrrole with a normal pyrrole and the second route would attempt to substitute an N-H for a Me group on a dipyrrole molecule (see Scheme 2.4.1) thus generating a dipyrrole containing one N-Me group: N-MeDipyrrole (N-MeDipyr).

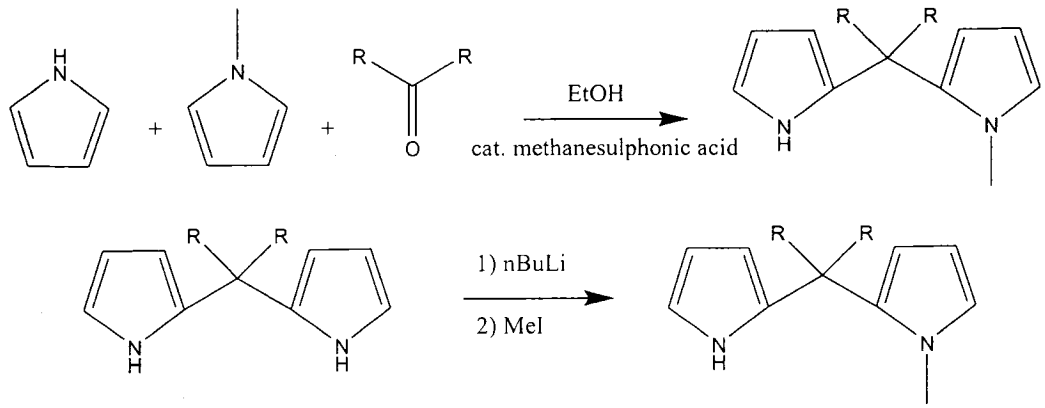

Scheme 2.4.1 Proposed Synthetic Routes to N-MeDipyr.

If neither of the previous two routes proved viable a third, more intensive, approach was proposed. The third technique will rely on first depronating an N-Mepyrrole,[25] followed by reaction of the nulceophilic N-Mepyrrolide with a ketone. After quenching, the resulting alcohol could then be condensed with a normal pyrrole in order to generate the desired product (see Scheme 2.4.2).

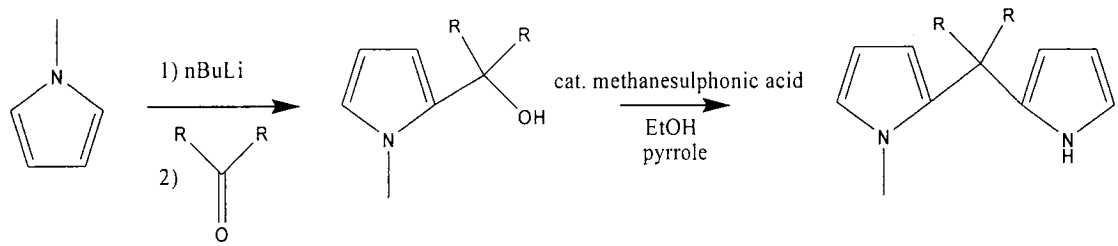

Scheme 2.4.2 Proposed Alternate Synthetic Route to N-MeDipyr.

2.5 Results and Discussion:

Since the first synthetic strategy was by far the easiest, it served as the starting point of this project. Unfortunately, the route quickly proved non-viable as the only products recovered were the unsubstituted dipyrroles. No N-Me products were found even when the stoichiometric ratio was 1000:1 (N-Mepyrrole:pyrrole) or even in the case of N-Mepyrrole without pyrrole. The use of different ketones had no impact on the outcome of this reaction, invariably leading to non-methylated dipyrrole products only. These results clearly show that N-Mepyrrole is incapable of undergoing the condensation reaction used to generate the traditional dipyrrole molecule.

Upon even a cursory inspection it can be seen that the second synthetic strategy also has a major problem. Since both N-H groups of the dipyrrole ligand are chemically and sterically equivalent, selective alkylation could prove problematic. A variety of deprotonating agents were used in conjunction with the diphenyldipyrrole ligand and methyliodide with varying success (see Table 2.5.2).

Table 2.5.1 Attempted Mono-Alkylation Reactions.

Alkylating Agent	Eq.	Total Yield (%)	Unsubstituted (%)[a]	Mono-Substituted (%)[a]	Di-Substituted (%)[a]
KH	1.0	62	40	trace	60
KH	0.5	68	77	4	19
LiMe	1.0	48	42	7	51
LiMe	0.5	53	63	9	28
t-BuLi	1.0	66	37	17	46
t-BuLi	0.5	54	35	37	28
$LiCH_2SiMe_3$	1.0	72	35	21	44
$LiCH_2SiMe_3$	0.5	66	34	41	25
$KN(TMS)_2$	1.0	79	29	26	45
$KN(TMS)_2$	0.5	76	47	31	22
$KN(TMS)_2$	0.8	82	30	50	20

[a] Based on relative NMR signals

In general it was observed that as the alkylating agent grew in steric bulk, the more mono-alkylated product was recovered. Conversely, the amount of di-substituted product

diminished with steric bulk. This was important as the unsubstituted product could be recycled back into the reaction, the di-substituted product, however, was considered to be waste. After much testing it was found that the reaction of 0.8 eq of $KN(TMS)_2$ was the best route for mainly producing the mono-substituted product. Unfortunately, the ligand was only obtained in sufficient purity after approximately five recrystallizations, depending on the scale. The resulting, recrystallized product was only 97 % pure with 3 % di-substituted product as a contaminant.

Due to the excessively long time required to recrystallize the ligand, the relatively small yields (maximum ~3 g) and the presence of the unsubstituted contaminant, it was decided to probe the third synthetic strategy (see Scheme 2.4.2). When N-Mepyrrole was reacted with 1.05 eq of nBuLi the α-position of the ring was deprotonated to yield **1** (see Figure 2.5.2). The corresponding nucleophilic N-Mepyrrolide was then added to a cooled solution of THF and benzophenone.

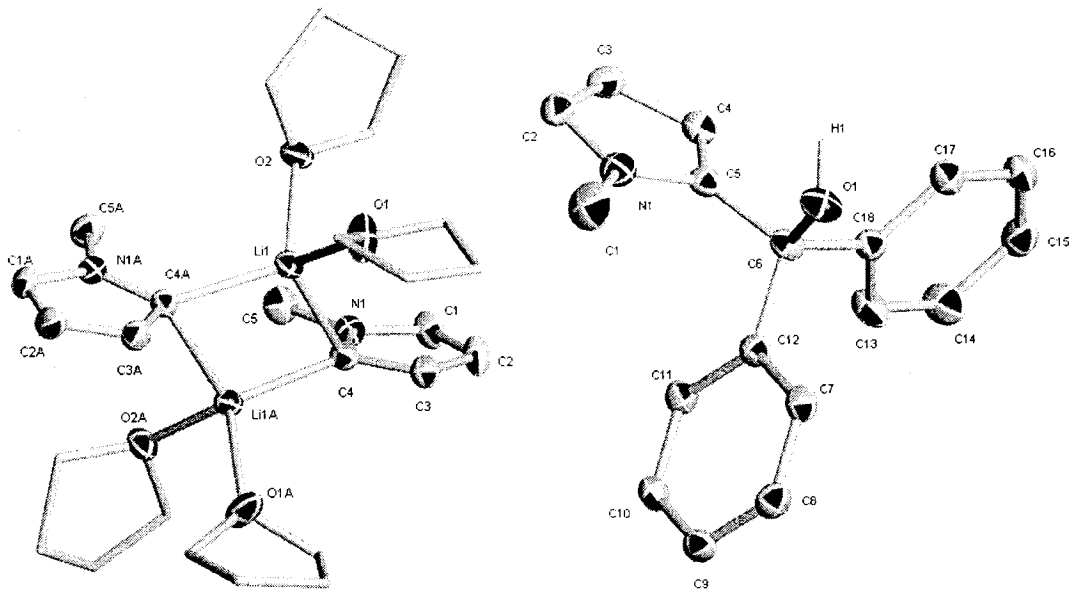

Figure 2.5.2 Structures of LiN-Mepyrrole (**1**) and Corresponding Alcohol (**2**).

After quenching of the reaction, the alcohol $[(1\text{-Me-}C_4H_3N)C(OH)Ph_2]$ (**2**) was recovered in good yield (56 %). Following the procedure for the conventional condensation reaction the alcohol was dissolved in ethanol with several equivalents of pyrrole and a catalytic amount of methanesulphonic acid. Surprisingly, the reaction did not proceed as

expected, but rather yielded a mixture of products, of which 36% was the desired product with 24% of the isolated product having an ethoxide substituted at the alcohol position (see Scheme 2.5.3).

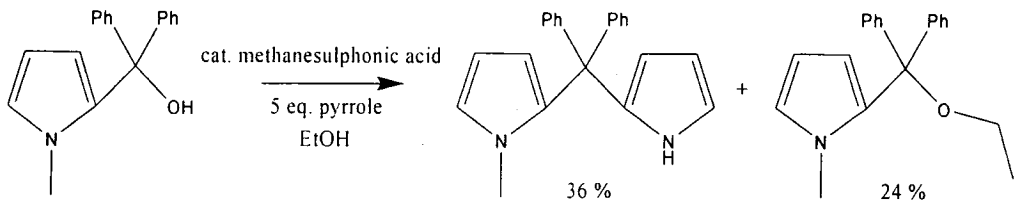

Figure 2.5.3 Condensation Reaction and Byproduct.

When the reaction was performed in methanol similar results were found with ~60% total yield, of which 70% was the desired product and 30% was the methoxide substituted product. To avoid the issue of solvent incorporation the reaction was performed in neat pyrrole with a catalytic amount of methanesulphonic acid, resulting in the desired product [(1-Me-C_4H_3N)(C_4H_3N)CPh_2] (**3**) being isolated in pure form in 82% yield (see Figure 2.5.4).

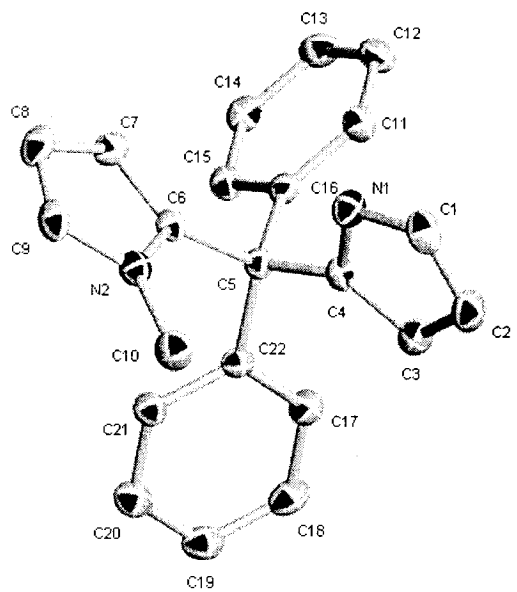

Figure 2.5.4 Structure of N-MeDipyr (**3**).

Since the preparation of N-MeDipyr could be successfully synthesized in large quantities (≥ 25 g) it was decided to attempt a similar reaction in order to generate an N-MeTripyrrole (N-MeTripyr). In order to generate the di-lithium salt of N-Mepyrrole,

slightly more forcing conditions are required.[24] The N-Mepyrrole was refluxed in the presence of TMEDA in a solution of hexanes in order to generate the salt. The salt was then added to a cooled THF solution containing benzophenone. After the reaction was quenched the di-alcohol [2,5-{$Ph_2C(OH)$}$_2$-1-Me-C_4H_2N] (**4**) was isolated in good yield (53%) (see Figure 2.5.5). Using the same neat pyrrole condensation used to prepare the N-MeDipyr (**3**), it was possible to isolate pure N-MeTripyr [2,5-{$Ph_2C(C_4H_3N)$}$_2$-1-Me-C_4H_2N] (**5**) in good yield (83%) after several days of stirring. This synthesis represents the first case in which an N-MeTripyrrole molecule has been rationally synthesized in a meaningful yield.[26]

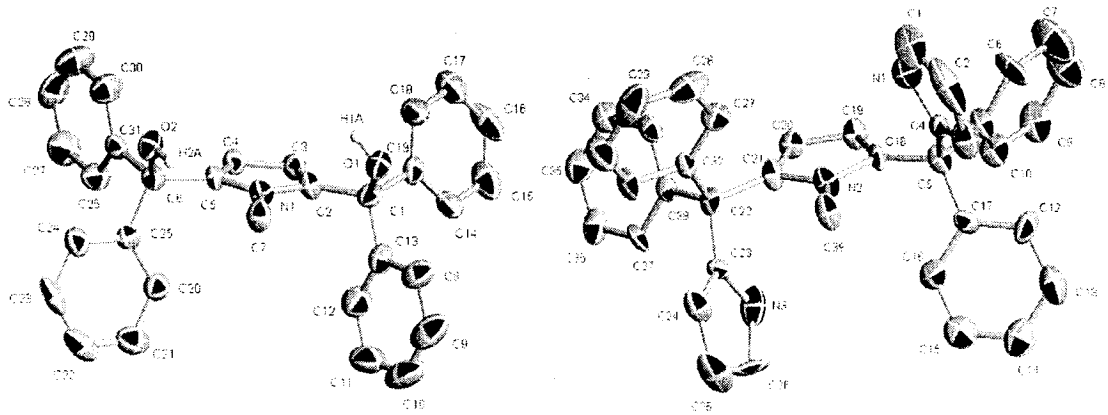

Figure 2.5.5 Structures of Di-alcohol (**4**) and N-MeTripyr (**5**).

Though the synthetic strategy used (see Scheme 2.5.6) involves the use of pyrophoric chemicals and takes several days to complete, the high purity of the products, and ability to produce the ligands in bulk ($\geq$ 25 g) makes this route the most viable for the production of the σ, π–bonding ligands **3** and **5**. Furthermore, the alcohols generated (**2** and **4**) can serve as ligands themselves, or building blocks for assembling other ligands via the simple S_N1 substitution reaction.

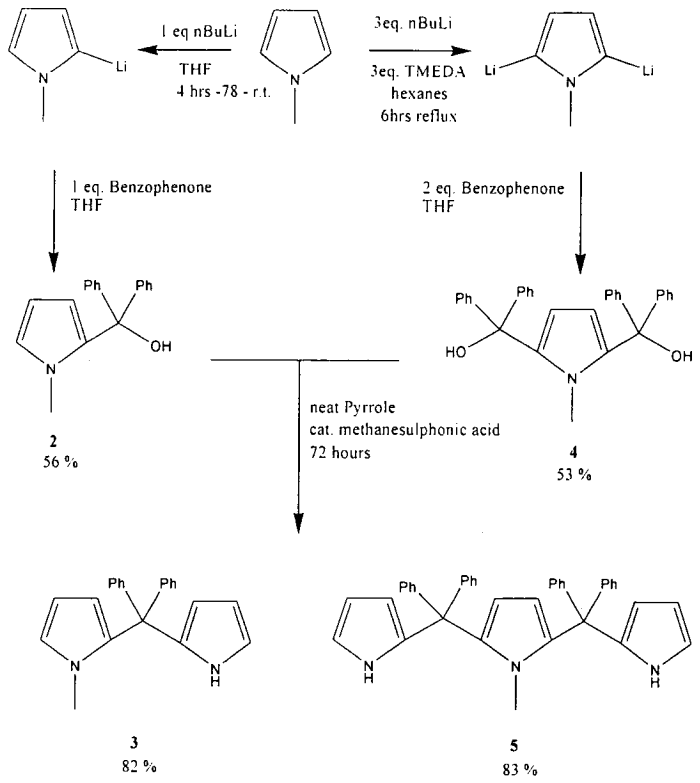

Scheme 2.5.6 Synthetic Routes to the σ, π-bonding ligands (**3**) and (**5**).

In order to increase the solubility of the N-MeDipyr (**3**) ligand, the reaction of LiN-Mepyrrolide was attempted with several other ketones. Unfortunately, even though the formation of the alcohol occurred, in all of the cases where a β - hydrogen was present, elimination of H_2O occurred during the pyrrole condensation step (see Scheme 2.5.7). This occurred even in the case of the more constrained rings: cyclohexanone and cyclopentanone which were expected to be more robust towards this type of reaction. These results indicated that this synthetic route appears valid only in the cases where there are no β -hydrogen present in the starting materials (as in the case of benzophenone).

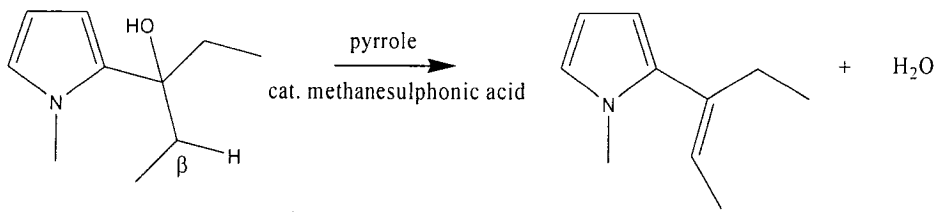

Scheme 2.5.7 Acid-Catalyzed Enolization.

In order to test this hypothesis, the reaction of LiN-Mepyrrolide with di-tertbutylketone was attempted. The reaction proceeded yielding the alcohol [(1-Me-C_4H_3N)C(OH)tBu_2] (**6**) in good yield (40%) (see Figure 2.5.8).

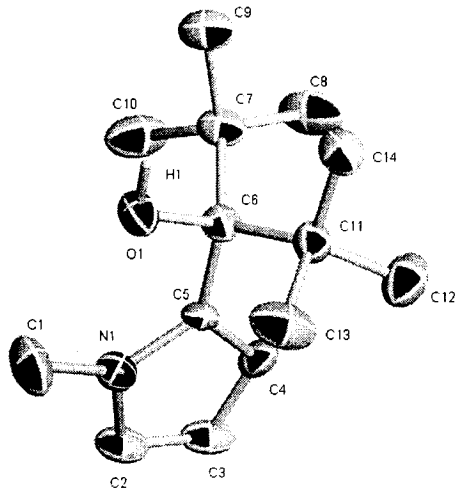

Figure 2.5.8 Structure of N-MePyrroledi-^{t}Bu alcohol (**6**).

Though no elimination route is open to form side-products, the steric bulk of the t-Bu groups appear to severely retard the condensation reaction of **6** with pyrrole, as only traces of the desired product were observed along with unreacted starting material, even after several days of stirring with heating.

As a further extension of the synthetic method for the preparation of σ, π-bonding ligands, it was decided to replace the central N-Me pyrrole ring with a benzene moiety (see Scheme 2.5.9).

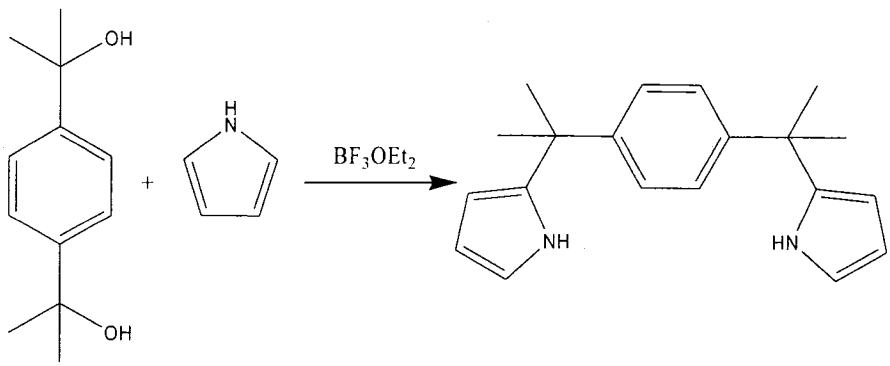

Scheme 2.5.9 Synthesis of PhenylDipyrrole (**7**).

Using a slightly modified literature preparation[26] the PhenylDipyrrole [*p*-{$Me_2C(C_4H_3N)$}$_2C_6H_4$] (**7**) was isolated in low yield (32%) via sublimation (See Figure 2.5.10). Interestingly, even though the diol precursor possesses *β*-hydrogens, the condensation occurs without the elimination reaction which was observed in the case of N-Me pyrrole.

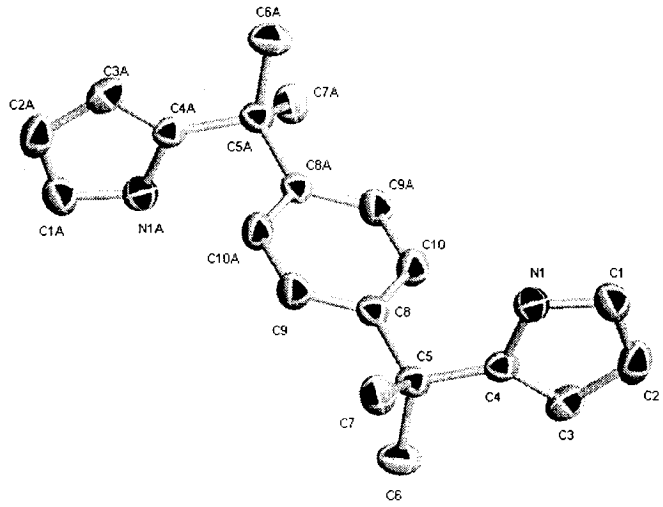

Figure 2.5.10 Structure of PhenylDipyrrole (**7**).

The PhenylDipyrrole (**7**), unfortunately, was found to have very poor solubility properties. Thus it was decided to attempt to substitute the methyl groups with groups that would provide better solubility in common organic solvents. Reacting 1,4-dibromo-benzene with 2 equivalents of *n*BuLi and then subsequently reacting the di-lithium salt with cyclohexanone in THF yielded the alcohol [*p*-{$CyC(OH)$}$_2C_6H_4$] (**8**) in low yield (27% see Figure 2.5.11).

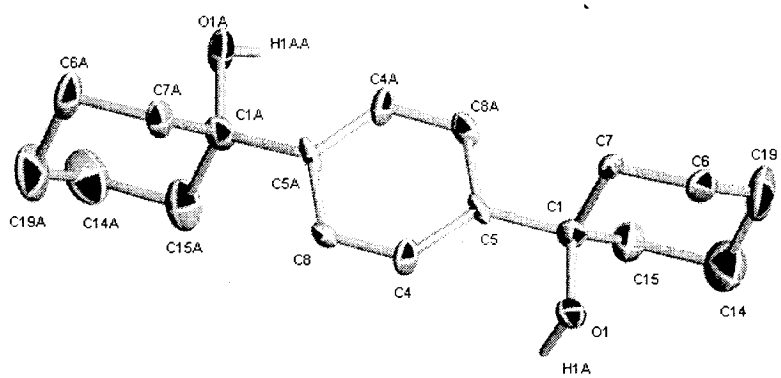

Figure 2.5.11 Structure of CyPhenylDiol (**8**).

As the work on **8** is so recent, the subsequent condensation with pyrrole has not been completed, and represents future work to be explored by our research group.

2.6 Conclusions:

Through the judicious selection of the proper synthetic strategy, several σ, π - donating ligands have been successfully synthesized in good yields. Both the N-MeDipyr and N-MeTripyr have already been utilized by our group to produce some remarkable chemistry ranging from low-valent Ti[27] and Th,[28] to ethylene oligomerization (see Chapter 5).[29] The versatility of this ligand bodes well for its future, and further demonstrates that rational ligand modifications can further enrich organometallic chemistry. Although the chemistry of the PhenylDipyrrole ligands is, as yet untested, rich chemistry is expected ensuring that future researchers will continue to develop this class of ligands.

Furthermore, this work demonstrates that N-MeTripyrrole and N-MeDipyrrole molecules can be rationally synthesized in large quantities, which is an unprecedented feat in the literature. The ability of these molecules to act as hemi-labile ligands with significant steric constraints will hopefully stimulate new research in the future.

2.7 X-Ray Crystallography Section:

The full crystallographic data and structural descriptions, including bond lengths and angles may be found in Appendix 2. The abbreviated crystallographic data for the structures contained within this chapter are as presented in Tables 2.7.1 - 2.7.3.

Table 2.7.1 Crystal Data and Structure Analysis Results.

	1	2	3
Formula	$C_{13}H_{22}LiNO_2$	$C_{18}H_{17}NO$	$C_{22}H_{20}N_2$
FW	231.26	263.33	312.40
space group	Monoclinic, ***C2/c***	Monoclinic, ***P2(1)/n***	Monoclinic, ***Cc***
a (Å)	19.619(10)	13.145(3)	10.138(15)
b (Å)	9.175(5)	10.553(3)	29.86(4)
c (Å)	15.720(8)	11.436(3)	7.408(8)
α (deg)	90	90	90
β (deg)	98.997(9)	115.223(15)	132.34(9)
γ (deg)	90	90	90
V ($Å^3$)	2795(3)	1435.2(7)	1658(4)
Z	8	4	4
radiation (Kα, Å)	0.71073	0.71073	0.71073
T (K)	200(2)	206(2)	209(2)
D_{calcd} (g cm^{-3})	1.099	1.219	1.252
μ_{calcd} (mm^{-1})	0.072	0.075	0.074
F_{000}	1008	560	664
R, R_w [2 a]	0.0775, 0.1878	0.0599, 0.1091	0.0435, 0.0817
GoF	1.039	1.029	1.022

[a] $R = \Sigma||Fo| - |Fc||/\Sigma|F|$. $Rw = [\Sigma(|Fo| - |Fc|)^2/\Sigma wFo^2]^{1/2}$.

Table 2.7.2 Crystal Data and Structure Analysis Results.

	4	5	6
Formula	$C_{31}H_{27}NO_2$	$C_{39.75}H_{34.50}Cl_{1.50}N_3$	$C_{14}H_{25}NO$
FW	445.54	607.38	223.35
space group	Monoclinic, ***C2/c***	Triclinic, ***P-1***	Orthorhombic, ***Pna2(1)***
a (Å)	32.396(7)	9.934(3)	8.033(3)
b (Å)	8.3912(17)	12.368(4)	14.786(6)
c (Å)	23.621(5)	14.173(4)	11.661(5)
α (deg)	90	89.491(5)	90
β (deg)	129.859(3)	80.429(4)	90
γ (deg)	90	72.618(4)	90
V ($Å^3$)	4929.0(18)	1637.0(8)	1385.0(10)
Z	8	2	4
radiation (Kα, Å)	0.71073	0.71073	0.71073
T (K)	206(2)	206(2)	213(2)
D_{calcd} (g cm^{-3})	1.201	1.232	1.071
μ_{calcd} (mm^{-1})	0.074	0.190	0.066
F_{000}	1888	639	496
R, R_w [2 a]	0.0757, 0.1116	0.1034, 0.1910	0.0619, 0.1287
GoF	1.013	1.014	1.053

[a] $R = \Sigma||Fo| - |Fc||/\Sigma|F|$. $Rw = [\Sigma(|Fo| - |Fc|)^2/\Sigma wFo^2]^{1/2}$.

Table 2.7.3 Crystal Data and Structure Analysis Results.

	7	**8**
Formula	$C_{20}H_{24}N_2$	$C_{18}H_{26}O_2$
FW	292.41	274.40
space group	Rhombohedral, ***R-3***	Orthorhomic, ***Cmca***
a (Å)	25.732(4)	53.339(6)
b (Å)	25.732(4)	24.289(6)
c (Å)	6.720(2)	10.026(4)
α (deg)	90	90
β (deg)	90	90
γ (deg)	120	90
V (Å^3)	3853.5(16)	12989.19(50)
Z	9	8
radiation (Kα, Å)	0.71073	0.71073
T (K)	213(2)	202(2)
D_{calcd} (g cm^{-3})	1.134	1.111
μ_{calcd} (mm^{-1})	0.066	0.132
F_{000}	1422	2923
R, R_w[2 a]	0.0548, 0.1438	0.1358, 0.2458
GoF	1.038	1.099

[a] $R = \Sigma||Fo| - |Fc||/\Sigma|Fo|$. $Rw = [\Sigma(|Fo| - |Fc|)^2/\Sigma wFo^2]^{1/2}$.

2.8 Experimental Section:

All reactions were carried out under a dry nitrogen or argon atmosphere unless otherwise stated. Solvents were dried using an aluminum oxide solvent purification system. Reagent grade (>98 %) 1,4-dibromobenzene, pyrrole and 1-MePyrrole were purchased from Aldrich. The pyrrole was vacuum distilled prior to use. Lithium reagents were purchased from Alrdich and used as they arrived. TMEDA was dried over Na/K amalgam and distilled before use. Diphenyldipyrrole was synthesized according to published procedure.[16] Infrared spectra were recorded on an ABB Bomem FTIR instrument from Nujol mulls prepared in a drybox. NMR were collected on an INOVA Varian 500 MHz instrument in $CDCl_3$. Elemental analysis was carried out with a Perkin-Elmer 2400 CHN analyzer. Data for X-ray crystal structure determination were obtained with a Bruker diffractometer equipped with a 1K Smart CCD area detector.

General Experimental Procedure for Table 2.5.1: Diphenyldipyrrole (0.500 g, 1.68 mmol) was dissolved in 100 ml of THF and cooled to 0 °C. The selected deprotonating

agent was then added and allowed to stir for two hours while warming to room temperature, after which MeI (0.238 g, 1.68 mmol) was added. The reaction was then dried *in vacuo*. The organics were then extracted with CH_2Cl_2 (3 X 15 mL) which was subsequently dried *in vacuo*. The resulting off-white powder was used to calculate the % yield. In order to determine the % yield of each product the NMR N-H peak of the unsubstituted product (7.83 ppm) was compared to the N-H peak of the mono-substituted product (7.74 ppm) and the N-CH_3 peak of the disubstituted product (2.88) was compared to the mono-substituted product (2.94 ppm). In order to purify the mono-substituted product several recrystallizations from hot hexanes were required which conveniently separated out the unsubstituted product, but always contained a minimum of 3% disubstituted product.

Synthesis of (1-methyl-1H-pyrrol-2-yl)diphenylmethanol (2): A 250 mL Schlenk flask was filled with 10 mL (9.14 g, 0.113 mol) of 99% 1-Methylpyrrole and 100 mL of THF. The solution was then cooled to -78 °C using a dry ice and acetone bath. 10 M n-BuLi in hexanes was then slowly added to the stirring solution over several minutes (1.05 eq, 11.83 mL, 0.118 mol). This resulted in the solution turning slightly brown and a precipitate forming. The solution was allowed to stir for 4 hours while warming to room temperature, after which time, it was slowly added to a cooled solution (-78 °C) of benzophenone (1 eq, 20.59 g, 0.113 mol) in THF. The solution immediately turned blue-green. The solution was then allowed to stir for 12 hours as it warmed to room temperature. After 12 hours the colour of the solution was again yellow-brown. The solution was then dried under reduced pressure and 100 mL of hexanes were added along with H_2O (2 eq, 4.068 g, 0.226 mol). The resulting suspension was filtered at the boiling point of hexane and washed with 3 X 20 mL of hot hexane in order to extract all organic product from the salt. The solution was then allowed to stand at room temperature for 12 hours after which slightly yellow crystals of the alcohol formed. The crystals were filtered and washed twice with cold hexanes 2 X 10 mL and dried yielding 16.72 g (56.2 %, 0.0635 mol).

Elemental Analysis calcd (Found) for $C_{18}H_{17}NO$: C 82.10 (82.12), H 6.51 (6.58), N 5.32 (5.58). MS (EI) m/z (found): 263 (263).

IR (neat): 3464 (br, s), 3058, 3025, 2947 (m), 1642, 1598 (m), 1490, 1447 (s), 1411 (w), 1329, 1293 (m), 1234(w), 1204, 1153 (m), 1092 (m), 1061(w), 1018, 1001 (m), 924, 899, 867 (m), 792 (w), 755, 721, 701 (s), 669 (m), 628 (w).

^{1}H NMR ($CDCl_3$, 500 MHz)(δ): 7.24 (br, 10H, phenyl), 6.58 (m, 1H, pyrrole), 5.92 (m, 1H, pyrrole), 5.47 (m, 1H, pyrrole), 3.32 (s, 3H, N-C**H**$_3$), 2.90 (1H, O**H**).

^{13}C NMR ($CDCl_3$, 500 MHz)(δ): 146.35 (phenyl, ipso), 136.06 (N-Me pyrrole ipso), 127.79 (phenyl), 127.09 (phenyl), 126.87 (phenyl), 124.80 (N-Me pyrrole), 112.14 (N-Me pyrrole), 105.52 (N-Me pyrrole), 78.44 (**C**-OH), 35.94 (N-**C**H$_3$).

Snythesis of 2-(diphenyl(1H-pyrrol-2-yl)methyl)-1-methyl-1H-pyrrole (N-MeDipyrrole) (3): The alcohol **2** (16.72 g, 0.0635 mol) was placed in neat pyrrole (~ 50 mL) using slight heating until fully dissolved at which time 12 drops of methanesulphonic acid were added which yielded a red solution. After stirring for 72 hours the grey product was filtered from pyrrole and washed 4 X 20 mL with cold MeOH yielding 16.21 g (81.8 %, 0.0519 mol) of white solid after drying under vacuum.
Elemental Analysis calcd (Found) for $C_{22}H_{20}N_2$: C 84.58 (84.62), H 6.45 (6.58), N 8.97 (8.88). MS (EI) m/z (found): 312 (312).

IR (neat): 3428 (m), 3083, 3061, 2956 (m), 1954, 1899, 1814 (w), 1591, 1549 (m), 1492, 1443, 1408, 1399 (m), 1321(w), 1298 (m), 1266, 1230, 1188 (m), 1155 (w), 1111, 1091 (m), 1041, 1031 (m), 1001 (w), 962 (m), 928 (w), 902, 888, 844 (m), 797 (s), 761, 744, 720, 702 (s), 620 (m), 566(s), 547(m), 492, 479 (w).

^{1}H NMR ($CDCl_3$, 500 MHz)(δ): 7.74 (br, 1H, N-**H**), 7.27 (m, 6H, phenyl), 7.13 (m, 4H, phenyl), 6.75 (m, 1H, pyrrole α), 6.65 (m, 1H, N-Me pyrrole α), 6.18 (m, 1H, N-Me pyrrole β), 6.14 (m, 1H, N-Me pyrrole γ), 6.02 (m, 1H, pyrrole β), 5.62 (m, 1H, pyrrole γ), 2.94 (s, 3H, N-C**H**$_3$).

^{13}C NMR ($CDCl_3$, 500 MHz)(δ): 145.97 (phenyl, ipso), 136.21 (N-Me pyrrole ipso), 134.71 (pyrrole ipso), 129.30 (phenyl), 127.64 (phenyl), 126.37 (phenyl), 124.32 (N-Me pyrrole α), 117.258 (pyrrole α), 111.99 (N-Me pyrrole β), 109.04 (pyrrole β), 107.72 (N-Me pyrrole γ), 105.81 (pyrrole γ), 55.44 (quaternary), 35.49 (N-$\mathbf{C}H_3$).

Synthesis of (1-methyl-1H-pyrrole-2,5-diyl)bis(diphenylmethanol) (4): 1-Methylpyrrole (10.0 mL, 0.113 mol) was added to a Schlenk flask containing 150 ml hexanes. 3.0 equivalents of TMEDA (51.0 mL, 0.338 mol) was then added to the flask and it was cooled to 0 °C in an ice bath. To the stirring solution was added 3.0 equivalents of 10.0 M nBuLi (33.8 mL, 0.338 mol). The solution was allowed to warm to room temperature and then the flask was fitted with a condenser, and the solution was refluxed for 4 hours. After refluxing the off-white suspension was filtered and the solid portion was washed (3 X 50 mL hexanes) yielding a white product. This product was dried briefly under vacuum (1 hour) and then redissolved in 100 mL of THF and cooled to -20 °C. In a separate flask, 2.0 equivalents of benzophenone (41.18 g, 0.226 mol) was added to 100 ml of stirring THF and cooled to -20 °C. The benzophenone solution was then canulated into the di-lithium pyrrolide solution, resulting in a deep blue colour. This solution was then stirred for 12 hours, after which time the solvent was removed under vacuum. 200 mL of hexanes was then added along with 4 equivalents of water (8 ml, 0.452 mol) resulting in an off-white suspension. This suspension was then filtered and washed with hexanes (4 X 50 mL). The purity of the solid can be tested via TLC (20:1 toluene:ether) diol R_f : 0.0; mono-substituted alcohol R_f : 0.3; benzophenone R_f : 0.45. If any impurities are detected a further washing (2 X 50 mL) by hexanes can be used to remove the impurities. The product is then extracted using several portions of CH_2Cl_2 (5 X 40 mL) and then dried under reduced vacuum yielding an off-white solid 26.75 g (53.2 %, 0.0601 mol). X-ray quality crystals of **4** were grown from CH_2Cl_2.

Elemental Analysis calcd (Found) for $C_{31}H_{27}NO_2$: C 83.57 (83.32), H 6.11 (6.18), N 3.14 (3.28). MS (EI) m/z (found): 445 (445).

IR (neat): 3484 (br, s), 3084, 3058, 3025, 2946 (m), 1597 (m), 1490, 1447 (s), 1411 (w), 1329, 1293 (s), 1234(s), 1204, 1153 (m), 1092 (m), 1061(w), 1018, 1001 (s), 924, 899, 867 (m), 792 (w), 755, 721, 701 (s), 670 (m), 628 (w), 612 (w), 559 (w), 472 (s).

^{1}H NMR ($CDCl_3$, 500 MHz)(δ): 7.27 (m, 20H, phenyl), 5.29 (s, 2H, pyrrole), 3.13 (s, 3H, N-C**H**$_3$), 2.87 (br, 2H, O**H**).

^{13}C NMR ($CDCl_3$, 500 MHz)(δ): 145.66 (ipso-phenyl), 138.83 (ipso N-Me pyrrole), 127.86 (phenyl), 127.25 (phenyl), 127.02 (phenyl), 110.17 (N-Me pyrrole), 78.83 (**C**-OH), 35.11 (N-**C**H$_3$)

Synthesis of 2,5-bis(diphenyl(1H-pyrrol-2-yl)methyl)-1-methyl-1H-pyrrole (N-MeTriyprrole) (5): The alcohol **4** 26.75 g (0.0601 mol)was dissolved in 60 mL of hot stirring pyrrole and 10 drops of methanesulphonic acid was added, resulting in a dark red solution. After 72 hours the suspension was filtered and the solid portion was washed with cold methanol (3 X 30 mL), yielding a white solid. This solid was then dried under vacuum. Alternately, the compound can be recrystallized from hot toluene, yielding a 1:1 (ligand:toluene) light beige final product. Yield 10.35 g (83.4%, 0.0501 mol).
Elemental Analysis calcd (Found) for $C_{39}H_{33}N_3$: C 86.15 (86.32), H 6.12 (6.18), N 7.73 (7.88). [M^+] 543, found 543.

^{1}H NMR ($CDCl_3$, 500 MHz)(δ): 7.69 (br, 2H, N-**H**), 7.18 (m, 8H, phenyl), 7.13 (m, 4H, phenyl), 7.07 (m, 8H, phenyl), 6.68 (m, 2H, pyrrole), 6.05 (m, 2H, pyrrole), 5.99 (m, 2H, pyrrole), 5.46 (s, 2H, N-Me pyrrole), 2.14 (s, 3H, N-C**H**$_3$).

^{13}C NMR ($CDCl_3$, 500 MHz)(δ): 145.52 (ipso-phenyl), 139.06 (ipso N-Me pyrrole), 129.66 (ipso-pyrrole), 127.93 (phenyl), 126.73 (phenyl), 117.26 (phenyl), 110.35 (pyrrole), 109.37 (pyrrole), 108.10 (pyrrole), 56.19 (quaternary), 34.80 (N-**C**H$_3$).

Synthesis of 2,2,4,4-tetramethyl-3-(1-methyl-1H-pyrrol-2-yl)pentan-3-ol (6): A 250 mL Schlenk flask was filled with 6.20 mL (5.67 g, 0.070 mol) of 99% 1-Methylpyrrole and 100 mL of THF. The solution was then cooled to -78 °C using a dry ice and acetone bath. 10 M n-BuLi in hexanes was then slowly added to the stirring solution over several minutes (1.05 eq, 7.33 mL, 0.073 mol). This resulted in the solution turning slightly brown. The solution was allowed to stir for 4 hours while warming to room temperature, after which time, it was slowly added to a cooled solution (-78 °C) of hexamethylacetone (1 eq, 9.96 g, 0.070 mol) in THF. The beige solution was then allowed to stir for 12 hours as it warmed to room temperature. The solution was then dried under reduced pressure and 50 mL of hexanes was added along with H_2O (2 eq, 2.520 g, 0.140 mol). The resulting suspension was filtered at the boiling point of hexanes and washed with 3 X 20 mL of hot hexane in order to extract all organic product from the salt. The solution was then allowed to stand at room temperature for 12 hours after which slightly yellow but no crystals formed. Removing the hexanes under reduced pressure and adding fresh pentanes (10 mL) followed by cooling (-35 °C) resulted in crystal formation after 24 hours 6.21 g (39.7 %, 0.0278 mol).
Elemental Analysis calcd (Found) for $C_{14}H_{25}NO$: C 75.28 (82.12), H 11.28 (6.58), N 6.27 (5.58). MS (EI) m/z (found): 223 (223).

IR (neat): 3472 (br, s), 3055, 3023, 2948 (m), 1690 (w), 1507 (m), 1450 (m), 1394 (m), 1288 (s), 1208 (w), 1097, 1054 (m), 983 (m), 942 (m), 864 (s), 671 (m), 652(s).

^{1}H NMR ($CDCl_3$, 500 MHz)(δ): 6.38 (m, 1H, pyrrole), 6.06 (m, 1H, pyrrole), 5.98 (m, 1H, pyrrole), 3.80 (s, 3H, N-C**H**$_3$), 1.89 (s, 1H, O**H**), 1.07 (s, 18H, t-Bu).

^{13}C NMR ($CDCl_3$, 500 MHz)(δ): 128.06 (N-Me pyrrole ipso), 114.60 (N-Me pyrrole), 107.34 (N-Me pyrrole), 100.33 (N-Me pyrrole), 68.46 (**C**-OH), 48.71 (tBu quaternary), 31.54 (N-**C**H$_3$), 22.31 (t-Bu).

Synthesis of 1,4-bis(2-(1H-pyrrol-2-yl)propan-2-yl)benzene (7): 2,2'-(1,4-phenylene) dipropan-2-ol 5.0 g (0.0257 mol) was dissolved in 25 mL of pyrrole. Then BF_3OEt_2 3.59 mL (1.10 eq, 0.0283 mol) was added drop-wise over 15 min. The beige solution was then stirred for 1 hr. The reaction was then diluted with 50 mL of CH_2Cl_2 and quenched with 8 mL of a 0.1 M NaOH solution. The organic layer was then washed 3 X 20 mL H_2O, dried with Na_2SO_4 and then dried under reduced pressure. The resulting brown oil was then sublimed (120 °C, 30 torr), resulting in a white solid 2.42 g (32.2%, 8.28 mmol). Elemental Analysis calcd (Found) for $C_{12}H_{18}O_2$: C 74.19 (74.32), H 9.34 (9.48). MS (EI) m/z (found): 194 (194).

IR (neat): 3368 (br, s), 3100, 2967, 2867 (w,s,w), 1561 (m), 1507 (m), 1468 (m), 1421, 1401 (m), 1382, 1362 (w), 1291 (m), 1254, 1226 (m), 1121, 1109 (s), 1084 (w), 1038, 1017 (m), 950 (m), 907 (s), 883 (w), 831 (s), 791 (s), 745 (s), 588 (s), 541 (m).

^1H NMR ($CDCl_3$, 500 MHz)(δ): 7.63 (br, 2H, N-**H**), 7.11 (s, 4H, phenyl), 6.68 (m, 2H, pyrrole), 6.14 (m, 2H, pyrrole), 6.08 (m, 2H, pyrrole), 1.64 (s, 12H, C-C**H**$_3$).

^{13}C NMR ($CDCl_3$, 500 MHz)(δ): 146.94 (ipso-phenyl), 140.67 (ipso-pyrrole), 126.63 (phenyl), 116.87 (pyrrole), 107.81 (pyrrole), 104.41 (pyrrole), 39.04 (quaternary), 27.15 (methyl).

Synthesis of 1,1'-(1,4-phenylene)dicyclohexanol (8): A 250 mL Schlenck flask was filled with ~100 mL of hexanes and 1,4-dibromobenzene 4.00 g (0.0169 mol). 10 M N-BuLi 42.4 mL (2.5 eq, 0.0425 mol) was then added to the stirring mixture. The flask was then refluxed for 2 hours resulting in a white precipitate. The precipitate was then filtered and washed (3 X 20 mL) with hexanes. The white solid was then redissolved in 50 mL of THF and slowly added to a cooled solution (-50 °C) of cyclohexanone 3.317 g (2 eq, 0.0338 mol) in 150 mL of THF. The solution was allowed to warm to room temperature and was stirred overnight. The solution was then dried under reduce pressure and hexanes was added ~100 mL along with H_2O 0.77 g (2.5 eq, 0.0425 mol). The resulting crude material was then filtered hot, and washed with 3 X 20 mL hot

hexanes. The volume was reduced ~25 mL and the colourless diol **8** slowly crystallized overnight 1.27 g (27.3 %, 4.61 mmol). Elemental Analysis calcd (Found) for $C_{18}H_{26}O_2$: C 78.79 (78.62), H 9.55 (9.58). MS (EI) m/z (found): 274 (274).

IR (neat): 3326 (br, s), 2845 (s), 1443, 1392, 1349 (m), 1289 (m), 1252 (m), 1216 (m), 1181, 1169 (w), 1146, 1132, 1117 (m), 1055 (w), 1034, 1007 (m), 971 (s), 928 (w), 898 (m), 847 (m), 824 (s), 772 (w), 738 (w), 695 (w), 665 (w), 569 (w).

^{1}H NMR ($CDCl_3$, 500 MHz)(δ): 7.46 (s, 4H, phenyl), 1.77 (m, 14H, Cy), 1.63 (s, 2H, **OH**), 1.61 (m, 4H, Cy), 1.27 (m, 2H, Cy).

^{13}C NMR ($CDCl_3$, 500 MHz)(δ): 147.99 (ipso-phenyl), 124.68 (phenyl), 73.18 (**C**-OH), 38.99 (Cy), 25.71 (Cy), 22.38 (Cy).

2.9 References:

1) Huheey, J. E *Inorganic Chemistry 3rd ed.: Principles of structure and reactivity.* Harper & Row Publishers; New York, **1983**.
2) *Coordination Chemistry Reviews*, Volumes 1-195 : Elsevier Pub. Co.: Amsterdam.
3) Bialek, M.; Czaja, K. *Macromolec. Chem. Phys.* **2006**, *207*, 1651. b) Barabanov, A. A.; Bukatov, G. D.; Zakharov, V. A.; Semikolenova, N. V.; Mikenas, T. B.; Echevskaja, L. G.; Matsko, M. A. *Macromolec. Chem. Phys.* **2006**, *207*, 1368.
4) Connelly, N. G.; Geiger, W. E. *Chem. Rev.* **1996**, *96*, 877.
5) Iqbal, J.; Bhatia, B.; Nayyar, N. K. *Chem. Rev.* **1994**, *94(2)*, 519. b) Burgess, K.; Ohlmeyer, M. J. *Chem. Rev.* **1991**, *91(6)*, 1179.
6) MacLachlan, E. A.; Fryzuk, M. D. *Organometallics* **2006**, *25*, 1530.
7) Butterick, R.; Ramachandran, B. M.; Carroll, P. J.; Sneddon, L. G. *J. Am. Chem. Soc.* **2006**, *128*, 8626.
8) Lubben, T, V,; Wolczanski, P. T.; Van Duyne, G. D. *Organometallics* **1984**, *3*, 977.
9) Lubben, T. V.; Wolczanski, P. T. *J. Am. Chem. Soc.* **1987**, *109*, 424.
10) Hirsekorn, K. F.; Veige, A. S.; Wolczanski, P. T. *J. Am. Chem. Soc.* **2006**, *128*, 2192. b) Hirsekorn, K. F.; Veige, A. S.; Marshak, M. P.; Koldobskaya, Y.; Wolczanski, P. T.; Cundari, T. R.; Lobkovsky, E. B. *J. Am. Chem. Soc.* **2005**, *127*, 4809.
11) Reardon, D.; Guan, J.; Gambarotta, S.; Yap, G. P. A. *Organometallics* **2002**, *21*, 4390.
12) Jubb, J.; Gambarotta, S. *J. Am. Chem. Soc.* **1994**, *116*, 4477.
13) Dube, T.; Conoci, S.; Gambarotta, S.; Yap, G. P. A.; Vasapollo, G. *Angew. Chem. Int. Ed.* **1999**, *38*, 3657.
14) Dube, T.; Gambarotta, S.; Yap, G. P. A. *Angew. Chem. Int. Ed.* **1999**, *38*, 1432.
15) Ganesan, M.; Gambarotta, S.; Yap, G. P. A. *Angew. Chem. Int. Ed.* **2001**, *40*, 766.

b) Dube, T.; Ganesan, M.; Conoci, S.; Gambarotta, S.; Yap, G. P. A. *Organometallics* **2000**, *19*, 3716.
16) Freckmann, D. M. M.; Dube, T.; Berube, C. D.; Gambarotta, S.; Yap, G. P. A. *Organometallics* **2002**, *21*, 1240. b) Dube, T.; Gambarotta, S.; Yap, G. P. A. *Organometallics* **2000**, *19*, 115. c) Dube, T.; Conoci, S.; Gambarotta, S.; Yap, G. P. A. *Organometallics* **2000**, *19*, 1182.
17) Dube, T.; Freckmann, D. M. M.; Conoci, S.; Gambarotta, S.; Yap, G. P. A. *Organometallics* **2000**, *19*, 209.
18) Slone, C. S.; Weinberger, D. A.; Mirkin, C. A. *Prog. Inorg. Chem.* **1999**, *48*, 233. b) Saito, T. *Adv. Inorg. Chem.* **1997**, *44*, 45. c) Bader, A.; Lindner, E. *Coord. Chem. Rev.* **1991**, *108*, 27.
19) Saito, T. *Early Transition Metal Clusters with π-Donor Ligands* VCH: New York, **1995**.
20) Chapman, C. J.; Frost, C. G.; Mahon, M. F. *Dalton Trans.* **2006**, 2251.
21) Deckers, P. J.; Hessen, B.; Teuben, J. H. *Angew. Chem. Int. Ed.* **2001**, *40*, 2516.
22) Ryppa, C.; Senge, M. O.; Hatscher, S. S.; Kleinpeter, E.; Wacker, P.; Schilde, U.; Wiehe, A. *Chem. Eur. J.* **2005**, *11*, 3427. b) Furuta, H.; Mormoto, T.; Osuka, A. *Org. Lett.* **2003**, *5*, 1427. c) Taniguchi, S.; Hasegawa, H.; Yanagiya, S.; Tabeta, Y.; Nakano, Y.; Takahashi, M. *Tetrahedron* **2001**, *57*, 2103. d) Ka, J-W.; Lee, C-H. *Tet. Lett.* **2000**, *41*, 4609. e) Sugiura, K.; Fujimoto, Y.; Sakata, Y. *Chem. Commun.* **2000**, 1105. f) Taniguchi, S.; Hasegawa, H.; Nishimura, M.; Takahashi, M. *Synlett* **1999**, *1*, 73.
23) Furusho, Y.; Kawaski, H.; Nakanishi, S.; Aida, T.; Takata, T. *Tet. Lett.* **1998**, *39*, 3537. b) Sawitzki, G.; von Schnering, H. G. *Angew. Chem. Int. Ed.* **1976**, *15*, 552. c) Franck, B.; Wegner, C. *Angew. Chem. Int. Ed.* **1975**, *14*, 424.
24) Dolphin, D.; Liu, B. Y.; Bruckner, C. *Chem. Commun.* **1996**, 2141. b) Lee, C. H.; Lindsey, S. *Tetrahedron* **1994**, *50*, 11 427.
25) Chadwick, D. J.; Willbe, C. *J. Chem. Soc.: Perkin I* **1977**, 887.
26) Sessler, J. L.; Cho, W-S.; Lynch, V.; Kral, V. *Chem. A Eur. J.* **2002**, *8*, 1134.
27) Nikiforov, G. B.; Crewdson, P.; Gambarotta, S.; Korobkov, I.; Budzelaar, P. H. M. *J. Am. Chem. Soc.* **2007**, *26*, 48.
28) Arunachalampillai, A.; Crewdson, P.; Korobkov, I.; Gambarotta, S. *Organometallics* **2006**, *25*, 3856.
29) Crewdson, P.; Gambarotta, S.; Djoman, M.-C.; Korobkov, I.; Duchateau, R. Organometallics **2005**, 24, 5214.

Chapter

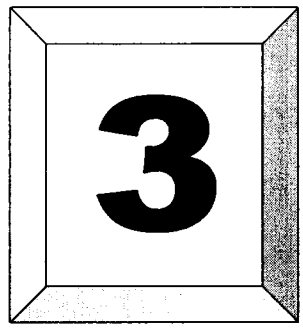

Preparation of Mn Alkyl Complexes

Table of Contents

3.1 Introduction:

The most ready source of divalent Mn complexes is provided by the simple chloride salt $[MnCl_2(THF)_{1.5}]$. However, one limitation of this reagent is that it often requires that ligands be used as their alkali metal salts via metal exchange reactions. As demonstrated in Chapter 2, the use of ligand alkali salts in metathesis reactions often leads to anionic metallate complexes in which the cationic alkali metal is retained.[1] This is a trend which will be further demonstrated in Chapter 6 (see Scheme 3.1.1) and can occur even in the case of polydentate ligands.

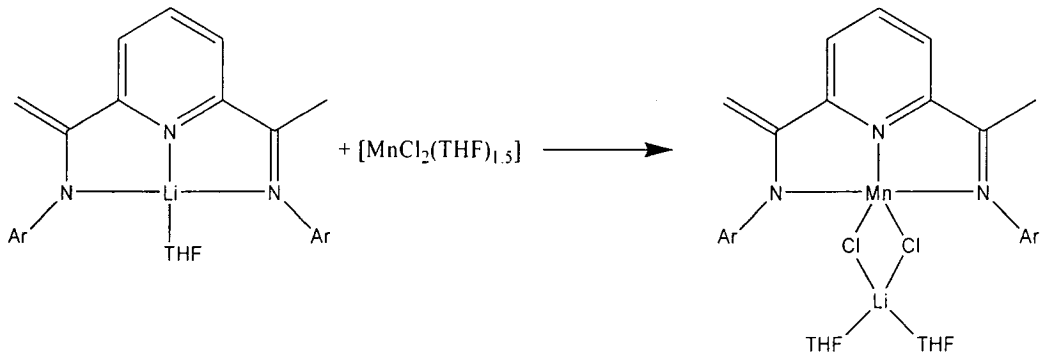

Scheme 3.1.1 Example of the Retention of an Alkali Cation.

The retention of the alkali cation, in turn, can lead to the assembly of cluster compounds via bridging interactions.[1] This type of reactivity can significantly compromise the ability to controllably prepare specific organometallic complexes, and was envisaged to be a potential problem. In order to avoid the issue of anionic metallate complex formation, it was decided to attempt the synthesis of various MnR_2 reagents. These reagents can be expected to react much cleaner via a hydrogen exchange reaction, as light hydrocarbons are released from the reaction, providing an irreversible driving force (see Scheme 3.1.2).

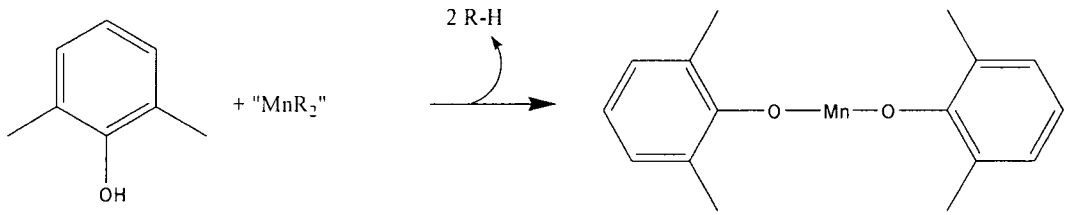

Scheme 3.1.2 Proposed Metathesis Reaction.

This type of reactivity is well documented with many different transition metals and many different R groups.[2]

3.2 Mn Alkyls:

The formation of organometallic complexes of $Mn^{(II)}$ was first reproducibly examined in the mid-1970's and followed the general trend of using Grignard reagents, or lithium salts in conjunction with $Mn^{(II)}$ halides. The group of Wilkinson pioneered the syntheses for $(MnR_2)_n$ (R = Neopentyl n = 4; Neophyl n = 2; Trimethylsilylmethyl n = ∞) using $MnCl_2$ and the appropriate Grignard reagents (see Scheme 3.2.1).[3]

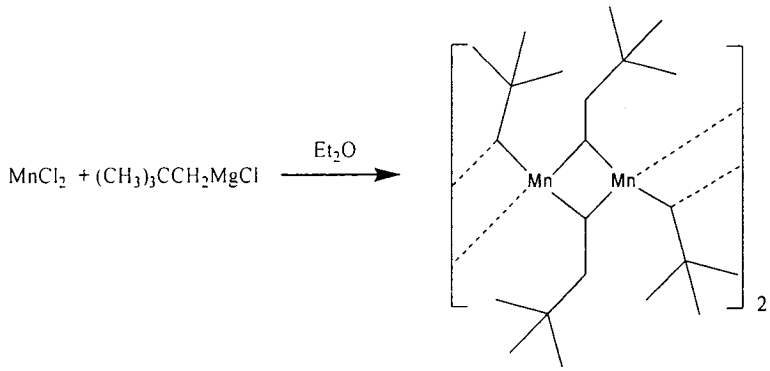

Scheme 3.2.1 Formation of $[Mn(Neopentyl)_2]_4$.

Though a crystal structure of the neophyl equivalent was reported, their diagrams of the crystal structures for the neopentyl, and trimethylsilylmethyl analogues referred to a personal communication as the source of the data. The monomeric complex $[Mn(CH_2SiMe_3)_2(PMe_3)_2]$ was isolated several years later using the same synthesis; indicating that the di-alkyl, in one form or another, was originally formed by the Wilkinson group.[4] In addition to the complexes of Wilkinson, several other $Mn^{(II)}$ alkyls have been synthesized. In 1983 the group of Floriani published the synthesis and crystal structure of the linear, trinuclear $[Mn_3(Mesityl)_6]$.[5] The monomeric homoleptic complex $[Mn\{C(SiMe_3)_3\}_2]$ was synthesized from the corresponding lithium salt, however the complex proved to be kinetically inert to any further transformations.[6]

Though no complexes of the formulation [MnRCl] have been reported yet, two cases of metallate complexes with the general formulae $Li[MnR_3]$ and $Li_2[MnR_4]$ have been reported. The Power's group has described the synthesis and characterization of $[Li(THF)_4]_2[Mn_2Ph_6]$ and $[Li(THF)_4][Mn(Mesityl)_3]$ from the corresponding lithium salts.[7] Similar di-anionic, metallate $Mn^{(II)}$ structures were produced in 1989 by the group of Girolami by simply combining methyl or ethyl lithium with $MnCl_2$ and subsequently treating the reaction with TMEDA in order to produce $[Li(TMEDA)]_2[MnR_4]$.[8]

In summary, the literature examples clearly indicate that homoleptic $Mn^{(II)}$ alkyls may be synthesized, and that they are sufficiently stable so as to serve as a bulk starting material for further chemical transformations.

3.3 Results and Discussion:

As enumerated in the previous section, several viable Mn di-alkyls have been synthesized which could serve as the starting point for this project. Perhaps the most attractive was the monomeric $[Mn\{C(SiMe_3)_3\}_2]$. However, given its apparent inertness,[6] it was decided that smaller R groups would allow for more facile metathetic reactions with the planned ligand systems. The mesityl group was also evaluated to be too sterically crowded. Thus the original Wilkinson complex $[Mn(CH_2SiMe_3)_2]_\infty$ was selected, since it was expected to be highly soluble and synthetically facile to produce. In addition, the steric bulk should be sufficiently small so as to allow for the planned metathesis reactions with a variety of ligands to occur rapidly.

The synthetic procedure utilized was straightforward. Either anhydrous $MnCl_2$ or the etherate form $[MnCl_2(THF)_{1.5}]$ would serve as a ready source of Mn for the reaction with solid $LiCH_2SiMe_3$ in different stoichiometric ratios (see Scheme 3.3.1).

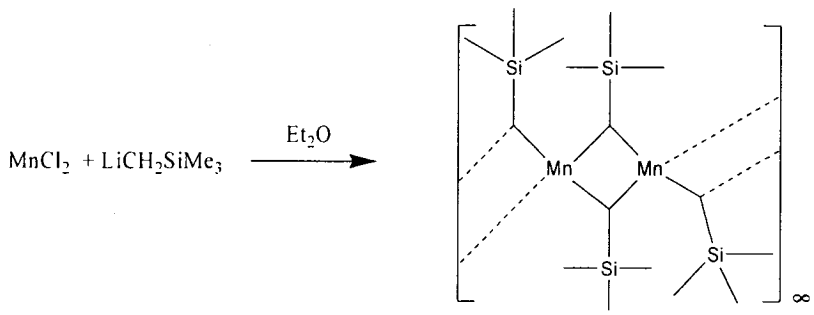

Scheme 3.3.1 Proposed Synthesis of $[Mn(CH_2SiMe_3)_2]_\infty$.

The alkylating agent would be used in stoichiometric ratios ranging from one two four equivalents in order to generate all possible combinations of Mn-alkyls. These various Mn alkyls could then be reacted with various ligand systems to generate a variety of Mn organometallic complexes.

In the case of the di-alkyl, it was quickly found that the choice of starting material had very little impact on the final product. Specifically the tetrahydrofuranate $[MnCl_2(THF)_{1.5}]$ or the anyhydrous $[MnCl_2]$ could be used interchangeably to produce the same complexes. Given the ease of producing $MnCl_2$ from $MnCl_2(H_2O)_6$, the anyhydrous complex was used for bulk preparations. Reacting 2.05 equivalents of $LiCH_2SiMe_3$ with Mn in ether lead to the desired $[Mn(\mu\text{-}CH_2SiMe_3)(CH_2SiMe_3)(Et_2O)]_2$

(**1**) or [Mn(μ-CH_2SiMe_3)(CH_2SiMe_3)(THF)]$_2$ (**2**) if the solvent THF was used, or if **1** was boiled in THF briefly (see Figure 3.3.2). Both **1** and **2** are extremely air and moisture sensitive; decomposing rapidly on exposure to either. However, both can be prepared in excess of 90 % yield and crystallized as large, dark orange block crystals from hexanes. Given that metal-carbon bonds tend to be quite unstable in homoleptic compounds, the thermal stability of these MnR_2 compounds (which are stable in boiling toluene for several hours) is rather remarkable.

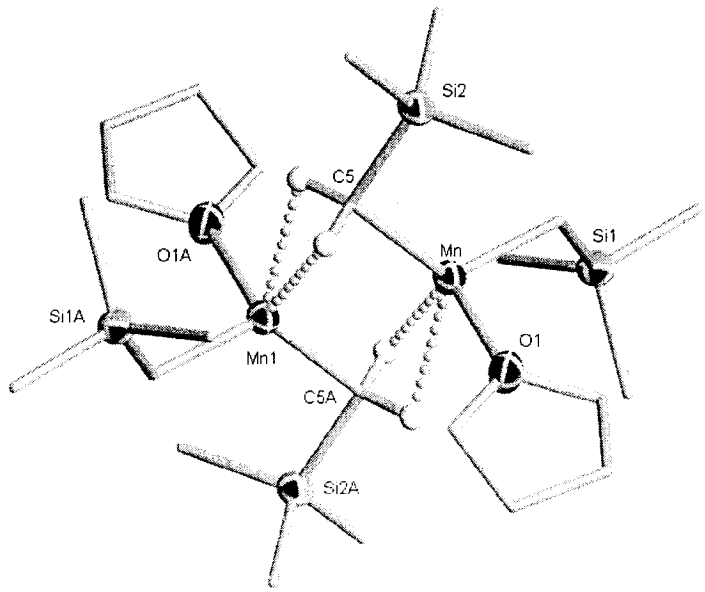

Figure 3.3.2 Crystal Structure of [Mn(μ-CH_2SiMe_3)(CH_2SiMe_3)(THF)]$_2$ (**2**) with 30% Thermal Ellipsoids.

Since the only structural difference between complexes **1** and **2** is the coordination of diethyl ether versus THF, only **2** will be described herein. The structure of **2** is a dinuclear complex in which each Mn atom is tetrahedrally coordinated, and bridged to the neighbouring Mn via a -CH_2SiMe_3 group. The Mn-Mn distance of 2.7878(9) Å is sufficiently short to be considered as falling within metal-metal bonding range, however anti-ferromagnetic exchange via the bridging alkyl groups was found to be the only interaction present between the two metal centres.[9] Three of the groups around each Mn atom can be considered as σ-bonded to the Mn centre [Mn–C(1) = 2.129(3), Mn–C(5) = 2.214(3), Mn–O(1) = 2.188(2) Å] while the fourth is the C atom of the bridging alkyl [Mn–C(5a) = 2.360(3) Å)]. Although the H atoms were not unequivocally located it seems quite likely that an agostic interaction between the hydrogens of the bridging alkyl

and the metal centre substantially contribute to the assembly of the dimeric structure and its stability (calculated hydrogens of C(5a)–Mn: 2.283(3) and 2.164(3) Å). The angles of the complex show a slight distortion from true tetrahedral [O(1)–Mn–C(1) = 108.19(11), O(1)–Mn–C(5) = 99.19(10), O(1)–Mn–C(5a) = 94.73(10)°]. The bridging angle is also quite narrow 75.07(9)° and is likely to responsible for the short Mn-Mn distance. These results are in sharp contrast to the structural formulation reported by Wilkinson, who stated that the structure was an ether-free infinite polymer. The reported structure is difficult to rationalize given that both the Wilkinson reaction and this reaction were performed in an ether solvent under virtually identical conditions, with the only difference being the use of the Grignard in Wilkinson's case. It is hard to rationalize how a Grignard could yield an infinite polymer, whereas the lithium reagent leads to the dimeric structure.

Given that our crystal structure was so different from the reported case a second Wilkinson compound, the tetrameric of $[Mn(Neopentyl)_2]_4$ (see Scheme 3.2.1) was prepared in order to verify our results. The neopentyl analogue was easily obtained from neopentyl lithium and either source of $MnCl_2$ in THF or ether. Once again a dimeric Mn complex resulted from the reaction $[Mn(\mu\text{-}CH_2CMe_3)(CH_2CMe_3)(THF)]_2$ (**3**) (see Figure 3.3.3).

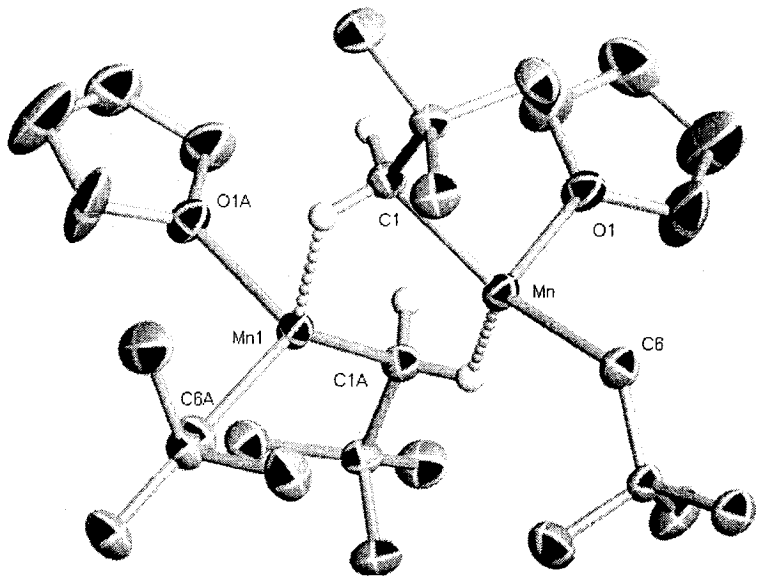

Figure 3.3.3 Crystal Structure of $[Mn(\mu\text{-}CH_2CMe_3)(CH_2CMe_3)(THF)]_2$ (**3**) with 30% Thermal Ellipsoids.

The structure is very similar to those of Complexes **1** and **2**, with a few minor differences. The most obvious is that while in **1** and **2**, the Mn-(μ-C)-Mn moiety was planar, it is puckered in the case of the neopentyl group. This distortion appears to be caused by a partial rotation of the bridging groups which orients one of the hydrogens closer to the Mn than in the previous case (calculated hydrogens of C(1)–Mn(1): 1.958(3) and 2.778(3) Å; 0.21 Å shorter than the closest contact in the CH_2SiMe_3 case). The rest of the tetrahedral environment shows very little other distortions [Mn–O(1) = 2.204(4), Mn–C(1) = 2.230(5), Mn–C(6) = 2.135(6) Å], although the distance to the bridging alkyls are now slightly longer [Mn–C(1a) = 2.482(6) Å]. The metal-metal distance is also slightly shorter in this case 2.718(6) Å, although there is very little change in the magnetic moment value (4.36 μ_B vs. 4.48 μ_B) indicating that there is probably no metal-metal bonding. The angles of the complex also show a distortion from true tetrahedral [O(1)–Mn–C(6) = 103.4(2), O(1)–Mn–C(1) = 127.3(2), O(1)–Mn–C(1a) = 88.96(10)°]. The bridging angle is also quite narrow 70.23(10)° which is once again probably responsible for the short Mn-Mn distance. Again, it is difficult to reconcile this structure with the reported tetrameric structure in the Wilkinson case, with the only explanation being that the Grignard reagents are reacting in a manner different from their lithium analogues.

In order to determine whether the dimeric $Mn^{(II)}$ complexes could be dissociated, the simple complexation reaction of **2** with TMEDA was performed. The formation of the expected monomeric complex [(TMEDA)Mn(CH_2SiMe_3)$_2$] (**4**), occurred in near quantitative isolated yield (see Figure 3.3.4).

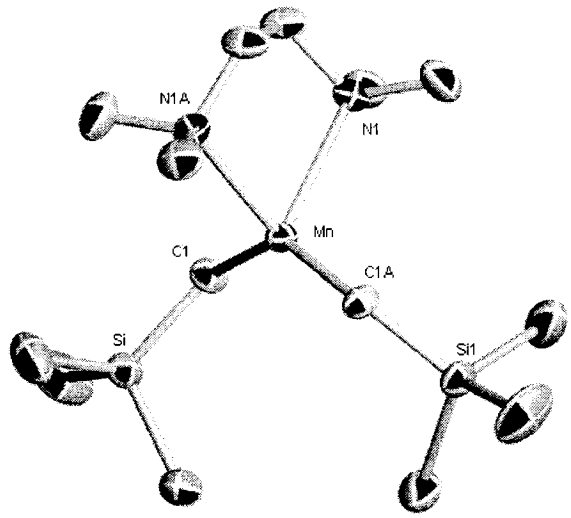

Figure 3.3.4 Crystal Structure of [(TMEDA)Mn(CH_2SiMe_3)$_2$] (**4**) with 30% Thermal Ellipsoids.

The complex is monomeric and tetrahedral as expected for the high-spin d^5 electronic configuration of a $Mn^{(II)}$ metal centre. The four coordination sites are filled by two alkyls, and the TMEDA molecule [Mn–C(1) = 2.1486(18), Mn–N(1) = 2.3433(16) Å, C(1)–Mn–C(1a) = 139.27(11), C(1)–Mn–N(1) = 101.79(6), C(1)–Mn–N(1a) = 109.32(7)°]. This structure demonstrates that the di-alkyls can be conveniently converted to monomeric forms via the simple addition of chelating Lewis bases. For a comparison of the bond distances and angles of the di-alkyl complexes see Table 3.3.5.

Table 3.3.5 Selected Bond Distances (Å) and Angles (°) for complexes **1-4**.

$[MnR_2(Et_2O)]_2$ (**1**) $R = CH_2SiMe_3$	$[MnR_2(THF)]_2$ (**2**) $R = CH_2SiMe_3$
Mn-Mn = 2.785(2)	Mn-Mn = 2.7878(9)
Mn-O(1) = 2.230(6)	Mn-O(1) = 2.188(2)
Mn-C(5) = 2.136(8)	Mn-C(1) = 2.129(3)
Mn-C(1a) = 2.210(8)	Mn-C(5) = 2.214(3)
Mn-H of C(1) = 2.052(8)	Mn-H of C(5a) = 2.164(3)
O(1)-Mn-C(5) = 128.1(4)	O(1)-Mn-C(1) = 108.19(11)
O(1)-Mn-C(1) = 104.7(4)	O(1)-Mn-C(5) = 99.19(10)
Mn-C(1)-Mn = 74.56(2)	Mn-C(5)-Mn = 75.07(9)

Table 3.3.5 continued.

$[MnR_2(THF)]_2$ (**3**) $R = CH_2CMe_3$	[(TMEDA)MnR_2(THF)] (**4**) $R = CH_2SiMe_3$
Mn-Mn = 2.7183(17)	Mn-N(1) = 2.3433(16)
Mn-O(1) = 2.204(4)	Mn-C(1) = 2.1486(18)
Mn-C(6) = 2.135(6)	
Mn-C(1) = 2.230(5)	N(1)-Mn-C(1) = 101.79(6)
Mn-H of C(1a) = 1.958(6)	N(1)-Mn-C(1a) = 109.32(7)
	N(1)-Mn-N(1a) = 79.52(8)
O(1)-Mn-C(6) = 103.4(2)	
O(1)-Mn-C(1) = 100.01(17)	
Mn-C(1)-Mn = 70.23(6)	

The formation of the di-alkyl is a stoichiometry-sensitive reaction. This was clearly indicated by the fact that when a slight excess of 2.35 eq of $LiCH_2SiMe_3$ was used during a synthesis of the di-alkyl, the reaction afforded an interesting side product. A *triangulo* structure consisting of three Mn atoms and seven alkyl anions, along with one

solvated lithium counter-anion resulted $[Mn_3(\mu_3\text{-}CH_2SiMe_3)(\mu_2\text{-}CH_2SiMe_3)_3(CH_2SiMe_3)_3][Li(THF)_4]$ (**5**) (see Figure 3.3.6).

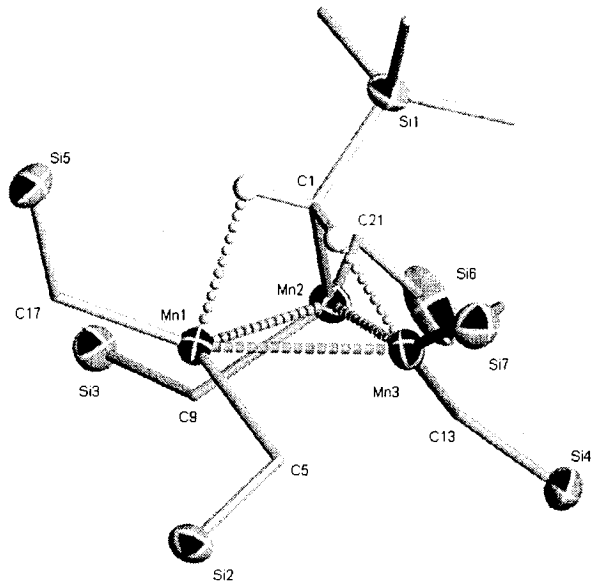

Figure 3.3.6 Crystal Structure of **5** with 30% Thermal Ellipsoids, $Li(THF)_4$ and Some Methyl Groups Omitted for Clarity.

Complex **5** consists of three Mn atoms defining the triangular core [Mn(1)–Mn(2) = 2.8521(13), Mn(1)–Mn(3) = 2.9665(13), Mn(2)–Mn(3) = 2.8145(14) Å, Mn(1)–Mn(2)–Mn(3) = 63.13(3), Mn(2)–Mn(1)–Mn(3) = 57.82(3)°]. Each Mn is pseudo-tetrahedrally coordinated by one terminal alkyl, two μ_2-bridging alkyls, and a final alkyl group which is μ_3-bridging all of the Mn atoms [Mn(1)–C(17) = 2.148(6), Mn(1)–C(5) = 2.238(6), Mn(1)–hydrogen-C(9) = 1.601(6), Mn(1) –hydrogen–C(1) = 2.289(6) Å, C(17)–Mn(1)–C(5) = 123.5(3), C(17)–Mn(1)–hydrogen-C(9) = 101.44(3), C(17)–Mn(1)– hydrogen-C(1) = 88.92(3)°]. One tetrahedrally coordinated $Li(THF)_4$ unit counter-balances the overall negative charge of the complex.

The unusual tri-alkyl anion $[Mn(\mu_2\text{-}CH_2SiMe_3)(CH_2SiMe_3)_2(LiOEt_2)]_2$ (**6**) was obtained by combining three equivalents of $LiCH_2SiMe_3$ with either $MnCl_2$ source in THF or ether (see Figure 3.3.7).

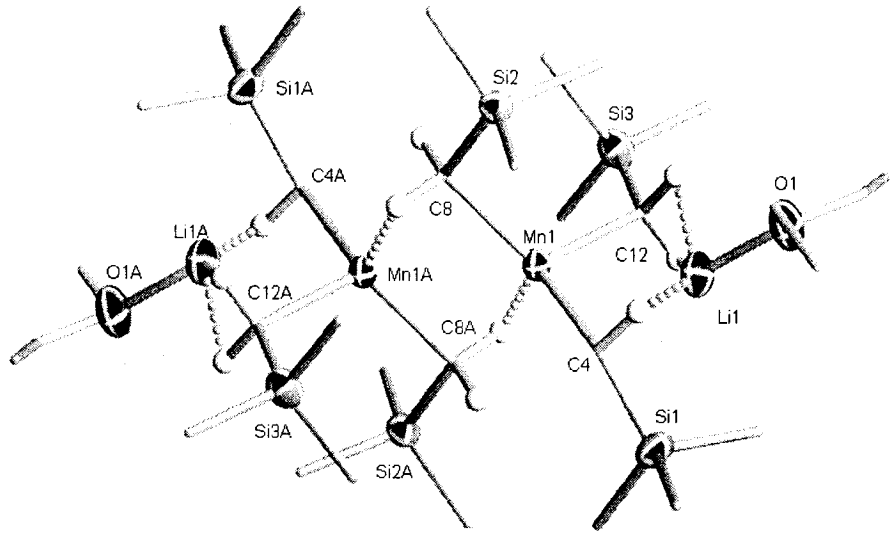

Figure 3.3.7 Crystal Structure of **6** with 30% Thermal Ellipsoids.

The complex adopts a linear arrangement along the Li-Mn-Mn-Li axis with each Mn atom bonded to two terminal and two bridging alkyls, along with the Li counter-cation which is hydrogen bonded to the terminal alkyl groups [Mn(1)–C(4) = 2.259(3), Mn(1)–C(12) = 2.222(3), Mn(1)–C(8) = 2.216(3), Mn(1)–hydrogen C(8a) = 2.085(3) Å, C(4)–Mn(1)–C(12) = 104.44(11), C(4)–Mn(1)–C(8) = 113.79(11), C(4)–Mn(1)–C(8a) = 103.847(11)°]. The Mn-Mn distance is slightly longer than in the previous cases [2.8208(19) Å] and as per usual there is a very tight Mn(1)-C(8)-Mn(1a) angle [75.07(11)°] which is probably enforced by the hydrogen bonding of the bridging alkyl groups similar to the previous cases.

Although exposure of any of the di-alkyls to atmosphere led almost instantaneously to dark coloured, completely insoluble materials, their exposure to CO_2 instead lead to a colourless hexane soluble product. The rate of this discolouration was qualitatively observed to be much faster in polar solvents like THF vs. the non-polar hexanes. Regardless of the solvent the complex was reacted in, all invariably lead to colourless single crystal formation out of cooled, concentrated, hexanes solutions. The crystal structure of $[Mn_5(\eta_2\text{-}\mu_3\text{-}O_2CCH_2SiMe_3)_6(CH_2SiMe_3)_4]\cdot(C_6H_{10})$ (**7**) revealed the species to be a carboxylate bridged penta-nuclear cluster with four of the five Mn centres retaining an intact alkyl group (see Figure 3.3.8).

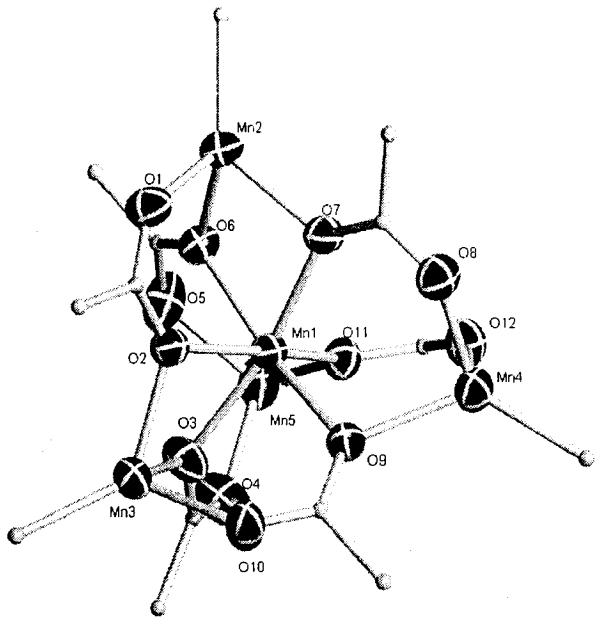

Figure 3.3.8 Crystal Structure of **7** with 30% Thermal Ellipsoids, $SiMe_3$ Groups and Lattice Hexane Omitted for Clarity.

The core of the cluster contains a central Mn(1) which is octahedrally coordinated by six carboxylate oxygens [Mn(1)–O(2) = 2.252(2), Mn(1)–O(3) = 2.211(2), Mn(1)–O(6) = 2.205(2), Mn(1)–O(7) = 2.223(2), Mn(1)–O(9) = 2.205(3), Mn(1)–O(11) = 2.171(2) Å, O(2)–Mn(1)–O(3) = 76.61(9), O(2)–Mn(1)–O(9) = 91.96(9), O(2)–Mn(1)–O(7) = 86.95(9), O(2)–Mn(1)–O(11) = 167.04(9)°]. Each of the four external Mn atoms are tetrahedrally coordinated by three bridging carboxylate groups and one terminal CH_2SiMe_3 group [Mn(2)–C(1) = 2.095(4), Mn(2)–O(1) = 2.071(3), Mn(2)–O(6) = 2.112(2), Mn(2)–O(7) = 2.152(2) Å, C(1)–Mn(2)–O(1) = 123.70(9), C(1)–Mn(2)–O(6) = 123.53(9), C(1)–Mn(2)–O(7) = 130.33(9)°]. The positioning of the four Mn atoms forms a tetrahedron with the octahedral Mn occupying the central position (see Figure 3.3.9).

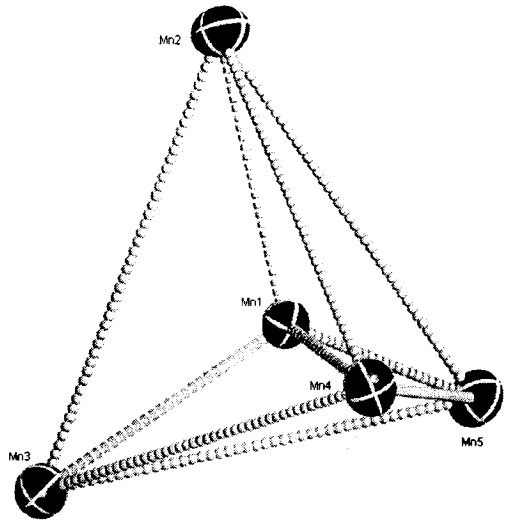

Figure 3.3.9 Three Dimensional Positions of Mn atoms in **7**.

Since the complex still possesses terminal alkyl groups along its exterior, this complex could readily serve as a building block for even larger cluster compounds, especially as the octahedrally coordinated central Mn should lend a large degree of structural strength.

3.4 Conclusions:

With this study we have demonstrated that several di-alkyl $Mn^{(II)}$ complexes can be readily synthesized in order to provide starting material for future metathesis reactions with protic ligands. The use of $[Mn(\mu_2\text{-}CH_2SiMe_3)(CH_2SiMe_3)(THF)]_2$ (**2**) will be more extensively investigated in the following chapters. Furthermore, it was demonstrated that the di-alkyl complexes could readily be made monomeric via the simple introduction of the chelating agent TMEDA.

In addition to the di-alkyls we have observed that the tris-alkyl $[Mn(\mu_2\text{-}CH_2SiMe_3)(CH_2SiMe_3)_2(LiOEt_2)]_2$ (**6**) can also be readily prepared, and could also serve as a precursor for future studies. The formation of the *triangulo* compound **5** does indicate that this type of chemistry is quite sensitive to the stoichiometry of the alkylating agent.

The reaction of the di-alkyl **2** with CO_2 led to the insertion of CO_2 into the alkyl ligand creating the robust carboxylate pentameric cluster compound **7**. This cluster could serve as an anchor for further transformations since it still contains four intact CH_2SiMe_3 alkyl groups that would easily support metathetic ligand exchange.

3.5 X-Ray Crystallography Section:

The full crystallographic data, including bond lengths and angles may be found in Appendix 3. The abbreviated crystallographic data for the structures contained within this chapter are as presented in Tables 3.5.1 to 3.5.3.

Table 3.5.1 Crystal Data and Structure Analysis Results for Complexes **1-2b**.

	1	**2**	**2b**
Formula	$C_{24}H_{64}Mn_2O_2Si_4$	$C_{24}H_{60}Mn_2O_2Si_4$	$C_{24}H_{60}Mn_2O_2Si_4$
FW	606.99	602.96	602.96
space group	Monoclinic, ***P2(1)/n***	Monoclinic, ***P2(1)/c***	Triclinic, ***P-1***
a (Å)	10.3807(16)	10.1991(16)	10.226(6)
b (Å)	10.4515(17)	15.568(2)	10.793(7)
c (Å)	17.653(3)	12.747(2)	38.76(2)
α (deg)	90	90	89.696(10)
β (deg)	90.802(3)	113.482(2)	89.864(9)
γ (deg)	90	90	63.284(9)
V (Å^3)	1915.0(5)	1856.4(5)	3821(4)
Z, Z'	2	2	2, 4
radiation (Kα, Å)	0.71073	0.71073	0.71073
T (K)	203(2)	203(2)	200(2)
D_{calcd} (g cm^{-3})	1.053	1.079	1.048
μ_{calcd} (mm^{-1})	0.800	0.825	0.802
F_{000}	660	652	1304
R, R_w[2 a]	0.0679, 0.1644	0.0488, 0.1300	0.0615, 0.1253
GoF	1.014	1.048	1.019

[a] $R = \Sigma||Fo| - |Fc||/\Sigma|F|$. $Rw = [\Sigma(|Fo| - |Fc|)^2/\Sigma wFo^2]^{1/2}$.

Table 3.5.2 Crystal Data and Structure Analysis Results for Complexes **3-5**.

	3	**4**	**5**
Formula	$C_{28}H_{60}Mn_2O_2$	$C_{14}H_{38}MnN_2Si_2$	$C_{44}H_{111}LiMn_3O_4Si_7$
FW	538.64	345.58	1072.72
space group	Monoclinic, *C2/c*	Monoclinic, *C2/c*	Monoclinic, *P2(1)/c*
a (Å)	10.028(2)	18.448(2)	12.5153(10)
b (Å)	17.698(5)	9.9379(12)	27.755(2)
c (Å)	19.227(4)	12.8427(16)	19.7478(16)
α (deg)	90	90	90
β (deg)	103.950(4)	108.487(2)	91.4790(10)
γ (deg)	90	90	90
V (Å^3)	3311.7(14)	2233.0(5)	6857.4(10)
Z	4	4	4
radiation (Kα, Å)	0.71073	0.71073	0.71073
T (K)	203(2)	203(2)	203(2)
D_{calcd} (g cm^{-3})	1.080	1.028	1.039
μ_{calcd} (mm^{-1})	0.781	0.692	0.696
F_{000}	1176	756	2332
R, R_w[2 a]	0.0668, 0.1655	0.0355, 0.0831	0.0799, 0.1942
GoF	1.041	1.064	1.013

[a] $R = \Sigma||Fo| - |Fc||/\Sigma|F|$. $Rw = [\Sigma(|Fo| - |Fc|)^2/\Sigma wFo^2]^{1/2}$.

Table 3.5.3 Crystal Data and Structure Analysis Results for Complexes **6-7**.

	6	**6b**	**7**
Formula	$C_{32}H_{86}Li_2Mn_2O_2Si_6$	$C_{32}H_{84}Li_2Mn_2O_2Si_6$	$C_{49}H_{117}Mn_5O_{12}Si_{10}$
FW	795.30	793.29	1454.03
space group	Monoclinic, *P2(1)/n*	Triclinic, *P-1*	Triclinic, *P-1*
a (Å)	10.745(9)	11.1960(13)	15.3309(19)
b (Å)	19.010(16)	12.4512(14)	15.379(2)
c (Å)	12.570(11)	20.741(2)	21.242(3)
α (deg)	90	93.144(2)	89.675(2)
β (deg)	92.964(14)	97.159(2)	69.448(2)
γ (deg)	90	115.671(2)	64.043(2)
V (Å^3)	2564(4)	2566.4(5)	4150.8(9)
Z, Z'	4, 2	2	2
radiation (Kα, Å)	0.71073	0.71073	0.71073
T (K)	203(2)	203(2)	293(2)
D_{calcd} (g cm^{-3})	1.030	1.027	1.163
μ_{calcd} (mm^{-1})	0.655	0.654	0.926
F_{000}	868	864	1544
R, R_w[2 a]	0.0437, 0.1128	0.0700, 0.1213	0.0526, 0.1220
GoF	1.064	1.023	1.005

[a] $R = \Sigma||Fo| - |Fc||/\Sigma|F|$. $Rw = [\Sigma(|Fo| - |Fc|)^2/\Sigma wFo^2]^{1/2}$.

3.6 Experimental Section:

All reactions were carried out under a dry nitrogen atmosphere. Solvents were dried using an aluminum oxide solvent purification system. $MnCl_2(THF)_{1.5}$ was prepared according to the literature preparation,[10] and anhydrous $MnCl_2$ was prepared by dehydrating $MnCl_2.6H_2O$ under vacuum at 300 °C for 24 hours. $LiCH_2SiMe_3$ was prepared via a modified literature preparation[11] and $LiCH_2CMe_3$ was preparped according to the literature.[12] TMEDA was purchased from Aldrich, dried over Na/K amalgam and distilled prior to use. CO_2 was research grade, and was passed through a P_2O_5 drying column prior to use. Infrared spectra were recorded on an ABB Bomem FTIR instrument from Nujol mulls prepared in a drybox. Samples for magnetic susceptibility were pre-weighed inside a drybox equipped with an analytical balance and measured on a Johnson Matthey Magnetic Susceptibility balance. Elemental analysis was carried out with a Perkin-Elmer 2400 CHN analyzer. Data for X-ray crystal structure determination were obtained with a Bruker diffractometer equipped with a 1K Smart CCD area detector.

Modified Synthesis of $LiCH_2SiMe_3$: 10.0 g of solid lithium (4.0 eq, 1.44 mol) was beaten flat and cut into thin strips in an Argon stream from a 500 mL round bottom Schlenk flask containing 300 mL of hexanes. Once the lithium was added to the flask was cooled to -30 °C and Me_3SiCH_2Cl (1.0 eq, 50.27 mL, 0.360 mol) was added dropwise at a rate that ensured that boiling did not occur. The solution was then refluxed for 24 hours, after which it was filtered and the filtrate was dried *in vacuo* yielding 26.3 g of a beige white solid (0.279 mol, 77.6 %).

General Synthesis $[MnR_2(THF)]_2$ R= CH_2SiMe_3, CH_2CMe_3 (1-3): Either $MnCl_2(THF)_{1.5}$ or $MnCl_2$ may be used for any of the preparations. A slurry of $MnCl_2$ (5.0 g, 39.7 mmol) in 50 mL of THF was cooled to -30 °C. In a separate flask $LiCH_2SiMe_3$ (2.05 eq, 7.67 g) was cooled to -30 °C in 10 mL of THF. The alkyl solution was then added to the stirring slurry and allowed to warm to room temperature. The colour of the solution quickly turned orange and the suspension became a clear solution. After stirring for 12 hours the THF was removed *in vacuo* and 75 mL of hexanes was added. The pure white LiCl was then centrifuged off yielding a dark orange solution.

This solution was progressively cooled in the following manner: 1 hr at 5 °C, 12 hrs at -17 °C, and 12 hrs at -35 °C. After the cooling extremely large dark orange block crystals of **2** (in excess of 5 cm) were recovered. The supernatant was then concentrated to ~10 mL and cooled to -35 °C in order to collect a second crop of crystals. Overall yield 11.05 g (36.6 mmol, Yield 92.3 %).

Characterization for $[Mn(\mu_2\text{-}CH_2SiMe_3)(CH_2SiMe_3)(Et_2O)]_2$ (**1**): IR (Nujol) ν: 1293 (w), 1243 (s), 1001 (m), 919 (s), 897 (s) 840 (s), 748 (s), 695 (s), 674 (s), 605 (m), 446 (s). Elemental Analysis calcd (Found) for $Mn_2C_{24}H_{64}Si_4O_2$: C 47.50 (47.63), H 10.64 (10.53). $\mu_{eff} = 4.52\ \mu_B$.

Characterization for $[Mn(\mu_2\text{-}CH_2SiMe_3)(CH_2SiMe_3)(THF)]_2$ (**2**): IR (Nujol) ν: 1294 (w), 1245 (s), 998 (m), 917 (s), 897 (s) 843 (s), 743 (s), 700 (s), 680 (s), 607 (m), 446 (s). Elemental Analysis calcd (Found) for $Mn_2C_{24}H_{60}Si_4O_2$: C 47.81 (47.73), H 10.03 (9.92). $\mu_{eff} = 4.48\ \mu_B$.

Characterization for $[Mn(\mu_2\text{-}CH_2CMe_3)(CH_2CMe_3)(THF)]_2$ (**3**): IR (Nujol) ν: 1292 (w), 1253 (s), 991 (m), 912 (s), 902 (s) 838 (s), 741 (s), 711 (s), 683 (s), 611 (m), 453 (s). Elemental Analysis calcd (Found) for $Mn_2C_{24}H_{60}Si_4O_2$: C 62.41 (62.59), H 11.23 (11.18). $\mu_{eff} = 4.36\ \mu_B$.

Synthesis [(TMEDA)Mn(CH_2SiMe_3)$_2$] (4): To a hexanes solution of **2** (0.250 g, 0.829 mmol) in 10 mL of hexanes was added TMEDA (1.05 eq, 0.131 mL, 0.871 mmol). The solution immediately went from orange to colourless. The solution was then cooled for 12 hours at -35 °C after which colourless block crystals were recovered 0.268 g (0.776 mmol, 93.6 % Yield).

IR (Nujol) ν: 2748 (s), 1293 (w), 1263 (s), 1150 (s), 1044 (s), 1001 (m), 924 (s), 894 (s) 856 (s), 741 (s), 692 (s), 669 (s), 600 (m), 426 (s).

Elemental Analysis calcd (Found) for $MnC_{14}H_{38}N_2Si_2$: C 48.66 (48.39), H 11.08 (11.23), N 8.11 (8.25). $\mu_{eff} = 5.53\ \mu_B$.

Synthesis $[Mn_3(\mu_3\text{-}CH_2SiMe_3)(\mu_2\text{-}CH_2SiMe_3)_3(CH_2SiMe_3)_3][Li(THF)_4]$ (5): The synthesis of the triangulo compound complex was never accomplished in full purity, but was found to be a side product in some cases when the stoichiometry was incorrect. When the stoichiometry was varied between 2.1-3.0 eq (of $LiCH_2SiMe_3$) some of the triangulo compound would sometimes results as prismatic dark orange crystals which were recovered from cold hexanes. No meaningful characterization data except the crystal structure was found due to the presence of other Mn species. Performing the reaction in non-polar solvents (ie. Hexanes) tended to lead to an increased amount of the triangulo complex.

Synthesis of $[Mn(\mu_2\text{-}CH_2SiMe_3)(CH_2SiMe_3)_2(LiOEt_2)]_2$ (6): Either $MnCl_2(THF)_{1.5}$ or $MnCl_2$ may be used for this preparation. A slurry of $MnCl_2$ (1.0 g, 7.94 mmol) in 25 mL of THF was cooled to -30 °C. In a separate flask $LiCH_2SiMe_3$ (3.05 eq, 2.28 g, 24.2 mmol) was cooled to -30 °C in 10 mL of THF. The alkyl solution was then added to the stirring slurry and allowed to warm to room temperature. The colour of the solution quickly turned orange and the suspension became a clear solution. After stirring for 12 hours the THF was removed *in vacuo* and 50 mL of hexanes was added. The pure white LiCl was then centrifuged off yielding a dark orange solution (much darker than in the MnR_2 synthesis). This solution was progressively cooled in the following manner: 1 hr at 5 °C, 12 hrs at -17 °C, and 12 hrs at -35 °C. After the cooling large dark orange block crystals of **6** were recovered. The supernatant was then concentrated to ~10 mL and cooled to -35 °C in order to collect a second crop of crystals. Overall yield 2.63g (6.61 mmol, Yield 83.3 %).

IR (Nujol) ν: 1278 (w), 1226 (s), 1021 (m), 932 (s), 867 (s) 833 (s), 752 (s), 720 (s), 631 (s), 588 (m), 427 (s).

Elemental Analysis calcd (Found) for $Mn_2C_{32}H_{86}Li_2O_2Si_6$: C 48.34 (48.51), H 10.91 (10.81). $\mu_{eff} = 4.36\ \mu_B$.

Synthesis of $[Mn_5(\eta_2\text{-}\mu_3\text{-}O_2CCH_2SiMe_3)_6(CH_2SiMe_3)_4]\cdot(C_6H_{10})$ (7): A solution of **2** (2.0 g, 6.63 mmol) in 50 mL of THF was exposed to CO_2 for ~2 hours. The solution quickly turned from orange to colourless over half an hour. The THF was then removed *in vacuo* and hexanes (50 mL) was added. The solution was then placed in the freezer at -35 °C for 12 hours after which time large block crystals of **7** which also contain half a molecule of hexane per pentamer, were recovered 1.73 g (1.19 mmol, 89.7 % Yield).

IR (Nujol) ν: 1610 (s), 1565 (s), 1249 (s), 1115 (s), 1003 (w), 968 (m), 847 (s), 711 (s), 639 (s), 557 (m), 496 (m), 471 (m).

Elemental Analysis calcd (Found) for $Mn_5C_{49}H_{117}O_{12}Si_{10}$: C 40.49 (40.34), H 8.12 (8.07). $\mu_{eff} = 12.83\ \mu_B$.

3.7 References:

1) Dube, T.; Freckmann, D. M. M.; Conoci, S.; Gambarotta, S.; Yap, G. P. A. *Organometallics* **2000**, *19*, 209.
2) Crewdson, P.; Gambarotta, S.; Yap, G. P. A.; Thompson, L. K. *Inorg. Chem.* **2003**, *42*, 8579. b) Jones, R. A.; Koschmieder, S. U.; Nunn, C. M. *Inorg. Chem.* **1988**, *27*, 4524. c) Murray, B. D.; Hope, H.; Power, P. P. *J. Am Chem. Soc.* **1985**, *107*, 169. d) Murray, B. D.; Power, P. P. *J. Am Chem. Soc.* **1984**, *106*, 7011.
3) Andersen, R. A.; Carmona-Guzman, E.; Gibson, J. F.; Wilkinson, G. *J. Chem. Soc., Dalton Trans.* **1976**, 2204.
4) Howard, C. G.; Wilkinson, G. *J. Chem. Soc., Dalton Trans.* **1983**, 2025. b) Davies, J. I.; Howard, C. G.; Skapski, A. C.; Wilkinson, G. *J. Chem. Soc., Chem. Commun.* **1982**, 1077.
5) Solari, E.; Musso, F.; Gallo, E.; Floriani, C.; Re, N; Chiesi-villa, A.; Rizzoli, C. *Organometallics* **1995**, *14*, 2265. b) Gambarotta, S.; Floriani, C.; Chiesi-Villa, A.; Guastini, J. *Chem. Soc., Chem. Commun.* **1983**, 1128.
6) Buttrus, N. H.; Eaborn, C.; Hitchcock, P. B.; Smith, J. D.; Sullivan, A. C. *J. Chem. Soc., Chem. Commun.* **1985**, 1380.
7) Bartlett, R. A.; Olmstead, M. M.; Power, P. P.; Shoner, S. C. *Organometallics* **1988**, *7*, 1801.
8) Morris, R. J.; Girolami, G. S. *Organometallics* **1989**, *8*, 1478.
9) Crewdson, P.; Gambarotta, S.; Yap, G. P. A.; Thompson, L. K. *Inorg. Chem.* **2003**, *42*, 8579.
10) Sobota, P.; Utko, J.; Jerzykiewicz, L. B. *Inorg. Chem.* **1998**, *37*, 3428.
11) Peterson, D. J. *J. Organomet.* **1967**, *9*, 373.12.
12) Screttas, C. G.; Micha-Screttas, M. *J. Org. Chem.* **1979**, *44*, 713.

Chapter

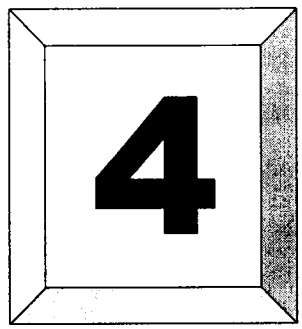

Manganese Complexes as Models for the Photosystem II Oxygen Evolving Complex

Table of Contents

4.1 Introduction:

Photosynthesis is a complex chain of intermingling physical and chemical events which not only are at the very beginning of the food chain but are also responsible for the production of oxygen and removal of carbon dioxide from the atmosphere. In its simplest terms photosynthesis is the process by which all plants convert the energy of the sun into

carbohydrates and oxygen, while utilizing water and carbon dioxide as reactants.[1] A photon absorbed by a chlorophyll molecule commences the process at an active site known as P680, which is located within a complex known as Photosystem II.[2] The light absorption oxidizes P680, forming $P680^+$ which is a strong oxidizing agent, while also passing the high-energy electron through a series of electron transfer agents to Photosystem I. At this particular site, another chain of events converts the photon's energy into chemical form by storing the energy in the ADP/ATP system.[3] The $P680^+$ species is sufficiently oxidizing to extract an electron from water via another electron transport chain, at a site known as the oxygen evolving complex (OEC), or alternately, the water oxidation complex (WOC).[4] Without the OEC, the plant would have no source of electrons to drive the formation of the crucial chemical energy carriers, and photosynthesis would cease to function (see Scheme 4.1.1).

$$2\,H_2O \xrightarrow[OEC]{h\nu} O_2 + 4H^+ + 2\,NADPH + 1.25\,ATP$$

Scheme 4.1.1 Products of Water Oxidation.

Attempts to model some aspects of the behaviour of the fascinating OEC complex was the target of our work. Incidentally, there is a spectacular growth of interest for a better understanding of this system because of the possible applications for the photo-oxidation of water as a convenient and plentiful supply of H_2 and O_2 gases, to be used cleanly and cyclically for harnessing the power of the sun through fuel cell technology (see Scheme 4.1.2).

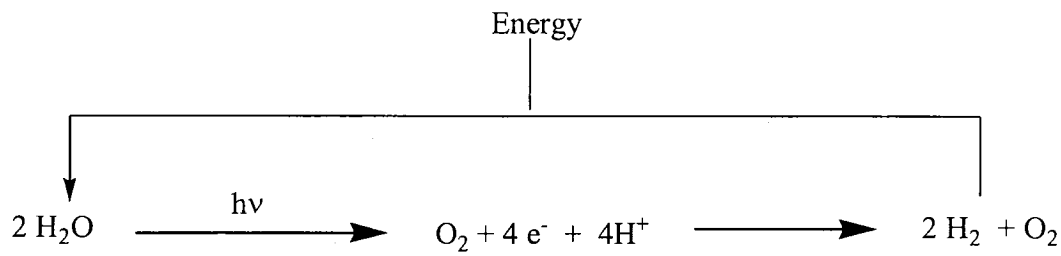

Scheme 4.1.2 Possible Source of Clean Energy.

The challenges associated with the elucidation of the exact structure of the OEC were quite formidable due to its incorporation within a protein structure in an active biological system. Nonetheless, it has been the object of intense scientific interest since the original discovery. In 2001, when this study was undertaken, several facts were known about the nature of the OEC. At the heart of the structure are 4 manganese atoms bridged by an unknown number of oxygens, one calcium, and one chloride atom.[5] It is this inorganic metal cluster which is believed to play the role of fixating, and oxidizing water. From EXAFS (Extended X-ray Absorbance Fine Structure) and XANES (X-ray Absorbance Near Edge Structure) measurements of the OEC, several geometries for the cluster were proposed (see Scheme 4.1.3).[6]

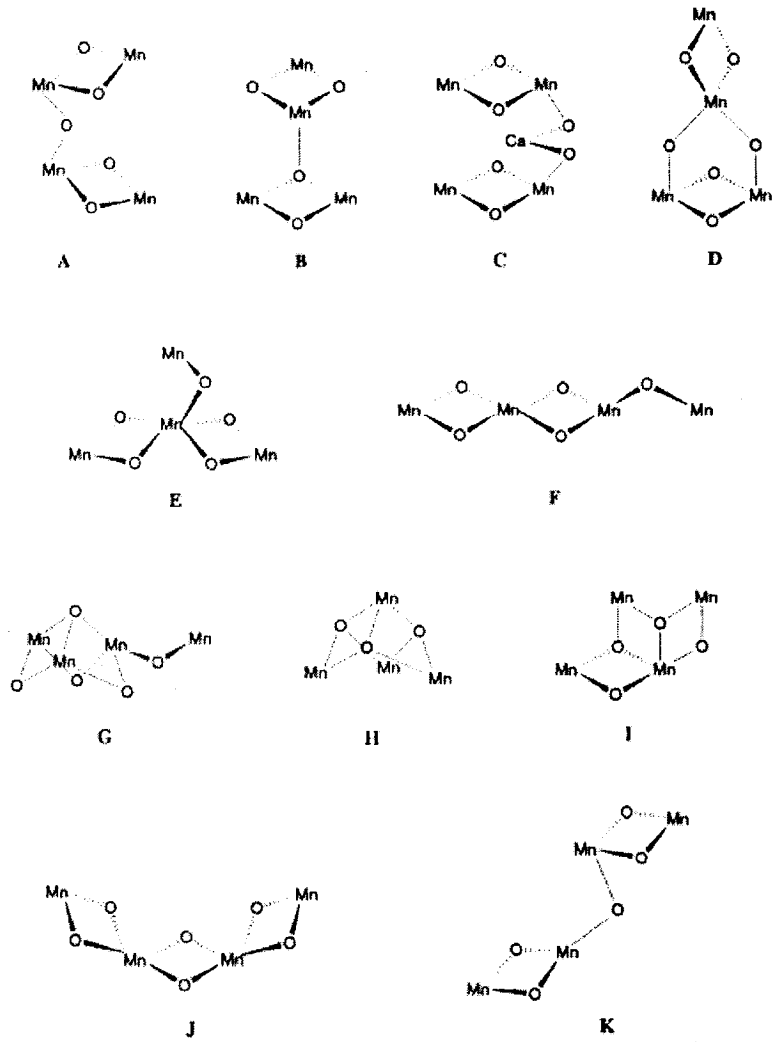

Scheme 4.1.3 Proposed Mn Clusters for the OEC.[6]

At that time structures A and F (Scheme 4.1.3) were the most popular among workers in the field, though none of the other could be conclusively ruled out. The amount of science produced on OEC is today so large that an entire volume of review articles was assembled, providing an excellent source for further reading.[7] The structure of the active site is also thought to be fluxional since the oxidation of water does not occur in one step, but rather four steps. These four steps were investigated by Joliet, and Kok in the late 1970's by using short bursts of light and measuring the amount of O_2 produced.[8] From their studies, they were able to show that O_2 was only evolved after every 4th flash of light, indicating that four photons were required to power each oxidative step in the water splitting reaction. These steps were referred to as the S–states of the Kok cycle. These S–states were later incorporated with the known 4-membered Mn cluster in order to attempt to explain the mechanism of H_2O oxidation. EPR studies (Electron Paramagnetic Resonance), along with the various X-ray techniques (EXAFS, and XANES) helped to elucidate the oxidation states of the Mn atoms within the OEC, however, there still remains some ambiguity (see Scheme 4.1.4).[9]

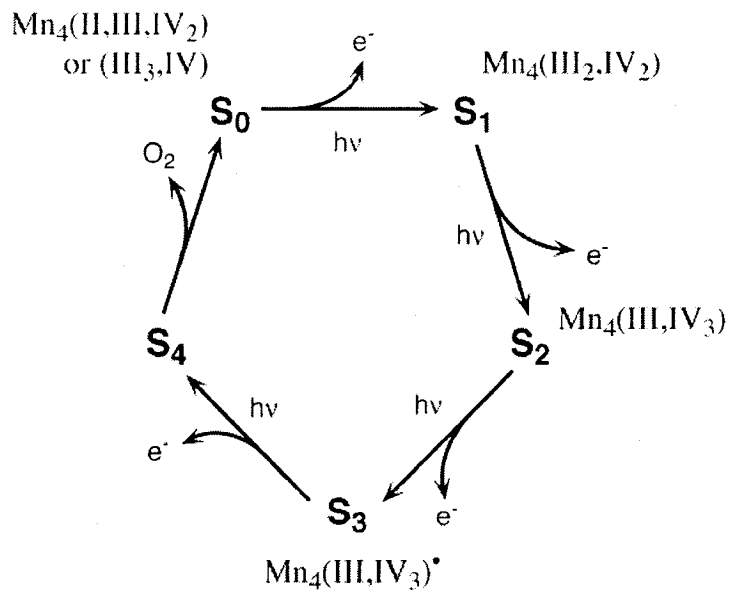

Scheme 4.1.4 Proposed Mn Oxidation States During Kok Cycle.[9]

The different S–states, which had appreciable lifetimes, were analyzed by using timed laser pulses in order to synchronize the OEC in each state. It should be noted that the $S_3 \rightarrow S_4 \rightarrow S_0$ transition occurs too quickly for any current spectroscopic techniques to garner information. From Scheme 4.1.4, it would appear that there is the possibility that two of the Mn atoms may never change their oxidation state from the +4 level. If this is true, they are most likely serving to anchor the remaining two Mn atoms in a specific geometry, within which the reaction is most likely occurring. It should be noted that the d^5, d^4 and d^3 electronic configurations of di-, tri- and tetravalent manganese have very specific requirement in terms of geometry. To model the behaviour of OEC system, many aqua- Mn compounds containing different numbers of oxo-bridges were synthesized in order to provide structural data closely matching the X-ray and EPR data of the naturally occurring system. However none of these synthetic models showed activity for O_2 production.[10]

4.2 Recent Advances:

The finding in 2004 by Ferreira *et al.*[11] solved the literature controversy over the geometry of the Mn cluster by conclusively clarifying by X-ray diffraction methods the structure of the OEC active site.[12] Within the structure, the Ca atom was located, as were the probable positions of the Cl^- and coordinated water molecules (see Figure 4.2.1).

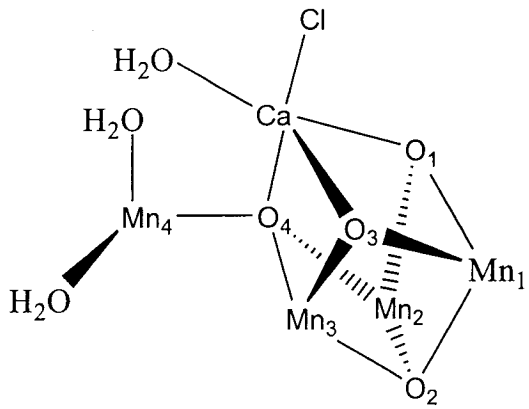

Figure 4.2.1 Mn Cluster Structure From X-Ray Crystal Structure; Mn ligands omitted for clarity.[11]

From this data a new model mechanism for the evolution of O_2 was proposed by Brudvig *et al.*,[13] although there still remains much debate in the current literature.[14]

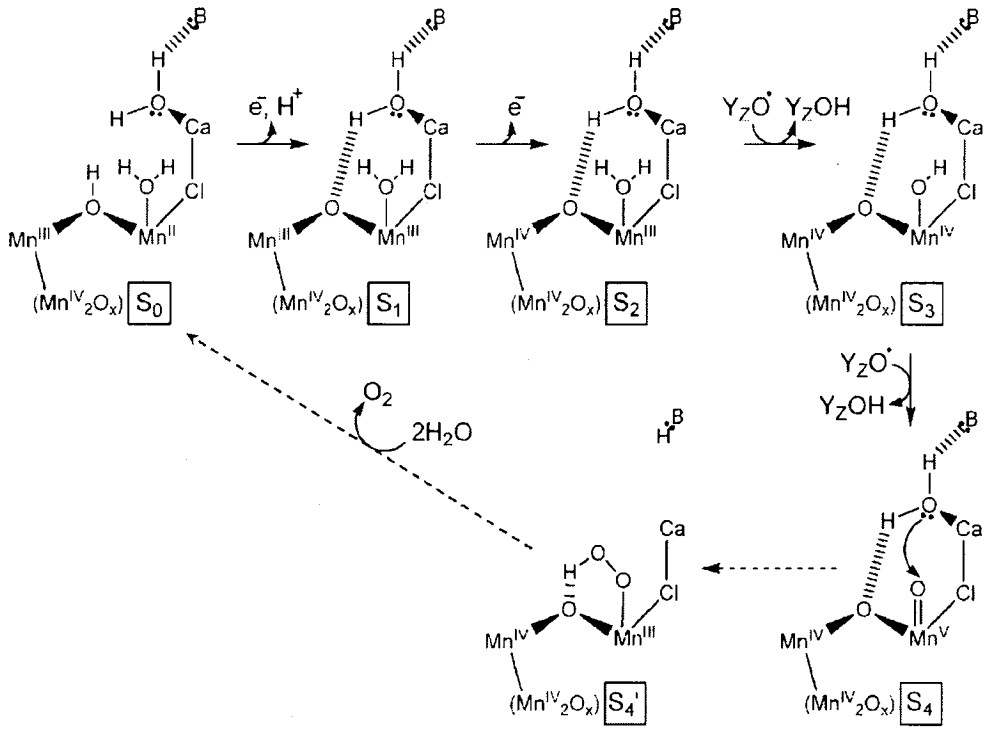

Scheme 4.2.2 Proposed Water Oxidation Mechanism.[12]

In this mechanism, it is important to note that only two of the Mn atoms are actually taking part in the redox process, while the remaining two appear to serve only as anchors for the cluster. According to the postulated cycle the two Mn centres go through the redox process from $Mn^{(II,III)}$ in the S_0 state to $Mn^{(IV,V)}$ at the S_4 state, after which they are restored to their original S_0 oxidation states while releasing a molecule of O_2. It is important to note that the proposed functional OEC is postulated to contain a Mn-OH group in close proximity to a bridging Mn-O-Mn, making the Mn-OH moiety an important target for synthesis.

Much literature has been published reporting on model compounds for the OEC,[15] which serve as references for the X-ray and EPR investigations. As mentioned above however, none were able to produce O_2 gas. The production of O_2 from a Mn compound is so rare that only four precedents exist in the literature. The first such example was claimed in 1994 using a $Mn^{(III)}$ porphyrin dimer (see Figure 4.2.3).

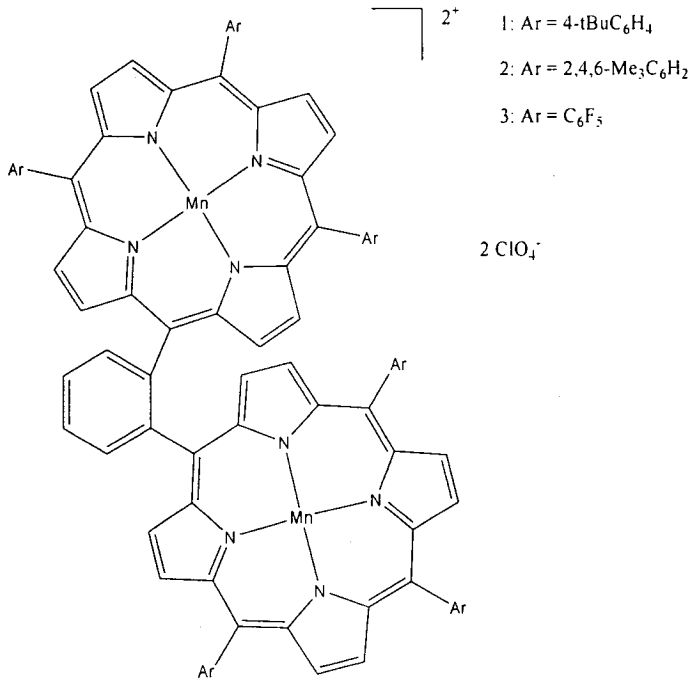

Figure 4.2.3 $Mn^{(III)}$ Dimer for O_2 Production.

Using an electrochemical cell, catalytic oxidation of water was observed. The best run was obtained with catalyst **3** (Figure 4.2.3) producing 9.2 mols. of O_2 per mol. of catalyst. Though the rate of catalysis was extremely low, this may offer the first real example of a Mn complex catalytically producing oxygen from water. Unfortunately, the water was not unambiguously shown to be the source of the oxygen gas, since the possibility that solvent, or even ClO_4^- counteranion degradation might be the actual sources could not conclusively be ruled out.

Brudvig and Crabtree published a series of papers detailing the production of oxygen gas from water, beginning with a Science publication in 1999.[16] Using a simple terpyridine mixed valent μ-oxo$_2$ Mn complex (see Figure 4.2.4) the group was able to produce up to 4 mols of O_2 per mol of catalyst using NaClO or Oxone (2 $KHSO_5 \cdot KHSO_4 \cdot K_2SO_4$) as an oxidant.

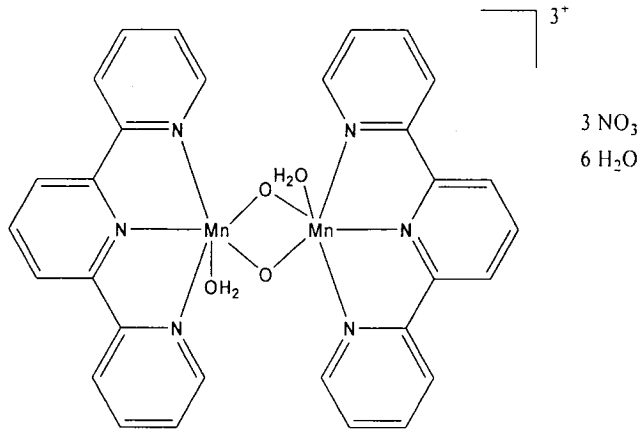

Figure 4.2.4 $Mn^{(III,IV)}$ Complex for Oxygen Evolution.

More findings were obtained by the same groups using similar terpy framework.[17] The common theme of all this chemistry was that either oxone or NaOCl were required as oxidants, and that the activities were always extremely low.

Very recently Deronzier, and Collomb *et al.* have revisited the Brudvig's system, after the finding that the Brudvig compounds did not produce O_2 when an oxidizing agent not containing oxygen was employed.[18] Their investigation found that using electrochemical methods, no O_2 was generated from the Brudvig compounds. The only time that O_2 production ensued was when oxygen containing oxidizing agents were employed (ie. NaOCl, and Oxone). These results quite clearly throw into question whether any of the reported cases of Mn-catalyzed water oxidations were truly produced by water, rather than from the oxidizing agent. Taken as a whole, all of these results quite clearly demonstrate that the activity of the OEC is still far from being fully understood, and thus encourages more research.

4.3 Research Rationale:

As briefly mentioned above, the overall goal of this work was to explore functional models for the OEC. As such, assembling either tetrameric, or dimeric Mn clusters is a key target. As discussed in Chapter 2 (see Chapter 2.1-2.2) the dipyrrolide ligand often assembles clusters of atoms, up to octameric, therefore offering a good potential (see Figure 4.3.1).

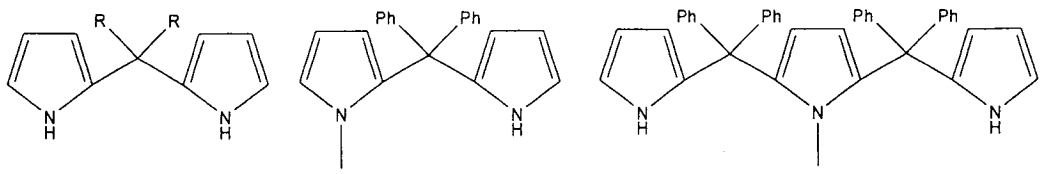

Dipyrrole N-MeDipyrrole N-MeTripyrrole

Figure 4.3.1 Pyrrole Ligand Systems.

In addition to the dipyrrole ligand, both the N-MeDipyrrole (N-MeDipyr), and N-MeTripyrrole (N-MeTripyr) ligands whose synthesis is discussed in Chapter 2 were utilized in an attempt to assemble $Mn^{(II)}$ cluster compounds. The generation of the $Mn^{(II)}$ compounds was expected to readily occur via a simple metathesis reaction with the Mn di-alkyl $[Mn(CH_2SiMe_3)_2(THF)]_2$ which was described in Chapter 3 (see Scheme 4.3.2). Although the possible hydrolysis of the Mn-N σ-bond was anticipated as a very realistic drawback for the use of these derivatives as model compounds, we were solely interested, at such an early stage, in the cluster chemistry of manganese by using ligand systems which in principle may cross the σ- and π-bonding modes. In the long term, we planned to oxidize these species with anhydrous oxygen with the hope that the corresponding oxo-clusters would have improved resistance to hydrolysis.

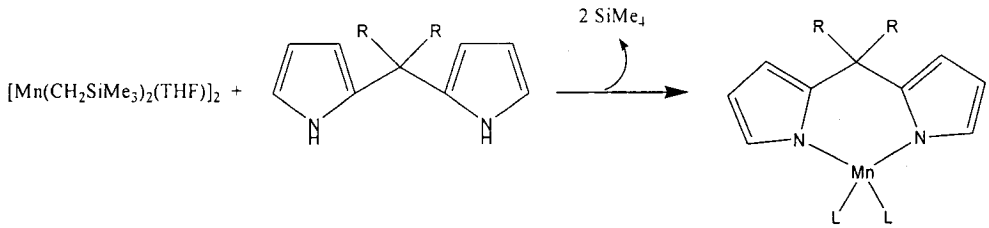

Scheme 4.3.2 Metathesis Reaction for Generating $Mn^{(II)}$ Complexes.

Given that the homoleptic Mn dialkyl species are soluble even in hexanes, the only expected limitation of the reaction will be the solubility of the ligand. As mentioned above, the idea was that Mn complexes generated by this technique could then be exposed to dry oxygen in an attempt to generate oxo-containing clusters of a higher oxidation state (see Scheme 4.3.2).

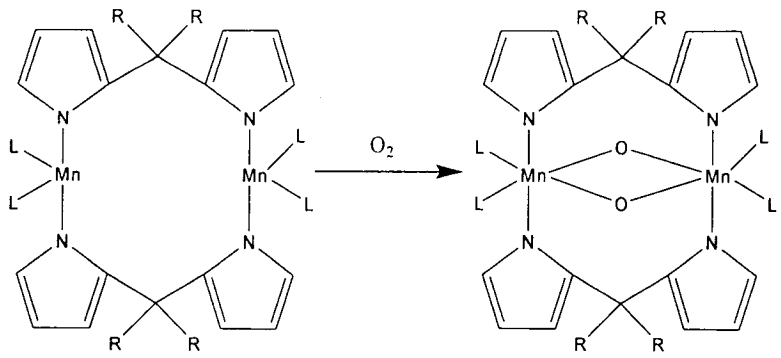

Scheme 4.3.3 Proposed Route for Generating oxo Mn Complexes.

Another ligand system which bears potential is the well known calix[4]arene system.[19] The ligand is easily tunable by varying the nature and sterics of the R groups attached to the phenyl backbones. The calix[4]arene ligand is also well known for assembling two transition metals in close proximity.[20]

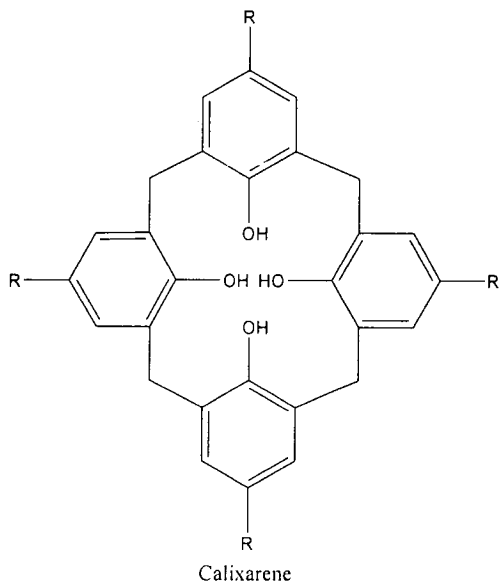

Calixarene

Figure 4.3.4 Calix[4]arene Ligand Structure.

By combining the calixarene ligand system with manganese according to the same synthetic strategy outlined in Schemes 4.3.2 and 4.3.3, further Mn oxo-containing compounds can be envisaged.

Once a collection of oxo-containing Mn compounds have been assembled, electrochemistry would be employed in aqueous media, in order to determine if any of

the compounds have any activity towards the oxidation of water and the concomitant production of gaseous oxygen.

4.4 Results and Discussion:

The dipyrrole ligand system was the first system utilized given that so many variations were readily available in our lab. Using the metathesis strategy outlined in Scheme 4.3.2 the diethyldipyrrole ligand ($Et_2DipyrH_2$) readily formed a dimeric $Mn^{(II)}$ compound $[Mn(\eta^1{:}\mu\text{-}\eta^1\text{-}Et_2Dipyr)(THF)_2]_2$ (**1**) which was crystallized from THF (See Figure 4.4.1). The crystal structure revealed that each diethyldipyrrolide ligand is σ-bound to one Mn atom, and μ^1-η^1 bridging to a second, creating the dimeric structure.

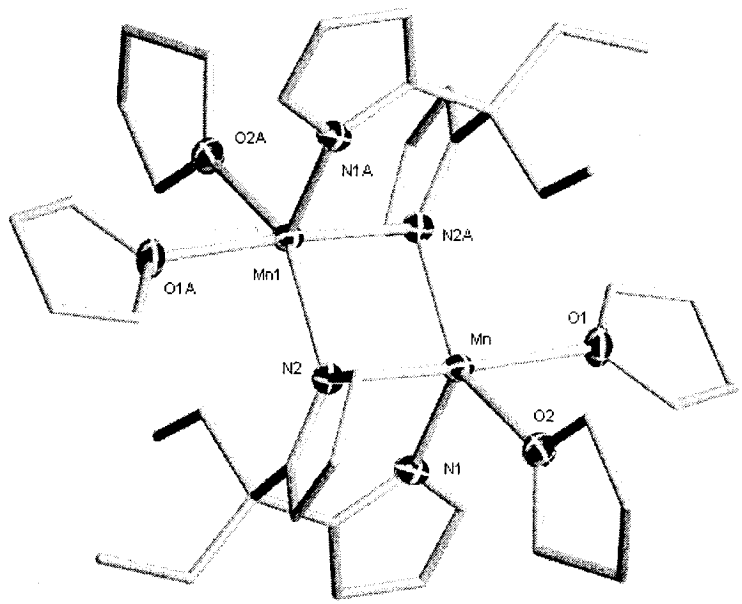

Figure 4.4.1 Crystal Structure of **1** with 30 % Thermal Ellipsoids, Carbon Ellipsoids not Drawn for Clarity.

Each Mn is present in a distorted trigonal bipyramidal coordination geometry. The equatorial plane is comprised of one σ-bound pyrrolide, one μ^1-η^1 bridging pyrrolide, and one molecule of THF [Mn–N(1) = 2.0711(17), Mn–N(2a) = 2.1886(17), Mn–O(2) = 2.1771(17) Å, N(1)–Mn–N(2a) = 114.35(6), N(1)–Mn–O(2) = 101.34(6)°]. The axial positions are fulfilled by the μ^1-η^1 bridging pyrrolide N(2) and the second molecule of THF [Mn–N(2) = 2.3080(16), Mn–O(1) = 2.2674(15) Å, N(2)–Mn–O(1) = 169.48(6)°].

The long Mn-Mn distance (3.2135(8) Å) precludes any direct metal-metal bonding, however the low room temperature magnetic moment of 7.14 μ_B indicates that there is electronic interaction between the Mn centres.

Utilizing a chiral menthone-based dipyrrole ligand (l-ment-dipyrH$_2$) and the same metathesis technique a dimeric structure [Mn(η^1:μ^1-η^1-l-ment-dipyr)(THF)$_2$]$_2$·(THF)$_2$ (**2**), and exhibited the identical pyrrolide bonding, with both σ–, and $\mu^1-\eta^1$ bonding (see Figure 4.4.2).

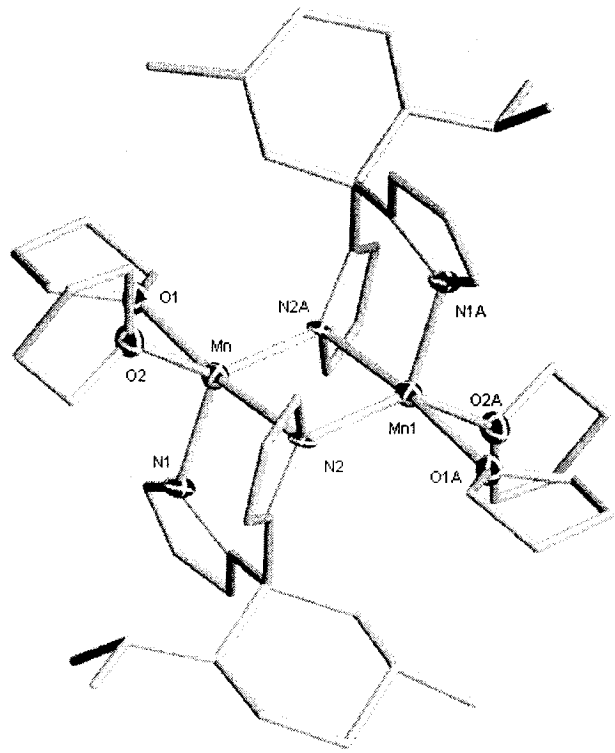

Figure 4.4.2 Crystal Structure of **2** with 30 % Thermal Ellipsoids, Carbon Ellipsoids not Drawn for Clarity.

As in the previous case the complex adopts a distorted trigonal bipyramidal geometry. The equatorial plane is again comprised of one σ-bound pyrrolide, one μ^1-η^1 bound pyrrolide, and a molecule of THF [Mn–N(1) = 2.077(7), Mn–N(2a) = 2.171(7), Mn–O(2) = 2.190(6) Å, N(1)–Mn–N(2a) = 111.6(3), N(1)–Mn–O(2) = 107.5(3)°]. The axial positions are fulfilled by the bridging pyrrolide N(2) and the second molecule of THF [Mn–N(2) = 2.270(7), Mn–O(1) = 2.269(6) Å, N(2)–Mn–O(1) = 173.9(3)°]. The long Mn-Mn distance (3.224(3) Å) once again precludes any direct metal-metal bonding,

though there again appears to be electronic interaction between the Mn centres as demonstrated by the low magnetic moment: 7.08 μ_B.

Using the highly soluble cyclohexyl dipyrrole ($CyDipyrH_2$) led to the expected dimeric complex $[Mn(\eta^1{:}\mu\text{-}\eta^1\text{-}CyDipyr)(THF)_2]_2{\cdot}(THF)$ (**3**). As in the previous two cases the dippyrolide ligand adopted both the σ-, and $\mu^1\text{-}\eta^1$ bonding modes (see Figure 4.4.3).

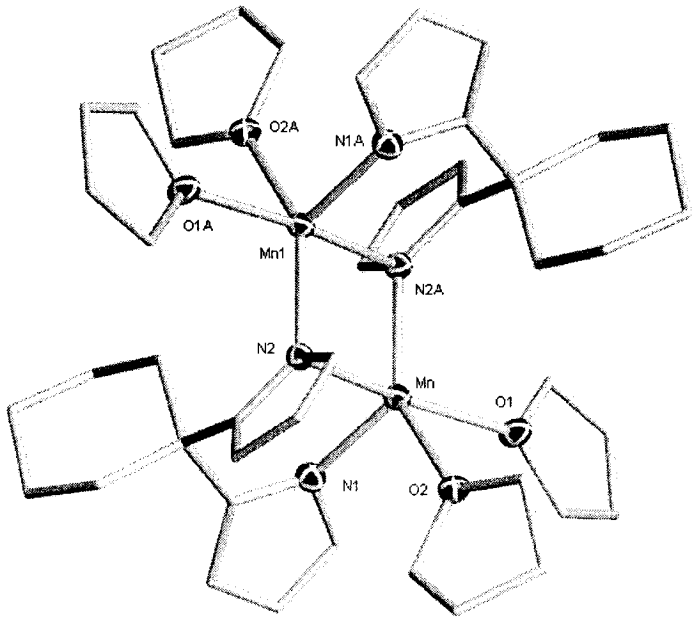

Figure 4.4.3 Crystal Structure of **3** with 30 % Thermal Ellipsoids, Carbon Ellipsoids not Drawn for Clarity.

The expected distorted trigonal bipyramidal coordination geometry is again present in complex **3**. The equatorial plane is again comprised of one σ-bound pyrrolide, one $\mu^1\text{-}\eta^1$ bound pyrrolide, and a molecule of THF [Mn–N(1) = 2.089(2), Mn–N(2a) = 2.1954(18), Mn–O(2) = 2.1933(16) Å, N(1)–Mn–N(2a) = 113.84(8), N(1)–Mn–O(2) = 99.27(7)°]. The axial positions are fulfilled by the bridging pyrrolide N(2) and the second molecule of THF [Mn–N(2) = 2.3211(19), Mn–O(1) = 2.2699(17) Å, N(2)–Mn–O(1) = 165.43(7)°]. As in the previous two cases there is a long Mn-Mn distance (3.2033(7) Å) and a low magnetic moment (7.02 μ_B). A comparison of selected bond distances and angles is provided in Table 4.4.4 demonstrates the close similarity among these dimeric structures.

Table 4.4.4 Selected Bond Distances (Å) and Angles (deg.) for Complexes **1-3**.

1	2	3
Mn-Mn = 3.2135(8)	Mn-Mn = 3.224(3)	Mn-Mn = 3.2033(7)
Mn-N(1) = 2.0711(17)	Mn-N(1) = 2.077(7)	Mn-N(1) = 2.089(2)
Mn-N(2a) = 2.1886(17)	Mn-N(2a) = 2.171(7)	Mn-N(2a) = 2.1954(18)
Mn-O(2) = 2.1771(17)	Mn-O(2) = 2.190(6)	Mn-O(2) = 2.1933(16)
Mn-N(2) = 2.3080(16)	Mn-N(2) = 2.270(7)	Mn-N(2) = 2.3211(19)
Mn-O(1) = 2.2674(15)	Mn-O(1) = 2.269(6)	Mn-O(1) = 2.2699(17)
N(1)-Mn-N(2a) = 114.35(6)	N(1)-Mn-N(2a) = 111.6(3)	N(1)-Mn-N(2a) = 113.84(8)
N(1)-Mn-O(2) = 101.34(6)	N(1)-Mn-O(2) = 107.5(3)	N(1)-Mn-O(2) = 99.27(7)
N(2a)-Mn-O(2) = 144.19(6)	N(2a)-Mn-O(2) = 140.7(3)	N(2a)-Mn-O(2) = 146.83(7)
N(2)-Mn-O(1) = 169.48(6)	N(2)-Mn-O(1) = 173.9(3)	N(2)-Mn-O(1) = 165.43(7)
N(2)-Mn-N(1) = 92.62(7)	N(2)-Mn-N(1) = 89.7(3)	N(2)-Mn-N(1) = 93.62(7)

The crystal structures described above were obtained from crystals grown in coordinating solvents such as THF. It is thus possible that the retention of THF in the coordination sphere of manganese may have played a significant role in the bonding mode adopted by the dipyrrolide ligand. When the metathetic exchange of the dipyrrole ligand was performed with the homoleptic manganese complex in toluene, crystalline material was also obtained in near quantitative yield (96 %). In the case of the CyDipyr ligand the crystallinity was of sufficient quality to enable crystal structure determination revealing an unprecedented octameric cluster $[Mn(\eta^1{:}\mu{-}\eta^5\text{-CyDipyr})]_8{\cdot}(toluene)_4$ (**4**) (see Figures 4.4.5 and 4.4.6).

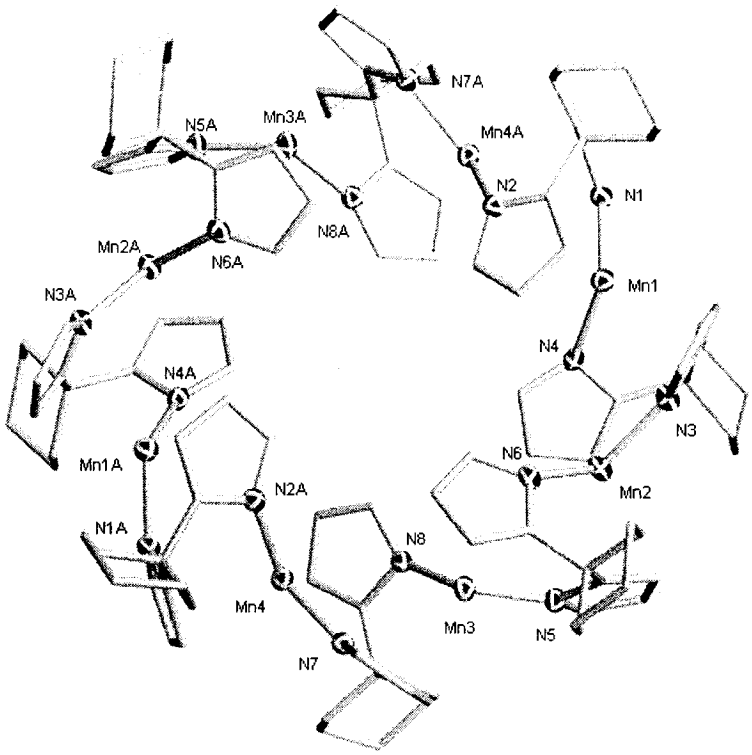

Figure 4.4.5 Crystal Structure of **4** with 30 % Thermal Ellipsoids, Carbon Ellipsoids and μ-η^4 Bonds Omitted for Clarity.

The structure of **4** consists of an octanuclear, cyclic structure with the eight Mn atoms (each formally having a 21-electron configuration) being nearly coplanar and forming a regular ring (see Figure 4.4.6). Each $Mn^{(II)}$ ion adopts a pseudotetrahedral coordination geometry defined by the centroids of two π-bonded rings from two different ligands and σ-bonded N atoms of two other rings also from the two ligands (See Figure 4.4.7).

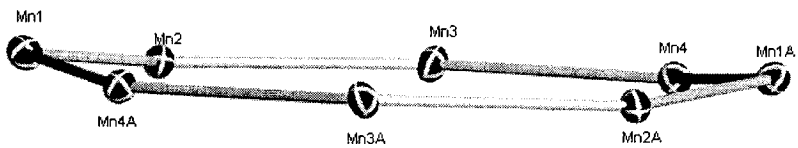

Figure 4.4.6 Ring Structure of Mn atoms in Octameric Cluster (**4**).

The Mn-Mn distances between two contiguous Mn atoms fall between 4.015 and 4.113 Å. A large circular void exists inside the ring with a diameter of ~10 Å. It should also be

noted that the cluster is remarkably thermally robust in boiling toluene, though it still exhibits extreme air sensitivity.

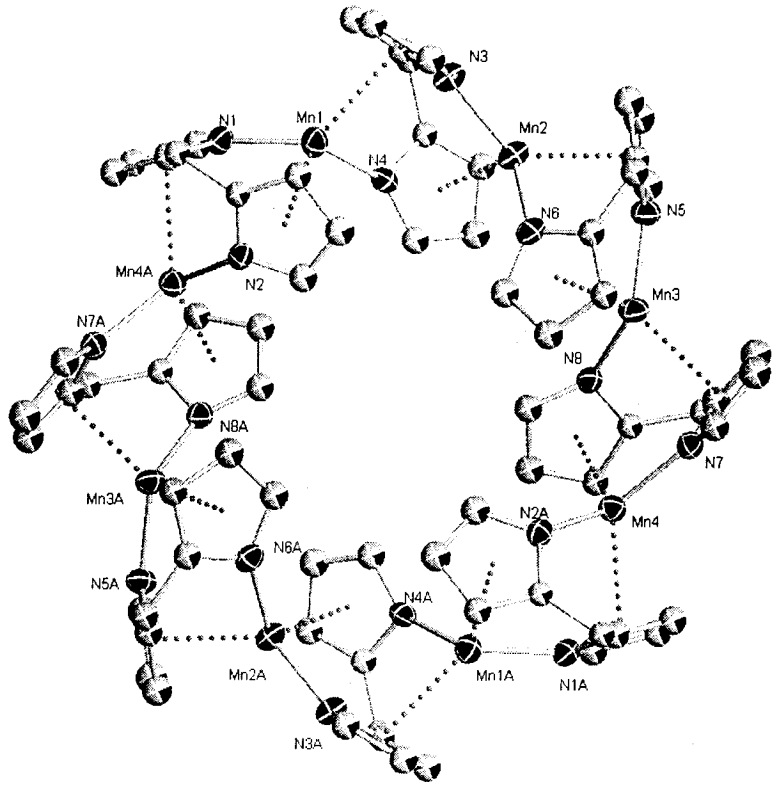

Figure 4.4.7 Crystal Structure of **4** with 30 % Thermal Ellipsoids, Cyclohexyl Groups not Drawn for Clarity.

The tetrahedral coordination geometry about each metal center is as expected for the d^5 high-spin electronic configuration of divalent manganese. The two σ-bound rings N(1) and N(4) display Mn-N distances within the normal pyrrolide bonding distances [2.117(5) and 2.116(5) Å respectively]. The two π-bound pyrrolide rings are somewhat non-equivalent as the ring containing N(2) (Mn(1)–centroid = 2.533 Å) is slightly closer than the ring containing N(3) (Mn(1)–centroid = 2.744 Å). This is most likely indicating that there is some ring-slippage occurring in order to reduce the amount of electron density on the metal towards a formal electron count closer to 18 e^-.

The behavior of the magnetic susceptibility of the octanuclear complex **4** as a function of the temperature shows the characteristic maximum at 35 K also indicative of the presence of intramolecular antiferromagnetic exchange (Figure 4.4.8).[21]

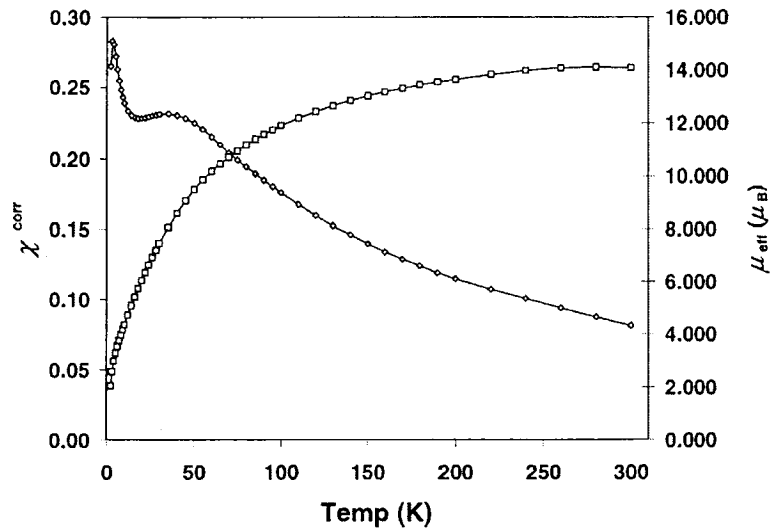

Figure 4.4.8 Diagram of the Magnetic Susceptibility (χ) and of the Magnetic Moment (μ_{eff}) versus T for **4**.

The rise in χ_M at low temperature signals a small proportion of paramagnetic impurity, typical in large clusters. The magnetic moment per mole displays normal behaviour for such a system rising from 3.13 μ_B at 4 K to a maximum value of 14.7 μ_B at 300 K (Figure 4.4.8). This is indicative of an antiferromagnetic/superexchange process through the pyrrolide fragments. The room temperature moment is somewhat lower than that expected for eight uncoupled $Mn^{(II)}$ centers (g = 2, 16.7 μ_B). The magnetic data (per mole) were not fitted to an exchange model based on a ring of eight $Mn^{(II)}$ (S = 5/2) centers, because of the computing difficulties of dealing with such a large calculation. Instead, since the ring is large, and approximates a 1-dimensional chain, the data were fitted to a 1-dimensional chain model[22] assuming a classical spin vector assembly of S = 5/2 centers. A successful fit was obtained with g = 1.96(2), J = -3.4(2) cm^{-1}, ρ = 0.015, TIP = 0 cm^3mol^{-1}, θ = 0 K (^2R = 3.0). The solid lines in Figure 4.4.8 were calculated with these parameters. The $Mn^{(II)}$ centers are therefore coupled uniformly throughout the ring with a moderate exchange integral, and coupling may occur (given the long Mn-Mn non-bonding distance) through the two types of pyrrolide bridging ligands connecting each adjacent pair of metal ions (superexchange). Definite information about the strength of the ligand field induced by a π-bonded pyrrolide ring is not available, and thus the possibility that an intermediate spin state might provide a more correct description for

$Mn^{(II)}$ in the type of coordination environment existing in **4** cannot confidently be excluded. Nevertheless, it seems questionable in light of the tetrahedral coordination environment.

Interestingly, complexes **3** and **4** are quantitatively converted from one to the other by dissolution in the appropriate solvent with heating, followed by recrystallization (see Scheme 4.4.9).

$$[Mn(\eta^1{:}\mu\text{-}\eta^1\text{-CyDipyr})(THF)_2]_2{\cdot}(THF)\ (\mathbf{3}) \underset{\Delta + THF}{\overset{\Delta + Toluene}{\rightleftharpoons}} [Mn(\eta^1{:}\mu\text{-}\eta^5\text{-CyDipyr})]_8{\cdot}(toluene)_4\ (\mathbf{4})$$

Scheme 4.4.9 Interconversion of Complexes **3** and **4**.

The ability of the negatively charged N donor atoms of the dipyrrolide dianion to form σ-bonds is obviously the basis of their poor tendency towards π-ligation. This is in spite of the success in obtaining the π-bond containing octameric structure via a non-coordinating solvent. Since the facile switch of bonding mode was regarded as a possible obstacle for molecular activation processes, we wondered whether the alkylation of one of the two rings might promote more robust π-ligation. We expected that the alkylation of one of the two pyrrolide rings would yield the π-ligation as the sole bonding mode for the second ring and the metal center. In turn, the consequently increased "soft" character of the metal center could provide more hydrolysis-resistant systems. Therefore, we have reacted the Mn di-alkyl successfully used above with N-MeDipyrH and N-MeTriyprH$_2$ according to the previous methodology. The monomeric complex [Mn(N-MeDipyr)$_2$] (**5**) was obtained regardless of the stoichiometry employed (see Figure 4.4.10).

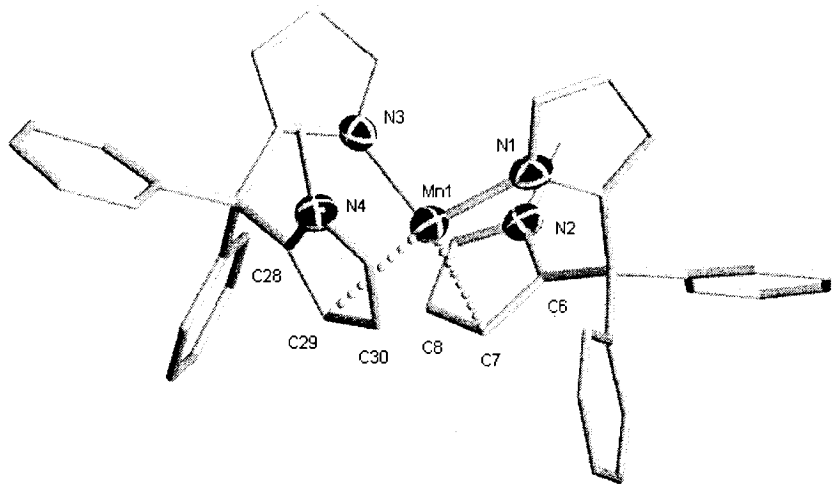

Figure 4.4.10 Structure of **5** with 30 % Thermal Ellipsoids, Carbon Ellipsoids not Drawn for Clarity.

The metal is in a pseudo tetrahedral geometry comprised of two σ-bonding pyrrolides, and two π-bonded N-Me pyrrole rings [N(1)–Mn(1)–N(3) = 105.8(3), N(1)–Mn(1)–C(29) = 140.9(3), N(1)–Mn(1)–C(7) = 97.7(3)°]. The sigma bonds are within the normal bonding distances observed for the previous Mn complexes [Mn(1)–N(1) = 2.067(7), Mn(1)–N(1) = 2.051(7) Å]. It is difficult to determine the extent of the π-bonding based on the bond distances alone. The closest contacts are shown in figure 4.4.9 [Mn(1)–C(7) = 2.523(7), Mn(1)–C(29) = 2.519(9) Å]. The other positions on the rings are then slightly longer [Mn(1)–C(8) = 2.798(9), Mn(1)–C(6) = 2.645(7) Å]. This would tend to indicate that there could possibly be a η^3 type of interaction with the Mn centre. This loose coordination at least demonstrates that the rationale behind the ligand design (ie. hemi-lability, see Chapter 2) may in fact be correct.

When $[Mn(CH_2SiMe_3)_2(THF)]_2$ was reacted with N-MeTriyprH$_2$ in toluene the tetrameric cluster $[Mn(\eta^1{}_2{:}\eta^5{:}\mu\text{-}\eta^3\text{-N-MeTripyr})]_4\cdot(toluene)_{4.85}$ (**6**) was obtained. Each Mn atom is σ-bonded to two pyrrolides, and η^5 π-bonded to an N-MePyrrole from the same ligand, a neighbouring ligand is η^3 bound to each Mn via one of its pyrrolide moieties (see Figure 4.4.11). The void space within the cluster measure 7.4 Å and is slightly bowl-shaped with two of the Mn atoms above the plane of the others.

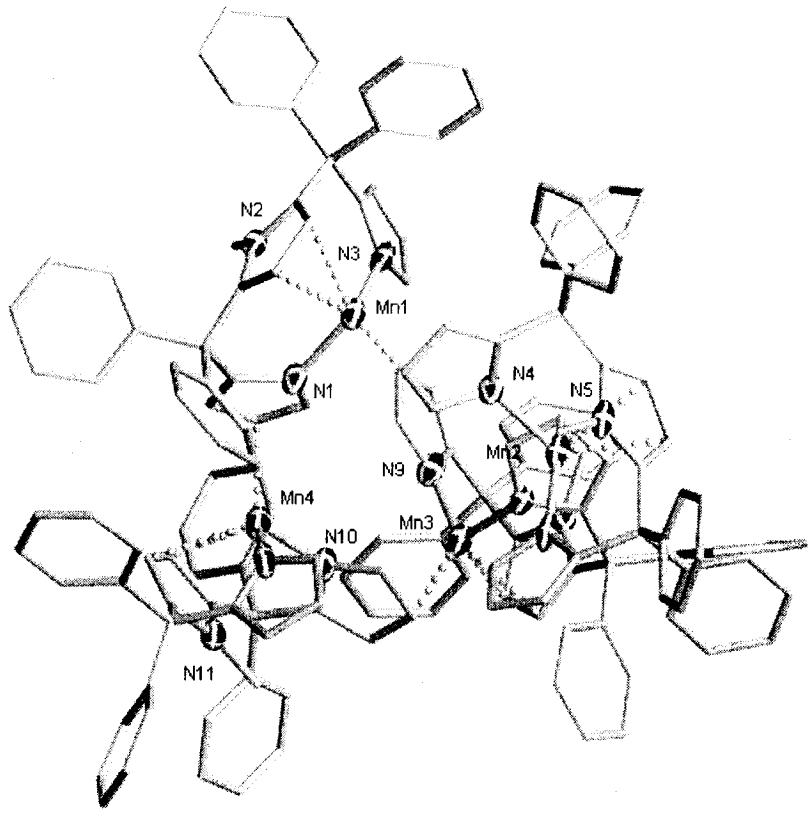

Figure 4.4.11 Structure of **6** with 30 % Thermal Ellipsoids, Carbon Ellipsoids not Drawn for Clarity.

For clarity, the cropped view of the cluster (see Figure 4.4.12) will be discussed with respect to the coordination geometry. Each Mn centre exhibits a pseudo-tetrahedral coordination geometry comprised of the N-MePyrrole ring centroid [Mn-centroid = 2.400(6) Å], the two σ-bound pyrrolides [Mn(1)–N(1) = 2.120(7), Mn(1)–N(3) = 2.038(9) Å], and finally what appears to be an η^3 bond from a neighbouring ligand pyrrolide [Mn(1)–C(41) = 2.335(9) Å].

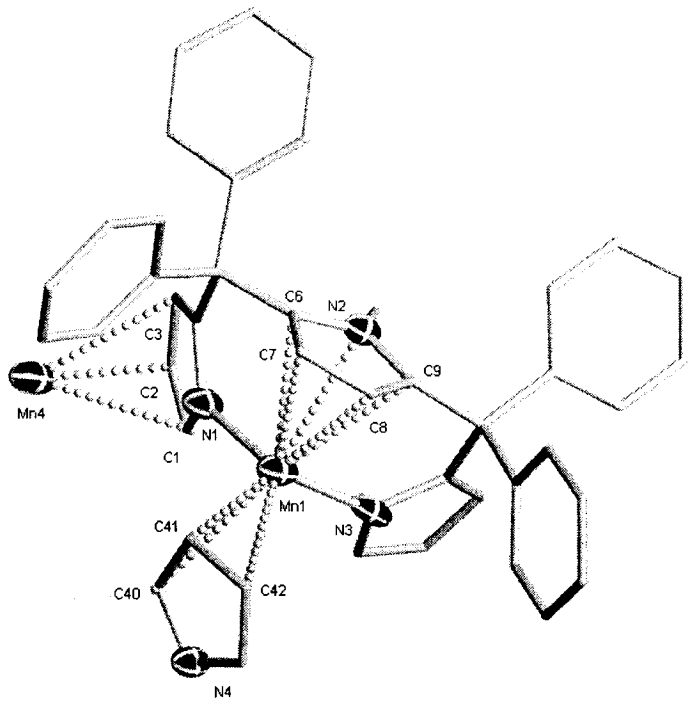

Figure 4.4.12 Mn(1) Portion of Structure **6** with 30 % Thermal Ellipsoids, Carbon Ellipsoids not Drawn for Clarity.

It is difficult to determine the bonding mode of the neighbouring ligand, though it does appear to be a weak η^3 interaction, since the next two nearest atoms are at 2.771(9) and 2.898(9) Å respectively for C(40) and C(42). The angles are quite distorted from tetrahedral [N(1)–Mn(1)–N(3) = 106.1(3), N(1)–Mn(1)–C(41) = 132.1(3), N(1)–Mn(1)–centroid = 94.7(3)°]. As in the previous cases the cluster displays a lower than expected magnetic moment indicating that there is electronic interactions between the Mn atoms: 10.37 μ_B.

As mentioned in the introductory part, oxygen based ligand systems and calix[4]arene in particular are regarded as providing probably the most versatile models for water activation reactions due to the robustness of the Mn-OR bond towards hydrolysis. The first reactions using the calix[4]arene ligand system proved to be quite disappointing as they invariably led to the formation of insoluble white gels regardless of either the stoichiometry, or the choice of solvents. Assuming that the jelly appearance of these products might be caused by polymeric aggregation, we have attempted the disruption of possible polymeric structures via coordination with pyridine, notoriously a

strongly coordinating ligand. Addition of pyridine and heating did not modify the outcome of the reaction. We speculated that perhaps the reaction is yielding a polymeric product in which the Mn centres are highly secluded. In order to avoid this possibility, the monomeric Mn-dialkyl [(TMEDA)Mn(CH_2SiMe_3)$_2$] was utilized (see Chapter 3 for synthesis) for the metathetic reaction with calixarene. The reactions of both one and two equivalents of the di-alkyl with the calixarene ligand were successful. When one equivalent was utilized the dimeric, partly deprotonated di-Manganese complex **7** (see Figure 4.4.13) was formed.

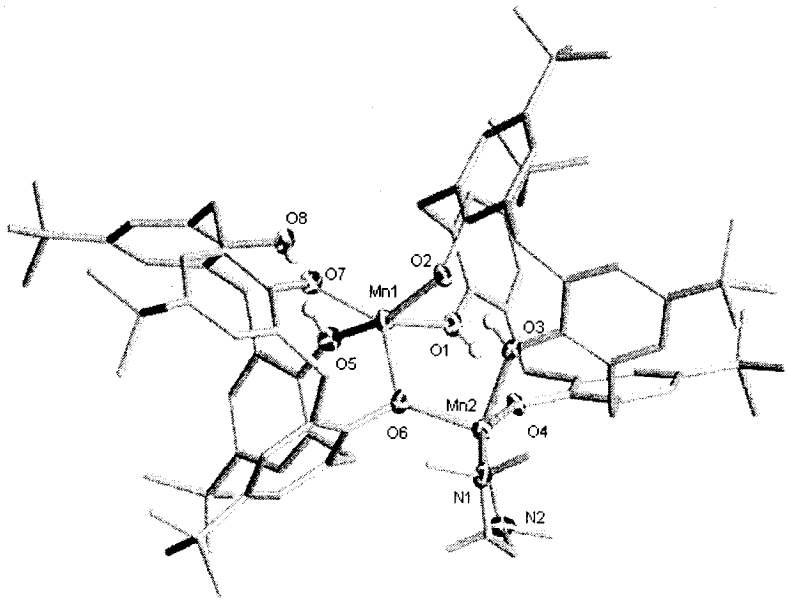

Figure 4.4.13 Structure of **7** with 30 % Thermal Ellipsoids, Carbon Ellipsoids not Drawn for Clarity.

Within the dimer each calixarene ligand has been deprotonated twice, retaining two OH functions each. Each Mn atom is in a distorted square pyramidal coordination geometry, and the two Mn atoms are linked via a bridging phenoxide group, one molecule of TMEDA per dimetallic unit is also retained. The basal plane about Mn(1) is composed of two oxygen atoms (one still carrying the proton) from each of the two macrocycles [Mn(1)–O(1) = 2.116(4), Mn(1)–O(2) = 2.133(4), Mn(1)–O(5) = 2.333(4), Mn(1)–O(7) = 2.099(5) Å, O(1)–Mn(1)–O(2) = 85.35(15), O(1)–Mn(1)–O(5) = 82.67(15), O(1)–Mn(1)–O(7) = 153.34(17)°]. The axial position is occupied by the last phenoxide group of the first ligand and which incidentally is also bridging the second manganese atom of

the dimetallic unit by occupying its axial position [Mn(1)–O(6) = 2.013(4) Å, O(6)–Mn(1)–O(1) = 91.44(16), O(6)–Mn(1)–O(2) = 98.03(16)°] (see Figure 4.4.14).

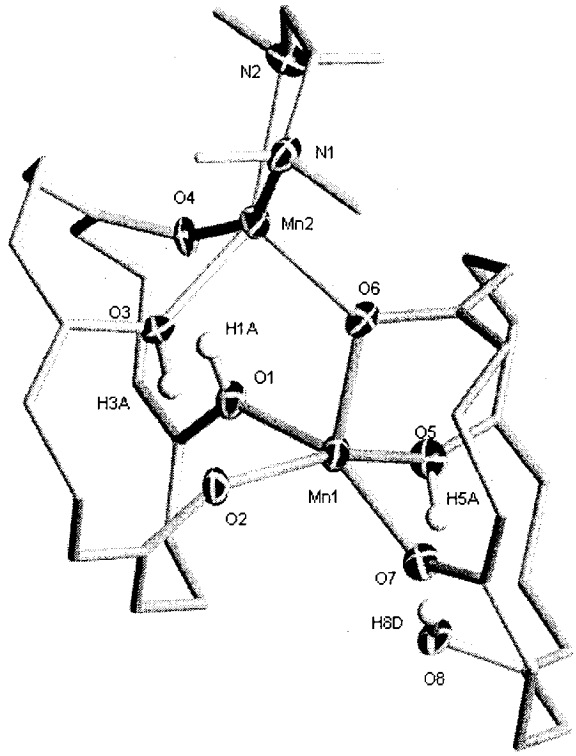

Figure 4.4.14 Core of Complex **7** with 30 % Thermal Ellipsoids, Carbon Ellipsoids not Drawn for Clarity.

The second Mn(2) atom is in a similar coordination environment with the only difference being that TMEDA now occupies two of the basal positions, along with the two oxygen atoms of one ligand, one having been deprotonated and the second carrying the proton [Mn(2)–N(1) = 2.308(5), Mn(2)–N(2) = 2.347(5), Mn(2)–O(3) = 2.136(4), Mn(2)–O(4) = 2.077(4) Å, N(1)–Mn(2)–N(2) = 76.5(2), N(1)–Mn(2)–O(3) = 93.9(2), N(1)–Mn(2)–O(4) = 155.96(18)°]. The phenoxide bridging the two manganese atoms occupy the axial position of both metals [Mn(2)–O(6) = 2.078(4) Å, O(6)–Mn(2)–N(1) = 111.15(18), O(6)–Mn(2)–N(2) = 115.29(19)°]. This complex represents the first time that we have successfully synthesized two of the most important motifs in the OEC. Those being a Mn-O-Mn bond and a Mn-OH bond in close proximity. Arguably, both the bridging

oxygen and the M-OH are still bonded to the calixarene ligand, but they do represent an important structural scaffold.

The reaction of two equivalents of the Mn-dialkyl [(TMEDA)Mn(CH_2SiMe_3)$_2$] with the calixarene ligand led to the expected, fully deprotonated, dinuclear calixarene complex [(η_1-TMEDA)Mn(η_3:μ_2-Calix)Mn(η_1-TMEDA)] (**8**) (See Figure 4.4.15).

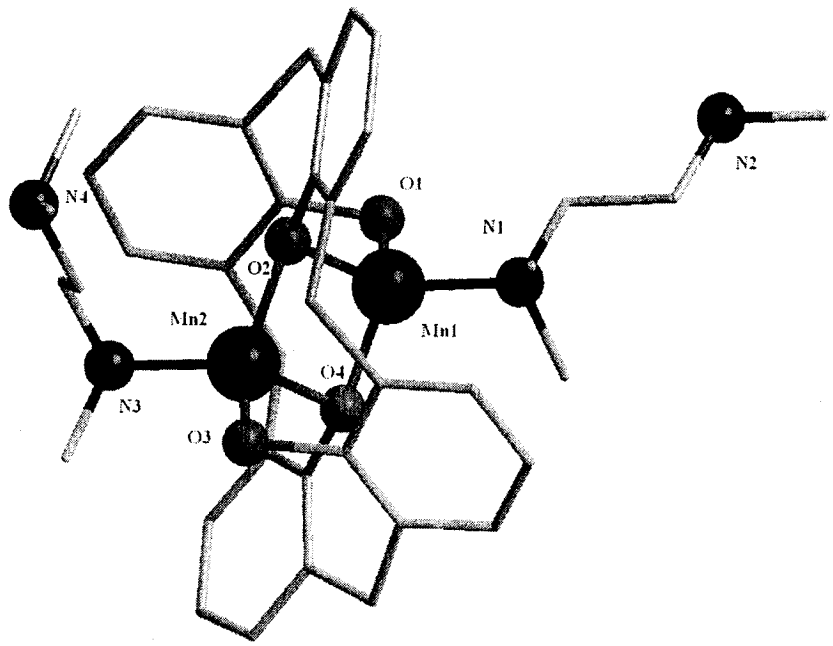

Figure 4.4.15 Structure of Complex **8**, *para*-^{t}Bu Groups Removed for Clarity.

The dinuclear structure contains two identical, tetrahedrally coordinated Mn atoms. Each atom is σ-bound to one phenoxide and shares two further bridging phenoxides, the final position of the tetrahedron is filled by an η_1-bound TMEDA molecule [Mn(1)–O(1) = 1.868(5), Mn(1)–O(2) = 1.911(4), Mn(1)–O(4) = 1.919(5), Mn(1)–N(1) = 2.070(4) Å, O(1)–Mn(1)–N(1) = 103.24(10), O(1)–Mn(1)–O(4) = 128.15(11) , O(1)–Mn(1)–O(2) = 103.21(10)°]. The short Mn-Mn distance (2.716 Å) and low magnetic moment (6.98 μ_B) indicates that there is most likely a magnetic interaction between the two metals. A unique feature of this complex is the unusual chair-like conformer that the calix[4]arene must adopt in order to accommodate the two Mn atoms. Replacement of the TMEDA molecules by water molecules is of course the next step in developing this molecule.

These two unprecedented compounds displayed a great potential for the water splitting reaction given their oxygen donor-atom-only type of environment and the compatibility with the presence of OH functions. It is therefore most unfortunate that attempts to oxidize the complex towards the oxidation state +4 (expected to be sufficiently reactive to extract a hydrogen atom from water) were unsuccessful. For this reason we have attempted the synthesis of other Mn complexes with a less restraining ligand system. The bis-phenoxide, a close relative to calixarene, was the most immediate choice. Reaction of the bis-phenol ligand with $[Mn(CH_2SiMe_3)_2(THF)]_2$ led to the dimeric structure $[Mn(\eta^1{:}\mu\text{-}\eta^1\text{-bisPhenoxide})(THF)]_2{\cdot}(hexane)_{0.875}$ (**9**) (see Figure 4.4.16). The dimeric structure is reminiscent of the dipyrrole complexes, with the exception that only one THF molecule remains coordinated to each Mn atom.

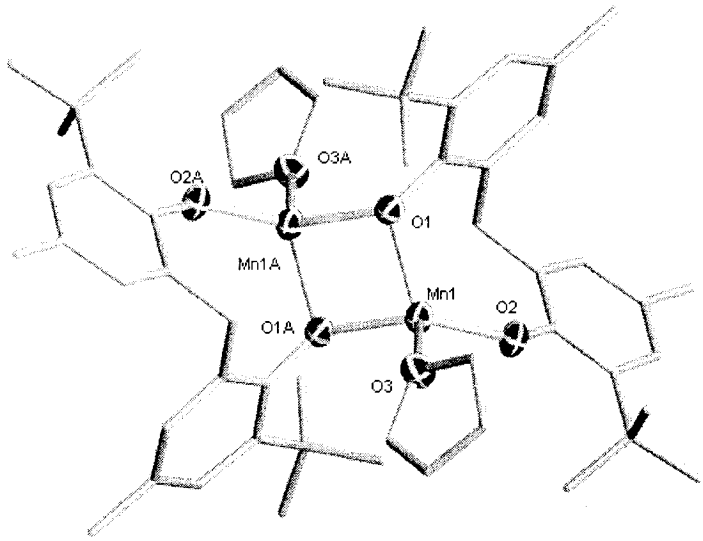

Figure 4.4.16 Structure of **9** with 30 % Thermal Ellipsoids, Carbon Ellipsoids not Drawn for Clarity.

Each Mn atom is in a tetrahedral coordination geometry comprised of one terminal phenoxide and two bridging phenoxides, the final position is occupied by a molecule of THF [Mn(1)–O(1) = 2.100(4), Mn(1)–O(1a) = 2.077(4), Mn(1)–O(2) = 1.953(4), Mn(1)–O(3) = 2.129(4) Å, O(2)–Mn(1)–O(1) = 115.95(16), O(2)–Mn(1)–O(1a) = 131.81(16), O(2)–Mn(1)–O(3) = 102.25(17)°]. The Mn-Mn distance of 2.767(4) Å is sufficiently short to allow for a direct metal-metal interaction. The low magnetic moment 6.84 μ_B is

slightly lower than the dipyrrolides ligand system, and is indicative of electronic interaction between the Mn centres. Even in this case attempts to oxidize these complexes with a variety of oxidizing agents were not successful, perhaps due to involvement of the aryloxide ligand system in the oxidation reaction.

The idea for the final complex synthesis stemmed from the research into CO_2 co-polymerization (see Chapter 5). It was observed that the [(NacNac)Mn(CH_2SiMe_3)] would be ideally suited to create a hydroxide bridge with another Mn atom if a hydrolysis was performed on the complex (see Scheme 4.4.17).

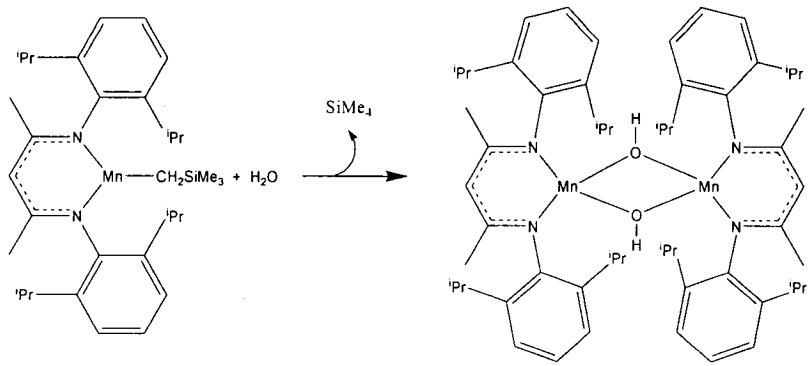

Scheme 4.4.17 Proposed Structure Formation.

A THF solution containing the stoichiometric amount of water was slowly added to another solution containing [(NacNac)Mn(CH_2SiMe_3)], and resulted in the dimeric complex [(NacNac)Mn(μ-OH)]$_2$ (**10**) (see Figure 4.4.18).

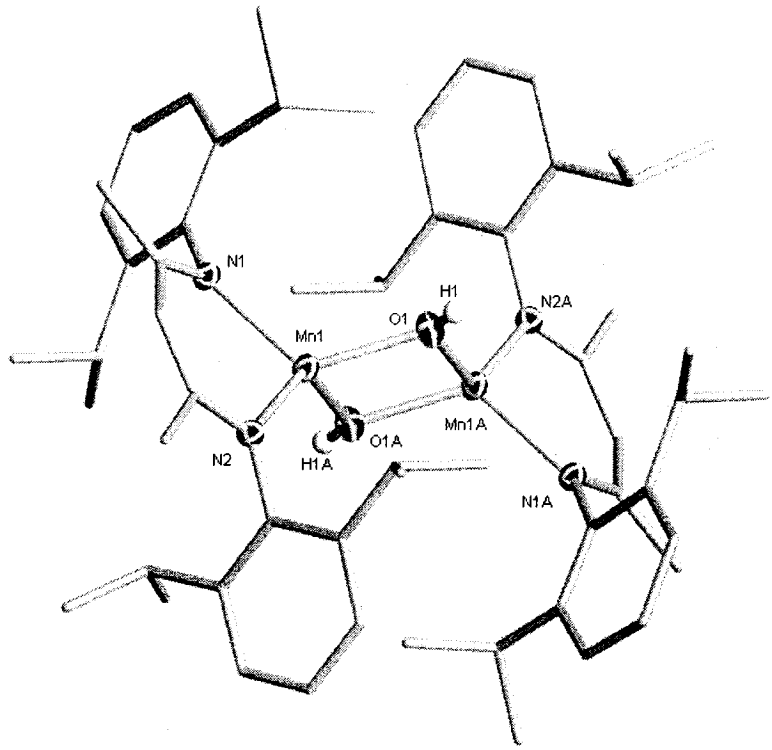

Figure 4.4.18 Structure **10** with 30 % Thermal Ellipsoids, Carbon Ellipsoids not Drawn for Clarity.

The complex adopts a tetrahedral geometry with two positions occupied by the NacNac ligand, and the remaining two filled by bridging OH groups [Mn(1)–N(1) = 2.113(4), Mn(1)–N(2) = 2.112(3), Mn(1)–O(1) = 2.054(4), Mn(1)–O(1a) = 2.039(4) Å, N(1)–Mn(1)–N(2) = 91.60(14), N(1)–Mn(1)–O(1) = 120.80(15), N(1)–Mn(1)–O(1a) = 122.37(16)°]. The long Mn-Mn distance (3.1456(14) Å) again precludes direct metal-metal bonding, but the low magnetic moment as per usual indicates that there is electronic interaction between the two Mn centres (μ_{eff} = 7.9 μ_B).

The presence of the isolable Mn-OH moiety was a major breakthrough in this project and represented the closest structural match with the proposed OEC. If the proposed reaction mechanism for oxygen evolution is correct, it may be possible to convert this Mn-OH species into the per-oxo derivative (see Scheme 4.2.2) and perhaps eventually even to eliminate dioxygen.

4.5 Reactivity with Oxygen Sources:

Once all of the cluster compounds had been synthesized, their reactivity with O_2 was systematically scanned. The oxygen was first dried in a P_2O_5 column in order to

remove any traces of water. In every case instantaneous reactions were observed as indicated by the immediate color change upon exposure of the various complex solutions to dry oxygen. Unfortunately, in all cases except the calixarene ligand, the reactions produced insoluble gel-like precipitates. The precipitates were insoluble in all available organic solvents, including pyridine. Further attempts at solubilization of the complexes included the use of polar solvents (ie. DMSO, DMF, acetonitrile); with similar results. Polar protic solvents including methanol, ethanol, and isopropanol also failed to solubilise the materials. In the case of the calixarene, the solutions quickly turned purple, and insoluble products were formed. The sudden darkening of the nearly colourless $Mn^{(II)}$ solutions is a clear indication that oxidation state of the metal was increased. It was argued that the lack of stoichiometry control in terms of calibrating the amount of oxygen could have been at the basis of the problem. Therefore it was decided to attempt the reaction using a single oxygen donor material. Triphenylphosphine oxide is a known molecular oxygen transfer agent and therefore the logical choice for further testing.[23] The reactions proceeded in much the same manner as the previous cases with the exception that the colour change to the brown or purple insoluble materials took significantly longer. This again indicates that higher valent manganese species were being generated. Regrettably, all these species proved impossible to crystallize in spite of the variety of ligands and solvents and therefore escape so far crystallographic characterization.

4.6 Aqueous Synthesis:

The failure to obtain higher valent manganese complexes via oxidation of the well-defined divalent compounds described above was disappointing and seemed to bring us to a deadlock. Therefore, we have decided as the last attempt to probe the self-assembling synthetic approach. Instead of preparing well-defined divalent complexes for further oxidation, we have now tried the in situ oxidation of a simple $Mn^{(II)}$ salt in water medium and in the presence of a variety of ligands. In one case, the reaction was very successful by providing a $Mn^{(IV)}$ complex which appears to spontaneously react with water through a redox process to eliminated O_2.

A screening of reactions was performed which combined $[Mn(OAc)_2]$ and $KMnO_4$ with many simple, poly-alcohol and carboxylic acid containing, organic molecules in water. The vast majority of these reactions led to intractable materials; however, in one instance a compound was successfully characterized. The equimolar reaction of $[Mn(OAc)_2]$ and $KMnO_4$ in the presence of aqueous tartaric acid led to the isolation of brown crystals of the polymeric $[Mn(\mu_3,\eta_2\text{-}O_2CCH(O)CH(O)CO_2)(H_2O)_{0.5}]_n \cdot H_2O_{1.5}$ (**11**) (n = ∞) (see Figure 4.6.1).

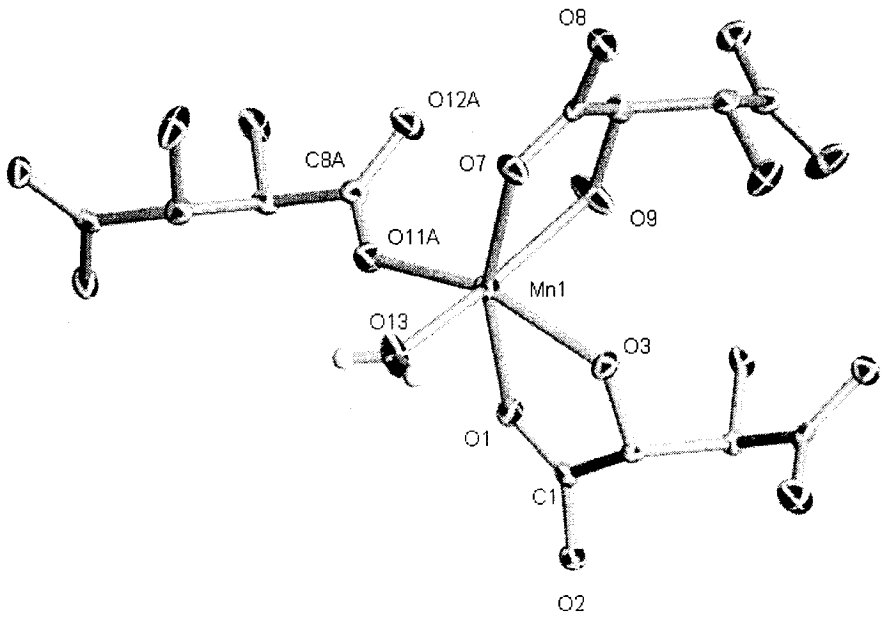

Figure 4.6.1 Truncated Structure of **11** with 30% Thermal Ellipsoids, Carbon Ellipsoids and Solvent Water Molecules not Drawn for Clarity.

Analysis of the crystal structure revealed an infinite three dimensional polymer in which each Mn atom is found in an octahedral coordination environment. Five of the octahedron positions are filled by the oxygen atoms of the fully deprotonated tartarate molecules, with the final position alternating regularly between a bound water molecule (as seen in Figure 4.6.1) or a tartarate oxygen atom. The slightly distorted octahedral geometry is comprised of three carboxylate donor groups and one alkoxide along the equatorial plane [Mn(1)–O(1) = 2.184(4), Mn(1)–O(7) = 2.135(4), Mn(1)–O(11a) = 2.105(3), Mn(1)–O(3) = 2.206(4) Å, O(1)–Mn(1)–O(3) 73.08(9), O(1)–Mn(1)–O(7) 160.88(12), O(1)–Mn(1)–O(13) 96.33(9)°]. The axial positions are filled by a water

molecule and an alkoxide donor from one of the fully deprotonated tartarate ligands [Mn(1)–O(13) = 2.134(4), Mn(1)–O(9) = 2.268(4) Å, O(13)–Mn(1)–O(9) = 166.82(13)°].

If the complex is allowed to stand at room temperature for several days the dark brown colour, which is normally associated with $Mn^{(IV)}$, slowly fades leaving a pale pink precipitate. Subsequent treatment with $KMnO_4$ restores the solution to its previous brown colouring. This observation led us to hypothesize that the compound may, in fact, be liberating O_2 from the water and concomitantly reducing to a lower valent oxidation state. Heating of the brown solution to 90 °C resulted in a very quick discolouration and the moderate evolution of a gas from the solution. Subsequent testing of the atmosphere of the solution with a portable oxygen sensor indicated that appreciable amounts of O_2 were being emitted.

This very preliminary work has sparked continuing research in this field which is even now being carried out by our group. Several very important questions must be answered about this observed O_2 evolution before it can truly be declared a breakthrough: 1) will careful quantification of the O_2 evolved indicate an appreciable activity per mol of Mn 2) is the source of the oxygen truly from the solvent water, or merely from the strong oxidant $KMnO_4$ 3) can this process be coupled with a photo-oxidant to provide a truly "green" reaction.

4.7 Conclusions:

This work has demonstrated that the assembly of dimeric, tetrameric, and even octameric Mn complexes is possible with the selected ligands. Furthermore, the nuclearity of the clusters was found to be strongly influenced by the nature of the solvent, with non-coordinating solvents tending to produce larger clusters. These clusters are assembled via the weak π-ligation of the pyrrolide rings. This weakness is demonstrated via the conversion of the cluster to dimers in the presence of co-ordinating solvents like THF. The results of the reactions of the clusters with oxygen sources were partly disappointing, as none proved to be characterizable. That said, the colour changes clearly indicate that higher oxidation state Mn centres have, indeed, been generated. Future work may yield the chemical structures of these higher oxidation state complexes. Literature published in 2006 has indicated that PhIO[24] may prove to be a more efficient

and cleaner oxygen transfer agent then the triphenylphophine oxide which was utilized, thus providing another avenue for future research into this area.

The calixarene, and NacNac Mn structures represent the most valuable contributions of this work towards assembling a surrogate for the OEC. The calixarene structure (**8**) contains both the Mn-O-Mn and Mn-OH moieties which have been proposed to be integral parts of the OEC cluster. In the case of the NacNac Mn complex (**10**) the two bridging Mn-OH moieties in close proximity to one another may yet yield the best chance of generating peroxo species, and maybe eventually even yield di-oxygen.

By far the most intriguing results to date though, are those produced by the aqueous tartarate system (**11**). The observation that O_2 is evolved from this system could elevate this system to the forefront of this type of chemistry. That said, much more testing is required, and is currently underway, to ensure that this system is as remarkable as this introductory evaluation makes it appear.

4.8 X-Ray Crystallography Section:

The full crystallographic data, including bond lengths and angles may be found in Appendix 4. The abbreviated crystallographic data for the structures contained within this chapter are as presented in Tables 4.8.1 to 4.8.4.

Table 4.8.1 Crystal Data and Structure Analysis Results for Complexes **1-3**.

	1	**2**	**3**
Formula	$C_{42}H_{64}Mn_2N_4O_4$	$C_{68}H_{112}Mn_2N_4O_8$	$C_{52}H_{80}Mn_2N_4O_5$
FW	798.85	1223.50	951.11
space group	Monoclinic, *P2(1)/n*	Triclinic, *P-1*	Monoclinic, *P2(1)/c*
a (Å)	9.516(2)	9.699(2)	10.6733(11)
b (Å)	13.816(3)	12.460(3)	11.8769(13)
c (Å)	15.259(4)	15.902(4)	19.867(2)
α (deg)	90	111.355(4)	90
β (deg)	94.354(4)	98.938(4)	97.054(2)
γ (deg)	90	101.703(4)	90
V (Å^3)	2000.4(8)	1696.6(6)	2499.4(5)
Z	2	1	2
radiation (Kα, Å)	0.71073	0.71073	0.71073
T (K)	203(2)	203(2)	203(2)
D_{calcd} (g cm^{-3})	1.326	1.198	1.285
μ_{calcd} (mm^{-1})	0.677	0.426	0.557
F_{000}	852	662	1036
R, R_w[2 a]	0.0622, 0.1246	0.0690, 0.1202	0.0503, 0.1379
GoF	1.051	1.010	1.023

[a] $R = \Sigma||Fo| - |Fc||/\Sigma|Fo|$. $Rw = [\Sigma(|Fo| - |Fc|)^2/\Sigma wFo^2]^{1/2}$.

Table 4.8.2 Crystal Data and Structure Analysis Results for Complexes **4-6**.

	4	**5**	**6**
Formula	$C_{140}H_{160}Mn_8N_{16}$	$C_{44}H_{38}MnN_4$	$C_{190}H_{170}Mn_4N_{12}$
FW	2506.36	677.72	2841.14
space group	Orthorhombic, *Pbcn*	Monoclinic, *C2/c*	Triclinic, *P-1*
a (Å)	26.483(9)	25.811(5)	18.65(4)
b (Å)	20.351(7)	10.2964(18)	19.51(2)
c (Å)	23.459(8)	26.128(5)	21.61(3)
α (deg)	90	90	98.20(9)
β (deg)	90	91.159(3)	95.53(16)
γ (deg)	90	90	100.96(15)
V (Å^3)	12 643(7)	6 942(2)	7 579(20)
Z	4	8	2
radiation (Kα, Å)	0.71073	0.71073	0.71073
T (K)	203(2)	206(2)	209(2)
D_{calcd} (g cm^{-3})	1.317	1.297	1.245
μ_{calcd} (mm^{-1})	0.828	0.418	0.385
F_{000}	5248	2840	2988
R, R_w[2 a]	0.0603, 0.1339	0.0735, 0.1639	0.0698, 0.1501
GoF	1.038	1.066	1.025

[a] $R = \Sigma||Fo| - |Fc||/\Sigma|Fo|$. $Rw = [\Sigma(|Fo| - |Fc|)^2/\Sigma wFo^2]^{1/2}$.

Table 4.8.3 Crystal Data and Structure Analysis Results for Complexes **7-9**.

	7	**8**	**9**
Formula	$C_{122}H_{156}Mn_2N_2O_8$	$C_{56}H_{84}Mn_2N_4O_4$	$C_{56.5}H_{81.5}Mn_2O_6$
FW	1888.37	987.17	966.60
space group	Orthorhombic, *P2(1)2(1)2(1)*	Monoclinic, *C2/c*	Monoclinic, *P2(1)/c*
a (Å)	17.378(5)	12.523(6)	12.473(3)
b (Å)	17.502(5)	17.288(8)	17.353(5)
c (Å)	37.511(10)	17.111(6)	17.081(4)
α (deg)	90	90	90
β (deg)	90	90.542(5)	108.568(4)
γ (deg)	90	90	90
V (Å^3)	11 409(5)	7 495(5)	3504.4(16)
Z	4	4	2
radiation (Kα, Å)	0.71073	0.71073	0.71073
T (K)	206(2)	206(2)	203(2)
D_{calcd} (g cm^{-3})	1.099	1.186	0.916
μ_{calcd} (mm^{-1})	0.275	0.563	0.396
F_{000}	4064	3053	1037
R, R_w[2 a]	0.0737, 0.1437	0.0841, 0.1782	0.0799, 0.1875
GoF	1.047	1.066	1.038

[a] $R = \Sigma||Fo| - |Fc||/\Sigma|F|$. $Rw = [\Sigma(|Fo| - |Fc|)^2/\Sigma wFo^2]^{1/2}$.

Table 4.8.4 Crystal Data and Structure Analysis Results for Complexes **10** and **11**.

	10	**11**
Formula	$C_{58}H_{84}Mn_2N_4O_2$	$C_8H_{12}Mn_2O_{16}$
FW	979.18	474.06
space group	Monoclinic, *C2/c*	Monoclinic, *P2(1)*
a (Å)	23.022(4)	7.6033(11)
b (Å)	14.820(2)	11.1919(16)
c (Å)	16.219(3)	8.9855(12)
α (deg)	90	90
β (deg)	91.294(3)	99.432(2)
γ (deg)	90	90
V (Å^3)	5 532.0(16)	754.29(18)
Z	4	2
radiation (Kα, Å)	0.71073	0.71073
T (K)	209(2)	213(2)
D_{calcd} (g cm^{-3})	1.176	2.087
μ_{calcd} (mm^{-1})	0.499	1.766
F_{000}	2104	476
R, R_w[2 a]	0.0749, 0.1400	0.0366, 0.0862
GoF	1.053	1.060

[a] $R = \Sigma||Fo| - |Fc||/\Sigma|F|$. $Rw = [\Sigma(|Fo| - |Fc|)^2/\Sigma wFo^2]^{1/2}$.

4.9 Experimental Section:

All reactions were carried out under a dry nitrogen or argon atmosphere. Solvents were dried using an aluminum oxide solvent purification system. The dipyrrolide,[25] calix[4]arene,[19] and NacNac[26] ligands were prepared using literature preparations. N-MeDipyr, and N-MeTripyr were prepared as detailed in Chapter 2. $[Mn(CH_2SiMe_3)(THF)]_2$ and $[(TMEDA)Mn(CH_2SiMe_3)_2]$ were prepared as detailed in Chapter 3, while $[NacNacMn(CH_2SiMe_3)]$ was prepared as detailed in Chapter 5. Infrared spectra were recorded on an ABB Bomem FTIR instrument from Nujol mulls prepared in a drybox. Samples for magnetic susceptibility were pre-weighed inside a drybox equipped with an analytical balance and measured on a Johnson Matthey Magnetic Susceptibility balance. Samples of **3** and **4** for magnetic susceptibility measurements were preweighed inside a drybox equipped with an analytical balance and flame sealed into calibrated 5 mm "o.d." quartz tubes. Magnetic measurements were carried out using a Quantum Design MPMS5S SQUID magnetometer at 0.1 T, in the temperature range 2-300 K. The accurate sample mass was determined by difference by breaking the tube after data collection. Background data on the cleaned, empty tube were obtained under identical experimental conditions. Standard corrections for underlying diamagnetism were applied to data.[27] Elemental analysis was carried out with a Perkin-Elmer 2400 CHN analyzer. Data for X-ray crystal structure determination were obtained with a Bruker diffractometer equipped with a 1K Smart CCD area detector.

Synthesis of $[Mn(\eta^1{:}\mu\text{-}\eta^1\text{-}Et_2Dipyr)(THF)_2]_2$ (1): $Et_2DipyrH_2$ (0.250 g, 1.24 mmol) was dissolved in 15 mL of THF and $[Mn(CH_2SiMe_3)(THF)]_2$ (0.5 eq, 0.186 g, 0.62 mmol) was dissolved in a separate vial in 15 ml of THF. The ligand was then added drop-wise to the Mn di-alkyl over the span of ~ 1 minute. The colour gradually lightened from light-orange to a light pink/colourless solution. The solution was then cooled to -35 °C and stored for 4 days after which time 0.401 g of pale pink block crystals of X-ray quality formed (1.00 mmol, 81.1% Yield).

IR (KBr, Nujol, cm^{-1}): 3083 (w), 3078 (w), 1162 (w), 1129 (w), 1063 (m), 1032 (s), 962 (w), 955 (w), 901 (m), 877 (m), 830 (w), 736 (m), 724 (m), 712 (m), 634 (w).

Elemental Analysis calcd (Found) for $Mn_2C_{42}H_{64}N_4O_4$: C 63.15 (63.25), H 8.08 (8.22), N 7.01 (7.22). $\mu_{eff} = 7.14\ \mu_B$.

Synthesis of [Mn(η^1:μ-η^1-MentDipyr) (THF)$_2$]$_2$·(THF)$_4$ (2): MentDipyrH$_2$ (0.250 g, 0.925 mmol) was dissolved in 15 mL of THF and [Mn(CH_2SiMe_3)(THF)]$_2$ (0.5 eq, 0.139 g, 0.462 mmol) was dissolved in a separate vial in 15 ml of THF. The ligand was then added drop-wise to the Mn di-alkyl over the span of ~ 1 minute. The colour gradually lightened from light-orange to a light pink/colourless solution. The solution was then cooled to -35 °C and stored for 8 days after which time 0.448 g of pale pink block crystals of X-ray quality formed (0.367 mmol, 79.3% Yield).

IR (KBr, Nujol, cm^{-1}): 3086 (w), 3084 (w), 1163 (w), 1125 (w), 1062 (m), 1026 (s), 964 (w), 951 (w), 902 (m), 871 (m), 828 (w), 737 (m), 729 (m), 715 (m), 633 (w).

Elemental Analysis calcd (Found) for $Mn_2C_{68}H_{112}N_4O_8$: C 66.75 (66.61), H 9.23 (9.22), N 4.58 (4.44). $\mu_{eff} = 7.08\ \mu_B$.

Synthesis of [Mn(η^1:μ-η^1-CyDipyr)(THF)$_2$]$_2$·(THF) (3): CyDipyrH$_2$ (0.250 g, 1.17 mmol) was dissolved in 15 mL of THF and [Mn(CH_2SiMe_3)(THF)]$_2$ (0.5 eq, 0.175 g, 0.583 mmol) was dissolved in a separate vial in 15 ml of THF. The ligand was then added drop-wise to the Mn di-alkyl over the span of ~ 1 minute. The colour gradually lightened from light-orange to a light pink/colourless solution. The solution was then cooled to -35 °C and stored for 1 day after which time 0.418 g of pale pink block crystals of X-ray quality formed (0.440 mmol, 75.4% Yield).

IR (KBr, Nujol, cm^{-1}): 3088 (w), 3086 (w), 1164 (w), 1127 (w), 1065 (m), 1030 (s), 965 (w), 952 (w), 905 (m), 874 (m), 829 (w), 738 (m), 726 (m), 714 (m), 631 (w).

Elemental Analysis calcd (Found) for $Mn_2C_{52}H_{80}N_4O_5$: C 64.85 (64.55), H 8.34 (8.29), N 5.79 (5.69). $\mu_{eff} = 7.02\ \mu_B$.

Synthesis of [Mn(η^1:μ–η^5-CyDipyr)]$_8$·(toluene)$_4$ (4): $CyDipyrH_2$ (0.250 g, 1.17 mmol) was dissolved in 15 mL of toluene and $[Mn(CH_2SiMe_3)(THF)]_2$ (0.5 eq, 0.175 g, 0.583 mmol) was dissolved in a separate vial in 15 ml of toluene. The ligand was then added drop-wise to the Mn di-alkyl over the span of ~ 1 minute. The colour gradually lightened from light-orange to a colourless solution. The solution was then allowed to stand for 24 hours at room temperature, followed by cooling to -35 °C for a subsequent 24 hrs after which time 0.418 g of colourless block crystals of X-ray quality formed (0.440 mmol, 96.2% Yield).

IR (KBr, Nujol, cm^{-1}): 3370 (w), 3088 (w), 1609 (w), 1300 (w), 1272 (m), 1200 (s), 1161 (s), 1129 (s), 1106 (m), 1033 (s), 965 (m), 906 (m), 872 (w), 851 (w), 830 (w), 790 (s), 744 (s), 693 (m), 621 (m).

Elemental Analysis calcd (Found) for $Mn_8C_{140}H_{160}N_{16}$: C 67.09 (67.01), H 6.43 (6.39), N 8.94 (8.88). μ_{eff} = 14.07 μ_B.

Synthesis of [Mn(N-MeDipyr)$_2$] (5): N-MeDipyrH (0.250 g, 0.800 mmol) was dissolved in 15 mL of toluene and $[Mn(CH_2SiMe_3)(THF)]_2$ (0.5 eq, 0.121 g, 0.400 mmol) was dissolved in a separate vial in 15 ml of toluene. The ligand was then added drop-wise to the Mn di-alkyl over the span of ~ 1 minute. The colour gradually lightened from light-orange to a colourless solution. The solution was then allowed to stand for 24 hours at room temperature, followed by cooling to -35 °C for another 24 hrs after which time 0.247 g of colourless block crystals of X-ray quality formed (0.365 mmol, 91.1% Yield).

IR (KBr, Nujol, cm^{-1}): 3088 (w), 3086 (w), 1164 (w), 1127 (w), 1065 (m), 1030 (s), 965 (w), 952 (w), 905 (m), 874 (m), 829 (w), 738 (m), 726 (m), 714 (m), 631 (w).

Elemental Analysis calcd (Found) for $MnC_{44}H_{38}N_4$: C 77.98 (78.01), H 5.65 (5.41), N 8.27 (8.43). μ_{eff} = 6.08 μ_B.

Synthesis of [Mn(η^1_2:η^5:μ-η^3-N-MeTripyr)]$_4$·(toluene)$_{4.85}$ (6): N-MeTripyrH·toluene (0.250 g, 0.393 mmol) was dissolved in 15 mL of toluene and [Mn(CH_2SiMe_3)(THF)]$_2$ (1.0 eq, 0.119 g, 0.393 mmol) was dissolved in a separate vial in 15 ml of toluene. The ligand was then added drop-wise to the Mn di-alkyl over the span of ~ 1 minute. The colour gradually lightened from light-orange to a colourless solution. The solution was then allowed to stand for 24 hours at room temperature, followed by cooling to -35 °C for another 24 hrs after which time 0.248 g of colourless block crystals of X-ray quality formed (8.73 X 10^{-5} mol, 88.9% Yield).

IR (KBr, Nujol, cm^{-1}): 3368 (w), 1607 (w), 1303 (w), 1261 (m), 1196 (s), 1158 (s), 1133 (s), 1106 (m), 1030 (s), 966 (m), 900 (m), 866 (w), 822 (w), 799 (s), 745 (s), 690 (m), 617 (m).

Elemental Analysis calcd (Found) for $Mn_4C_{190}H_{170}N_{12}$: C 80.32 (80.51), H 6.03 (6.11), N 5.92 (6.09). μ_{eff} = 10.37 μ_B.

Synthesis of [(Calix(OH)$_2$)Mn-(μ-O)-Mn(Calix(OH)$_2$)(TMEDA)] (7): 4-^{t}Bu$_4$-Calix[4]arene·(toluene)$_{1.5}$ (0.250 g, 0.318 mmol) was dissolved in 15 mL of THF and [(TMEDA)Mn(CH_2SiMe_3)$_2$] (1.0 eq, 0.110 g, 0.318 mmol) was dissolved in a separate vial in 15 ml of THF. The Mn di-alkyl was then added drop-wise to the ligand solution over the span of ~ 1 minute. The colour gradually lightened from light-orange to a colourless solution. The solution was then allowed to stand for 24 hours at room temperature, followed by cooling to -35 °C for another 24 hrs after which time 0.251 g of colourless crystals of X-ray quality formed (0.133 mmol, 83.6% Yield).

IR (KBr, Nujol, cm^{-1}): 3155 (s,br), 1604 (s), 1477 (s), 1362 (s), 1304 (s), 1237 (m), 1109 (m), 1118 (w), 899 (m), 870 (s), 816 (s), 782 (s), 729 (m), 695 (w), 673 (w), 591(w).

Elemental Analysis calcd (Found) for $Mn_2C_{122}H_{156}N_2O_8$: C 77.59 (77.54), H 8.33 (8.49), N 1.48 (1.62). μ_{eff} = 7.36 μ_B.

Synthesis of [(Calix)Mn_2(TMEDA)$_2$] (8): 4-^{t}Bu_4-Calix[4]arene·(toluene)$_{1.5}$ (0.125 g, 0.159 mmol) was dissolved in 15 mL of THF and [(TMEDA)Mn(CH_2SiMe_3)$_2$] (2.0 eq, 0.110 g, 0.318 mmol) was dissolved in a separate vial in 15 ml of THF. The Mn di-alkyl was then added drop-wise to the ligand solution over the span of ~ 1 minute. The colour gradually lightened from light-orange to a colourless solution. The solution was then allowed to stand for 24 hours at room temperature, followed by cooling to -35 °C for another 24 hrs after which time 0.196 g of colourless crystals of X-ray quality formed (0.099 mmol, 62.2% Yield).

IR (KBr, Nujol, cm^{-1}): 1606 (w), 1303 (m), 1303 (m), 1278 (w), 1201 (m), 1127 (w), 872 (m), 820 (m), 788 (w), 727 (m), 694 (w).

Elemental Analysis calcd (Found) for $Mn_2C_{56}H_{84}N_4O_4$: C 68.13 (68.54), H 8.58 (8.49), N 5.68 (5.62). μ_{eff} = 6.98 μ_B.

Synthesis of [NacNacMn(μ-OH)]$_2$ (10): [NacNacMn(CH_2SiMe_3)] (0.250 g, 0.447 mmol) was dissolved in 15 mL of THF and 8.93 mL of a 0.05 M water solution in THF was added drop-wise. The yellow solution did not progress through any colour change except a very slight lightening of the colour. The solution was then allowed to stand for 24 hours at room temperature, followed by cooling to -35 °C for another 24 hrs after which time 0.210 g of colourless block crystals of X-ray quality formed (0.215 mmol, 96.3% Yield).

IR (KBr, Nujol, cm^{-1}): 3688 (s), 1960 (m), 1815 (m), 1575 (m), 1558 (m), 1539 (m), 1506 (s), 1476 (s), 1457 (s), 1430 (s), 1386 (s), 1318 (s), 1261 (s), 1122 (m), 1070 (w).

Elemental Analysis calcd (Found) for $Mn_2C_{58}H_{84}N_4O_2$: C 71.14 (71.32), H 8.65 (8.59), N 5.72 (5.82). μ_{eff} = 7.27 μ_B.

Synthesis of [Mn(μ_3,η_2-O_2CCH(O)CH(O)CO_2)(H_2O)$_{0.5}$]$_n$· $H_2O_{1.5}$ (11): [Mn(OAc)$_2$] (0.150 g, 0.86 mmol) and tartaric acid (0.141 g, 0.94 mmol, 1.1 eq.) were dissolved in 15 mL of stirring distilled deionized water. $KMnO_4$ (0.135 g, 0.86 mmol, 1.0 eq) was then

added to the stirring mixture resulting in a dark purple solution, which over the course of several hours gradually turned dark brown. After stirring for 8 hours the stir bar was removed and the solution was left at room temperature for several days. After several days crystals of X-ray quality were collected (0.213 g, 0.45 mmol, 52.2% yeild).

IR (KBr pellet, cm^{-1}): 3598 (m,br), 3359 (m,br), 1610 (s,br), 1397 (m, br), 1294 (m), 1234 (m), 1215 (m), 1123 (m), 1047 (m), 1002 (w), 933 (w), 895 (w), 835 (w), 713 (m).

Elemental Analysis calcd (Found) for $MnC_4H_6O_8$: C 26.53 (26.54), H 2.78 (2.88). μ_{eff} = 3.36 μ_B.

4.10 References:

1) Das, V. R. M. *Photosynthesis : regulation under varying light regimes* Science Publishers: Enfield, New Hampshire, **2004**.
2) McIntosh, L. *Photosynthesis : molecular biology of energy capture* Academic Press: San Diego, CA, **1998**.
3) biochem book
4) Sauer, K.; Yachandra, V. K. *Biochim. Biophys. Acta: Bioenerg.* **2004**, *1655*, 140.
5) Dau, H.; Iuzzolino, L.; Dittmer, J. *Biochim. Biophys. Acta: Bioenerg.* **2001**, *1503*, 24.
6) Szalai, V. A.; Kuhne, H.; Brudvig, G. W. *Biochemistry* **1998**, *37*, 13594.
7) *Biochimica et Biophysica Acta: Bioenergetics* **2001**, *1503*, 1-259
8) Joliot, P.; Barbieri, G.; Chabaud, R. *Photochem. Photobiol.* **1969**, *10*, 309. b) Kok, B.; Forbush, B.; McGloin, M. *Photochem. Photobiol.* **1970**, *11*, 457.
9) Robblee, J. H.; Cinco, R. M.; Yachandra, V. K. *Biochim. Biophys. Acta.: Bioenerg.* **2001**, *1503*, 7.
10) Philouze, C.; Blondin, G.; Girerd, J. –J.; Guilhem, J.; Pascard, C.; Lexa, D. *J. Am. Chem. Soc.* **1994**, *116*, 8557. b) Plaskin, P. M.; Stoufer, R. C.; Mathew, M.; Palenik, G. K. *J. Am .Chem. Soc.* **1972**, *94*, 2121. c) Auger, N.; Girerd, J. –J.; Corbella, M.; Gleizes, A.; Zimmermann, J. –L. *J. Am. Chem. Soc.* **1990**, *112*, 448.
11) Boussac, A.; Zimmermann, J. –L.; Rutherford, A. W. *Nature* **1990**, *347*, 303.
12) Biesiadka, J.; Loll, B.; Kern, J.; Irrgang, K. –D.; Zouni, A. *Phys. Chem. Chem. Phys.* **2004**, 4733. b) Zouni, A.; Witt, H. –T.; Kern, J.; Fromme, P.; Krauss, N.; Saenger, W.; Orth, P. *Nature* **2001**, *409*, 739.
13) McEvoy, J. P.; Gascon, J. A.; Batista, V. S.; Brudvig, G. W. *Photochem. Photobiol. Sci.* **2005**, *4*, 940. b) McEvoy, J. P.; Brudvig, G. W. *Phys. Chem. Chem. Phys.* **2004**, *6*, 4754.
14) Isobe, H.; Shoji, M.; Koizumi, K.; Kitagawa, Y.; Yamanaka, S.; Kuramitsu, S.; Yamaguchi, K. *Polyhedron* **2005**, *24*, 2767.
15) Sarneski, J. E.; Thorp, H. H.; Brudvig, G. W.; Crabtree, R. H.; Schulte, G. K. *J. Am. Chem. Soc.* **1990**, *112*, 7255. b) Philouze, C.; Blondin, G.; Menage, S.; Auger, N.;

Girerd, J. –J.; Vigner, D.; Lance, M.; Nierlich, M. *Angew. Chem. Int. Ed.* **1992**, *31*, 1629.
16) Limburg, J.; Vrettos, J. S.; Liable-Sands, L. M.; Rheingold, A. L.; Crabtree, R. H.; Brudvig, G. W. *Science* **1999**, *283*, 1524.
17) Chen, H.; Tagore, R.; Das, S.; Incarvitto, C.; Faller, J. W.; Crabtree, R. H.; Brudvig, G. W. *Inorg. Chem.* **2005**, *44*, 7661. b) Limburg, J.; Vrettos, J. S.; Chen, H. Y.; de Paula, J. C.; Crabtree, R. H.; Brudvig, G. W. *J. Am. Chem. Soc.* **2001**, *123*, 423. c) Limburg, J.; Brudvig, G. W.; Crabtree, R. H. *J. Am. Chem. Soc.* **1997**, *119*, 2761.
18) Baffert, C.; Sophie Romain, S.; Richardot, A.; Jean-Claude Lepretre, J-C.; Lefebvre, B.; Alain Deronzier, A.; Collomb, M-N. *J. Am. Chem. Soc.* **2005**, *127*, 13694. b) Yagi, M.; Narita, K. *J. Am. Chem. Soc.* **2004**, *126*, 8084.
19) Simaan, S.; Biali, S. E. *J. Org. Chem.* **2003**, *68*, 3634. b) Gutsche, D. C.; Iqbal, M.; Stewart, D. *J. Org. Chem.* **1986**, *51*, 742.
20) Bukhaltsev, E.; Goldberg, I.; Vigalok, A. *Organometallics* **2005**, *24*, 5732. b) Cotton, F. A.; Daniels, L. M.; Lin, C.; Murillo, C. A. *Inorg. Chim. Acta* **2003**, *347*, 1. c) Iwasa, K.; Kochi, T.; Ishii, Y. *Angew. Chem. Int. Ed.* **2003**, *42*, 3658. d) Attner, J.; Radius, U. *Z. Anorg. Allg. Chem.* **2002**, *628*, 2345. e) Caselli, A.; Solari, E.; Scopelliti, R.; Floriani, C.; Re, N.; Rizzoli, C.; Chiesi-Villa, A. *J. Am. Chem. Soc.* **2000**, *122*, 3652. f) Chisholm, M. H.; Folting, K.; Strib, W. E.; Wu, D.-D. *Inorg. Chem.* **1999**, *38*, 5219. g) Zanotti-Gerosa, A.; Solari, E.; Giannini, L.; Floriani, C.; Chiesi-Villa, A.; Rizzoli, C. *J. Am. Chem. Soc.* **1998**, *120*, 437. h) Chisholm, M. H.; Folting, K.; Streib, W. E.; Wu, D.-D. *Chem. Commun.* **1998**, 379. i) Gardiner, M. G.; Lawrence, S. M.; Raston, C. L.; Skelton, B. W.; White, A. H. *Chem.Commun.* **1996**, 2491. j) Olmstead, M. M.; Sigel, G.; Hope, H.; Xu, X.; Power, P. P. *J. Am. Chem. Soc.* **1985**, *107*, 8087.
21) Crewdson, P.; Gambarotta, S.; Yap, G. P. A.; Thompson, L. K. *Inorg. Chem.* **2003**, *42*, 8579.
22) Fisher, M. E. *Am. J. Phys.* **1964**, *32*, 343.
23) Renehan, M. F.; Schanz, H. –J.; McGarrigle, E. M.; Dalton, C. T.; Daly, A. M.; Gilheany, D. G. *J. Molec. Catal. A.: Chem.* **2005**, *231*, 205.
24) Conley, B. L.; Ganesh, S. K.; Gonzales, J. M.; Tenn, W. J.; Young, K. J. H.; Oxgaard, J.; Goddard, W. A.; Periana, R. A. *J. Am. Chem. Soc.* **2006**, *128*, 9018. b) Bukowski, M. R.; Comba, P.; Lienke, A.; Limberg, C.; de Laorden, C. L.; Mas-Ballest, R.; Merz, M.; Que, L. *Angew. Chem. Int. Ed.* **2006**, *45*, 3446. c) Suh, Y.; Seo, M. S.; Kim, K. M.; Kim, Y. S.; Jang, H. G.; Tosha, T.; Kitagawa, T.; Kim, J.; Nam, W. *J. Inorg. Biochem.* **2006**, *100*, 627. d) Lansky, D. E.; Mandimutsira, B.; Ramdhanie, B.; Clausen, M.; Penner-Hahn, J.; Zvyagin, S. A.; Telser, J.; Krzystek, J.; Zhan, R.; Ou, Z.; Kadish, K. M.; Zakharov, L.; Rheingold, A. L.; Goldberg, D. P. *Inorg. Chem.* **2005**, *44*, 4485.
25) Bambirra, S.; van Leusen, D.; Meetsma, A.; Hessen, B.; Teuben, J. H. *Chem. Commun.* **2003**, *4*, 522.
26) Dolphin, D.; Liu, B. Y.; Bruckner, C. *Chem. Commun.* **1996**, 2141. b) Lee, C. H.; Lindsey, S. *Tetrahedron* **1994**, *50*, 11 427.
27) Mabbs, M. B.; Machin, D. *Magnetism and Transition Metal Complexes*; Chapman and Hall: London, **1973**. b) Foese, G.; Gorter, C. J.; Smits, L. J. *Constantes Selectionnes, Diamagnetisme, Paramagnetism, Relaxation Paramagnetique;* Masson: Paris, **1957**.

Chapter

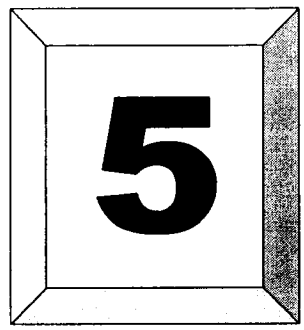

CO_2 CHO Epoxide Co-Polymerization

Table of Contents

5.1 Introduction:

The use of CO_2 as a chemical feedstock is not only attractive from the environmental point of view, but is also an economically profitable practice. Today, CO_2 is inexpensive and largely available as a high purity condensed gas. However, there are major challenges thwarting its common use. The large thermodynamic stability of CO_2 poses a formidable barrier towards the formation of C-C bonds in a catalytic fashion,

though this stability does make it an ideal medium for other processes.[1,2,3] This is not to say, however, that CO_2 cannot be combined with highly reactive molecules (ie. epoxides) in order to produce a polycarbonate co-polymer. Using CO_2 as a carbon source is also a safer alternative to the traditional use of the highly toxic phosgene gas for polycarbonate synthesis.

The two epoxides which have garnered the most interest to date have been cyclohexene oxide (CHO) and propylene oxide (PO). When combined with CO_2 they can form either monomeric cyclic carbonates or polycarbonates (see Scheme 5.1.1). For the scope of this thesis only the polycarbonate case will be examined in detail even though traces of the monomeric cyclic product are always present due to its thermodynamic stability.[4]

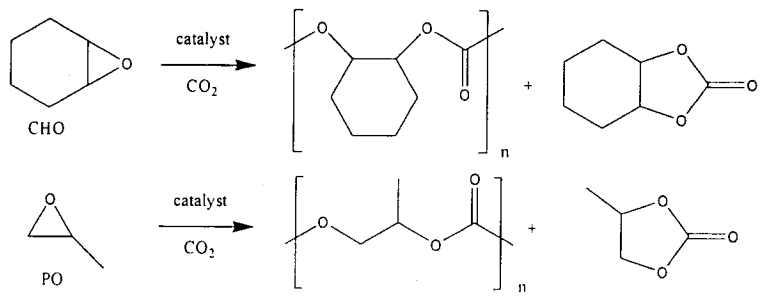

Scheme 5.1.1 CHO and PO Polycarbonate and Monomer Formation.

Polycarbonates are known for their optical clarity and are used to make useful items, such as CD's and safety glasses. Aliphatic polycarbonates have also found uses in packaging materials, thermoplastics, resins, pyrotechnics and interliners for safety glasses.[5,6,7] It has also been found that polypropylene carbonate decomposes controllably and uniformly to form the cyclic carbonate,[8] which makes it a useful binder for ceramics, adhesives, and propellants.[9] According to Coates,[10] the most promising use for the polypropylene carbonate will be as a mid-segment of polyurethanes. Cyclohexene polycarbonate possesses a much higher T_g than propylene polycarbonate (115 °C vs. 38 °C) giving it characteristics much like those of polystyrene.[11] Due to the higher decomposition temperature of cyclohexene polycarbonate (~300 °C), industrial melt-processing is a feasible refinement process. Another unique application for cyclohexene polycarbonates is their use for the construction of microfluidic devices.[12] Given the wide range of

applications for these polycarbonate materials it readily becomes apparent why this field has received much scientific interest.

The initial discovery of the CO_2 co-polymerization reaction was made by Inoue in 1969,[13] with the discovery that a 1:1 mixture of $ZnEt_2$ and H_2O catalyzed the alternating co-polymerization of CO_2 and propylene oxide at 20-50 atm of CO_2. It was found that the activity for the reaction (given in Turn-Over Frequency [TOF]) was 0.12 h^{-1} and the resulting polymer had 88% carbonate linkages. Presumably an EtZnOH complex generated *in situ* is the catalytically active species. Remarkably, polycarbonates were not formed when methanol was used in lieu of water. Subsequent work by the Inoue group explored the use of diprotic compounds such as: resorcinol,[14] dicarboxylic acids,[15] and primary amines.[16] These systems formed catalysts with only moderate improvements in activity over the original: TOF's 0.17, 0.43, and 0.06 h^{-1} respectively. Further work by Kuran on the $ZnEt_2$ system demonstrated that mono-protic molecules led exclusively to the cyclic monomer, whereas di- and tri- protic molecules led to co-polymerization.[17]

5.2 Recent Advances:

Given the vast volume of literature concerning CO_2 co-polymerization (over 500 publications and patents) only the most relevant examples for the scope of this thesis will be discussed. For a complete overview of the literature several reviews have been written by the likes of Walther,[18] Darensbourg,[19] Kuran,[20] and Coates.[10]

In 1978 Inoue made another major breakthrough in the field by introducing the first single-site catalyst for epoxidation.[21] The catalyst was based upon the porphyrin framework and utilized Al as the metal centre (see Figure 5.2.1).

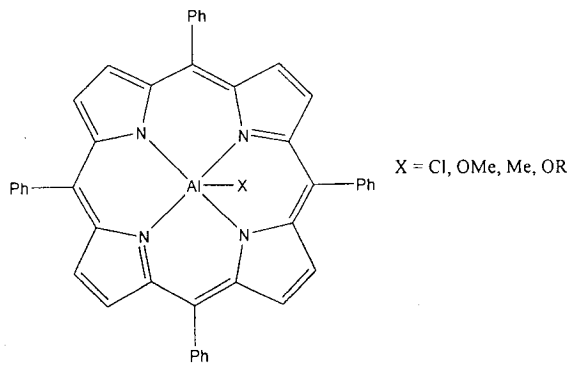

Figure 5.2.1 Inoue Porphyrin Catalyst Framework.

It was found that when X = OMe the co-polymerization of PO and CO_2 (20 °C, 8 atm CO_2) proceeded to yield propylene polycarbonate with 40% carbonate linkages over 19 days with a M_w = 4 485 g/mol and a PDI (polydispersity indice [M_w/M_n]) of 1.15.[22] Inoue also reported that the incorporation of carbonate linkages was drastically increased when the salt $EtPh_3PBr$ was combined with the complex wherein X = Cl. In the case of PO, the polycarbonate was found to have >99% carbonate linkages after treatment with 48 atm CO_2 at 20 °C (M_w = 3 815 g/mol, PDI = 1.09, TOF = 0.18 h^{-1}). Further investigation of the same system by Ree in 1999 did cast some doubt on the results by finding that the system only yielded 72% carbonate linkages at 20 °C and 52 atm CO_2 (M_w = 2 090 g/mol, PDI = 1.10).[23] Inoue also reported that the porphyrin system with X = Cl also co-polymerized CHO and CO_2 with >99 % carbonate linkages in the presence of the phosphorous salt (M_w = 6 572 g/mol, PDI = 1.06, TOF = 0.30 h^{-1}).[24] Though the activities of these systems were quite low, the extremely low PDI's and living nature of the catalyst marked a milestone in this field.

The heterogeneous nature of the Zn based catalytic systems severely hampered the reproducibility of this family of catalysts and made them unsuitable for mechanistic studies. Darensbourg attempted to solve these issues by way of generating discrete Zn complexes.[25] Several square-planar complexes were synthesized from phenols and the starting material [$Zn(N(SiMe_3)_2)_2$] and characterized by X-ray crystallography (See Figure 5.2.2).

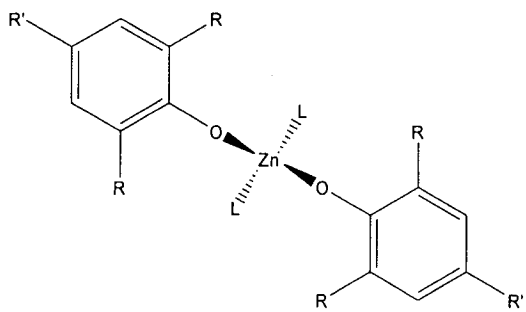

1: R = Ph, R' = H, L = Et2O
2: R, R' = tBu, L = THF
3: R= tBu, R' = H, L = THF
4: R,R' = Me, L = pyridine

Figure 5.2.2 Darensbourg's Discrete Zn Complexes.

It was found that **1** was able to co-polymerize CHO with 91% carbonate linkages under 55 atm CO_2 at 80 °C (M_w = 171 000 g/mol, PDI = 5.5, TOF = 2.4 h^{-1}). Further investigations examined the effects of the *ortho* substituents. It was found that in the case of catalysts **2-4**, the least bulky catalyst **4** was the most active.[26] In order to round out the

analysis of the effect of the *ortho*-substituents, phenols with bis-*ortho* F, Cl, and Br were reacted to form the corresponding Zn complexes. The results of these tests clearly showed that the electron withdrawing ability of the groups attached to the phenol (F>Cl>Br), is directly related to an increase in activity for CHO co-polymerization.[27]

Though the Darensbourg catalysts were an improvement over the traditional systems, they still suffered from having two possible active sites formed by the two bulky aryloxide groups. This problem was solved by utilizing the NacNac ligand (see Figure 5.2.3) in order to synthesize discrete, single-site catalysts with Zn.

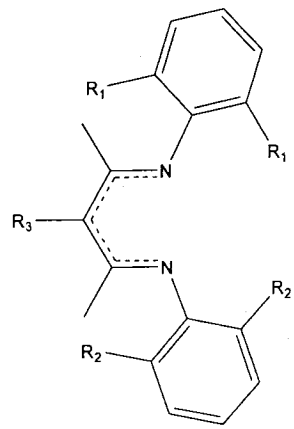

5: R_1=R_2 = Me, R_3 = H
6: R_1 = R_2 = Et, R_3 = H
7: R_1 = R_2 = iPr, R_3 = H
8: R_1 = R_2 = Et, R_3 = CN
9: R_1 = Me, R_2 = iPr, R_3 = CN

Figure 5.2.3 NacNac Ligand Framework Used by Coates.

From this basic framework the Coates group has built up a large array of complexes synthesizing alkoxide and acetate bridged Zn structures with many alterations of the NacNac framework. Remarkably, these catalysts are very active even under exceedingly mild conditions (7 atm CO_2 and 50 °C).[28] The effect of the bulkiness of the group on the *ortho*-position of the phenyl rings (R_1 and R_2) was the first trend to emerge from this work. The Zn complex of the di-methyl substituted phenyl ligand (**5**) shows no co-polymerization activity, whereas the Zn complexes containing bulkier phenyl side-groups (**6**) and (**7**), showed remarkable activities with TOF's of 431 h^{-1} and 360 h^{-1} respectively.[29] The substitution of an electron withdrawing group onto the NacNac backbone (R_3) such as in the ligand **8**, led to a highly active catalyst that yielded cyclohexene polycarbonate with 90% carbonate linkages (M_w = 20 585 g/mol, PDI = 1.15, TOF = 917 h^{-1}) in only 20 minutes.[30] It was also found that making an asymmetric

ligand system $R_1 \neq R_2$ led to very active catalysts, especially when coupled with the electron withdrawing effects of a CN group. The Zn methoxide complex of **9** proved to be the most active catalyst yielding a TOF of 2290 h^{-1} with a PDI = 1.09-1.11 in only 10 minutes.

5.3 Co-polymerization Mechanism:

Many mechanistic studies have been undertaken in order to gain a better understanding of how to improve the co-polymerization systems. The most succinct summary of these many studies is presented in a review article by Coates.[10] Since the inception of this chemistry and the observation that poly-hydridic compounds were able to facilitate polycarbonate formation while mono-hydridic compounds led only to monomeric cyclic products, a multi-nuclear (with respect to Zn) mechanism has been invoked. Regardless of the actual mechanism, it is apparent that there are two reaction pathways accessible whenever CO_2 and an epoxide are combined. These two routes are the formation of the monomeric cyclic product, or the linear polycarbonate chain (see Scheme 5.3.1).

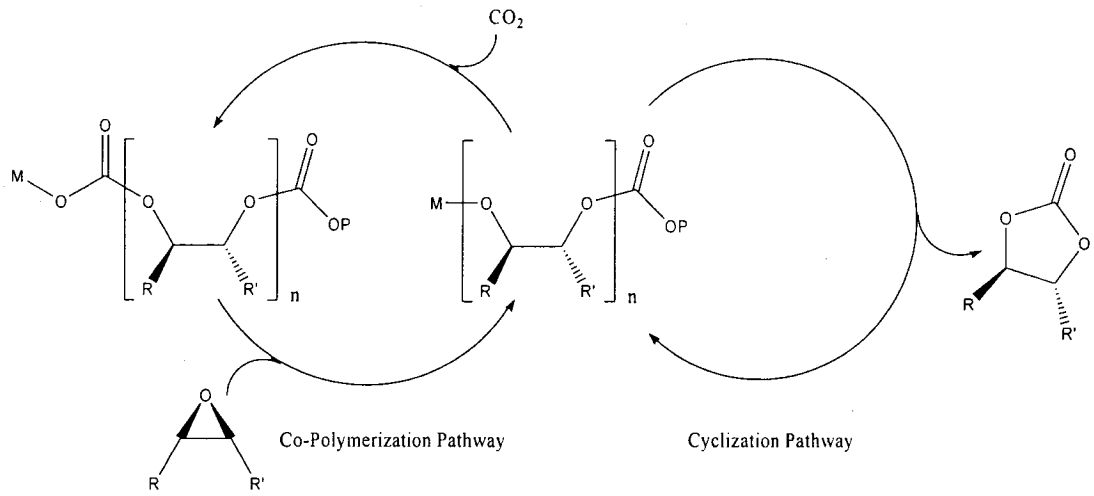

Scheme 5.3.1 Possible Reactivity Pathways.

The mechanism is a two-step process which commences when a CO_2 molecule inserts into either a metal-alkoxide or metal-phenoxide bond, forming the corresponding carbonate. It is for this reason that all catalysts contain a metal oxygen bond. A second subsequent insertion of another CO_2 molecule to form a pure polycarbonate is so

thermodynamically unfavourable that it has yet to be observed. The second step involves the insertion of the epoxide into the metal carbonate bond. In the case of aliphatic epoxides, ring-opening usually, though not exclusively, occurs at the least hindered C-O bond. The observed stereochemistry of the epoxide ring-opening is typical of an S_N2 attack, giving an inversion of the stereochemistry and yielding the *trans* ring-opened product.[31] At this stage the metal alkoxide species may either enter into the cyclization or co-polymerization pathway (see Scheme 5.3.1). It has been demonstrated that the cyclization process most likely occurs when a metal-alkoxide back-bites into an adjacent carbonate linkage (see Scheme 5.3.2).[32]

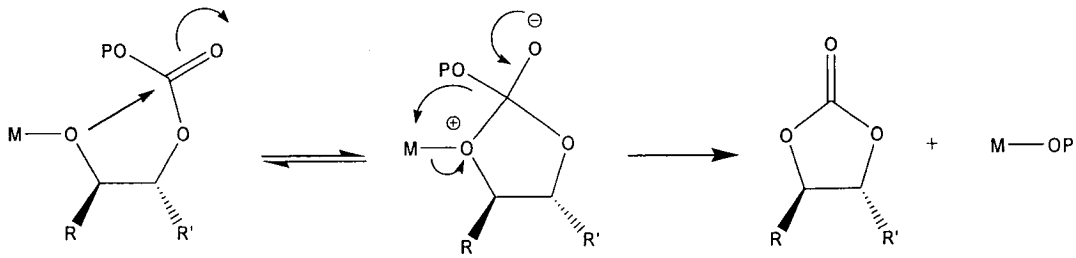

Scheme 5.3.2 Proposed Back-Biting Mechanism.

Higher temperatures and lower pressures of CO_2 favour the thermodynamically stable cyclic species. The final side-product pathway which is common in the CO_2 co-polymerizations is the formation of ether linkages. These occur when two or more epoxide units concurrently insert into the polymer chain (see Scheme 5.3.3).

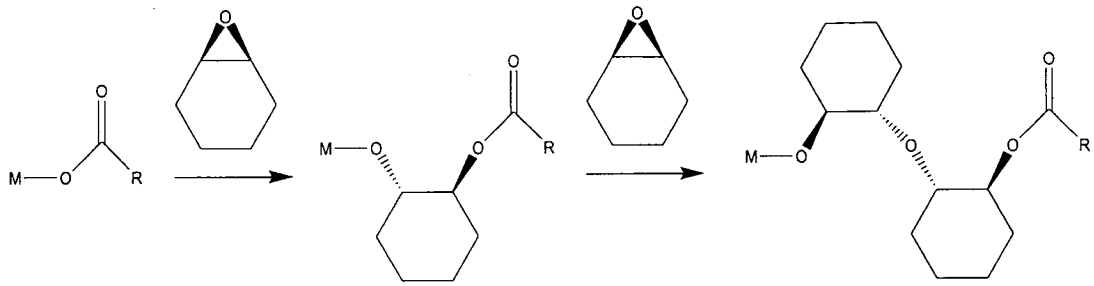

Scheme 5.3.3 Ether Linkage Formation.

Darensbourg hypothesized that two coordination sites were required on the metal in order to effect polyether formation, whereas alternating co-polymerization requires only one site.27 In order to test this hypothesis the PCy_3 adduct **10** versus its THF counterpart **11** (see Figure 5.3.4) were compared.

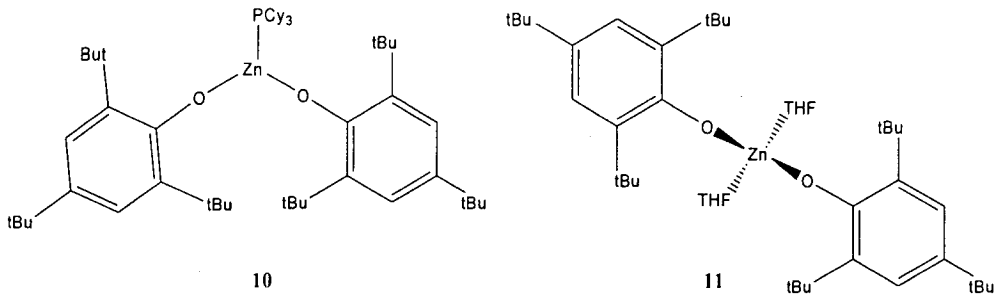

Figure 5.3.4 PCy_3 Adduct for Probing Ether Linkage Formation.

As expected, complex **10** produced polycarbonate with no ether linkages, while complex **11** yielded co-polymer with only 50% carbonate linkages.[33] These and other similar results tend to support the hypothesis that two coordination sites are indeed required for polyether formation.

Recent structurally characterized complexes have provided evidence for the co-polymerization mechanism depicted in Scheme 5.3.1, according to Coates.[29] When a Zn-isopropoxide complex of the NacNac ligand was exposed to CO_2, a rapid insertion reaction occurred to yield a carbonate bridged structure which was characterized by X-ray crystallography (see Scheme 5.3.5).

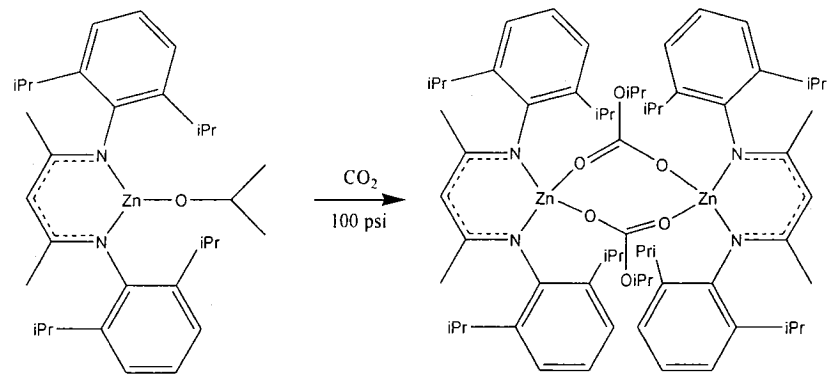

Scheme 5.3.5 CO_2 Insertion Into Zn-Alkoxide Bond.

The same work has also crystallographically characterized the insertion of CHO into a Zn-acetate bond, which occurred over the course of a few days (see Scheme 5.3.6).[29]

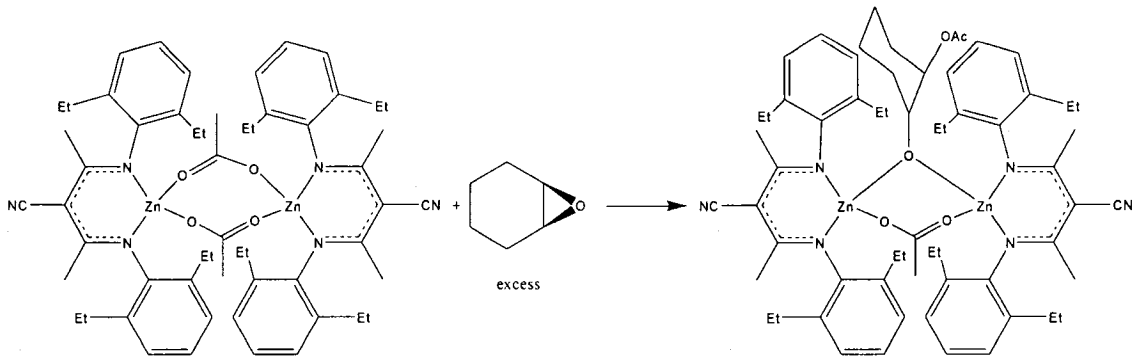

Scheme 5.3.6 Insertion of CHO Into a Zn-Acetate Bond.

Kinetic work which was performed in conjunction with the structural characterizations indicated that the rate-determining step for the co-polymerization process is the insertion of the epoxide into the carbonate bond. Furthermore, Coates reports that his kinetic data supports the hypothesis that co-polymerization requires two metal centres.[29]

5.4 Research Rationale:

Many metals have been explored for the co-polymerization of CO_2 and epoxides ranging from Al,[22] Cr,[34] Co,[35] and even encompassing the lanthanide Y.[36] However, the most performing systems to date have always been based on $Zn^{(II)}$.

When attempting to mimic the behaviour of a compound the concept of isolobality can be used to search for complexes that should, in principle, provide similar chemical properties. Isolobality is an indication that two atoms or compounds have similar types of valence orbitals. In the case of $Zn^{(II)}$, the metal producing the most performing catalysts, the electronic configuration is d^{10} which indicates a completely full valence shell. A high-spin $Mn^{(II)}$ complex with its d^5 high-spin electronic configuration, should therefore be a very good mimic of the d^{10} Zn complexes. Furthermore, its larger atomic radius, and greater oxophilicity may further facilitate the rate of binding and reacting with the epoxides and CO_2.

The Mn-dialkyl ($[Mn(CH_2SiMe_3)_2(THF)]_2$) synthesized in Chapter 3 could in principle provide an excellent starting material for the exploration of this chemistry as it readily and cleanly reacts with either CO_2 or any protic ligand (See Scheme 5.5.1).

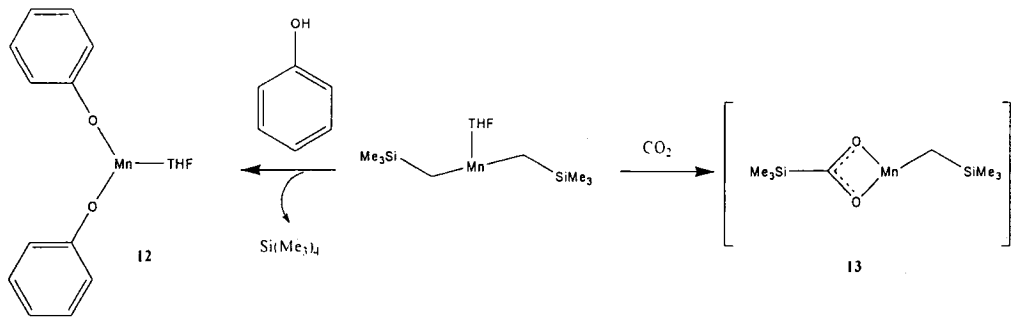

Scheme 5.5.1 $[Mn(CH_2SiMe_3)_2(THF)]_2$ Simplified Reactivity.

Complexes related to the structure of **12** would be a close mimic to the classic Zn phenoxide complexes, or in the case of aliphatic alcohols, the Zn alkoxide compounds. The Mn carboxylate compound depicted in a simplified form as **13** (see Figure 5.5.1 for full structure) provides the same framework as in Scheme 5.3.6 and should allow for the ready insertion of CHO into the complex, in turn leading to co-polymer formation. Furthermore, reaction of a Mn di-alkyl with bulky amine ligands which are known to generate single-site catalysts will provide a good contrast to the Coates NacNac complexes.

5.5 Results and Discussion:

The first attempts to explore the CO_2 co-polymerization process were performed using the *in situ* reaction of the electron withdrawing 2,6-difluoro-phenoxide ligand and $[Mn(CH_2SiMe_3)_2(THF)]_2$ (See Table 5.5.1). This ligand was selected as it has been found that electron withdrawing groups attached to the metal centre are typically able to increase the reactivity. Unfortunately, no polymerization was observed using 2 equivalents of the phenol (entry **2**), and only traces of polymer were observed via NMR in the case of 1 equivalent of phenol (entry **1**). The active site of the one eq. reaction is most likely the alkyl group which is able to insert CO_2 in order to form a carboxylate. Since the original work of Inoue has established that mono-protic alcohols often do not lead to polymerization, and that poly-protic alcohols were often required, the bis-phenol depicted in entry **3** was used. Just as in the case of entry **1**, only traces of polymer were observable via NMR. These results tended to indicate, that in the case of Mn, phenoxide based ligand systems provided only very poor performance. Aliphatic alcohols were then

examined in order to determine the influence of a more electron rich alcohol on the metal centre. The cyclohexanol adduct (entry **4**) proved to be a successful candidate as it was the first alkoxide catalyst to produce a measurable amount of polymer. The polymer had a large PDI of 13.93 and a M_w of 100 637 g/mol and contained greater than 98% carbonate linkages, indicating almost perfect co-polymerization. The TOF (see Appendix 4 for TOF and % carbonate linkage calculations) of 0.168 h^{-1} places the catalyst in the "low" activity range according to the classification system defined by Coates.[10] Entry **5** utilized the same cyclohexanol framework, but with the addition of a pendant OMe group which should be able to loosely co-ordinate to the metal in order to increase the electron density thereon. Although the pendant OMe group alkoxide appears to slightly retard the reaction when compared to cyclohexanol (TOF 0.158 vs. 0.168), the polymer exhibited a similar PDI and M_w and % carbonate linkages (>98%), indicating a similar reaction mechanism. Since all subsequent active runs invariably yielded >98 % carbonate linkages, this attribute will not be further discussed. It is important to note that this value does indicate that all of the active $Mn^{(II)}$ catalysts were exhibiting nearly perfect co-polymerization activity.

Table 5.5.1 Catalytic Conditions and Results for Alcoholic Ligands.[a]

Proposed Catalyst (entry number)	**Conditions**	**Results**
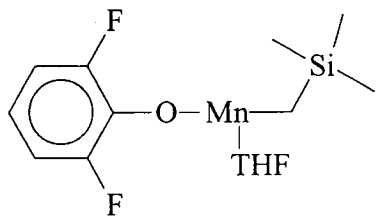 (1)	80 °C 24 h	Trace polymer via NMR TOF ~ 0 h^{-1}
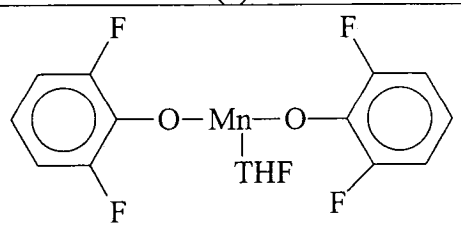 (2)	80 °C 24 h	No Polymer TOF = 0 h^{-1}

Table 5.5.1 Conditions and Results for Alcoholic Ligands continued.[a]

Proposed Catalyst (entry number)	**Conditions**	**Results**
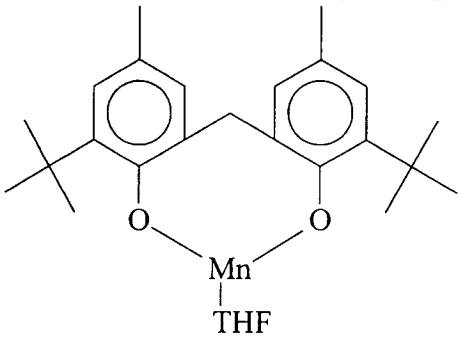 **(3)**	80 °C 24 h	Trace polymer via NMR TOF ~ 0 h^{-1}
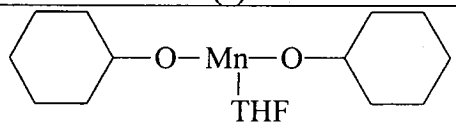 **(4)**	80 °C 24 h	0.172 g Polymer M_w = 100 637 g/mol PDI = 13.929 TOF = 0.168 h^{-1}
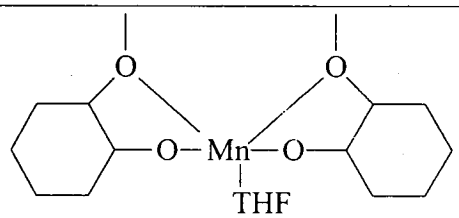 **(5)**	80 °C 24 h	0.162 g Polymer M_w = 95 322 g/mol PDI = 15.582 TOF = 0.158 h^{-1}

[a] All catalysis runs were conducted using 300 μmol of catalyst and 15 mL (0.15 mol) CHO in 35 mL of toluene and 80 bar CO_2 unless otherwise stated. All catalysts were pre-treated at 60 °C, 40 bar CO_2 for 3 hours prior to the runs in order to ensure carbonate formation.

Although the performance of the *in situ* generated Mn alkoxides was somewhat disappointing, it did clearly indicate that the insertion of CO_2 into the Mn-OR function was indeed possible. The poor activity of these *in situ* generated catalysts could be ascribed to an intrinsic low ability of a $Mn^{(II)}$ centre to support this type of catalysis. However, it is also possible that the reaction of MnR_2 with ROH was more complicated than anticipated, perhaps also leading to oxidation of the metal centre. For this reason it was decided to utilize complexes of well-defined structures, from which the oxidation state could conclusively be proven via the magnetic moment. As demonstrated in Chapter 3 the Mn di-alkyl ($[Mn(CH_2SiMe_3)_2(THF)]_2$) reacts readily with CO_2 in any

solvent to yield a pentameric carboxylate structure $[Mn_5(O_2CCH_2SiMe_3)_6(CH_2SiMe_3)_4]$ (See Figure 5.5.1) in which Mn retains the +2 oxidation state.

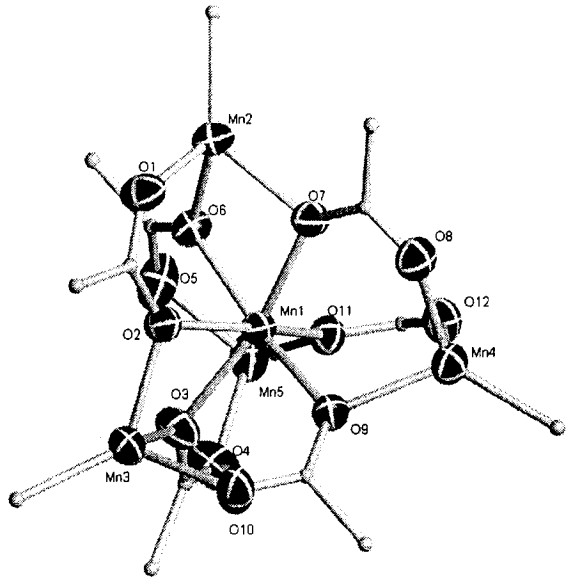

Figure 5.5.1 Crystal Structure of Mn-Carboxylate; Terminal $SiMe_3$ Groups Omitted for Clarity.

This carboxylate should be a good model for the carbonate structure required in the co-polymerization cycle (see Scheme 5.3.1) and should therefore allow the facile insertion of CHO, leading to co-polymerization. In order to ensure that a carboxylate structure is present the $[Mn(CH_2SiMe_3)_2(THF)]_2$ was pre-treated with 40 bar CO_2 at 60 °C for 3 h prior to all runs. Using the same conditions as in the case of the alcohols (80 °C, 24 h, 80 bar CO_2) it was quickly found that the Mn di-alkyl ($[Mn(CH_2SiMe_3)_2(THF)]_2$) was an effective catalyst (see entry **9** in Table 5.5.2). The catalyst was twice as active as the best alkoxide case (TOF 0.387 h^{-1} vs 0.168 h^{-1}) and yielded polymer that was about 60 000 g/mol (60 %) heavier, but with a similar PDI. Varying the time of reaction was found to have a significant impact on the polymerization. When the reaction was run for only 3 h (entry **8**) only traces of polymer were found via NMR. In contrast to this, when the reaction was run for 64 h (entry **10**) the overall activity was about half of the 24 h case (TOF 0.142 vs. 0.387 h^{-1}). A 19% decrease in the M_w was also observed, indicating that *depolymerization may be occurring* over longer reaction times. The effect of the solvent was also examined by using both THF and toluene (entries **6** and **9**). It was found that the presence of THF completely inhibited the reaction as only traces of polymer were found

via NMR. When the reaction was run in 50 mL of neat CHO (entry **12**) similar results to the standard conditions (entry **9**) were obtained with only a slight drop-off in activity: TOF 0.240 vs. 0.387 h^{-1} and M_w's 156 029 vs. 159 312 g/mol. In order to determine if the pre-treatment of the Mn di-alkyls with CO_2 had any impact on the reaction, a run was performed with no pre-treatment of CO_2 pressure at 60 °C (entry **13**). It was found that the activity was about half (TOF 0.157 vs. 0.387 h^{-1}) of the standard case (entry **9**) and the M_w was slightly lower (M_w = 102 597 vs. 159 213 g/mol). The decrease in activity can probably be attributed to the lack of carboxylate groups for the insertion of CHO, which would take some time to form before the catalytic cycle could become active. The most active run was found to occur at the elevated temperature of 120 °C (entry **11**). A five-fold increase in activity was observed (TOF 1.692 vs. 0.387 h^{-1}) with very little change in the M_w (156 029 vs. 159 213 g/mol), though the PDI was somewhat broader than the standard (entry **9**).

Table 5.5.2 Catalytic Conditions and Results for Mn Dialkyls.[a]

Catalyst (entry number)	**Conditions**	**Results**
$[Mn(CH_2SiMe_3)_2(THF)]_2$ **(6)**	80 °C 24 h in THF	Trace polymer via NMR TOF ~ 0 h^{-1}
$[Mn(CH_2SiMe_3)_2(THF)]_2$ **(7)**	20 bar CO_2 50 °C 24 h	No Polymer
$[Mn(CH_2SiMe_3)_2(THF)]_2$ **(8)**	80 °C 3 h	Trace polymer via NMR TOF ~ 0 h^{-1}
$[Mn(CH_2SiMe_3)_2(THF)]_2$ **(9)**	80 °C 24 h	0.396 g Polymer M_w = 159 213 g/mol PDI = 16.873 TOF = 0.387 h^{-1}
$[Mn(CH_2SiMe_3)_2(THF)]_2$ **(10)**	80 °C 64 h	0.388 g Polymer M_w = 118 755 g/mol PDI = 17.124 TOF = 0.142 h^{-1}
$[Mn(CH_2SiMe_3)_2(THF)]_2$ **(11)**	120 °C 24 h	1.733 g Polymer M_w = 167 376 g/mol PDI = 19.438 TOF = 1.692 h^{-1}

$[Mn(CH_2SiMe_3)_2(THF)]_2$ **(12)**	80 °C 24 h neat CHO	0.246 g Polymer M_w = 156 029 g/mol PDI = 19.335 TOF = 0.240 h^{-1}
$[Mn(CH_2SiMe_3)_2(THF)]_2$ **(13)**	80 °C 24 h No CO_2 Pre-treatment	0.161 g Polymer M_w = 102 597 g/mol PDI = 13.084 TOF = 0.157 h^{-1}

[a] All catalysis runs were conducted using 300 μmol of catalyst and 15 mL (0.15 mol) CHO in 35 mL of toluene and 80 bar CO_2 unless otherwise stated. The $[Mn(CH_2SiMe_3)_2(THF)]_2$ was pre-treated at 60 °C, 40 bar CO_2 for 3 hours prior to the runs in order to ensure carboxylate formation.

The results of the catalysis testing with the Mn di-alkyls proved that the $Mn^{(II)}$ system was quite capable of co-polymerization. However, the Mn di-alkyls have two possible active sites and no ligands which remain tightly coordinated to the metal in order to influence the polymerization. We hypothesized that the lack of sterically demanding ligands attached to the metal centre could be the reason for the observed broad PDI's. Thus we endeavoured to test well-defined catalysts by placing a variety of imine-based ligands about the metal centre. The choice of the imine-based ligand systems was prompted by the robustness of their coordination mode and also since the class of ligand has been used for a variety of catalytic systems and metal-promoted organic reactions. The bis-imino pyridinato ligand, introduced in the literature by Gibson and Brookhart,[37] attracted our interest because of its superb electronic flexibility and ability to sustain PE polymerizations with a variety of metals. When the ligand was combined with a solution of $[Mn(CH_2SiMe_3)_2(THF)]_2$ an immediate reaction took place changing the colour of the solution from a light orange to a dark purple. This type of reactivity has been reported before, resulting in one $-C(=NAr)CH_3$ being deprotonated.[38] Based on the previous example we propose that the structure of the catalyst is a mono-deprotonated form (see Figure 5.5.2), however other possible structures are described in Chapter 6.

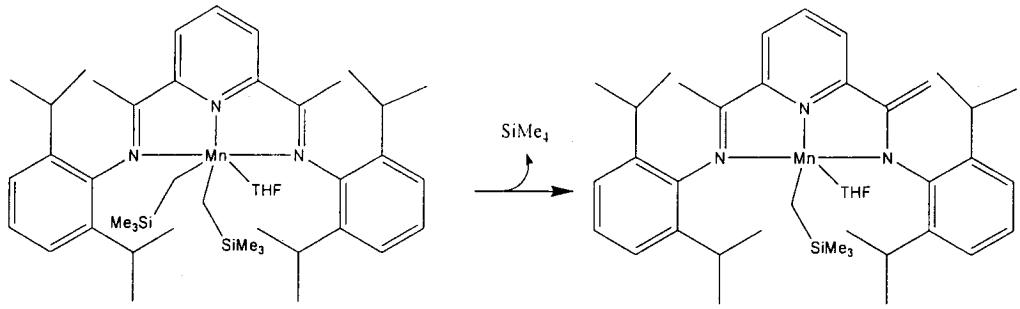

Figure 5.5.2 Proposed Structure for Entry **15**.

When the catalyst was tested it was found to be about half as active as the standard entry **9**. The catalyst (entry **14**) had a TOF of 0.126 h^{-1} and produced a polymer with a PDI of 9.687 and a M_w of 76 049 g/mol. When a similar reaction was attempted with the di-imine of entry **15** the same deep colour change was observed leading us to propose the same type of structure as seen in Fig. 5.5.2. The less bulky di-imine ligand only exhibited half of the activity of the Brookhart case TOF 0.053 h^{-1} but yielded a nearly identical PDI with a slightly higher M_w 85 892. The similarity of the PDI's and M_w found for these two catalysts most likely indicates that they have a similar active site. Another di-imine ligand which was examined was the Bazan ligand.[39] This ligand is known to co-ordinate via the enolic moiety as the oxygen penetrates better in the metal coordination sphere than does nitrogen, especially as Mn is quite oxophilic (see Figure 5.5.3).

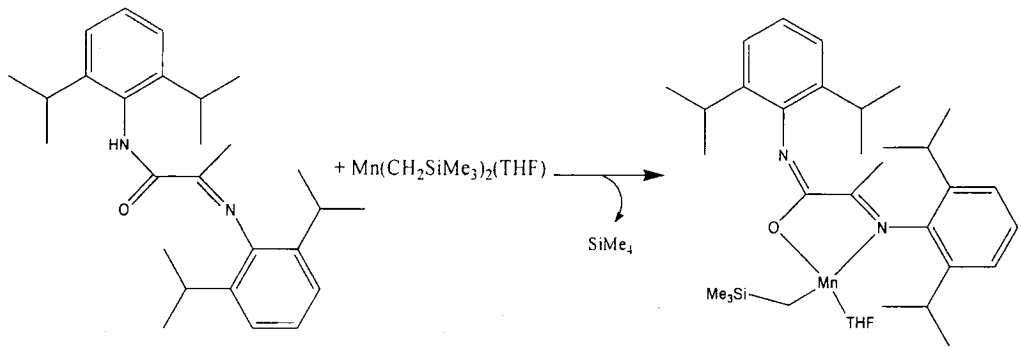

Figure 5.5.3 Proposed Structure for Entry **16**.

Entry **16** yielded polymer with a TOF of 0.112 h^{-1} and a PDI of 16.134 which is much broader than the previous di-imines, the M_w was also significantly higher at 118 274 g/mol. The higher M_w and PDI observed in this case could perhaps be attributed to the much less sterically crowded metal centre.

In order to enable a better comparison with the Coates' Zn-NacNac system, we prepared a $Mn^{(II)}$ catalyst with the same ligand. When the catalyst in entry **17** was tested under the usual conditions it yielded roughly half of the activity as the Mn di-alkyl entry **9**: TOF 0.159 vs. 0.387 h^{-1}. This was not entirely unanticipated as the catalyst is expected to have only one active site, as opposed to two on the Mn di-alkyl. The PDI (15.839) was very similar to the di-alkyl, though the polymer produced was about 60 000 g/mol lighter (M_w = 103 115 g/mol, ~60%). When the same catalyst run was performed at 120 °C the activity rose by a factor of 3 (TOF = 0.512 h^{-1}), however both the M_w and PDI remained virtually unchanged. This would tend to indicate that heating this catalyst increases the rate of reaction, with no observable detrimental effects.

The last attempt to prepare a satisfactory $Mn^{(II)}$ catalyst was carried out via the reaction of Mn di-alkyl with the simple amidinate depicted in entry **19**. Amidinates are quite versatile ligands since both their electronics and sterics are easily tuned by adjusting their side-groups, just as in the case of the NacNac ligand. The only major difference between the NacNac and amidinate ligands is the size of the "bite-angle" the ligand adopts. Amidinates have a much narrower 3-atom "bite", compared to NacNac's 5-atom "bite". The amidinate system **19** was slightly more active than the NacNac system (TOF = 0.177 vs. 0.159 h^{-1}), however the polymer it produced was about 50 000 g/mol heavier (150 456 g/mol) while the PDI remained relatively unchanged (PDI = 13.559). When the catalysis was conducted at 120 °C a seven-fold increase in activity was observed (TOF = 1.188 h^{-1}) as well as a large increase in the M_w 233 296 g/mol, however the PDI was also negatively affected as it increased from 13.559 at 80 °C to 21.828 at 120 °C.

In conclusion, this work proved that $Mn^{(II)}$ complexes can, indeed, catalyze co-polymerization of CHO and CO_2 with promising activity although they are not competitive with the current generation of Zn systems.

Table 5.5.3 Catalytic Conditions and Results for Imine Based Ligands.[a]

Proposed Catalyst (entry number)	**Conditions**	**Results**
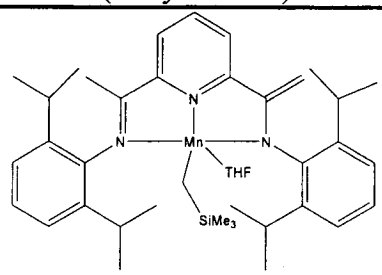 **(14)**	80 °C 24 h	0.129 g Polymer M_w = 76 049 g/mol PDI = 9.687 TOF = 0.126 h^{-1}
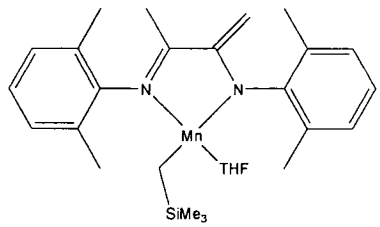 **(15)**	80 °C 24 h	0.054 g Polymer M_w = 85 892 g/mol PDI = 10.244 TOF = 0.053 h^{-1}
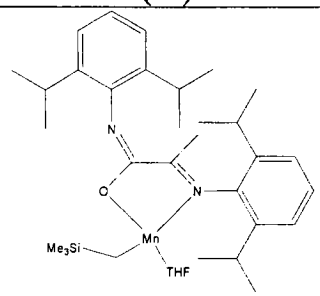 **(16)**	80 °C 24 h	0.115 g Polymer M_w = 118 274 g/mol PDI = 16.134 TOF = 0.112 h^{-1}
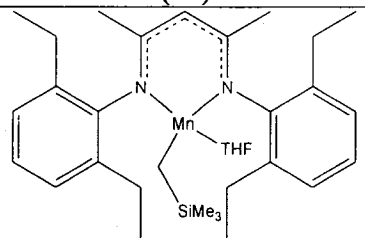 **(17)**	80 °C 24 h	0.163 g Polymer M_w = 103 115 g/mol PDI = 15.839 TOF = 0.159 h^{-1}
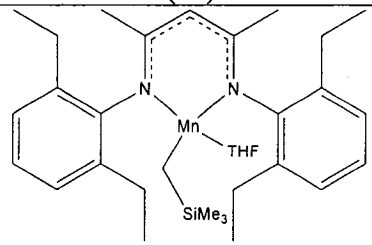 **(18)**	120 °C 24 h	0.524 g Polymer M_w = 97 682 g/mol PDI = 15.51 TOF = 0.512 h^{-1}

Table 5.5.3 cont'd Catalytic Conditions and Results for Imine Based Ligands[a]

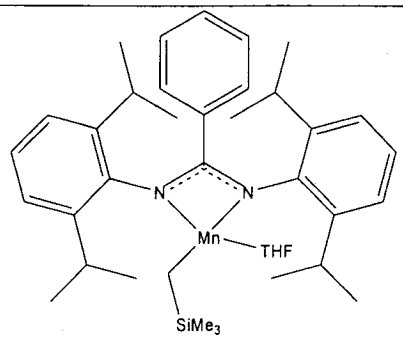 **(19)**	80 °C 24 h	0.181 g Polymer M_w = 150 456 g/mol PDI = 13.559 TOF = 0.177 h^{-1}
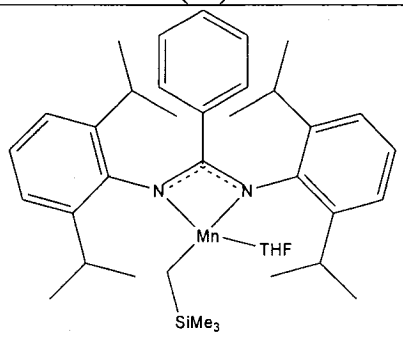 **(20)**	120 °C 24 h	1.217 g Polymer M_w = 233 296 g/mol PDI = 21.828 TOF = 1.188 h^{-1}

[a] All catalysis runs were conducted using 300 μmol of catalyst and 15 mL (0.15 mol) CHO in 35 mL of toluene and 80 bar CO_2 unless otherwise stated. All catalysts were pre-treated at 60 °C, 40 bar CO_2 for 3 hours prior to the runs in order to ensure carboxylate formation.

5.6 Structural and Mechanistic Investigations:

Although the activities exhibited by the Mn catalysts were quite reasonable when compared to the literature examples, the PDI's and supporting GPC traces proved intriguing. The lowest PDI produced by these catalysts was 9.687 whereas the highest was 21.828. This trend was disappointing, since changing the ligands and even reaction temperature appear to have very little impact on the polydispersity. The three SEC/GPC traces depicted in Figs. 5.6.1-3 represent the typical results found. The regions between the first triangle and the diamond indicate where the co-polymers elute.

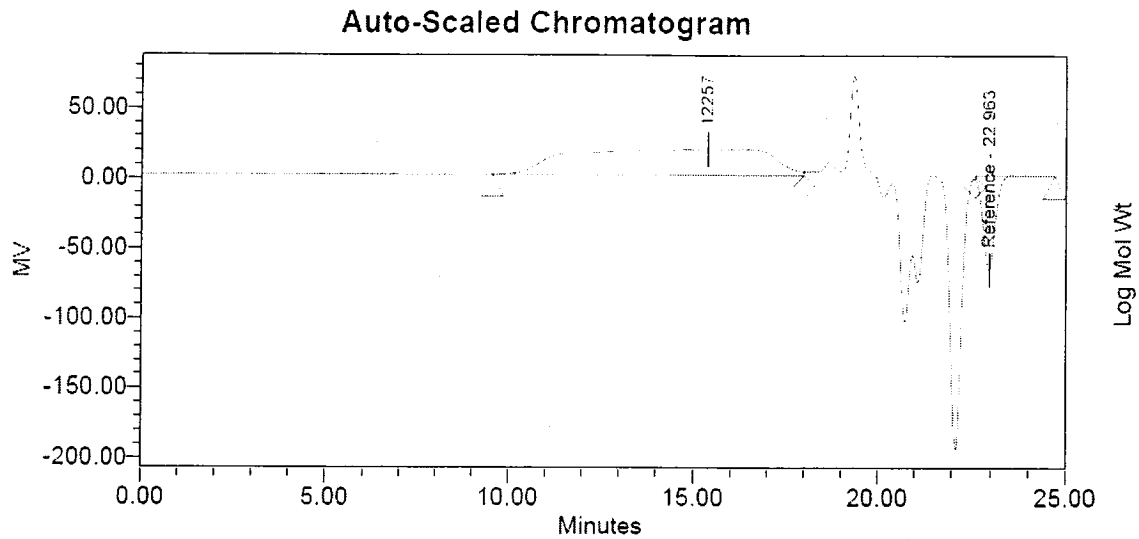

Figure 5.6.1 GPC Trace for Entry **9** (Table 5.5.2).

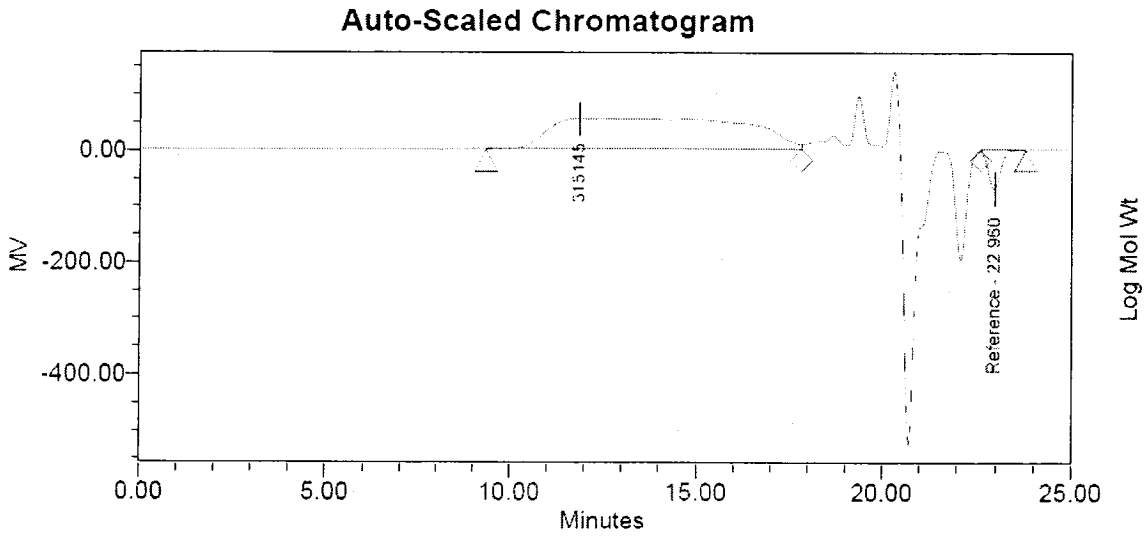

Figure 5.6.2 GPC Trace for Entry **19** (Table 5.5.3).

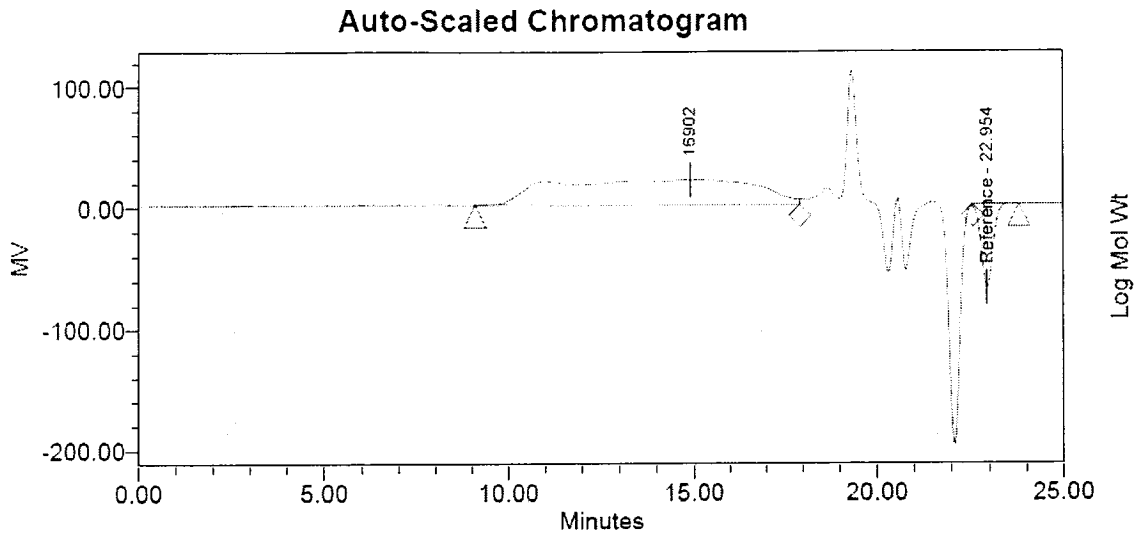

Figure 5.6.3 GPC Trace for Entry **20** (Table 5.5.3).

Each trace depicts a near uniform distribution of M_w's between 5 000 and 800 000 g/mol. There appears to be absolutely no modality present which would tend to indicate that there may be a very long initiation time or a very long termination time. If the catalyst is either dying, or initiating very slowly the plateau-shape would be expected as many different catalysts would have many different chain-lengths attached to them. Alternately, many different active sites with overlapping polymer distributions could generate these types of plateaus; however this possibility is so remote that it can be discounted.

In order to probe the mechanics of this reaction, several organometallic reaction studies were initiated. Firstly, in order to demonstrate that the *in situ* reactions of Table 5.5.1 were producing the proposed structures, the reaction of $[Mn(CH_2SiMe_3)_2(THF)]_2$ with the bi-phenol ligand from entry **3** (see Scheme 5.6.4) was carried out.

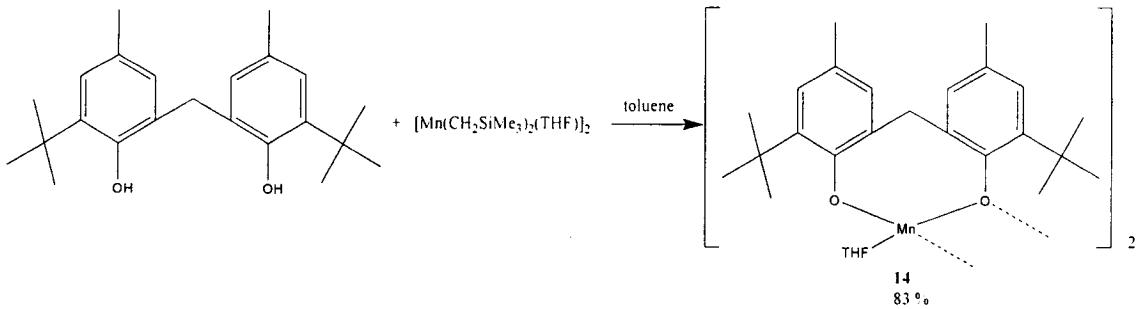

Scheme 5.6.4 Reaction of Biphenol with $[Mn(CH_2SiMe_3)_2(THF)]_2$.

Complex **14** was isolated in 83% crystalline yield from hexanes and is actually a dimeric structure where one phenol is σ-bound to Mn while the second is μ_2-bound to two Mn centres (see Figure. 5.6.5).

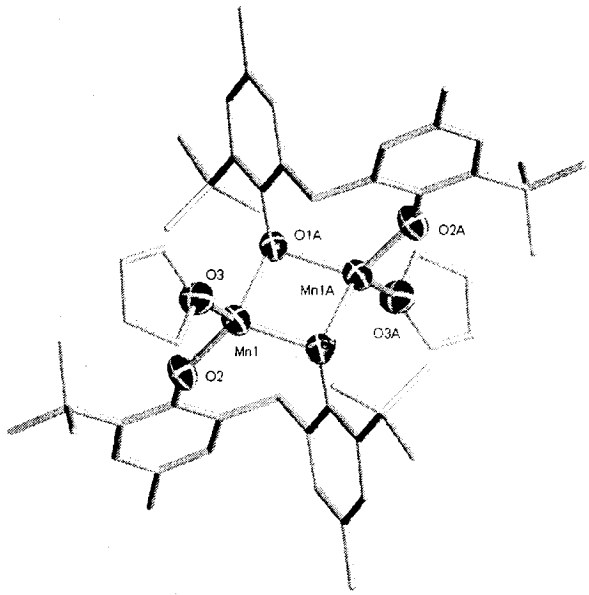

Figure 5.6.5 Crystal Structure of (**14**) with 30 % Thermal Ellipsoids.

The structure supports the hypothesis that the *in situ* reaction is a valid way of generating the tested Mn-alkoxide species from Table 5.5.1.

Using the NacNac ligand depicted in Scheme 5.5.3 the $[(NacNac)Mn(CH_2SiMe_3)(THF)]$ complex **15** was synthesized in 93 % crystalline yield as yellow blocks (see Scheme 5.6.6).

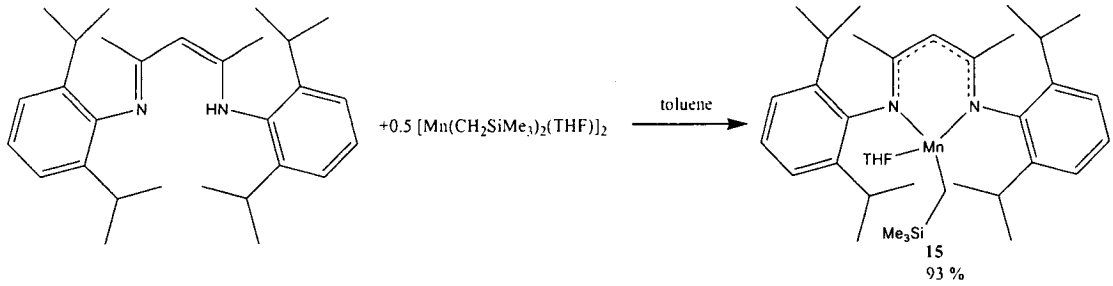

Scheme 5.6.6 Synthesis of [(NacNac)Mn(CH_2SiMe_3)(THF)] (**15**).

Over the course of days, or if heated slightly, the complex loses THF to form the monomeric species **16** which was crystallized in near quantitative yield from hexanes as yellow block crystals (See Figure 5.6.7).

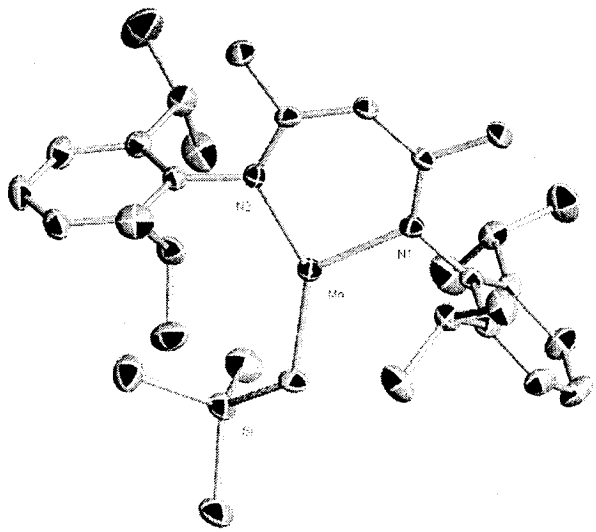

Figure 5.6.7 Crystal Structure of [(NacNac)Mn(CH_2SiMe_3)] (**16**) With 30% Thermal Ellipsoids.

Upon exposure to 1.1 atm of CO_2 gas for several hours a yellow solution of either **15** or **16** in hexanes slowly becomes colourless. Crystals of **17** were grown from cold hexanes in near quantitative yield. The structure of **17** clearly shows that CO_2 inserted into the Mn-C bond forming a dimeric carboxylate structure (see Figure 5.6.8). The structure is analogous to the Coates' Zn carbonate structure[29] which further indicates that $Mn^{(II)}$ behaves much the same way as Zn. Unfortunately, unlike the Coates' system, prolonged exposure of compound **17** to an excess of CHO did not result in any isolable insertion products, but rather led to dark-coloured solutions after several days, from which only intractable materials resulted. This most likely indicates that the epoxide is oxidizing Mn

to a higher valency, thus reiterating that the Mn-R moiety can be responsible for an array of side-reactions which are detrimental to catalytic performance.

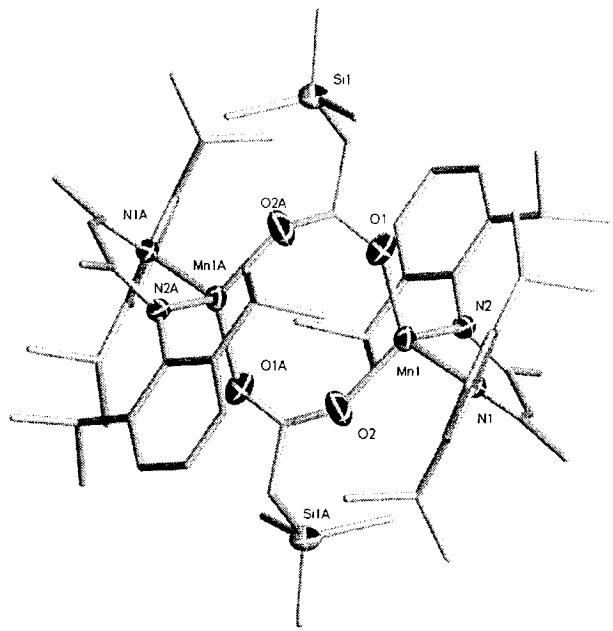

Figure 5.6.8 Crystal Structure of (**17**) with 30% Thermal Ellipsoids.

Since the CHO insertion product was not isolated it was proposed to explore whether substituting the alkyl group for a phenol, and then attempting the reaction would be a more successful route. Some very interesting, and quite unexpected chemistry resulted from these investigations. When the [(NacNac)Mn(CH_2SiMe_3)] complex (**16**) was reacted with 3,5-^{t}Bu-Phenol an unanticipated product was formed. Instead of the expected Mn-phenoxide bond, ligand leaching was observed (see Fig. 5.6.9).

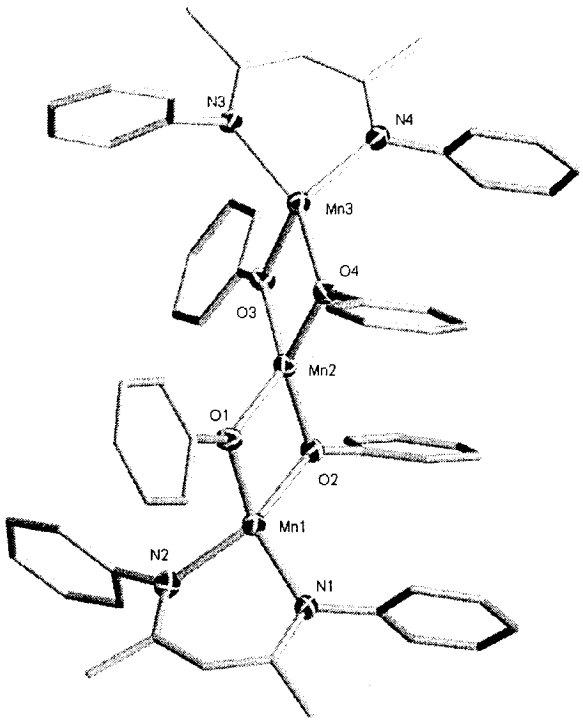

Figure 5.6.9 Crystal Structure of (**18**), with 30 % Thermal Ellipsoids; Side Groups Omitted for Clarity.

Complex **18** is a tri-nuclear structure with three tetrahedrally co-ordinated $Mn^{(II)}$ atoms. What is quite surprising is that the central Mn atom has completely lost the NacNac ligand system in order to bond with four bridging oxygen atoms. This implies that during the course of catalysis it is quite possible that any ligand on the Mn centre may be replaced with an oxide ligand, thus leaving the metal centre with little ability to control the growth of the polymer chains. This reactivity is probably attributable to the high oxophilicity of Mn, especially when compared to Zn. When the 3,5-^{t}Bu groups are placed at the *ortho* positions, the reactivity was quite different. The reaction of 3,5-^{t}Bu-Phenol resulted in the formation of the expected Mn-phenoxide complex (**19**) which was crystallized from cold hexanes (see Figure 5.6.10).

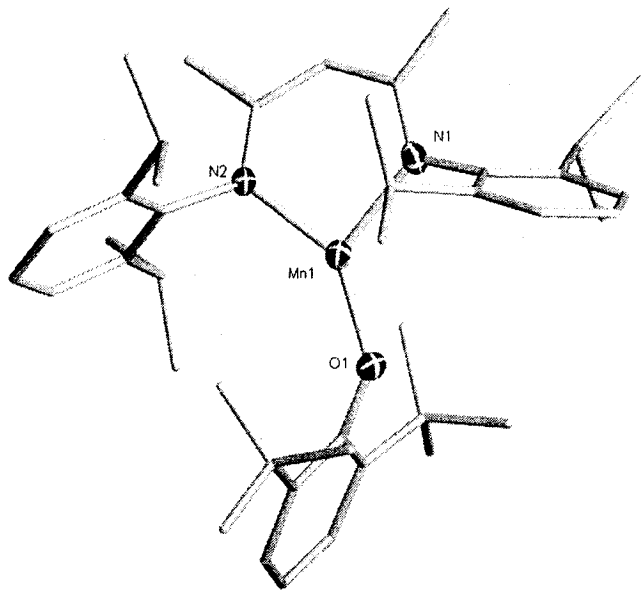

Figure 5.6.10 Crystal Structure of (**19**) with 30 % Thermal Ellipsoids.

Oddly, it was observed that when a solution of **19** was allowed to stand at room temperature, the colour slowly darkened over time. This observation was perplexing as the molecule should be quite stable. It was found that when the dark red-brown solution was cooled, colourless crystals of **20** were recovered (see Figure 5.6.11). The formation of diphenylquinone implies the loss of a molecule of H_2 from two phenoxides, with a concomitant two-electron reduction of one or two Mn centres (See Scheme 5.6.12). This process is known to be a radical type of reaction and has been performed using Mn complexes.[40] This indicates that the $Mn^{(II)}$ centre is able to initiate radical chemistry which might well account for the broad PDI's, as the presence of radicals within a polymerization can lead to a poor product distributions. This gradual reduction also precluded the isolation of any complexes from the reaction of **19** with CHO. Therefore the question of whether the epoxide is able to readily insert into the Mn-OR bond is unknown in this case.

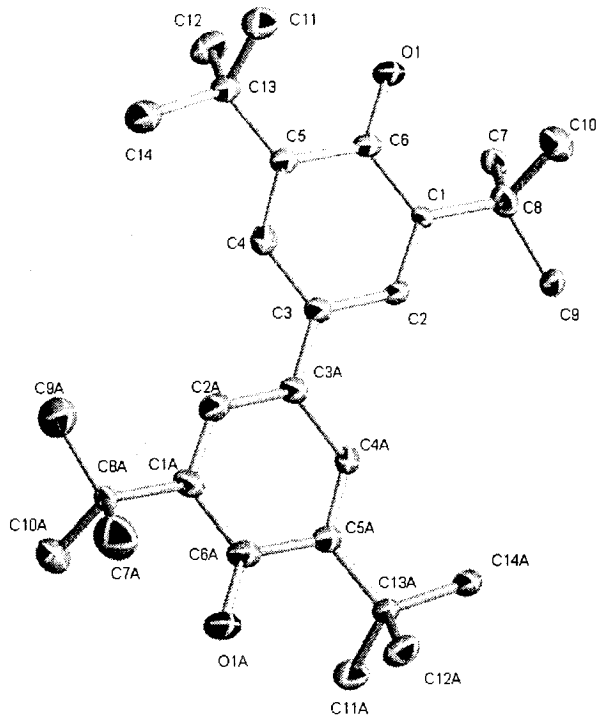

Figure 5.6.11 Crystal Structure of (**20**) with 30 % Thermal Ellipsoids.

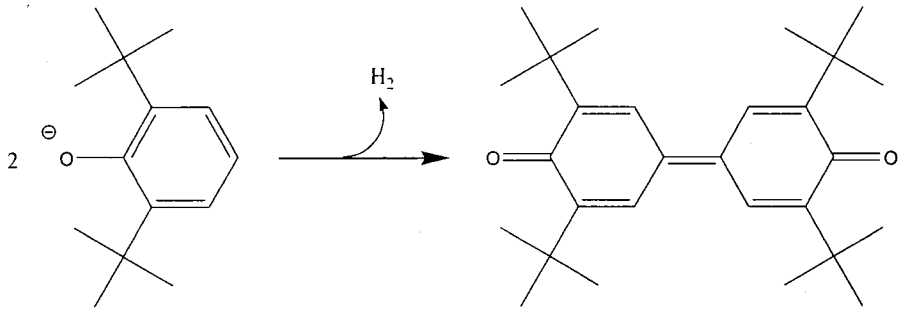

Scheme 5.6.12 Formation of Quinone Complex (**20**).

5.7 Conclusions:

Subsequent to our investigations the group of Inoue published a paper detailing the first case of Mn co-polymerizing CO_2 with CHO.[41] Based on the same porphyrin structure as in Fig. 5.2.1 the complex utilized $Mn^{(III)}$ as the active catalyst. However, the very best run only yielded an activity of 16.3 h^{-1} with a M_w of 8 710 g/mol and a PDI of 1.3 (99% carbonate linkages). Remarkably, their catalyst was able to function at 1 atm of CO_2, albeit at a slow rate (when compared to the Zn catalysts).

The results of our investigations have shown that $Mn^{(II)}$ could perhaps produce viable catalysts, and produces significantly higher M_w's than the $Mn^{(III)}$ catalyst of Inoue. In addition, the $Mn^{(II)}$ catalysts are capable of producing nearly perfectly alternating co-polymer, given that the % carbonate linkages were always found to be in excess of 98%. That said, further tuning is definitely required in order to gain better control over the large PDI's produced by $Mn^{(II)}$. The cause of which, we have demonstrated, may be attributed to the presence of radicals in the polymerization or leaching of the ligand from the metal. Furthermore, the activities will need to be drastically increased if they are to compete with the Zn-based catalysts.

5.8 X-Ray Crystallographic Section:

The full crystallographic data and structural descriptions, including bond lengths and angles may be found in Appendix 5. The abbreviated crystallographic data for the structures contained within this chapter are as presented in Tables 5.8.1 and 5.8.2.

In complex **14** two Mn atoms are each pseudo-tetrahedrally coordinated with one σ –bound phenol [Mn(1)–O(2) = 1.953(4) Å] and two μ_2 –bridging phenols [Mn(1)–O(1) = 2.100(4), Mn(1)–O(1') = 2.077(4) Å]. The final coordination site is filled by a molecule of THF [Mn(1)–O(3) = 2.129(4) Å]. The Mn-Mn distance (3.1289(18) Å) places the two metal centres outside of typical bonding range, although electronic exchange via the bridging phenols is quite probable. Three highly disorderd, and partially occupied hexane molecules were found in each unit cell, leading to the non-integer value of the empirical formula. When the complex is crystallized from Et_2O the THF is displaced yielding the structurally identical structure **14b**.

Complex **15** is best described as a distorted trigonal pyramid. The basal plane is comprised of the two nitrogens (N(1) and N(2)) of the NacNac ligand and C(30) of the CH_2SiMe_3 group. The Mn atom sits very slightly above the plane formed by the previously mentioned three atoms [Mn(1)–N(1) = 2.119(3), Mn(1)–N(2) = 2.101(4), Mn(1)–(C30) = 2.107(3) Å]. The ligand enforces a narrower angle between the two nitrogens [N(1)–Mn(1)–N(2) = 91.29(9)°] then between the nitrogens and the alkyl group [N(1)–Mn(1)–C(30) = 117.57(13)°, N(2)–Mn(1)–C(30) = 136.55(10)°]. The pyramidal

structure is capped by a molecule of THF [Mn(1)–O(1) = 2.204(3) Å]. The THF free analogue **16** shows significantly less distortion along the basal plane, yielding an almost perfectly flat trigonal planar geometry. The plane is compromised of the ligand Mn bonds [Mn(1)–N(1) = 2.064(2), Mn(1)–N(2) = 2.0654(19) Å] with the alkyl group filling the final position [Mn(1)–C(30) = 2.100(3) Å]. The same distorted angle enforced by the ligand as seen in **15** was again observed [N(1)–Mn(1)–N(2) = 91.73(8)°] although the angles between the nitrogens and the alkyl were slightly more relaxed in this case [N(1)–Mn(1)–C(30) = 123.35(10)°, N(2)–Mn(1)–C(30) = 143.60(10)°].

The CO_2–insertion adduct **17** adopts a distorted tetrahedral geometry compromised of the ligand system [Mn(1)–N(1) = 2.092(3), Mn(1)–N(2) = 2.082(3) Å] and two bridging carboxylate groups [Mn(1)–O(1) = 2.037(3), Mn(1)–O(2) = 2.047(3) Å]. Sterics are probably the cause of the large angle observed between the bridging carboxylates [O(1)–Mn(1)–O(2) = 121.66(14)°]. The ligand again enforces the tight angle that was previously seen [N(1)–Mn(1)–N(2) = 92.58(12)°]. The Mn-Mn distance (5.142(3) Å) is well outside of bonding range, therefore any electronic coupling is strictly ligand mediated.

Complex **18** is quite convoluted. The structure contains three Mn atoms in a linear arrangement, each in a pseudo-tetrahedral geometry. Each end of the tri-nuclear cluster is capped with a NacNac ligand [Mn(1)–N(1) = 2.117(8), Mn(1)–N(2) = 2.151(8), Mn(3)–N(3) = 2.127(8), Mn(3)–N(4) = 2.107(8) Å]. The central Mn is bridged to each terminal Mn via briding phenoxides [Mn(2)–O(1) = 2.070(6), Mn(2)–O(2) = 2.118(7), Mn(2)–O(3) = 2.088(6), Mn(2)–O(4) = 2.071(7)]. Three toluene molecules (with two disordered over two positions) complete the asymmetric unit.

Complex **19** is isostructural to complex **16**, although it shows slightly more distortion from planarity which is most likely a result of the much larger steric bulk of the phenoxide. The distorted trigonal planar structure is composed of the ligand [Mn(1)–N(1) = 2.073(4), Mn(1)–N(2) = 2.037(4) Å] and the phenoxide ligand [Mn(1)–O(1) = 1.891(3) Å] which rests slightly above the plane of the ligand. As per usual the NacNac ligand enforces a tight angle with the metal [N(1)–Mn(1)–N(2) = 93.85(16)°], while the phenoxide is slightly skewed to one side [N(1)–Mn(1)–O(1) = 125.15(16)°, N(2)–Mn(1)–O(1) = 141.80(16)°]. If crystallization is initiated too quickly the half-reacted complex

19b is recovered, although it is fully converted to product if redissolved into the mother liquor. The structure of **19b** includes one molecule of **19** and one molecule of **16**. The bond distances and angles of the two complexes within **19b** are identical to their pure forms.

Since the molecule **20** rests on an inversion centre a corrected Z factor (Z') was required in order to correctly describe the chemical structure. The distance between C(6) and O(1) (1.243(3) Å) clearly reveals that a double bond is present. While the intra-ring distances are a little more vague [C(1)–C(6) = 1.472(4), C(1)–C(2) = 1.351(4), C(3)–C(4) = 1.440(4) Å], they are consistent with a single bond between C(1) –C(2) and C(3) –C(4) and a double bond between C(1)–C(2). The C(3) – C(3') distance (1.416(6) Å) is slightly long for a double bond, however the complete planarity of the structure indicates the sp^2 character of each atom, necessitating the presence of a double bond.

Table 5.8.1 Crystal Data and Structure Analysis Results for Complexes **14-17**.

	14	**16**	**17**
Formula	$C_{28.25}H_{40.75}O_3Mn$	$C_{33}H_{52}N_2SiMn$	$C_{34}H_{52}N_2O_2SiMn$
FW	483.30	559.80	603.81
space group	Monoclinic, ***P2(1)/c***	Monoclinic, ***P2(1)/n***	Monoclinic, ***P2(1)/n***
a (Å)	12.473(3)	10.7504(13)	12.6721(13)
b (Å)	17.353(5)	21.524(3)	12.6426(13)
c (Å)	17.081(4)	15.0063(19)	22.342(2)
α (deg)	90	90	90
β (deg)	108.568(4)	96.700(2)	92.690(2)
γ (deg)	90	90	90
V (Å^3)	3505.4(16)	3448.5(7)	3575.4(6)
Z	4	4	4
radiation (Kα, Å)	0.71073	0.71073	0.71073
T (K)	203(2)	203(2)	209(2)
D_{calcd} (g cm^{-3})	0.916	1.078	1.122
μ_{calcd} (mm^{-1})	0.396	0.439	0.432
F_{000}	1037	1212	1300
R, R_w[2 a]	0.0799, 0.1875	0.0598, 0.1668	0.0675, 0.1262
GoF	1.038	1.044	1.087

[a] $R = \Sigma||Fo| - |Fc||/\Sigma|F|$. $Rw = [\Sigma(|Fo| - |Fc|)^2/\Sigma wFo^2]^{1/2}$.

Table 5.8.2 Crystal Data and Structure Analysis Results for Complexes **18-20**.

	18	**19**	**20**
Formula	$C_{135}H_{190}N_4O_4Mn_3$	$C_{43}H_{62}N_2OMn$	$C_{24}H_{40}O2$
FW	2097.73	677.89	408.60
space group	Orthorhombic, *Pca2(1)*	Monoclinic, *P2(1)/n*	Triclinic, *P-1*
a (Å)	28.55(4)	19.548(3)	6.0664(15)
b (Å)	15.69(2)	9.7800(15)	10.355(2)
c (Å)	32.15(5)	22.978(4)	10.418(3)
α (deg)	90	90	81.561(5)
β (deg)	90	115.912(3)	76.564(5)
γ (deg)	90	90	81.358(5)
V (Å^3)	13481(37)	3985.2(11)	625.0(3)
Z, (Z')	4	4	2, (1)
radiation (Kα, Å)	0.71073	0.71073	0.71073
T (K)	213(2)	213(2)	209(2)
D_{calcd} (g cm^{-3})	1.034	1.130	1.086
μ_{calcd} (mm^{-1})	0.325	0.364	0.066
F_{000}	4540	1468	224
R, R_w[2 a]	0.0803, 0.1805	0.0606, 0.1393	0.0617, 0.0968
GoF	1.040	1.010	1.049

[a] $R = \Sigma|Fo| - |Fc|/\Sigma|F|$. $Rw = [\Sigma(|Fo| - |Fc|)^2/\Sigma wFo^2]^{1/2}$.

5.9 Experimental Section:

All reactions were carried out under a dry nitrogen or argon atmosphere. Solvents were dried using an aluminum oxide solvent purification system, CHO was purchased from Aldrich (>98 %) and was freshly distilled and degassed prior to each run. All alcohols were purchased from Aldrich and used after drying *in vacuo*. $[Mn(CH_2SiMe_3)_2(THF)]_2$ was prepared as described in Ch 3. The ligands used for entries **14**,[40] **15**,[40] **16**,[39] **17**,[42] and **19**[43] were prepared according to literature references and were only used once the purity was > 98% by NMR. Infrared spectra were recorded on an ABB Bomem FTIR instrument from Nujol mulls prepared in a drybox. Samples for magnetic susceptibility were pre-weighed inside a drybox equipped with an analytical balance and measured on a Johnson Matthey Magnetic Susceptibility balance. Molecular weight and product dispersity was measured on a Splatastic GPC/SEC. NMR were collected on an INOVA Varian 300 MHz instrument in $CDCl_3$. Elemental analysis was carried out with a Perkin-Elmer 2400 CHN analyzer. Data for X-ray crystal structure

determination were obtained with a Bruker diffractometer equipped with a 1K Smart CCD area detector.

Polymerization Details: The 150 mL reactor was dried at 120 °C under vacuum for a minimum of 4 hours prior to each run. The catalyst and solvent mixture was then injected under a stream of argon gas, following which the reactor was pressurized to 40 bar CO_2 at 40 °C for 4 hours. CHO was then injected and the pressure and temperature were raised to those required for the run. After the run was complete, the reactor was vented and 30 mL of MeOH was injected in order to quench the reaction. The reactor was then drained and a portion removed for NMR. The bulk of the solution from the reactor was then stirred with ~500 mL of petroleum ether in order to precipitate the polycarbonate portion.

Synthesis of $[Mn(CH_2\{4\text{-}Me\text{-}2\text{-}tBu\text{-}6'C_6H_2O\}_2)(THF)]_2(C_7H_8)_{0.75}$ (14): A solution of the alcohol (0.150 g, 0.440 mmol) in toluene (5 mL) was slowly added to a solution of $[Mn(CH_2Si(CH_3)_3)_2(THF)]_2$ (0.133 g, 0.440 mmol) also in toluene (4 mL). The orange solution quickly discoloured to yield a clear solution. The solution was then cooled to -35 °C and allowed to stand for 24 hours, after which, colourless extremely air-sensitive X-ray quality crystals of **14** were formed (0.176 g, 0.365 mmol, 83%).

IR (Nujol) cm $^{-1}$: 2928 (s), 2824 (s), 1606 (w), 1303 (m), 1303 (m), 1278 (w), 1220 (w),1201 (m), 1127 (w), 872 (m), 848 (w), 807 (w), 704 (w).

Elemental Analysis (Found) for $MnC_{28.25}H_{40.75}O_3Mn_4$: C 70.20 (70.38), H 8.50 (8.62). $\mu_{eff} = 6.85\ \mu_{BM}$.

Synthesis of $[Mn(^{iPr}NacNac)(CH_2SiMe_3)]$ (16): A solution of the ^{iPr}NacNac ligand (0.250 g, 0.597 mmol) in hexanes (5 mL) was slowly added to a solution of $[Mn(CH_2Si(CH_3)_3)_2(THF)]_2$ (0.180 g, 0.597 mmol) also in toluene (4 mL). The orange solution quickly turned a clear yellow. If the solution was allowed to stand at room temperature overnight, crystals of the THF adduct **15** were isolated. These crystals

slowly converted to a hexanes soluble solution over the course of several days. If the hexanes soluble solution is cooled to -35°C and allowed to stand for 24 hours, yellow extremely air-sensitive X-ray quality block crystals of **16** were formed. After two subsequent concentrations and recrystallizations the total crop of crystalline material was (0.321 g, 0.573 mmol, 96%).

IR (Nujol) cm $^{-1}$: 3088 (w), 3076 (w), 1172 (w), 1131 (m), 1071 (s), 1022 (s), 961 (w), 944 (m), 900 (w), 875 (m), 831 (w), 733 (m), 726 (m), 711 (m), 630 (w).

Elemental Analysis (Found) for $MnC_{33}H_{52}N_2Si$: C 70.80 (70.48), H 9.36 (9.62), N 5.00 (5.08). $\mu_{eff} = 7.25\ \mu_{BM}$.

Synthesis of [Mn(^{iPr}NacNac)(μ-$O_2CH_2SiMe_3$)]$_2$ (17): A solution of **16** (0.250 g, 0.447 mmol) in hexanes (10 mL) was exposed to 1.1 atm of dry CO_2. The yellow solution slowly turned colourless over several hours. The solution was then cooled to -35°C and allowed to stand for 24 hours, after which X-ray quality block crystals of **17** were formed (0.256 g, 0.424 mmol, 95%).

IR (Nujol) cm $^{-1}$: 3087 (w), 3076 (w), 1160 (w), 1128 (w), 1066 (s), 1020 (s), 952 (w), 888 (m), 870 (m), 824 (w), 730 (m), 722 (w), 710 (m), 605 (w).

Elemental Analysis (Found) for $MnC_{34}H_{52}N_2O_2Si$: C 67.63 (67.50), H 8.68 (8.62), N 5.64 (5.52). $\mu_{eff} = 6.51\ \mu_{BM}$.

Synthesis of [(^{iPr}NacNac)Mn(μ$_2$-O-3,5-di-tBu-C_6H_3)$_2$Mn(μ$_2$-O-3,5-di-tBu-C_6H_3)$_2$Mn (^{iPr}NacNac)](C$_7$H$_8$)$_3$ (18): A solution of **16** (0.250 g, 0.447 mmol) in toluene (5 mL) was mixed with a toluene solution of 3,5-di-tBu-phenol (0.092 g, 0.447 mmol). The yellow solution slowly turned colourless over several hours. The solution was then cooled to -35°C and allowed to stand for 24 hours, after which X-ray quality crystals of **18** were formed (0.200 g, 0.095 mmol, 64% based on Mn).

IR (Nujol) cm $^{-1}$: 3079 (m), 3064 (w), 1155 (m), 1122 (w), 1075 (s), 1020 (s), 955 (m), 943 (m), 911 (m), 871 (m), 825 (w), 739 (m), 735 (m), 711 (m), 630 (w).

Elemental Analysis (Found) for $Mn_3C_{135}H_{190}N_4O_4$: C 77.29 (77.50), H 9.13 (9.62), N 2.67 (2.52). $\mu_{eff} = 4.12\ \mu_{BM}$.

Synthesis of [(^{iPr}NacNac)Mn(O-2,6-di-tBu-C_6H_3)] (19): A solution of **16** (0.250 g, 0.447 mmol) in toluene (5 mL) was mixed with a toluene solution of 2,6-di-tBu-phenol (0.092 g, 0.447 mmol). The yellow solution slowly turned colourless over several hours. The solution was then evaporated *in vacuo* and re-dissolved in hexanes. The solution was then cooled to -35°C and allowed to stand for 24 hours, after which X-ray quality crystals of **19** were formed (0.224 g, 0.331 mmol, 74%).

IR (Nujol) cm $^{-1}$: 3088 (w), 3070 (m), 1130 (m), 1078 (s), 1029 (s), 958 (m), 951 (w), 888 (w), 873 (m), 825 (w), 736 (m), 716 (m), 710 (m), 620 (w).

Elemental Analysis (Found) for $MnC_{43}H_{62}N_2O$: C 76.18 (76.50), H 9.22 (9.52), N 5.13 (5.22). $\mu_{eff} = 6.72\ \mu_{BM}$.

Synthesis of 3,3',5,5'-tetra-tert-butyl(bi-2,5-cyclohexadien-1-ylidene)-4,4'-dione (20): It was found that after sitting at room temperature for several days a hexanes solution of **19** (0.200 g, 0.295 mmol) gradually darkened in colour. The dark brown/red solution was placed in the freezer at -35 °C. After several days colourless crystals of **20** grew from the solution (0.077 g, 0.188 mmol, 32 % based on **19**).

IR (neat) cm $^{-1}$: 2930, 2820 (s), 1632 (w), 1620 (s), 1608 (w), 1450 (s), 1360, 1348 (s), 1250, 1220 (w), 1090 (m), 906 (m), 899 (w), 848 (w), 807 (w), 704 (w).

Elemental Analysis (Found) for $MnC_{43}H_{62}N_2O$: C 76.18 (76.50), H 9.22 (9.52), N 5.13 (5.22).

^{1}H NMR (300 MHz): 6.21 (4H), 1.05 (36 H).

5.10 References:

1) Cooper, A. I. *J. Mater. Chem.* **2000**, *10*, 207.
2) Jessop, P. G.; Ikariya, T.; Noyori, R. *Chem. Rev.* **1999**, *99*, 475.
3) Kendall, J. L.; Canelas, D. A.; Young, J. L.; DeSimone, J. M. *Chem. Rev.* **1999**, *99*, 543.
4) Behr, A. *Carbon Dioxide Activation by Metal Complexes*, VCH Publishers, New York **1988.**
5) Pang, H.; Liao, B.; Huang, Y. H.; Cong, G. M. *Chin. J. Appl. Chem.* **2001**, *18*, 347.
6) http://www.empowermaterials.com
7) Thorat, S. D.; Phillips, P. J.; Semenov, V.; Gakh, A. *J. Appl. Polym. Sci.* **2003**, *89*, 1163.
8) Peng, S. M.; An, Y.; Chen, C.; Fei, B.; Zhuang, Y.; Dong, L. *Polym. Degrad. Stab.* **2003**, *80*, 141.
9) Liu, B.; Chen, L.; Zhang, M.; Yu, A. *Macromol. Rapid Commun.* **2002**, *23*, 881.
10) Moore, D. R.; Coates, G. W. *Angew. Chem. Int. Ed.* **2004**, *43*, 6618.
11) Koning, C.; Wildeson, J.; Parton, R.; Plum, B.; Steeman, P.; Darensbourg, D. J. *Polymer* **2001**, *42*, 3995.
12) Jayachandran, J. P.; Reed, H. A.; Zhen, H.; Rhodes, L. F.; Henderson, C. L.; Allen, S. A. B.; Kohl, P. A. *J. Microelectromech. Syst.* **2003**, *12*, 147. b) Czaplewski, D. A.; Kameoka, J.; Mathers, R.; Coates, G. W.; Craighead, H. G. *Appl. Phys. Lett.* **2003**, *83*, 4836. c) Harnett, C. K.; Satyalakshmi, K. M.; Coates, G. W.; Craighead, H. G. *J. Photopolym. Sci. Technol.* **2002**, *15*, 493. d) Harnett, C. K.; Coates, G. W.; Craighead, H. G.; *J. Vac. Sci. Technol. B* **2001**, *19*, 2842.
13) Inoue, S.; Koinuma, H.; Tsuruta, T. *J. Polym. Sci. Part B* **1969**, *7*, 287. b) Inoue, S.; Koinuma, H.; Tsuruta, T. *Makromol. Chem.* **1969**, *130*, 210.
14) Kobayashi, M.; Tang, Y. L.; Tsuruta, T.; Inoue, S. *Makromol. Chem.* **1973**, *169*, 69. b) Kobayashi, M.; Inoue, S.; Tsuruta, T. *Macromolecules* **1971**, *4*, 658.
15) Kobayashi, M.; Inoue, S.; Tsuruta, T. *J. Polym. Sci. Polym. Chem. Ed.* **1973**, *11*, 2383.
16) Inoue, S.; Kobayashi, M.; Koinuma, H.; Tsuruta, T. *Makromol. Chem.* **1972**, *155*, 61.
17) Kuran, W.; Listos, T. *Macromol. Chem. Phys.* **1994**, *195*, 977.
18) Walther, D. *Coord. Chem. Rev.* **1987**, 136.
19) Darensbourg, D. J.; Holtcamp, M. W. *Coord. Chem. Rev.* **1996**, *153*, 155.
20) Kuran, W. *Prog. Polym. Sci.* **1998**, *23*, 919.
21) Inoue, S. *J. Polym. Sci. Part A* **2000**, *38*, 2861.
22) Aida, T.; Inoue, S. *Macromolecules* **1982**, *15*, 682. b) Takeda, N. ; Inoue, S. *Makromol. Chem.* **1978**, *179*, 1377.
23) Jung, J. H.; Ree, M.; Chang, T. *J. Polym. Sci. Part A* **1999**, *37*, 3329.
24) Aida, T.; Ishikawa, M.; Inoue, S. *Macromolecules* **1986**, *19*, 8.
25) Darensbourg, D. J.; Holtcamp, M. W. *Macromolecules* **1995**, *28*, 7577.
26) Darensbourg, D. J.; Holtcamp, M. W.; Struck, G. E.; Zimmer, M. S.; Niezgoda, S. A.; Rainey, P.; Robertson, J.B.; Draper, J. D.; Reibenspies, J. H. *J. Am. Chem. Soc.* **1999**, *121*, 107.
27) Darensbourg, D. J.; Wildeson, J. R.; Yarbrough, J. C.; Reibenspies, J. H. *J. Am. Chem. Soc.* **2000**, *122*, 12487.

28) Cheng, M.; Lobkovsky, E. B.; Coates, G. W. *J. Am. Chem. Soc.* **1998**, *120*, 11 018.
29) Moore, D. R.; Cheng, M.; Lobkovsky, E. B.; Coates, G. W. *J. Am. Chem. Soc.* **2003**, *125*, 11 911.
30) Moore, D. R.; Cheng, M.; Lobkovsky, E. B.; Coates, G. W. *Angew. Chem. Int. Ed.* **2002**, *41*, 2599.
31) Inoue, S.; Koinuma, H.; Yokoo, Y.; Tsuruta, T. *Makromol. Chem.* **1971**, 143.
32) Kuran, W.; Listos, T. *Macromol. Chem. Phys.* **1994**, *195*, 1011. b) Gorecki, P.; Kuran, W. *J. Polym. Sci. Part C* **1985**, *23*, 299.
33) Darensbourg, D. J.; Zimmer, M. S.; Rainey, P.; Larkins, D. L. *Inorg. Chem.* **2000**, *39*, 1578.
34) Kruper, W. J.; Dellar, D. V. *J. Org. Chem.* **1995**, *60*, 725. b) Kruper, W. J.; Dellar, D. US Patent 4,663,467 **1987**.
35) Qin, Z. Q.; Thomas, C. M.; Lee, S.; Coates, G. W. *Angew. Chem. Int. Ed.* **2003**, *42*, 5485. b) Soga, K.; Uenishi, K.; Ikeda, S. *J. Polym. Sci. Polym. Sci. Ed.* **1979**, *17*, 415.
36) Chen, X. H.; Shen, Z. Q.; Zhang, Y. F. *Macromolecules* **1991**, *24*, 5305.
37) Small, B. L.; Brookhart, M. *Polymer Prepr.* **1998**, *39*, 213. b) Johnson, L. K.; Mecking, S.; Brookhart, M. *J. Am. Chem. Soc.* **1996**, *118*, 267. c) Johnson, L. K.; Killian, C. M.; Brookhart, M. *J. Am. Chem. Soc.* **1995**, *117*, 6415.
38) Reardon, D.; Aharonian, G.; Gambarotta, S.; Yap, G. P. A. *Organometallics* **2002**, *21*, 786.
39) Lee, B. Y.; Bazan, G. C.; Vela, J.; Komon, Z. J. A.; Bu, X. *J. Am. Chem. Soc.* **2001**, *123*, 5352.
40) Matsushita, M.; Kamata, K.; Yamaguchi, K.; Mizuno, N. *J. Am. Chem. Soc.* **2005**, *127*, 6632. b) Mukherjee, S.; Weyhermuller, T.; Bothe, E.; Wieghardt, K.; Chaudhuri, P. *Dalton Trans.* **2004**, 3842.
41) Sugimoto, H.; Ohshima, H.; Inoue, S. *J. Polym. Sci. Part A: Polym. Chem.* **2003**, *41*, 3549.
42) Chamberlain, B. M.; Cheng, M.; Moore, D. R.; Ovitt, T. M.; Lobkovsky, E. B.; Coates, G. W. *J. Am. Chem. Soc.* **2001**, *123*, 3229.
43) Bambirra, S.; van Leusen, D.; Meetsma, A.; Hessen, B.; Teuben, J. H. *Chem. Commun.* **2003**, *4*, 522.

Chapter

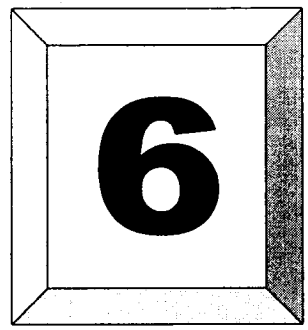

Low-Valent Manganese Complexes Supported by the Bis-Iminopyridinato Ligand

Table of Contents

6.1 Introduction:

Since the discovery Ziegler-Natta catalysts the science of olefin polymerization has progressed in leaps and bounds. Perhaps one of the biggest breakthroughs was made by the groups of Gibson,[1] Brookhart,[2] and Bennett[3] in the mid-1990's who pioneered a sterically bulky ligand bis-iminopyridinato ligand, [{2,6-(*i*Pr)$_2$PhN=C(Me)}$_2$(C$_5$H$_3$N)]

(see Figure 6.1.1), which produced extremely active late-metal olefin polymerization catalysts for the first time.

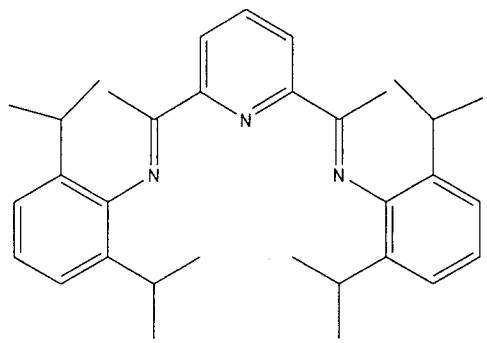

Figure 6.1.1 Structure of the Bis-Iminopyridinato (BisImine) Ligand.

This, and related ligand systems, spawned intense academic and industrial research into late-metal catalyzed polymerization. In addition, the observation that this ligand system is promoting a high degree of activity with many disparate metals across the periodic table suggests that the direct involvement of the ligand system in the reactivity of the metal could very well play a very significant role in the performance of the catalytic system.

6.2 Recent Advances:

Our group first became interested in the bis-iminopyridinato [2,6-(2,6-$\{^{i}Pr\}_2PhN=C\{CH_3\})_2(C_5H_3N)$] (BisImine) ligand system in 1999 when it was observed that reacting the [(BisImine)VCl_3] adduct with common alkylating agents led to alkylation of the pyridine ring as well as reduction to the rare $V^{(I)}$ oxidation state.[4] These results were the first step in exposing the non-innocent behaviour of this ligand system, and sparked subsequent study by our group.

Manganese has yet to be reported to support any meaningful level of polymerization with ethylene, as was the case for the late metals Fe, Co, Ni etc. before the advent of the bis-iminato (the so-called Brookhart/Gibson) ligands. [5] However, the Bis-Iminopyridinato ligand system is able to induce spectacular polymerization activity in both the late and early metals. Thus, the production of complexes and polymerization

attempts of the notoriously inactive metal Mn with this ligand system was of significant interest. Reaction of the ligand with $[MnCl_2(THF)_{1.5}]$ led to the expected, trigonal bipyramidal, [(BisImine)$MnCl_2$] adduct.[6] Surprisingly, even though the Mn complex exhibited the same coordination geometry as the highly active Fe, and Co analogues,[7] no polymerization activity resulted upon the activation of the complex with MAO in the presence of ethylene (under the same conditions as for Fe, and Co). In order to explore the reason for this lack of reactivity the [(BisImine)$MnCl_2$] compound was reacted with LiMe and $LiCH_2SiMe_3$ in an attempt to generate the alkylated pre-catalyst. Instead of the expected alkylation, reduced complexes which were assigned the $Mn^{(I)}$ and $Mn^{(0)}$ oxidation states (see Figure 6.2.1), respectively, were recovered, in line with the behaviour of the $V^{(III)}$ analogues.

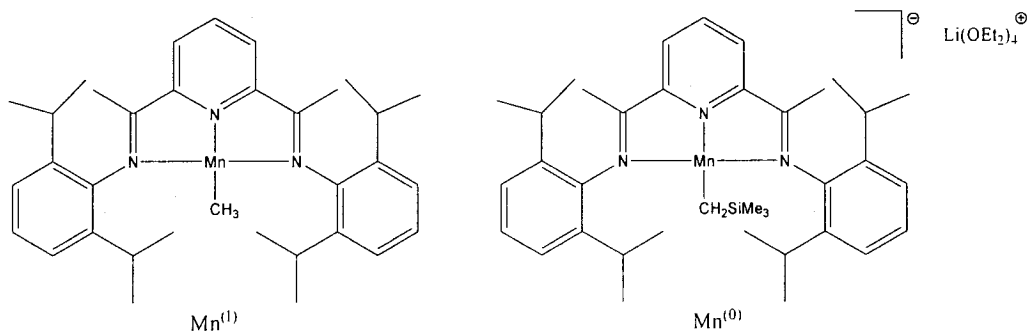

Figure 6.2.1 Suspected $Mn^{(I)}$ and $Mn^{(0)}$ Structures.

Though the one electron reduction from $Mn^{(II)}$ to $Mn^{(I)}$ is not unprecedented,[8] the two electron reduction to $Mn^{(0)}$ seemed quite unrealistic. Careful examination of the crystal structure and DFT calculations, revealed that the structure which was initially thought to contain a $Mn^{(0)}$ was actually most likely a $Mn^{(II)}$ complex. The dianionic ligand charge was attributed to the two imino methyl groups of the ligand having been deprotonated (see Scheme 6.2.2).[9] The same deprotonation had been previously observed in a similar ligand system adding further weight to this new structural assignment.[10] The $Mn^{(I)}$ structure, on the other hand, was never re-examined in order to determine if the oxidation state was truly +1.

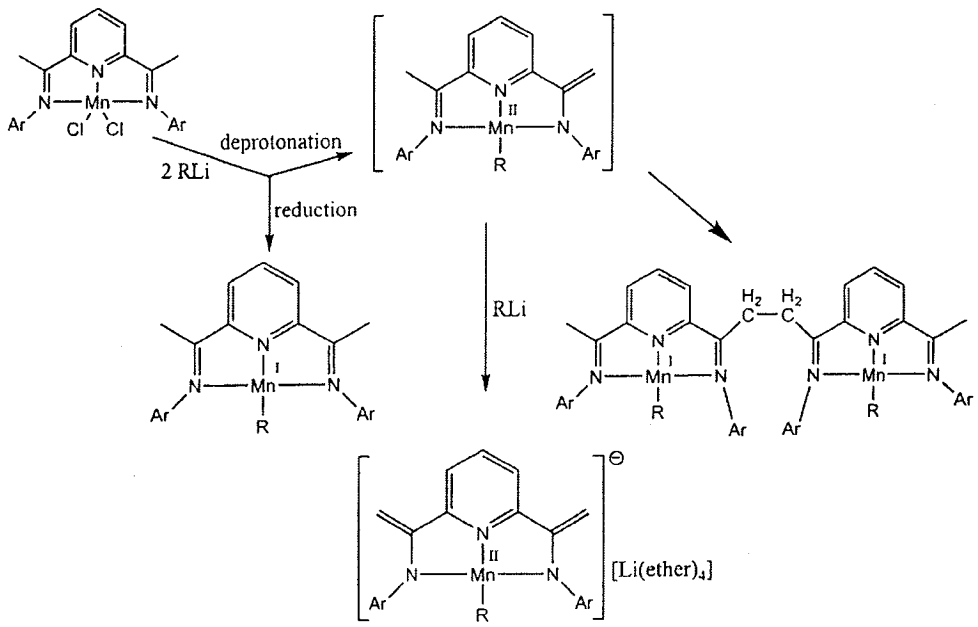

Scheme 6.2.2 Reaction Pathways for [(BisImine)Mn] Complexes.[9]

During the course of exploring the deprotonation reactions, a new dimeric complex was isolated which added further evidence that the imino methyl groups of the ligand were being deprotonated. This observation, together with literature data, indicates that the original [(BisImine)$MnCl_2$] complex undergoes several possible transformations when exposed to alkylating agents (see Scheme 6.2.2). Along with the deprotonation pathway it was thought that a mono-deprotonated transient Mn-R species was generated which would then either undergo a radical coupling to generate the dimeric $Mn^{(I)}$ complex, or react with another equivalent of alkylating agent in order to generate the doubly deprotonated [(BisIminato)$Mn^{(II)}$][Li(ether)$_4$] complex. Alternatively, instead of deprotonation, the reduction pathway may also be followed, generating a monomeric non-deprotonated [$Mn^{(I)}$-R] complex. Though the connectivity of the monomeric non-deprotonated complex assigned the formal oxidation state as $Mn^{(I)}$, the magnetic moment and DFT calculations actually indicated that the complex should be described as a $Mn^{(II)}$ complex which is anti-ferromagnetically coupled to a ligand radical anion.[9] This finding further confused the role of the Bis-iminopyrdinato ligand, as it appeared that the ligand

was able to store electrons, forming organic radicals, thus making oxidation state assignment dubious.

The ambiguity involved in whether or not the ligand was retaining delocalized radicals led our group to explore the reactions of the free ligand with various equivalents of either Li metal or lithium naphthalenide in THF under an argon atmosphere. The investigations found that the ligand was able to retain up to three electrons within the delocalized system, to yield the paramagnetic complex **1** (see Scheme 6.2.3).[11]

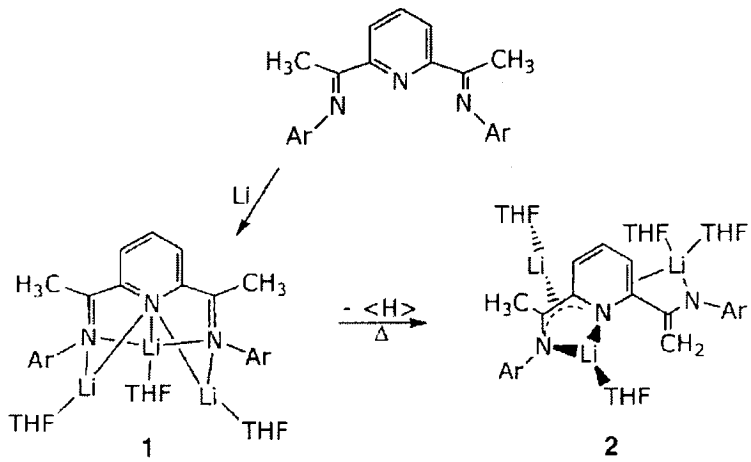

Scheme 6.2.3 Bis-Iminopyridinato Li Complexes.[10]

Complex **1** spontaneously decomposed to the diamagnetic, tri-anionic compound **2** if heated in toluene, or if generated from lithium naphthalenide via a one electron oxidation. These results clearly demonstrate that: 1) the ligand is capable of storing up to 3 electrons and; 2) there is significant radical character located on the imino methyl groups of the ligand which could explain coupling observed above.

The formally tri-anionic ligands generated by the reaction of three equivalents of Li with the free ligand proved to be synthetically uninteresting due to its thermal instability. Therefore, the rational preparation of the mono-anionic ligand was explored. It was found that reaction of LiMe with the ligand led to a dimeric compound (the Y group is an identical unit bound at the para position, except that an ether molecule is coordinated to Li) in which the pyridine nitrogen is alkylated (see Scheme 6.2.4).[12]

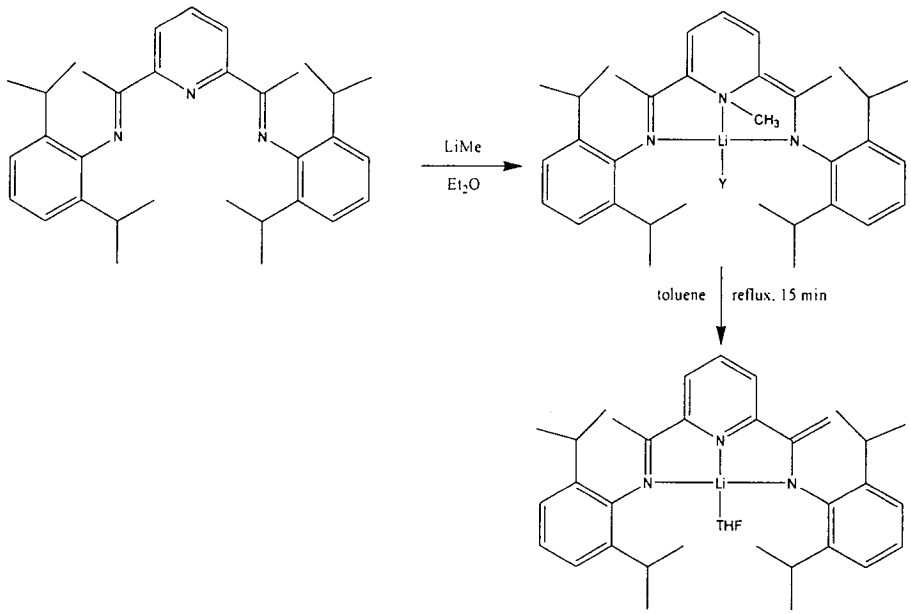

Scheme 6.2.4 Generation of Mono-Deprotonated BisImine Ligand (BisImine=CH_2).

If the nitrogen alkylated complex is then placed into toluene and refluxed briefly the mono-deprotonated ligand (BisImine=CH_2) results. Formation of this ligand again reiterates the fact that the imino methyl groups of the ligand are quite susceptible to attack by alkylating agents.

The ability of this ligand to form complexes with the deceiving appearance of low-valent complexes is not limited to Mn. In fact it seems a rather general behaviour having been observed with lanthanide, Al and Fe complexes. An intriguing question obviously arises as to whether or not the ability of storing electrons can be used for purposes other than simply preparing complexes with the formal appearance of low-valent states. In our group it was found that when the [(BisImine)VCl_3] was reacted with excess NaH in THF, a di-nitrogen bridged dimeric structure resulted (see Scheme 6.2.5).[13] The generation of di-nitrogen bound organometallic complexes isn't limited to V, as it was also observed that [(BisImine)Co] complexes were also able to form analogous di-nitrogen structures.[14]

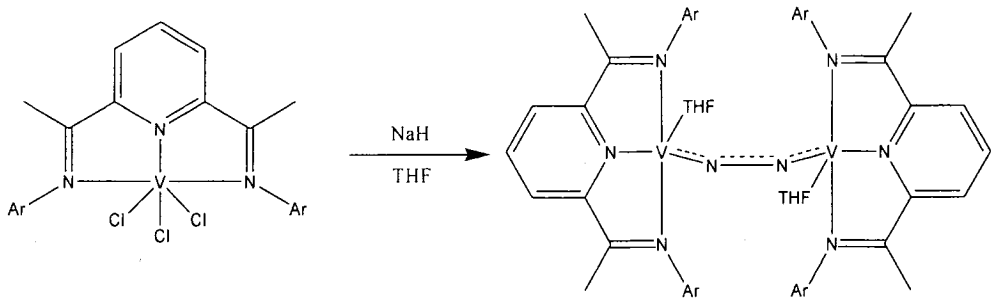

Scheme 6.2.5 Formation of [(BisImine)V] Di-Nitrogen Complex.

Once again, the metal may formally be regarded as the very rare case of a zero-valent complex. However, DFT calculations, and the distorted bond lengths within the ligand system would tend to indicate that each V is in the +3 oxidation state and each ligand is carrying a -2 charge. In turn this implies a substantial amount of reduction of the coordinated di-nitrogen unit, as it is also demonstrated by the lengthening of the N-N distance. Therefore, the ligand system is capable of stabilizing complexes whose appearance as low-valent is exclusively a formalism. However, the metal seems to retain the very high reactivity expected from a genuinely low-valent species, as the ability to coordinate an exceedingly stable molecule such as N_2 seems to suggest.

6.3 Research Rationale:

The target of this sub-project was to probe the ability of the bis-imine pyridinato ligand to sustain catalytic activity even with a metal, Mn, which notoriously does not produce catalysts. Thus, the immediate synthetic target was to prepare a complex containing two Mn-R functions, which eventually could be activated by Lewis acids.

The Mn di-alkyl $[Mn(CH_2SiMe_3)_2(THF)]_2$ (see Chapter 3) offers to provide new insights into the reactivity of [(BisImine)Mn] complexes as the metal centre already contains two alky groups. This will preclude the need for external alkylating agents which could detrimentally react with the ligand, therefore allowing the formation of the elusive $[(BisImine)MnR_2]$ type of complex (see Scheme 6.3.1).

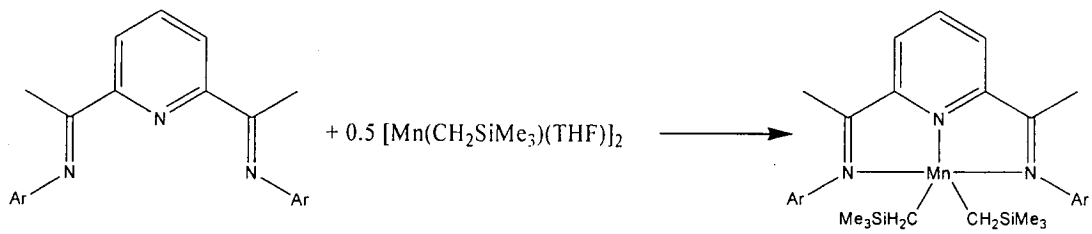

Scheme 6.3.1 Proposed Formation of [(BisImine)MnR_2].

The [(BisImine)MnR_2] complex would then be tested for ethylene polymerization activity, to evaluate whether this new synthetic strategy will finally lead to a functional catalyst.

As was previously reported, the mono-deprotonated ligand (BisImine=CH_2) may be readily synthesized via the addition of LiMe to the free ligand. This mono-anionic ligand, should react with $MnCl_2(THF)_{1.5}$ (see Scheme 6.3.2) to form a species analogous to the supposed $Mn^{(I)}$ complex found in Scheme 6.2.1

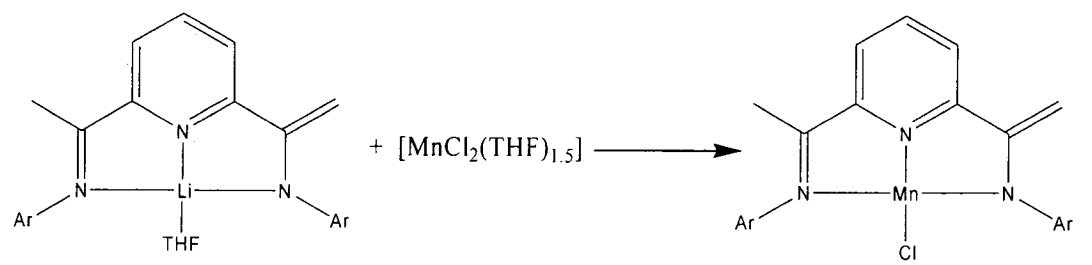

Scheme 6.3.2 Proposed Formation of [(BisImine=CH_2)MnCl].

This model structure should allow for a better comparison of the electronics and crystal structure in order to determine the proper oxidation state of the supposed $Mn^{(I)}$ complex.

We wish also to test whether it would be possible to use the electron storage ability of this ligand for the preparation of an unprecedented Mn di-nitrogen complex. The formation of low-valent Mn via the reduction of [(BisImine)$MnCl_2$] with NaH will be attempted in order to determine whether di-nitrogen coordination by Mn is possible with this unique ligand system (see Scheme 6.3.3).

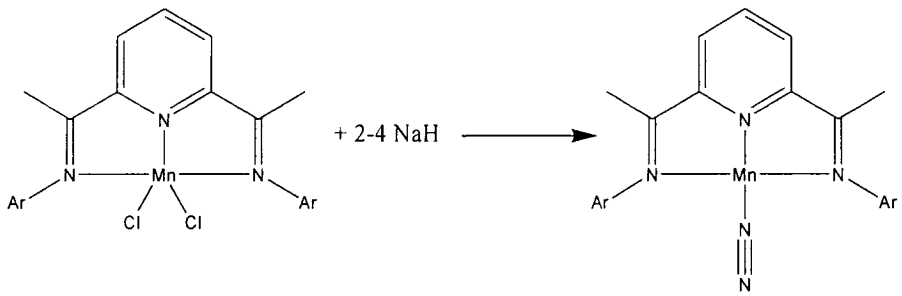

Scheme 6.3.3 Proposed Formation of Mn Di-Nitrogen Complex.

Di-nitrogen complexes of Mn are exceedingly rare, the only reliable example to date exists in the +1 oxidation state $[MnH(N_2)(dmpe)_2]$.[15]

6.4 Results and Discussion:

In order to have a good point of reference the neutral ligand was crystallized from toluene (see Figure 6.4.1).

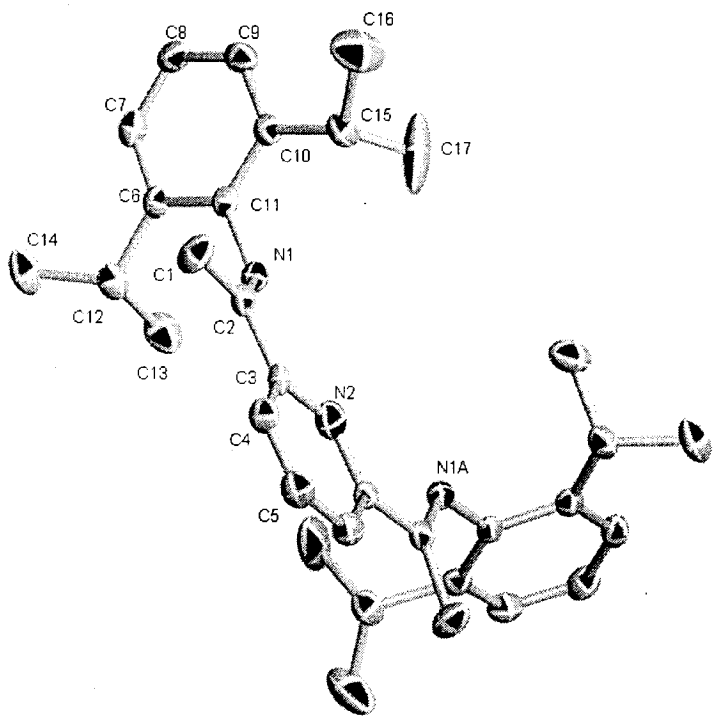

Figure 6.4.1 Structure of BisImine (**3**) with 30% Thermal Ellipsoids.

The imine bond and imino methyl groups quite obviously are composed of a double and single bond respectively [N(1)–C(2) = 1.278(4), C(1)–C(2) = 1.503(4) Å]. All other

bonds in the structure are within the expected distances, for a comparison of the bonds, along with the other complexes synthesized in this chapter see Table 6.6.1.

Upon mixing the Mn di-alkyl $[Mn(CH_2SiMe_3)_2(THF)]_2$ with the free ligand in either toluene or THF the colour immediately turned a very dark purple, which generally indicates a redox reaction as $Mn^{(II)}$ tends to be either colourless, or only very lightly coloured. X-ray quality crystals were eventually grown of the dimeric complex **4** (see Figure 6.4.2).

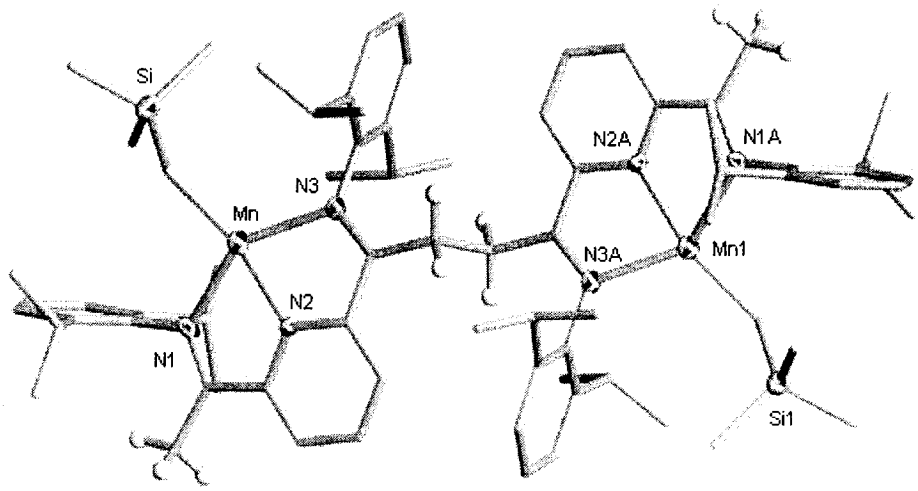

Figure 6.4.2 Structure of **4** with 30% Thermal Ellipsoids, Carbon Ellipsoids Omitted for Clarity.

The complex was formed via the radical coupling of two of the ligand imino methyl groups in order to generate what appears to be two $Mn^{(I)}$ metal centres. Unfortunately, this structure is identical to the previously published example,[9] indicating that the Mn di-alkyl is incapable of creating a discrete [(BisImine)MnR_2] type of complex. Furthermore, this result would tend to indicate that the alkylating agents used in the introduction examples do not attack the ligand first, but rather add to the metal centre, and then subsequently are transferred to the ligand system. Since this complex was already obtained by our group via a different synthetic route, its coordination geometry will not be discussed here, however a comparison with the other complexes synthesized in this chapter can be found in Table 6.6.1.

Reaction of $[MnCl_2(THF)_2]$ with the mono-deprotonated ligand (BisImine=CH_2) led to the formation of the monomeric metallate structure [(BisImine=CH_2)Mn-μ_2-

$Cl_2Li(THF)_2)$] (**5**) (See Figure 6.4.3). The Mn is found in a distorted trigonal bi-pyramidal coordination geometry with the equatorial plane occupied by the two bridging chlorides, and the pyridine nitrogen [Mn–Cl(1) = 2.436(3), Mn–Cl(2) = 2.417(3), Mn–N(2) = 2.209(5) Å, N(3)–Mn–Cl(1) = 124.92(17), N(3)–Mn–Cl(2) = 139.01(18)°].

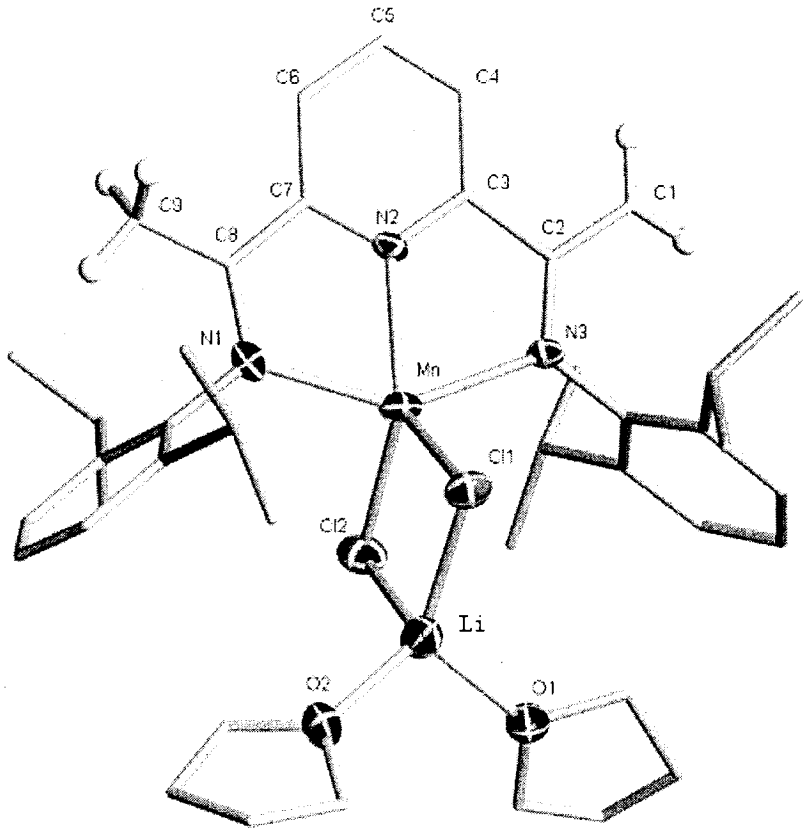

Figure 6.4.3 Structure of **5** with 30% Thermal Ellipsoids, Carbon Ellipsoids Omitted for Clarity.

The axial positions are filled by the remaining two nitrogen atoms [Mn–N(1) = 2.295(7), Mn–N(3) = 2.334(6) Å, N(1)–Mn–N(3) = 145.1(2), N(1)–Mn–Cl(1) = 103.13(19)°]. It appears that the anionic charge is delocalized over the ligand framework as the C(1)–C(2) and C(8)–C(9) distances are longer than expected [1.439(10) and 1.486(10) Å respectively]. The imine bonds reflect this delocalized charge by their significant lengthening [C(2)–N(3) = 1.338(8), C(8)–N(1) = 1.366(9) Å]. A comparison of this structure with the published structure, which was assumed to be $Mn^{(I)}$, reveals some striking similarities between the two structures (see Table 6.4.4).

Table 6.4.4 Comparison of Supposed $Mn^{(I)}$,[6] and $Mn^{(II)}$ [(BisImine=CH_2)Mn-μ_2-$Cl_2Li(THF)_2$)] (**5**) Bond Distances.

[(BisImine)$Mn^{(I)}CH_3$][6]	[(BisImine=CH_2)Mn-μ_2-$Cl_2Li(THF)_2$)] (**5**)
C(1)–C(2) = 1.467	C(1)–C(2) = 1.439(10)
C(8)–C(9) = 1.482	C(8)–C(9) = 1.486(10)
C(2)–C(3) = 1.449	C(2)–C(3) = 1.527(10)
C(7)–C(8) = 1.451	C(7)–C(8) = 1.437(10)
C(2)–N(3) = 1.333	C(2)–N(3) = 1.338(8)
C(8)–N(1) = 1.320	C(8)–N(1) = 1.366(9)

If the averaged distance for the $Mn^{(I)}$ and $Mn^{(II)}$ complexes are compared (1.475 vs. 1.463 Å) a difference of only 0.01 Å is observed which may very well indicate that the $Mn^{(I)}$ has actually lost one proton from an imino methyl group. The imine bonds are also remarkably close to one another with only a 0.03 Å difference between their averaged values. Given the similarity of the crystal structure of the two complexes, along with near identical magnetic moments ($Mn^{(I)}$ = 4.82 μ_B vs $Mn^{(II)}$ 4.98 μ_B) it would seem a reasonable assumption to make that the $Mn^{(I)}$ complex would more correctly be formulated as the $Mn^{(II)}$ complex [(BisImine=CH_2)$MnCH_3$].

The reduction of [(BisImine)$MnCl_2$] with 2.1 equivalents of NaH led to the formation of the formally $Mn^{(I)}$ structure [(BisImine)MnCl(THF)] (**6**) (See Figure 6.4.5). The coordination geometry of the Mn centre is best described as square pyramidal with the basal plane comprised of the ligand and the chloride atom [Mn(1)–N(1) = 2.280(4), Mn(1)–N(2) = 2.072(4), Mn(1)–N(3) = 2.305(4), Mn(1)–Cl(1) = 2.316(2) Å, N(1)–Mn(1)–N(2) = 73.46(14), N(1)–Mn(1)–N(3) = 142.39(13), N(1)–Mn(1)–Cl(1) = 103.72(11)°].

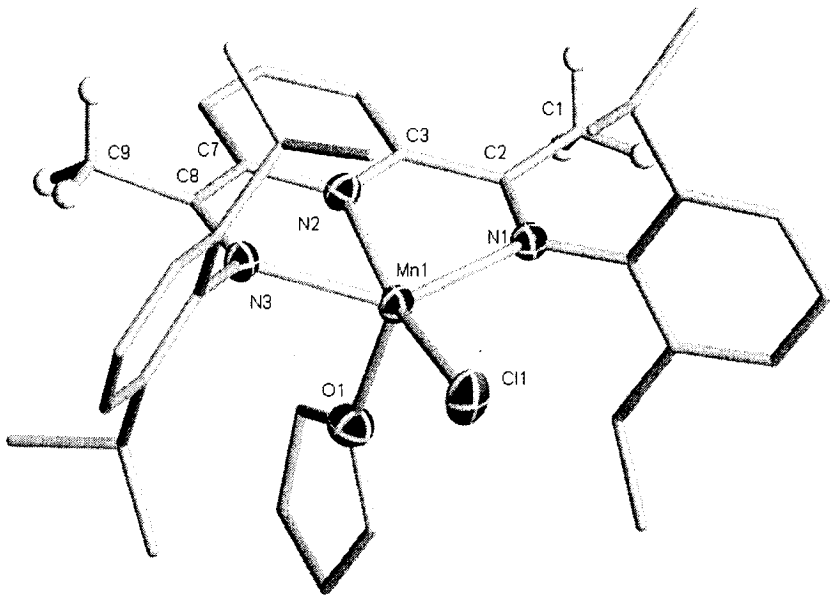

Figure 6.4.5 Structure of **6** with 30% Thermal Ellipsoids, Carbon Ellipsoids Omitted for Clarity.

The axial position is occupied by a molecule of coordinated THF [Mn(1)–O(1) = 2.171(4) Å, O(1)–Mn(1)–Cl(1) = 99.62(11)°]. The imino methyl groups of the ligand appear to be completely intact [C(1)–C(2) = 1.519(6), C(8)–C(9) = 1.511(6) Å] showing no signs of deprotonation. There is a slight lengthening of the imine bonds [N(1)–C(2) = 1.311(4), N(3)–C(8) = 1.303(4) Å] and the bonds adjacent to the pyridine [C(2)–C(3) = 1.444(5), C(7)–C(8) = 1.443(5) Å] which may indicate that the ligand is, in fact, carrying a negative charge which would make the complex $Mn^{(II)}$. The rather low magnetic moment (4.14 μ_B) would tend to favour a formulation that the metal is in the +2 oxidation state and that a radical character exists on the ligand, however without detailed calculations this must remain a conjecture.

As stated in the introduction, Mn catalysts tend to produce abysmal activities when used for the production of PE. However, to not even attempt polymerization with the newly synthesized complexes **4-6** would do this thesis a disservice. As such each was tested under standard conditions (see Table 6.4.6).

Table 6.4.6 Polymerization Results[a] for Mn Catalysts **4-6**.

Catalyst	Amount (mmol)	PE Produced (g)	Activity (g PE/mmol·h·atm)
[Fe(BisImine)Cl_2][16b]	0.01	3.90	678
4	3.0	0.48	0.320
5	3.0	0.44	0.293
6	3.0	0.51	0.340
Blank	0	0.11	-

[a] Conditions: 500 eq MAO activator, 1 atm ethylene, 24 °C, 30 minutes reaction time, total volume 150 mL in toluene.

From the table it is readily apparent that these Mn complexes are no exception to the general trend of being poor PE catalysts. The Mn complexes **4-6** only produce measurable quantities for PE when used in mmol amounts, as compared to their Fe analogues which utilize μmol amounts and yield better results. On the whole these results are not terribly surprising, and serves to confirm the trend of poor activity for Mn based PE catalysts.

6.5 Conclusions:

This work has confirmed that even with Mn the Bis-Iminopyridinato ligand system continues to have a fickle nature[16] which is difficult to fully grasp. The reaction of the preformed Mn di-alkyl [$Mn(CH_2SiMe_3)(THF)]_2$ with the ligand system clearly shows that the presence of alkyl groups on the metal centre triggers the ligand transformation/reductive pathways regardless if the alkyl groups begin the reaction attached to the metal, or are added as their alkali-metal salts. Construction of the model $Mn^{(II)}$ compound [(BisImine=CH_2)Mn-μ_2-Cl_2Li$(THF)_2$)] (**5**) appears to have solved the oxidation state questions of the previously published $Mn^{(I)}$ complex [(BisImine)$MnCH_3$], which should now be considered as the $Mn^{(II)}$ [(BisImine=CH_2)$MnCH_3$] complex. Finally, though the reduction of the [(BisImine)$MnCl_2$] complex with NaH did not yield the hoped for di-nitrogen complex, it does appear that an actual $Mn^{(I)}$ complex may have been generated in this case, though the possibility that it is in the +2 oxidation state can not conclusively be ruled out. Further study with increased equivalents of NaH may lead to even lower oxidation states, or even the ever elusive Mn di-nitrogen complex.

6.6 X-Ray Crystallography Section:

The full crystallographic data, including bond lengths and angles may be found in Appendix 5. The abbreviated crystallographic data for the structures contained within this chapter are as presented in Tables 6.6.1 to 6.6.3.

Table 6.6.1 Selected Bond Distances for Complexes **3, 5,** and **6**.

(BisImine) (**3**)	[(BisImine=CH_2)Mn-μ_2-$Cl_2Li(THF)_2$)] (**5**)	[(BisImine)MnCl(THF)] (**6**)
C(1)–C(2) = 1.503(4) C(2)–C(3) = 1.500(4) C(2)–N(1) = 1.278(4)	C(1)–C(2) = 1.439(10) C(8)–C(9) = 1.486(10) C(2)–C(3) = 1.527(10) C(7)–C(8) = 1.437(10) C(2)–N(3) = 1.338(8) C(8)–N(1) = 1.366(9)	C(1)–C(2) = 1.519(6) C(8)–C(9) = 1.511(6) C(2)–C(3) = 1.444(5) C(7)–C(8) = 1.443(5) C(2)–N(1) = 1.311(4) C(8)–N(3) = 1.303(4)

Table 6.6.2 Crystal Data and Structure Analysis Results for Complexes **3** and **4**.

	3	**4**
Formula	$C_{33}H_{43}N_3$	$C_{74}H_{106}Mn_2N_6Si_2$
FW	481.70	1245.71
space group	Orthorhombic, ***Pbcn***	Monoclinic, ***P2(1)/c***
a (Å)	24.03(3)	17.469(3)
b (Å)	7.654(9)	12.0207(19)
c (Å)	16.105(19)	18.372(3)
α (deg)	90	90
β (deg)	90	110.800(3)
γ (deg)	90	90
V (Å^3)	2 962(6)	3618.9(10)
Z	4	2
radiation (Kα, Å)	0.71073	0.71073
T (K)	217(2)	203(2)
D_{calcd} (g cm^{-3})	1.080	1.143
μ_{calcd} (mm^{-1})	0.063	0.425
F_{000}	1048	1340
R, R_w[2 a]	0.0789, 0.1467	0.0818, 0.1541
GoF	1.182	1.088

[a] $R = \Sigma|Fo| - |Fc|/\Sigma|F|$. $Rw = [\Sigma(|Fo| - |Fc|)^2/\Sigma wFo^2]^{1/2}$.

Table 6.6.3 Crystal Data and Structure Analysis Results for Complexes **5** and **6**.

	5	**6**
Formula	$C_{51.50}H_{70}Cl_2LiMnN_3O_2$	$C_{37}H_{51}ClMnN_3O$
FW	895.89	644.20
space group	Tetragonal, ***P4(1)2(1)2***	Monoclinic, ***P2(1)/c***
a (Å)	14.230(4)	10.105(8)
b (Å)	14.230(4)	16.075(12)
c (Å)	51.930(9)	22.708(15)
α (deg)	90	90
β (deg)	90	102.01(4)
γ (deg)	90	90
V ($Å^3$)	10 516(7)	3 608(5)
Z	8	4
radiation (Kα, Å)	0.71073	0.71073
T (K)	203(2)	198(2)
D_{calcd} (g cm^{-3})	1.312	1.186
μ_{calcd} (mm^{-1})	0.391	0.471
F_{000}	3824	1376
R, R_w [2 a]	0.0723, 0.1082	0.0533, 0.1125
GoF	1.029	1.030

[a] $R = \Sigma||Fo| - |Fc||/\Sigma|F|$. $Rw = [\Sigma(|Fo| - |Fc|)^2/\Sigma wFo^2]^{1/2}$.

6.7 Experimental Section:

All reactions were carried out under a dry nitrogen or argon atmosphere. Solvents were dried using an aluminum oxide solvent purification system. The [{2,6-(iPr)$_2$PhN=C(Me)}$_2$(C_5H_3N)] and the deprotonated [(BisImine=CH_2Li(THF)] ligands were prepared according to literature procedure.[1a, 12] [Mn(CH_2SiMe_3)(THF)]$_2$ was prepared as detailed in Chapter 3. Infrared spectra were recorded on an ABB Bomem FTIR instrument from Nujol mulls prepared in a drybox. Samples for magnetic susceptibility were pre-weighed inside a drybox equipped with an analytical balance and measured on a Johnson Matthey Magnetic Susceptibility balance. Elemental analysis was carried out with a Perkin-Elmer 2400 CHN analyzer. Data for X-ray crystal structure determination were obtained with a Bruker diffractometer equipped with a 1K Smart CCD area detector.

Synthesis of Dimeric Complex (4): (BisImine) (0.250 g, 0.519 mmol) was dissolved in 15 mL of THF and $[Mn(CH_2SiMe_3)(THF)]_2$ (0.5 eq, 0.078 g, 0.259 mmol) was dissolved in a separate vial in 15 ml of THF. The two solutions were then mixed which led to an immediate colour change to dark purple. After reacting for 4 hours the solution was dried *in vacuo* and redissolved in 15 mL of toluene and layered with hexanes. After several days of standing at room temperature dark crystals of X-ray quality formed (0.063 g, (5.06×10^{-5} mol, 39.1% Yield).

IR (KBr, Nujol, cm^{-1}): 1644 (s), 1567 (m), 1530 (s), 1493 (s), 1365 (s), 1317 (w), 1266 (s), 1253 (s), 1227 (s), 1194 (w), 1162 (s), 1135 (w), 1110 (s), 1092 (s), 1050 (s), 1022 (s), 991 (s), 958 (s), 872 (s), 823 (s), 784 (m), 775 (w), 765 (m), 748 (s), 722 (s), 691 (s), 670 (w), 617 (w). $\mu_{eff} = 5.72\ \mu_B$.

Synthesis of $[(BisImine{=}CH_2)Mn\text{-}\mu_2\text{-}Cl_2Li(THF)_2]$ (5): $[BisImine{=}CH_2Li(THF)]$ (0.300 g, 0.536 mmol) was dissolved in 15 mL of THF and $[MnCl_2(THF)_2]$ (1.0 eq, 0.145 g, 0.536 mmol) was suspended in a separate vial in 15 ml of THF. The two solutions were then mixed which led to an immediate colour change to dark green. After reacting for 4 hours the solution was dried *in vacuo* and redissolved in 15 mL of toluene and centrifuged to remove small amounts of solid. The solution was then cooled to -35 °C, after standing for several days dark green crystals of X-ray quality formed (0.364 g, (0.406 mmol, 75.8% Yield).

IR (KBr, Nujol, cm^{-1}): 1624 (s), 1530 (s), 1393 (s), 1377 (s), 1278 (s), 1244 (s), 1217 (s), 1172 (m), 1100 (s), 1072 (m), 1038 (w), 1022 (s), 981 (s), 952 (m), 872 (s), 826 (s), 789 (m), 743 (w), 771 (m), 732 (s), 712 (s).

Elemental Analysis calcd (Found) for $MnC_{51.50}H_{70}N_3Cl_2LiO_2$: C 69.04 (69.21), H 7.88 (7.82), N 4.69 (4.66). $\mu_{eff} = 4.98\ \mu_B$.

Synthesis of [(BisImine)MnCl(THF)] (6): (BisImine) (0.300 g, 0.623 mmol) was dissolved in 15 mL of THF and $[MnCl_2(THF)_2]$ (1.0 eq, 0.68 g, 0.623 mmol) was suspended in a separate vial in 15 ml of THF. The two solutions were then mixed which and refluxed overnight, which led to the expected orange $[(BisImine)MnCl_2]$ complex. NaH (2.05 eq, 0.031 g, 1.28 mmol) was then added and the suspension was stirred for one week. Over the course of the week the colour slowly turned dark blue/black. The solution was then dried *in vacuo* and redissolved in 15 mL of hexanes after which it was centrifuged. The hexanes solution was then cooled to -35 °C for several days after which time orange crystals of X-ray quality were recovered (0.263 g, 0.408 mmo, 65.5% Yield).

IR (KBr, Nujol, cm^{-1}): 1565(m), 1461(s), 1377(s), 1309(m), 1300(w), 1263(m), 1231 (m), 1138(w), 1101(m), 1077 (w), 999(w), 960(w), 873(w), 820(m), 798(w), 766(s), 721(m), 696(w).

Elemental Analysis calcd (Found) for $MnC_{37}H_{51}N_3ClO$: C 68.98 (69.04), H 7.98 (8.09), N 6.52 (6.52). $\mu_{eff} = 4.14\ \mu_B$.

6.8 References:

1) Britovsek, G. J. P.; Bruce, M.; Gibson, V. C.; Kimberley, B. S.; Maddox, P. J.; Mastroianni, S.; McTavish, S. J.; Redshaw, C.; Solan, G. A.; Stromberg, S.; White, A. J. P.; Williams, D. J. *J. Am. Chem. Soc.* **1999**, *121*, 8728. b) Britovsek, G. J. P.; Dorer, B. A.; Gibson, V. C.; Kimberley, B. S.; Solan, G. A. (BP Chemicals Limited), WO 99/12981, **1999**. c) Britovsek, G. J. P.; Mastroianni, S.; Solan, G. A.; Baugh, S. P. D.; Redshaw, C.; Gibson, V. C.; White, A. J. P.; Williams, D. J.; Elsegood, M. R. J. *Chem. Eur. J.* **2000**, *6*, 2221. d) Bruce, M.; Gibson, V. C.; Redshaw, C.; Solan, G. A.; White, J. P. A.; Williams, D. J. *Chem. Commun.* **1998**, 2523.

2) Dias, E. L.; Brookhart, M.; White, P. S. *Chem. Commun.* **2001**, 423. b) Small, B. L.; Brookhart, M. *Polymer Prepr.* (Am. Chem. Soc., Div. Polym. Chem.) **1998**, *39*, 213. c) Johnson, L. K.; Mecking, S.; Brookhart, M. *J. Am. Chem. Soc.* **1996**, *118*, 267. d) Killian, C. M.; Tempel, D. J.; Johnson, L. K.; Brookhart, M. *J. Am. Chem. Soc.* **1996**, *118*, 11664. e) Johnson, L. K.; Killian, C. M.; Arthur, S. D.; Feldman, J.; McCord, E. F.; McLain, S. J.; Kreutzer, K. A.; Bennett, M. A.; Coughlin, E. B.; Ittel, S. D.; Parthasarathy, A.; Tempel, D. J.; Brookhart, M. S. (DuPont) WO 96/23010, **1996**. f) Johnson, L. K.; Killian, C. M.; Brookhart, M. *J. Am. Chem. Soc.* **1995**, *117*, 6414.

3) Bennett, A. M. A. CHEMTECH **1999**, July, 24-28. b) Bennett, A. M. A. (DuPont) WO 98/27124, **1998**.

4) Reardon, D.; Conan, F.; Gambarotta, S.; Yap, G. P. A.; Wang, Q. *J. Am. Chem. Soc.* **1999**, *121*, 9318.
5) Small, B. L.; Brookhart, M.; Bennett, A. M. A. *J. Am. Chem. Soc.* **1998**, *120*, 4049. b) Britovsek, G. J. P.; Gibson, V. C.; Kimberley, B. S.; Maddox, P. J.; McTavish, S. J.; Solan, G. A.; White, A. J. P.; Williams, D. J. *Chem. Commun.* **1998**, 849.
6) Reardon, D.; Aharonian, G.; Gambarotta, G.; Yap, G. P. A. *Organometallics* **2002**, *21*, 786.
7) Small, B. L.; Brookhart, M.; Bennett, A. M. A. *J. Am. Chem Soc.* **1998**, *120*, 4049. b) Britovsek, G. J. P.; Gibson, V. C.; Kimberley, B. S.; Maddox, P. J.; McTavish, S. J.; Solan, G. A.; White, A. J. P.; Williams, D. *Chem. Commun.* **1998**, 849.
8) Danilovtseva, E. N.; Annenkov, V. V.; Skushnikova, A. I.; Svyatkina, L. I. *J. Appl. Polym. Sci.* **2000**, *78*, 101. b) Rai, S. K.; Shivakumar, K.; Sherigara, B. S. *Eur. J. Polym.* **2000**, *36*, 1339. c) Jocheska, N.; Petrov, G.; Janevski, A.; Sebenik, A. *Eur. Polym. J.* **1996**, *32*, 209. d) Sumi, K.; Kimura, M.; Nakamura, I. *J. Polym. Sci., Part A: Polym. Chem.* **1994**, *32*, 1243.
9) Sugiyama, H.; Aharonian, G.; Gambarotta, S.; Yap, G. P. A.; Budzelaar, P. H. M. *J. Am. Chem. Soc.* **2002**, *124*, 12 268.
10) Nuckel, S.; Burger, P. *Organometallics* **2001**, *20*, 4345. b) Nuckel, S.; Burger, P. *Organometallics* **2000**, *19*, 3305.
11) Enright, D.; Gambarotta, S.; Yap, G. P. A.; Budzelaar, P. H. M. *Angew. Chem. Int. Ed.* **2002**, *41*, 3873.
12) Khorobkov, I.; Gambarotta, S.; Yap, G. P. A. *Organometallics* **2002**, *21*, 3088.
13) Vidyaratne, I.; Gambarotta, S.; Korobkov, I.; Budzelaar, P. H. M. *Inorg. Chem.* **2005**, *44*, 1187.
14) Scott, J.; Gambarotta, S.; Korobkov, I. *Can. J. Chem.* **2005**, *83*, 279.
15) Perthuisot, C.; Fan, M.; Jones, W. D. *Organometallics* **1992**, *11*, 3622.
16) Scott, J.; Gambarotta, S.; Korobkov, I.; Knijnenburg, Q.; de Bruin, B.; Budzelaar, P. H. M. *J. Am. Chem. Soc.* **2005**, *127*, 17204. b) Scott, J.; Gambarotta, S.; Korobkov, I.; Budzelaar, P. H. M. *J. Am Chem. Soc.* **2005**, *127*, 13 019.

Chapter

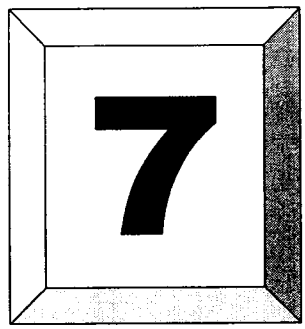

Chromium Catalyzed Ethylene Oligomerization

Table of Contents

7.1 Introduction:

Linear α–olefins are valued commodity chemicals for industrial applications as they have a variety of uses as precursors to detergents, co-polymers, synthetic lubricants and plasticizers.[1] In particular, the C_6 and C_8 fractions are in the highest demand as co-monomers for the production of LLDPE (Linear Low-Density PolyEthylene).

Traditionally, α–olefins were produced as a Shultz-Flory[2] distribution ranging from C_4-C_{20} (eg. the SHOP[3] process), making the production rather inconvenient, especially as extensive distillation is required in order to adequately separate the desired fractions. The highest market demand is currently for 1-butene, 1-hexene and 1-octene. While satisfactory processes for the production of 1-butene are conveniently available by using Ni-based catalyst systems, a selective system for producing 1-hexene has only recently been commercialized by Chevron Phillips in Qatar. The groundwork for the selective trimerization of ethylene was actually laid 39 years ago. In 1967, Manyik and Walker of the Union Carbide Corporation made the observation that a $Cr^{(III)}$ catalyst activated by PIBAO (partially hydrolyzed tri-isobutylaluminum) produced a polymer with regular butyl side-chains.[4] The authors later rationalized, and provided experimental evidence, that the presence of the butyl side-groups was a result of 1-hexene being formed and subsequently incorporated into the growing polymer chain.[5] It was further observed that the formation of 1-hexene was more influenced by the pressure of ethylene, than was the formation of PE. From these observations, they were able to derive a rate law for 1-hexene formation which was second order with respect to ethylene. This observation was incompatible with the known rate laws for polymer formation which, invariably, are first order with respect to ethylene; thus indicating that some, as yet, unknown mechanism was responsible for the selective formation of 1-hexene.

7.2 Recent Advances:

Since the original discovery of selective oligomerization a tremendous increase in interest has occurred for developing commercial catalysts, with over 200 patents being filed since 1987. In 2004, John Dixon of Sasol Technology published the most comprehensive review of both the patent and academic literature to date.[6] Due to the sheer number of publications in the field, only the most relevant to the scope of this chapter will be discussed.

The first major contribution to the field of selective oligomerization was made in a patent filed in 1991 by Reagan[7] describing the reaction of sodium pyrrolide with different stoichiometric ratios of $Cr^{(II)}$ and $Cr^{(III)}$ reagents. Though the resulting complexes were often poorly characterized, they all had one important feature in

common. When combined with various alkylating agents in the presence of ethylene, all these species performed oligomerization. Subsequent work by the Phillips company utilized 2,5-dimethylpyrrole, which had superior thermal and light stability along with [$Cr^{(III)}(2\text{-EH})_3$] (2-EH = 2-ethylhexanoate) which would soon become a standard source of Cr for oligomerization catalysts. Eventually, a catalyst that produced 156 666 (g/g·Cr·h) at 115 °C with a 93 % yield of 1-hexene was patented.[8] This system was subsequently optimized through the judicious use of activators and additives to yield one of the most active catalysts for 1-hexene production to date, again utilizing [$Cr^{(III)}(2\text{-EH})_3$] (see Scheme 7.2.1).[9]

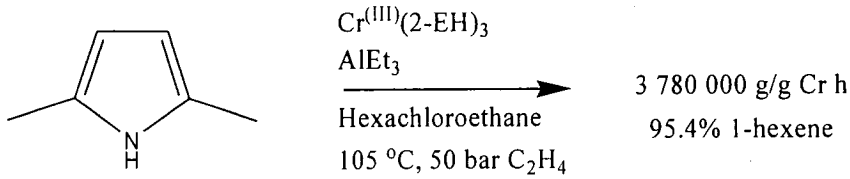

Scheme 7.2.1 Optimized Phillips System.

Quite similar to pyrrole in terms of both electronic and molecular orbital arrangement, the maleimidyl ligand was expected to also yield a viable catalyst. The Tosoh Corporation patented such a system in 1997 (see Scheme 7.2.2).[10]

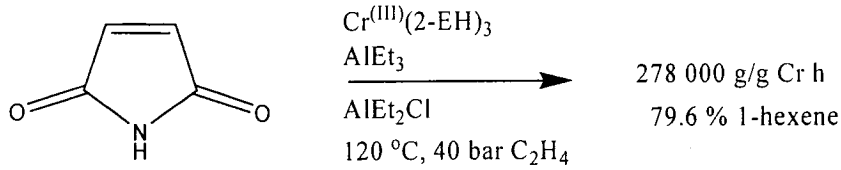

Scheme 7.2.2 Maleimidyl Ligand System.

It was observed that both the selectivity and activity could be increased via the addition of a chloro-derivatized alkylating agent $AlEt_2Cl$ in this case,[11] a similar trend was also noted in the case of the 2,5-dimethylpyrrole system.[12]

Given that the pyrrolide molecule is isoelectronic with the Cp ligand (Cp = cyclopentadienyl), it is quite odd that "CpCr" systems were known only for ethylene polymerization, with no traces of incorporated oligomers.[13] In fact, it is possible to convert a "CpCr" complex into a trimerization catalyst, but it requires the substitution of the ring by bulky aryl groups (see Scheme 7.2.3).[14]

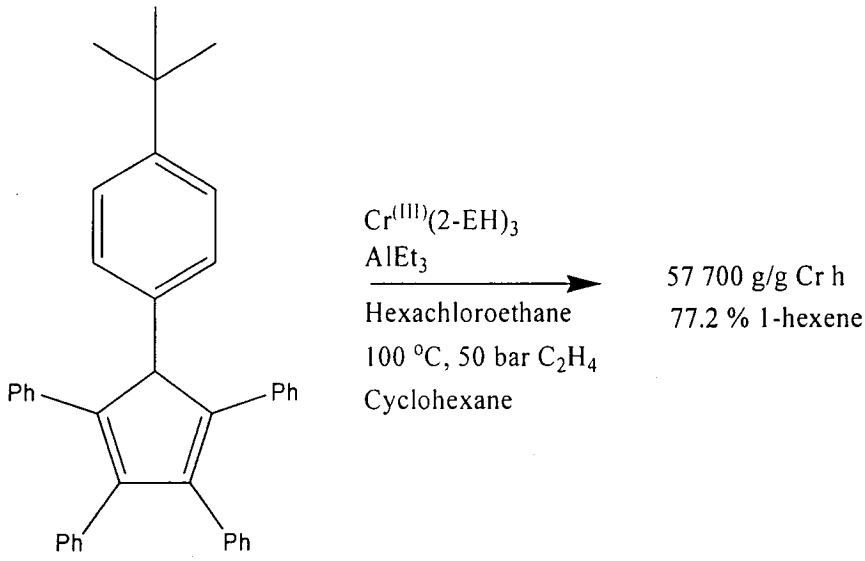

Scheme 7.2.3 Cp Based Ligand System.

The major drawback of the system, besides the exorbitant price of the ligand, is that a substantial amount of internal hexenes (14 %) are produced, which are very difficult to separate from the desired α-product. If less bulky groups are used the production of 1-hexene rapidly decreases, indicating that the steric bulk is an important prerequisite for the selective production of 1-hexene.

Recently, Hessen found that by substituting one of the Cp ring positions with a -$C(CH_3)_2Ph$ group, switched the output of a traditionally ethylene polymerization catalyst from PE production to 1-hexene. This remarkable discovery was ascribed to the hemi-labile nature of the phenyl ring, which was thought to stabilize intermediates in the trimerization cycle (see Scheme 7.2.4).[15,16]

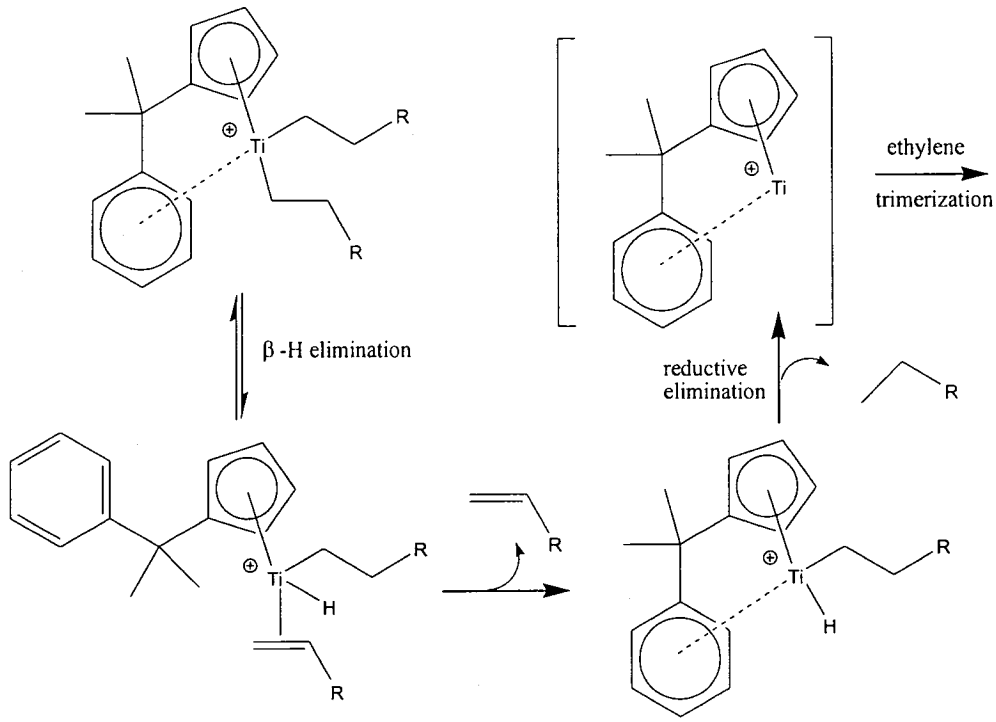

Scheme 7.2.4 Proposed Mechanism for Entrance Into Trimerization Pathway.

It was proposed that the hemi-labile properties of the ligand allowed both coordinative and electronic flexibility. This flexibility was thought to allow for the generation a $Ti^{(II)}$ species (top right Scheme 7.2.4) which would subsequently enter into the metallacyclic oligomerization cycle (see Section 7.3 for a mechanistic discussion). The most striking feature of the catalytic system was that it performed successfully at pressures and temperatures very low in comparison to the chromium systems (see Scheme 7.2.5).

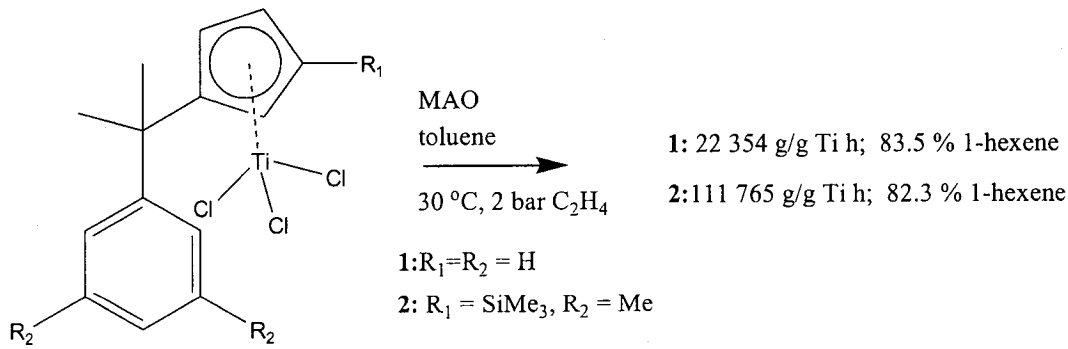

Scheme 7.2.5 Hemi-Labile Cp ligand (**1**) and Optimized Ligand (**2**).

Through the introduction of steric bulk to both the Cp ring and the pendant phenyl ring the authors were further able to increase the activity of the ligand with only a minute drop in selectivity.

Although these catalysts are highly performing, the absolute record in terms of selectivity is attributed to the so-called SNS Sasol ligand. The catalyst precursor is very simple and consists of a $CrCl_3$ unit octahedrally coordinated to the tridentate sulphur/ amine ligand [$(RSCH_2CH_2)_2NH$] (see Scheme 7.2.6).[17]

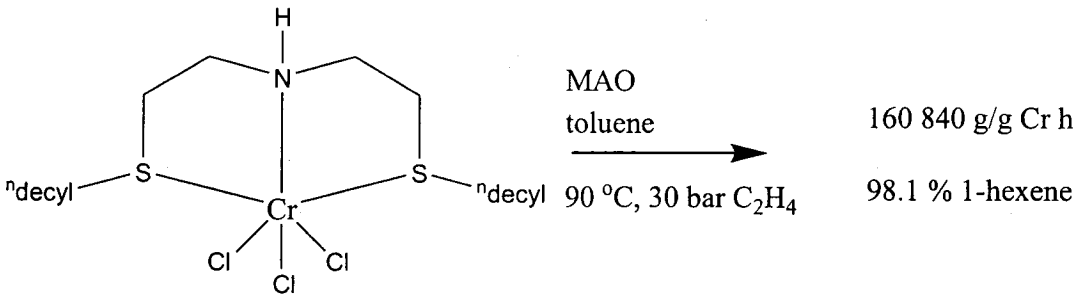

Scheme 7.2.6 SNS Ligand System.

By varying the groups attached to the sulphur atoms, Sasol's scientists were able to synthesize a variety of catalysts, which all showed remarkable selectivity for 1-hexene. The best catalyst reported utilized n-decyl groups. The catalyst was quite active while using only 30 eq. of MAO activator and yielded one of the highest overall selectivity for 1-hexene yet reported. The use of such a remarkably low amount of activator is of course an attractive feature in terms of cost-savings, safety and simplicity of the system.

Perhaps one of the largest advances in the field of ethylene oligomerization came with the publication of the PNP catalyst systems. The first major breakthrough using the PNP system occurred in 2002 when Wass of BP published an extremely active and selective catalyst (see Scheme 7.2.7).[18]

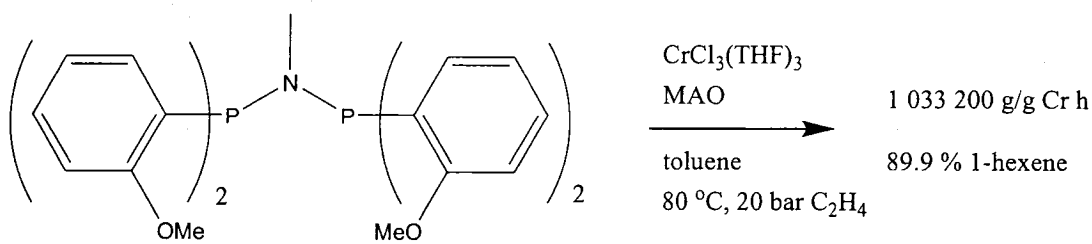

Scheme 7.2.7 PNP Ligand System.

The activity of the system is quite remarkable and is characterized by a very slow decrease of ~10 % /h of catalytic activity. This is in stark contrast to most other trimerization systems which lose most of their activity during the first 30 minutes.[6] What is even more outstanding about this catalyst system is that the C_6 oligomer fraction is 99.9 % composed of 1-hexene which was an unprecedented level of selectivity. Even more desirable, the authors didn't report the formation of PE, though this is most likely an oversight rather than a characteristic of the catalyst, as no catalyst has been reported to date which was free of PE production. It should be noted that formation of PE during the oligomerization process is highly undesirable, due to the fouling of the reactors requiring lengthy and costly clean up procedures. The second, and most significant, breakthrough in PNP based oligomerizations was reported by Sasol. Exchanging the methyl group attached to the central nitrogen with a bulkier group (^{n}pentyl, ^{i}Pr, Ph, Cy, etc.) significantly affected the outcome of the oligomerization. The selectivity switched from predominantly 1-hexene, to 1-octene.[19] The activity of these catalysts, though not quite to the level of the BP PNP system are still quite respectable (see Scheme 7.2.8). It should be reiterated that no other catalysts reported in the literature, at the time, produced predominantly 1-octene. Incidentally, 1-octene is the most requested α-olefin for industrial purposes, which demonstrates the value of these findings.

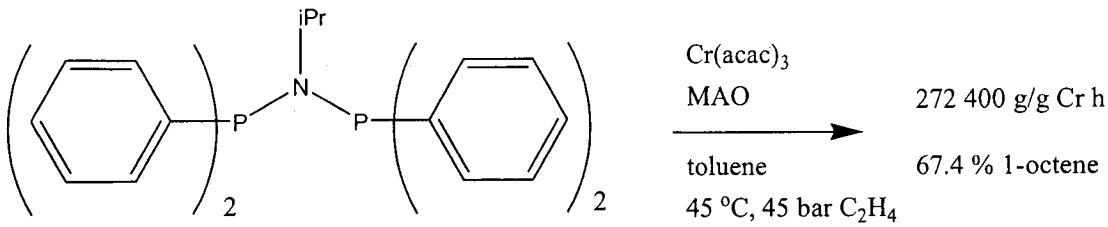

Scheme 7.2.8 1-Octene Producing PNP Ligand.

As a general trend in this family of catalysts, the production of 1-octene was favoured at lower temperature, and higher pressure conditions. In addition, substituents in the *ortho* positions had a remarkable impact on selectivity. In the absence of substituents, the catalyst produced 1-octene as the main oligomer (33% C_6 vs 61% C_8). However, the presence of the more bulky ethyl group changed the distribution more towards 1-hexene (47% C_6 vs 47% C_8). Finally, the presence of a dative bonding group (OMe) completely changes the selectivity to 1-hexene (74% C_6 vs 6% C_8).

7.3 Oligomerization Mechanism:

A rapid survey of the scientific and patent literature clearly pointed out that chromium is by far the most recurrent metal among all the reported catalytic systems. Although catalysts based on other metal systems (Ti,[15,16] V,[20] Ni,[21] and even U[5]) have been found, none can be compared to the chromium based systems in terms of activity and selectivity. Perhaps as a result of the great industrial interest in obtaining performing catalysts, the large majority of chromium catalysts are based on poorly defined *in situ* generated systems, or on simple coordination compounds which clearly are catalyst precursors. As a result, our understanding of the mechanism of the oligomerization process and especially of the factors which favour a selective process instead of a statistical distribution of oligomers or even polymerization remains very limited. It should be noted that selective and non-selective oligomerization and polymerization belong to the same category of process, through which C-C bonds are generated from ethylene coupling. The current level of understanding can basically be summarized with two current mechanistic proposals. The first may be regarded as an "aborted" polymerization: a polymerization occurring in the presence of a highly competitive β-H elimination process. As usual, the alkylation of the metal center and possible cationization may provide the conditions for the insertion reaction and chain growth. The extent of selectivity in this case will be determined by the same factors governing the β-H elimination process and which could be related to either steric factors or the thermal stability of the M-C bond or a combination of both. An important point is that the chain-growth mechanism does not require a redox reaction at the metal center. Therefore, the fact that the vast majority of chromium catalysts are based on the trivalent state makes good sense, given the stability of these d^3 octahedral compounds and the sometimes surprising chemical inertness of the Cr-C bond.[22] This mechanistic proposal was published by Cossee in 1964 to explain observations from Ziegler-Natta polymerization and, though unlikely, may account for the selective oligomerization process.

An alternative proposal, which is currently the most supported by observations, is known as the metallacyclic ring expansion mechanism, which is commonly abbreviated to the "metallacyclic mechanism". The cycle is initiated when two molecules of ethylene oxidatively add to a Cr centre, generating a metallacyclopentane (**A**) (see Scheme 7.3.1).

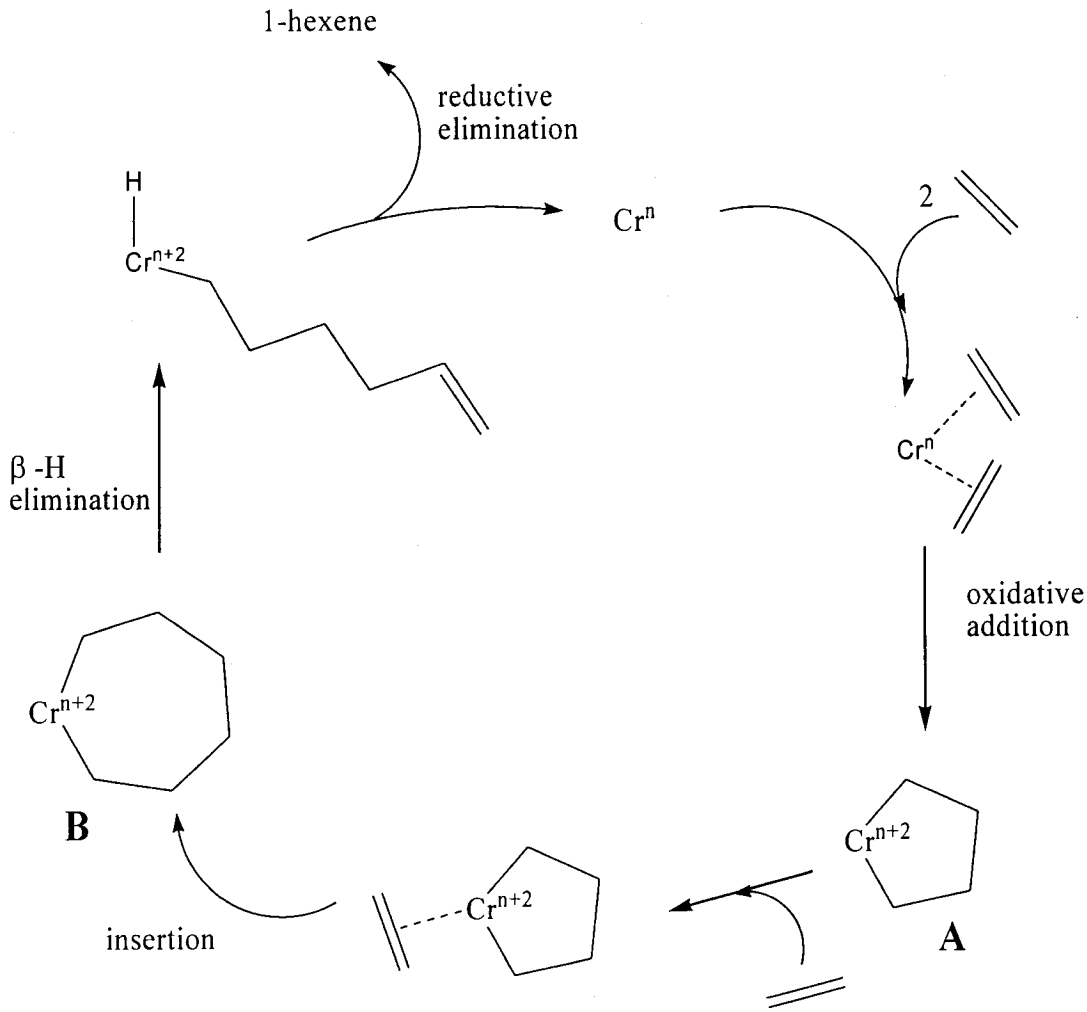

Scheme 7.3.1 Accepted Mechanism for Selective Trimerization.

At this point one of two events may occur. During the constructive pathway another molecule of ethylene coordinates to the metal and inserts into the ring expanding it to a metallacycloheptane. The other option is that a β–hydride elimination occurs followed by a subsequent reductive elimination of 1-butene. Once at position (**B**) two competing events may occur. If the rate of ethylene insertion is greater than the rate of β–hydride elimination, another ethylene molecule will insert into the ring generating a metallacyclononane. If, however, the rate of β–hydride elimination is greater (as in the case of selective trimerization), 1-hexene will be generated and the catalyst will be returned to its resting oxidation state (n).

There was debate[6] as to why the 5–membered ring should be more stable than the 7–membered, with the possible explanation that the 5–membered ring was too sterically constrained to allow β–hydride elimination. This hypothesis was further proven when Jolly synthesized, and crystallographically characterized both the five and seven membered chromacyclic rings using a Cp-based ligand system.[23] It was found that the 5-membered ring decomposed at 20 °C, while the 7–membered ring decomposed at 0 °C and liberated 1-hexene. These results showed that the metallacyclopentane species was much more stable than the corresponding metallacycloheptane, thus providing rather strong evidence as to why 1-hexene was selectively formed. Furthermore, when the metallacyclopentane compound was exposed to ethylene, and subsequently protonated, hexane was formed. These results quite clearly indicated that the metallacyclic mechanism was plausible, and that the insertion of ethylene into the 5–membered ring was also a viable route.

Several calculations have also been performed on the system in order to better elucidate the mechanism. The most accurate calculations were performed on Ti since it has a closed shell, allowing easier data processing with the currently available computational models. Not surprisingly, it was found that there is a significant energy barrier for the β-hydride elimination from the 5-membered ring and that the energy required for the insertion of another ethylene unit is minute in comparison, making it the preferred pathway.[24] Perhaps the only surprise revealed by the computational work was for the β–hydride elimination step. It was found that rather than the accepted two step process [β–hydride elimination to the metal followed by reductive elimination to yield an alkene (see Scheme 7.3.1)] a concerted hydride transfer takes place utilizing a linear C·····H·····C spatial arrangement (see Scheme 7.3.2).[25]

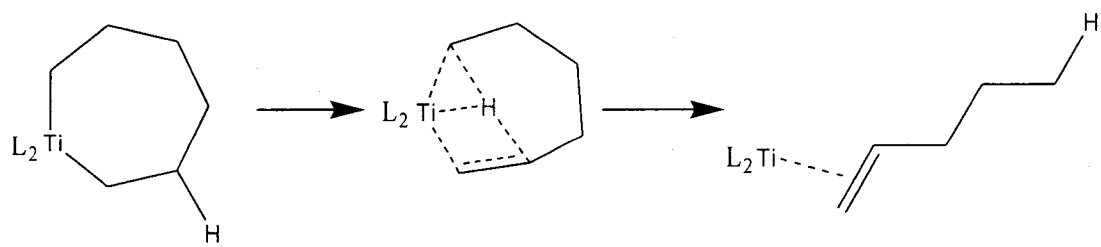

Scheme 7.3.2 Concerted Hydride Transfer Mechanism.

The 5-membered ring was incapable of attaining this transition state, further explaining the selectivity for 1-hexene. Of course, all calculation chemistry should be taken with a grain of salt, as several of the authors postulated that further growth to form 1-octene would be highly unlikely, if not impossible.[26]

It is important to note that this process requires a two electron redox couple. Namely there is a two-electron oxidative addition of the metal centre to the ethylene double bond and then, after subsequent insertions, a reductive elimination of α-olefin which restores the original catalyst oxidation state for further cycles. The fact that this mechanism explains very well the variety of the by-products occasionally observed during the oligomerization process is considered to be convincing evidence in favour for this type of mechanism. However, if a two electron process is at the very heart of the process the major question is: *which oxidation state of the chromium centre may be sufficiently reactive to perform reversible oxidative addition to ethylene.* Ethylene chromium complexes are exceedingly rare. The only example of a crystallographically characterized ethylene complex was reported by Jolly, with the fixation of ethylene at a $[CpCr(PMe_3)_2]$ residue.[22] Remarkably, this complex is non-reactive with ethylene, tentatively suggesting that the formally monovalent oxidation state of chromium is producing complexes which are too stable to initiate the insertion mechanism, although it is likely that the coordination of PMe_3 may be quenching the reactivity. Nonetheless, convincing evidence has been reported in the literature that a $Cr^{(I)}/Cr^{(III)}$ redox couple in some cases may be entering the catalytic cycle. Evidence has also been reported that other redox couples such as $Cr^{(0)}$-$Cr^{(II)}$,[27] $Cr^{(I)}$-$Cr^{(III)}$,[28] $Cr^{(II)}$-$Cr^{(IV)}$,[29] $Cr^{(III)}$-$Cr^{(V)}$,[30] may be involved. Of these the $Cr^{(II)}$-$Cr^{(IV)}$ couple appears to be the most likely candidate as they proceed through the most accessible and reactive oxidation states. Deuterium labelling experiments also are strong supporting evidence that the reaction proceeds via a metallacyclic mechanism (see Scheme 7.3.1), rather than a linear chain growth mechanism.[31]

One of the final points of the literature controversy for the selective trimerization reaction is with respect to the rate determining step. Several authors have noted a 2nd order dependence on ethylene, which would tend to indicate that the initial 5-membered ring formation is the rate determining step.[5,12] Whilst others have instead observed a 1st

order dependence on ethylene which would imply that the limiting step is the insertion of ethylene into a metallacycle.[15,32] Neither calculations, nor experimental evidence have solved this controversy. It is possible that the rate determining step is ligand dependant, therefore causing the discrepancies between the several observations.

It is important to note that with a few very rare exceptions,[33] all oligomerization catalysts require activation. The activator is usually an aluminum alkyl (MAO, $AlEt_3$, etc.) and its role is generally accepted to be the alkylation of the metal in order to generate an active catalyst. However, as will be explored later in this chapter, the role of the activators is not necessarily so straightforward.

7.4 Research Rationale:

It should be noted that while the results presented here are based exclusively on Cr, the σ,π-bonding pyrrolide complexes of Mn (See Chapter 4) were also tested given that the main thrust of this thesis was the investigation of the metal Mn. Not surprisingly, absolutely no oligomerization activity was ever observed in the case of Mn. The most likely reason for this is that if the metallacyclic mechanism is the true mechanism for this reaction, a metal must then possess a readily accessible two electron redox pair in order to participate. Manganese +2, with its highly stable d^5 electron configuration does not have access to a facile two-electron redox couple, and therefore was never expected to be active for this process.

The Cr project had three main directions which were explored. Foremost, was the utilization of the hemi-labile and σ,π–bonding pyrrole ligands developed in Chapter 2, to study the reactivity of chromium-based catalysts. Secondly, several amidinate (NCN) and amidate (NCO) ligands were explored as they bear a structural resemblance to the PNP tetramerization catalysts. Finally, an attempt was made to better determine the active oxidation state for the process via the careful exploration of $Cr^{(II)}$ and $Cr^{(III)}$ PNP and SNS ligand systems using well defined, rather than *in situ* generated catalysts.

Given the tremendous activity of the pyrrole based Phillips catalyst, we hoped that the N-MeDipyr and N-MeTripyr ligands (see Figure 7.4.1) developed in Chapter 2 may also provide promising results.

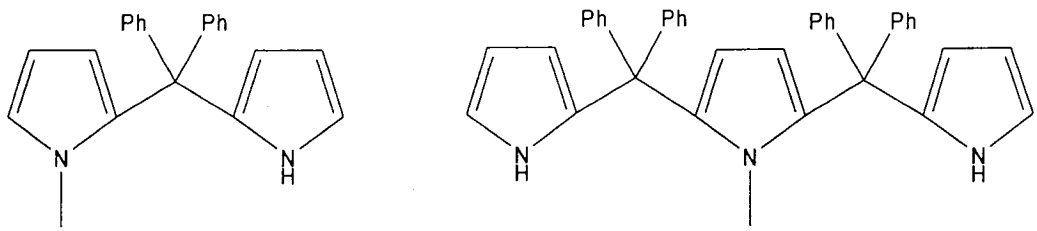

Figure 7.4.1 Structures N-MeDipyr and N-MeTripyr.

In other words, by combining the known effectiveness of the pyrrole ligand system, with the hemi-labile motif of the Hessen system (see Scheme 7.2.5), it was hoped that a potent catalyst would be created.

The strategy adopted for exploring this system was quite straight-forward (see scheme 7.4.2).

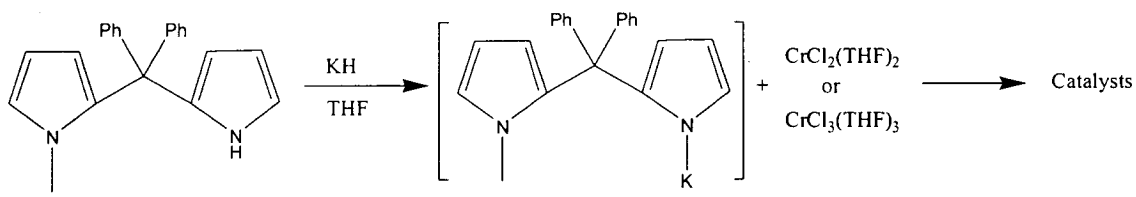

Scheme 7.4.2 Proposed Catalyst Synthesis Strategy.

The potassium salt of either ligand will be combined with either $Cr^{(II)}$ or $Cr^{(III)}$ in varying stoichiometries in order to generate well-defined complexes for testing. The catalysts will then be tested in conjunction with an activator according to commonly used conditions. It was anticipated that the N-MeDipyr ligand will behave in much the same hemi-labile manner as the Hessen system providing flexible electronic and steric interactions. The σ,π,σ–bonding N-MeTripyr ligand on the other hand, was not expected to have quite as much flexibility since the two σ–bonds effectively lock the N-Me pyrrole ring in close proximity to the metal centre. That said, the N-Me pyrrole ring should still offer electronic flexibility by donating more or less electrons (2 vs. 6 e^-) depending on ring-slippage, or quaternization of the N-Me group.

Given that the PNP ligand is performing so well in terms of formation of 1-octene, it was decided that it would be an optimum template for rationale modification. In order to explore the effects of the bite angle, a system with the same 3-atom bite was

selected. However, rather than the PNP framework, the NCN amidinate framework (CyNC(R)NCy) was chosen. This ligand is mono-anionic and serves as a 4 e^- donor versus the PNP system which is neutral but also a 4 e^- donor. Since nitrogen is a harder donor than phosphorous it will be interesting to see how this affects the overall activity. Also, since the amidinate system can only have one terminal group attached to the nitrogen instead of the two attached to the phosphorous of the PNP ligand, there will be less steric constraint. Nonetheless, the use of the bulky cyclohexyl groups should still provide the steric bulk which is seemingly so important. The amidinate ligand system is readily available with a large variety of substituents since it can be obtained via reaction of the appropriate RLi reagent with carbodiimides some of which are commercially available at very reasonable prices (see Scheme 7.4.3).[34] With this methodology, several compounds can be synthesized. Since any changes in electronic factors are readily transmitted throughout the conjugated π–system of the amidinate ligand, the possibility of altering the *para* position with both electron donating and electron withdrawing groups was regarded as beneficial for mechanistic studies. In turn, this will affect the electronic environment of the metal center allowing us to evaluate how catalytic performance may be related to the electron density on the metal center.

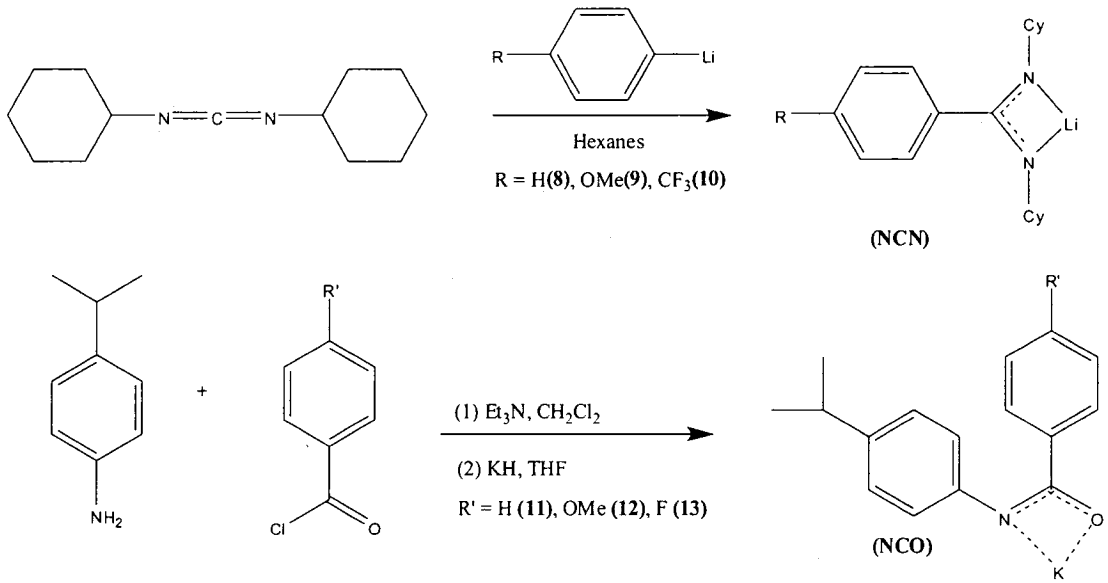

Scheme 7.4.3 Amidinate (NCN) and Amidate (NCO) Synthesis Strategy.

Following the same line of reasoning, the amidate (NCO) ligand[35] (see Scheme 7.4.3) is isostructural with the amidinate ligand, showing a similar bite angle, the major difference being the presence of the oxygen donor atom as part of the ligand backbone. The oxygen group acts as an even harder donor atom than nitrogen, and can act as a binding site for the aluminum activator. In addition, the replacement of the steric bulk of the N-Cy group by an oxygen atom will allow for the further evaluation of steric effects on catalysis.

Finally, we wish to revisit a family of established compounds which have been reported in the literature as mediocre polymerization catalysts when combined with Cr.[36] The NacNac ligand system[37] (see Figure 7.4.4) is comparable to the NCN amidinate systems as it too is a mono-anionic bi-dentate, and based on two nitrogen donor atoms. The main difference is that the ligand "bite" has been widened. Furthermore, the NacNac ligand provides quite extensive steric bulk leaving a well-defined pocket within which ethylene may react, and is quite good at generating monomeric species.[38]

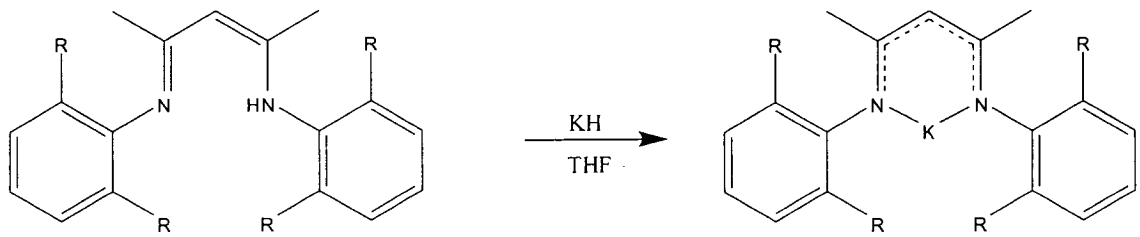

R = iPr (**14**)
R = Me (**15**)

Figure 7.4.4 NacNac Ligand Framework.

Both the NCN, and NCO derivatives **8-13** (see Scheme 7.4.3) and the KNacNac (**14-15**) ligand will be reacted with various stoichiometries of $CrCl_3(THF)_3$ and $CrCl_2(THF)_2$ in order to attempt to isolate well-defined complexes for catalysis. The impact of the various bite-angles, hetero-atoms, and electron withdrawing/donating groups will then be evaluated with respect to oligomerization selectivity and activity.

The final thrust of this project was to evaluate well-defined catalyst systems in order to determine the most likely oxidation state of the catalyst. To address the important point of the chromium oxidation state in the catalytically active species and of

how this may affect the selectivity of the oligomerization process, we have embarked on a project aimed at isolating and characterizing complexes arising from the reaction of trivalent or divalent chromium complexes with alkyl aluminum derivatives. To this end, we have analyzed the remarkable BP/Sasol PNP ligand, and Sasol's SNS ligand (see Figure 7.4.5). These ligands were selected as they provide the most selective systems to date, with published literature conditions for testing which will offer us a good base-line indication to compare our results with.

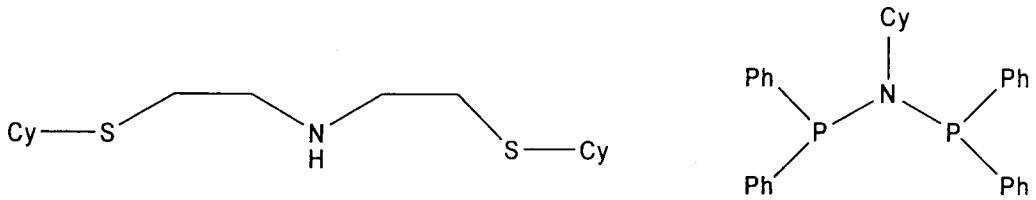

SNS PNP

Figure 7.4.5 SNS and PNP Ligands Utilized.

Just as in the previous cases the two ligand systems will be reacted with various stoichiometric ratios of both $Cr^{(II)}$ and $Cr^{(III)}$ in order to attempt to isolate well-defined complexes. In addition, the interaction of the isolated complexes with Al activators will be critically examined in order to gain insights as to the nature of the catalytically active species.

7.5 Results and Discussion:

Given the sheer volume of results, breaking them down into separate sub-sections is required in order to maintain clarity. The interpretation of each sub-section will be presented individually while the overall trends, especially comparing different catalysts, will be presented in the concluding section of this chapter (see Section 7.9 – Conclusions).

7.6 σ,π-Bonding Pyrrolide Ligands:

The reaction of two equivalents of KN-MeDipyr (see Figure 7.4.1) with $CrCl_2(THF)_2$ provided good yields of Complex **1** (see Figure 7.6.1).

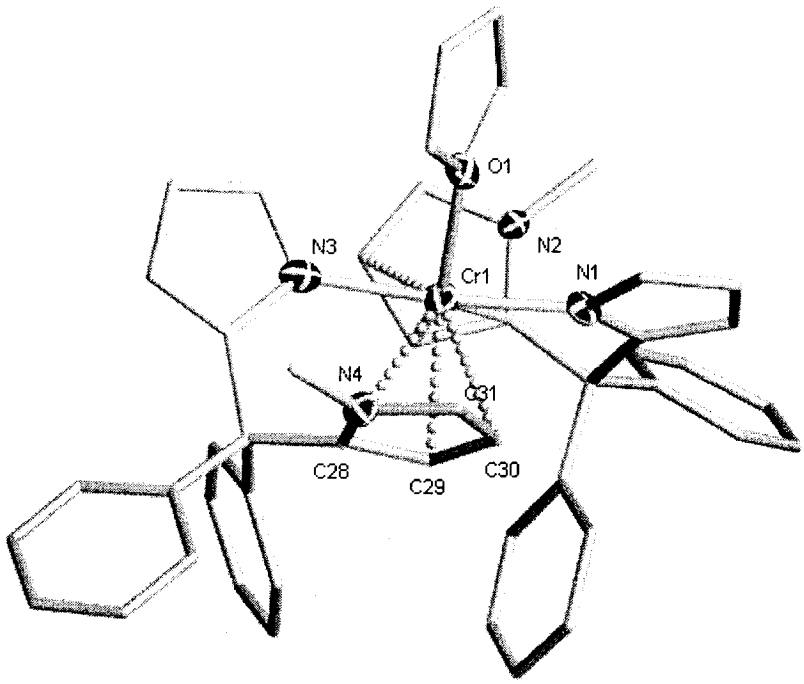

Figure 7.6.1 Crystal Structure of (**1**) with 30% Thermal Ellipsoids.

The structure consists of a pseudo-trigonal bipyramidally coordinated chromium centre with N(1)–Cr(1) = 2.079(7) Å and N(3)–Cr(1) = 2.068(8) Å occupying the axial positions [N(1)–Cr(1)–N(3) = 173.4(3)°]. One equatorial position is filled by a molecule of THF [O(1)–Cr(1) = 2.097(6) Å]. The final two equatorial positions are filled by two N-Me pyrroles [O(1)–Cr(1)–C(29) = 122.8(8)°, O(1)–Cr(1)–C(7) = 134.5(8)°] which both appear to be bonding in either an η^1 or η^3 fashion. The closest contact occurs between C(29)–Cr(1) = 2.558(7) Å and C(7)–Cr(1) = 2.579(7) Å, the distances, though long, are still considered to be within bonding range.[39] Whether the pyrroles could be η^3 bonding is slightly more doubtful as the interatomic distances grow quite far apart [C(28)–Cr(1) = 2.997(7) Å, C(30)–Cr(1) = 2.992(7) Å]. Finally, the remaining two atoms of the ring [C(31) and N(4)] are over 3.5 Å from the Cr centre, excluding any bonding interaction. The second N-Me pyrrole ring [based on N(2)] shows nearly identical distances from the ring positions, indicating that both N-Me pyrroles are coordinated in the same fashion. The results would tend to indicate that the N-MeDipyr ligand system is indeed acting as a hemi-labile ligand with a very loose coordination to the metal as demonstrated by the very long bond distances.

For the case of the N-MeTripyr ligand (see Figure 7.4.1) a slightly more complex situation arose. When K_2N-MeTripyr was reacted with $CrCl_2(THF)_2$ in THF, an insoluble light blue product formed nearly instantaneously. This solid was insoluble in all common solvents, including CH_2Cl_2 and acetonitrile which led to great difficulty in separating the complex from the two equivalents of KCl, which must concomitantly form. Crystals suitable for X-ray crystallography were obtained by layering a THF solution of K_2N-MeTripyr on a buffering solution of pure THF which had been layered on a solution of $CrCl_2(THF)_2$ in THF. This trinary system was then left undisturbed for several days, after which time crystals of [(N-MeTripyr)Cr(THF)$_2$] (**2**) of appropriate size grew out of the solution (see Figure 7.6.2). Although this technique does not allow for the bulk preparation of materials, the crystalline and dried non-crystalline samples displayed identical IR spectra, therefore indicating that KCl was likely the sole contaminant.

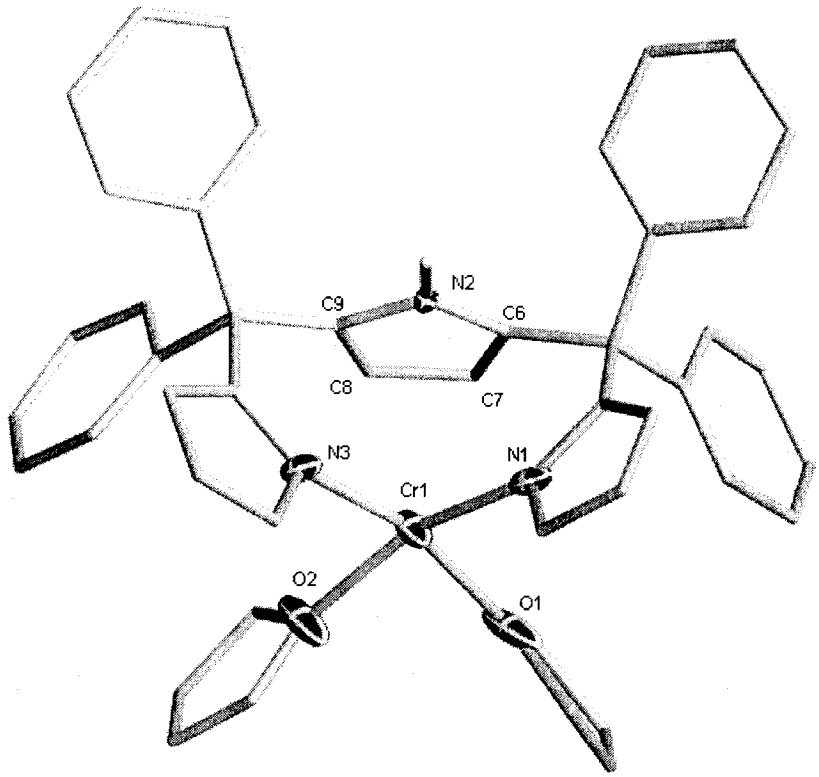

Figure 7.6.2 Crystal Structure of (**2**) with 30% Thermal Ellipsoids.

The Cr atom is in a square-planar geometry with each pyrrolide *trans* to a coordinated THF molecule [N(1)–Cr(1) = 2.065(7) , N(3)–Cr(1) = 2.053(7), O(1)–Cr(1) = 2.091(7),

O(2)–Cr(1) = 2.107(7) Å, N(1)–Cr(1)–N(3) = 96.3(7), N(1)–Cr(1)–O(1) = 88.8(7), O(1)–Cr(1)–O(2) = 83.1(7)°]. The N-Me pyrrole ring appears to be outside the typical bonding range [ring centroid is 2.70 Å from Cr(1)]; although a bonding interaction with a large Jahn-Teller distortion can not be discounted. The N-Me pyrrole ring is perfectly centred above the Cr atom so it is possible that a very weak, and probably dynamic interaction is occurring, especially in solution state.

Complex **2** was treated with pyridine in boiling toluene in an attempt to completely separate the [(N-MeTripyr)Cr(THF)$_2$](THF)$_{1.4}$ from KCl, thus generating an analytically pure, well-defined complex. This treatment solubilised the complex, forming the intensely purple [(N-MeTripyr)Cr(pyridine)$_2$] (**3**) while allowing the KCl to be centrifuged off (see Figure 7.6.3).

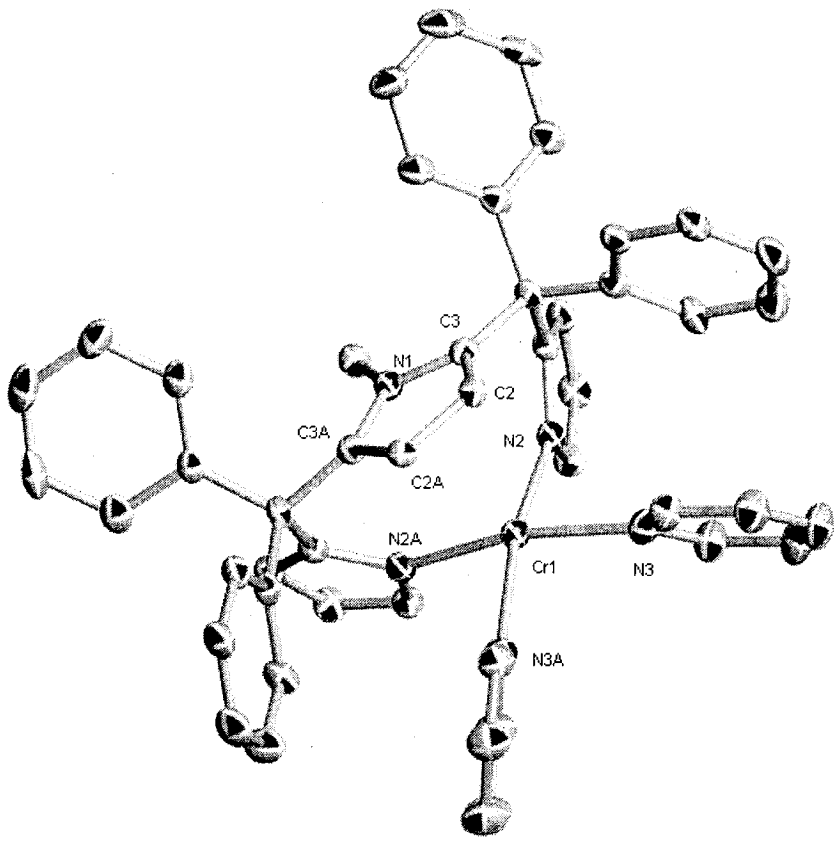

Figure 7.6.3 Crystal Structure of (**3**) with 30% Thermal Ellipsoids.

Not surprisingly, Complex **3** is isostructural with **2**, as the only difference between the two species is that the THF molecules have now been replaced with pyridine. Once again the complex assumes a square planar geometry with the N-Me ring perfectly centred over

Cr(1) [centroid–Cr(1) = 2.70, Cr(1)–N(2) = 2.093(3), Cr(1)–N(3) = 2.158(3) Å, N(2)–Cr(1)–N(3) = 88.80(11), N(2)–Cr(1)–N(2a) = 92.97(15)°].

Conversely, if the lithium salt (Li_2N-MeTripyr) is used in the synthesis, the metallate structure [(N-MeTripyr)Cr(ClLi(THF)$_3$)] (**4**) was isolated in good yield (see Figure 7.6.4).

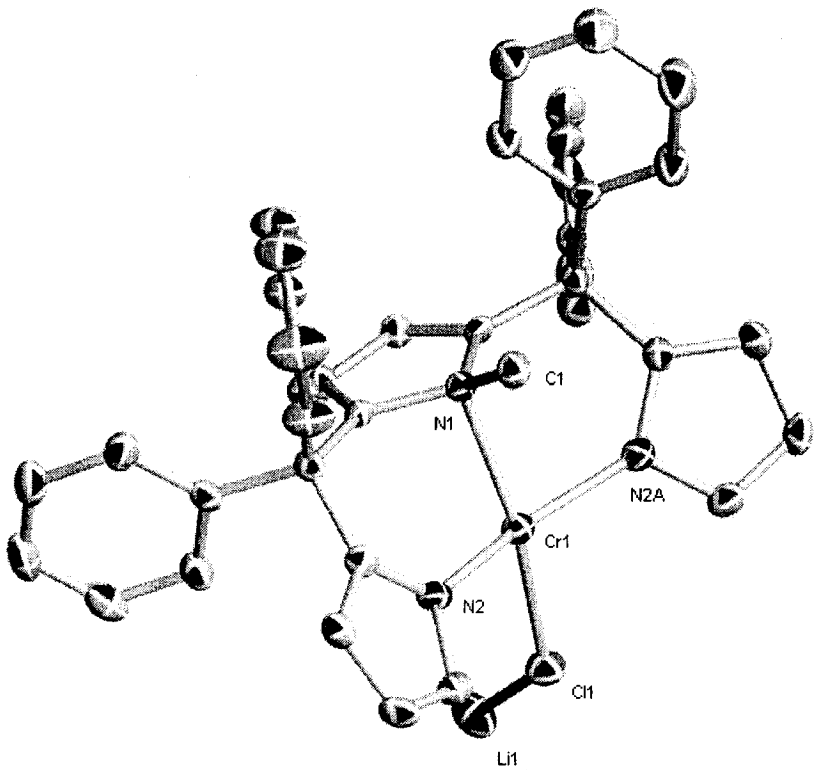

Figure 7.6.4 Crystal Structure of (**4**) with 30% Thermal Ellipsoids, THF Molecules Have Been Omitted for Clarity.

Complex **11** assumes a distorted square-planar geometry in which Cr(1) lies slightly below the N(2)–N(2a) plane and slightly above the N(1)–Cl(1) plane. The pyrrolides are *trans* to one another as are Cl(1) and the N-Me pyrrole N(1) [N(2)–Cr(1) = 2.053(11), N(1)–Cr(1) = 2.239(13), Cl(1)–Cr(1) = 2.359(12) Å]. The most striking feature of the complex is that the N-Me group has lost it's sp^2 geometry and has become quaternized as indicated by the sp^3 configuration of the nitrogen atom directly σ-bonding with Cr(1) [C(1)–N(1)–Cr(1) = 104.3(3)°]. This is in striking contrast to complexes **2** and **3** in which the N-Me ring appears to be non-bonding, and further demonstrates the flexibility of the N-MeTripyr ligand system.

Reaction of the K_2N-MeTripyr ligand with $CrCl_3(THF)_3$ proceeded smoothly to yield the expected [(N-MeTripyr)CrCl] (**5**) complex (see Figure 7.6.5). The d^3 metal centre adopts a tetrahedral geometry comprised of the two pyrrolide rings, a fully η^5 coordinating N-Me pyrrole ring, and finally one Cl atom [N(1)–Cr(1) = 1.958(4), N(3)–Cr(1) = 1.981(4), centroid–Cr(1) = 1.997, Cl(1)–Cr(1) = 2.221(2) Å, N(1)–Cr(1)–N(3) = 105.74(15), N(1)–Cr(1)–Cl(1) = 100.55(13), N(1)–Cr(1)–centroid = 108.3°].

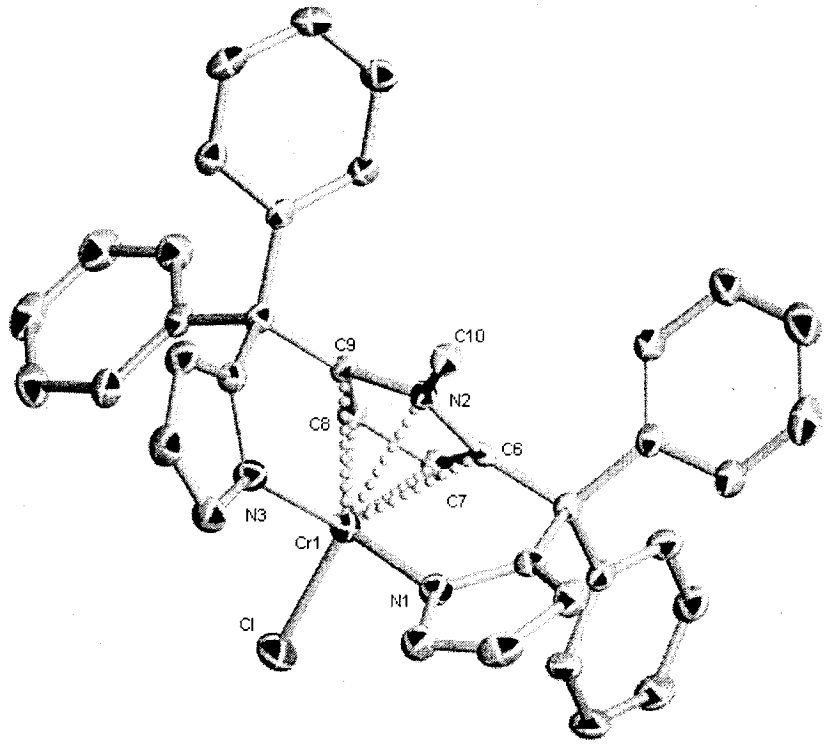

Figure 7.6.5 Crystal Structure of (**5**) with 30% Thermal Ellipsoids.

The greater Lewis acidity of the $Cr^{(III)}$ metal may be the driving force for the formation of the fully η^5-coordinated N-Me pyrrole ring in this case. For full bond angles and distances for the N-MeDipyr and N-MeTripyr complexes see Appendix 7.

All catalyst testing was performed at the Technical University of Eindhoven (the Netherlands) under the supervision of Dr. Rob Duchateau, using a temperature controlled 250 mL Büchi reactor with mechanical stirring. During the first round of testing in May

2005, the σ,π-bonding pyrrolide ligands N-MeDipyr and N-MeTripyr (see Figure 7.6.6 and Table 7.6.7) were investigated.

[N-MeDipyr$_2$CrTHF]

1

Figure 7.6.1

$Cr^{(II)}$

[N-MeTripyrCr(THF)$_2$]

2

Figure 7.6.2

$Cr^{(II)}$

[N-MeTripyrCr(pyridine)$_2$]

3

Figure 7.6.3

$Cr^{(II)}$

[N-MeTripyrCr(ClLiTHF$_3$)]

4

Figure 7.6.4

$Cr^{(II)}$

[N-MeTripyrCrCl]

5

Figure 7.6.5

$Cr^{(III)}$

Figure 7.6.6 Catalysts Used in Tables 7.6.7 and 7.6.8.

Table 7.6.7 Catalyst Testing for Ethylene Oligomerization.[a]

Entry	Catalyst	Activator (eq.)	PE (g)	Alkenes (mL)	Activity g/mol·h	Activity g/g·Cr·h
1	1	2000	10.13	56.3	1 261 875	24 267
2	2	2000	4.95	35.0	942 200	18 119
3	3	2000	2.30	54.0	1 211 400	23 296
4	4	2000	16.18	48.0	1 076 800	20 708
5	5	2000	1.75	8.3	1 982 945	3 813
6	blank	2000	0.82	0	0	0

[a] Conditions: 30 μmol of catalyst, MAO activator, 40 bar ethylene, 50 °C, 1 hour reaction time, total volume 150 mL in toluene.

From the results presented in the table it readily becomes apparent that the N-MeDipyr and N-MeTripyr ligands produce active catalysts. Furthermore, a clear difference is visible between the $Cr^{(II)}$ and $Cr^{(III)}$ oxidation states. Even the least active $Cr^{(II)}$ catalyst (entry 2) is almost five times more active than the $Cr^{(III)}$ catalyst (entry 5). This would tend to indicate that $Cr^{(II)}$ is able to generate an active species capable of oligomerizing ethylene better than the $Cr^{(III)}$ oxidation state. Amongst the $Cr^{(II)}$ catalysts there is very little deviation in overall reactivity, with the only real differences being the amount of PE which was produced during the runs. It can be observed that entries 1 and 4 produce significantly more polymer than the other catalysts. The Li alkali metal present in entry 4

could somehow be influencing this increase in PE production; however, it is difficult to rationalize a reason for the increased PE production found in entry 1.

Table 7.6.8 α-Olefin Product Distriubtion.[a]

Entry	Catalyst	Activity g/g·Cr·h	mol % C_4	C_6	C_8	C_{10}	C_{12}	C_{14}	C_{16}
1	1	24 267	8.9	32.8	23.4	15.0	9.7	6.0	4.2
2	2	18 119	16.2	36.7	22.1	12.4	6.8	3.7	2.2
3	3	23 296	12.3	36.8	22.7	13.2	7.8	4.6	2.7
4	4	20 708	0.1	13.7	33.1	23.6	14.8	9.0	5.7
5	5	3 813	14.7	40.1	22.5	11.6	6.0	3.4	1.7

[a] Determined by GC-FID, against standard solutions of authentic α-olefin samples.

The product distributions for the α-olefins produced in each run are presented in Table 7.6.8. It must be noted that very small amounts (<0.5 % of each oligomer fraction) of what was assumed to be internal olefins would often be detected, but their extremely low concentrations made meaningful quantification impossible. From this table it becomes apparent that a Shulz-Flory distribution is occurring for all of the catalysts tested. The majority of which (entries 1-3, 5) are centred upon the C_6 fraction. A deviation from this trend is observed in entry 4 which utilizes a catalyst, [N-MeTripyrCr(ClLiTHF$_3$)] (**4**), that contains a Li cation. In this case the production of 1-butene has been almost completely retarded, and the overall Shulz-Flory distribution of α-olefins is now centred on C_8 (33.1 %). The production of the higher α-olefins has also been increased in the case of entry 4, indicating that the presence of the alkali metal is most likely affecting the catalysis by shifting the oligomer production to higher chain lengths. It should also be noted that there is virtually no difference between the product distributions of the $Cr^{(II)}$ and $Cr^{(III)}$ complexes that do not contain an alkali metal (entries 1-3 vs. 5).

Since the [N-MeTripyrCr(pyridine)$_2$] (**3**) complex oligomerized ethylene with a respectable rate and very little PE produced, it was decided to investigate other reaction conditions utilizing this species. The first variable which was investigated was the effect of changing the pressure of ethylene while holding all other conditions constant (see Table 7.6.9).

Table 7.6.9 Effect of Pressure on Catalyst **3**.[a]

Entry	Pressure (bar)	PE (g)	Alkenes (mL)	Activity g/mol·h	Activity g/g·Cr·h
6	1	0.49	1.0	22 433	431
7	10	0.21	33.0	740 300	14 237
8	20	0.69	50.3	1 127 275	21 678
9	40	2.30	54.0	1 211 400	23 296
10	60	3.54	32.3	723 475	13 913

[a] Conditions: 30 μmol of catalyst, 2000 eq. of MAO activator, 50 °C, 1 hour reaction time, total volume 150 mL in toluene.

There is a marked decrease in oligomerization activity when the pressure is reduced to 1 bar of ethylene (entry 1), yielding a fifty-fold decrease in activity from the most active case (entry 9) which utilized 40 bars of ethylene. Overall the activity appears to increase from 1-40 bar, at which point it plateaus and then falls when the pressure is increased in the 60 bar run (entry 10).

Table 7.6.10 Effect of Pressure on the α-Olefin Product Distriubtion of **3**.[a]

Entry	Pressure (bar)	Activity g/g·Cr·h	α-olefin mol %						
			C_4	C_6	C_8	C_{10}	C_{12}	C_{14}	C_{16}
6	1	431	8.6	51.0	22.9	10.4	4.4	1.7	1.1
7	10	14 237	16.4	37.4	22.1	11.8	6.7	3.6	2.0
8	20	21 678	17.0	35.2	21.4	12.5	7.2	4.3	2.4
9	40	23 296	12.3	36.8	22.7	13.2	7.8	4.6	2.7
10	60	13 913	20.7	35.6	21.7	8.6	7.0	4.1	2.3

[a] Determined by GC-FID, against standard solutions of authentic α-olefin samples.

There appears to be very little influence on the selectivity of the catalyst over the pressure ranges tested, as all produced a Shulz-Flory distribution centred at 1-hexene. At the low 1 bar pressure (entry 6) there appears to be a slight reduction in the production of 1-butene. Though this could also represent a sample which has lost more of the 1-butene gas into the atmosphere than have the other samples, especially since such a small volume of oligomers was produced to begin with (~1 mL).

Temperature often has quite a large influence on catalytic processes, hence it was deemed prudent to investigate the effect of temperature on **3** (see Table 7.6.11).

Table 7.6.11 Effect of Temperature on Catalyst **3**.[a]

Entry	Temperature (°C)	PE (g)	Alkenes (mL)	Activity g/mol·h	Activity g/g·Cr·h
11	30	1.61	28.5	639 350	12 295
12	50	2.30	54.0	1 211 400	23 296
13	70	1.05	54.8	1 228 225	23 630

[a] Conditions: 30 μmol of catalyst, 2000 eq. of MAO activator, 40 bar ethylene, 1 hour reaction time, total volume 150 mL in toluene.

From entries 11-13 it would appear that the catalyst prefers operating at slightly elevated temperature as both the 50 °C and 70 °C runs produced almost identical activities. When the catalysis is run at the slightly lower temperature of 30 °C, the activity is nearly halved (entry 11).

Table 7.6.12 Effect of Temperature on the α-Olefin Product Distribution of **3**.[a]

Entry	Temperature (°C)	Activity g/g·Cr·h	α-olefin mol %						
			C_4	C_6	C_8	C_{10}	C_{12}	C_{14}	C_{16}
11	30	12 295	22.2	40.1	19.4	9.9	4.9	2.4	1.2
12	50	23 296	12.3	36.8	22.7	13.2	7.8	4.6	2.7
13	70	23 630	11.5	32.5	22.2	14.5	9.4	6.0	3.9

[a] Determined by GC-FID, against standard solutions of authentic α-olefin samples.

Upon examination of the α-olefin selectivities it can be observed that temperature has very little impact. Similar to their activities, entries 12 and 13 displayed nearly identical selectivities, yielding a Shulz-Flory distribution centred on 1-hexene. At the lower reaction temperature (30 °C, entry 11), the reaction displayed slightly higher selectivity for the lower α-olefins C_4 and C_6.

By examining the activity of a catalyst over different time periods, it can be determined whether the catalyst is highly active but quickly deactivated, or working at a lower rate over a longer period of time. For this reason, the catalyst activity at three different times was measured (see Table 7.6.13).

Table 7.6.13 Effect of Reaction Time on Catalyst **3**.[a]

Entry	Time (min)	PE (g)	Alkenes (mL)	Activity g/mol·h	Activity g/g·Cr·h
14	30	0.97	1.2	56 083	1 079
15	60	1.20	3.6	76 650	1 347
16	120	2.20	9.0	100 950	1 941

[a] Conditions: 30 μmol of catalyst, 1000 eq. of MAO activator, 40 bar ethylene, 50 °C, total volume 150 mL in toluene.

As displayed in entries 14-16 the activities of the catalyst appears to increase over longer reaction times. Specifically, the activity at 120 min (entry 16) is nearly double that of the 30 min (entry 14) run. This would tend to indicate that the catalyst does not decompose very rapidly and, in fact, may require longer reaction times in order to fully activate.

Table 7.6.14 Effect of Reaction Time on the α-Olefin Product Distribution of **3**.[a]

Entry	Time (min)	Activity g/g·Cr·h	α-olefin mol %						
			C_4	C_6	C_8	C_{10}	C_{12}	C_{14}	C_{16}
14	30	1 079	19.2	37.3	23.4	10.5	5.4	2.6	1.5
15	60	1 347	13.5	38.7	24.4	11.5	6.4	3.2	2.1
16	120	1 941	11.2	38.9	22.8	13.4	7.3	4.1	2.3

[a] Determined by GC-FID, against standard solutions of authentic α-olefin samples.

There is virtually no effect on the selectivity of the catalyst over the different reaction times, indicating that the same species is present throughout the catalytic run.

Perhaps one of the most difficult tasks of this project was the search for an appropriate activator, and the correct stoichiometric ratio required. When the catalyst testing was first commenced very low loadings of MAO were used (entry 20) which resulted in some oligomerization activity, but the amount produced was so low (0.5-1.0 mL), that it made quantification very difficult. Other known activators were used in an attempt to generate better activity (entries 17-19), but all failed.

Table 7.6.15 Effect of Activator Type and Equivalents on Catalyst **3**.[a]

Entry	Activator (eq.)	PE (g)	Alkenes (mL)	Activity g/mol·h	Activity g/g·Cr·h
17	$ZnMe_2$ (100)	0	0	0	0
18	$AlEt_3$ (300)	0.12	0	0	0
19	$AlMe_3$ (300)	0	0	0	0
20	MAO (500)	1.30	1.0	22 433	431
21	MAO (1000)	1.20	1.5	33 650	647
22	MAO (2000)	2.30	54.0	1 211 400	23 296
23	MAO (3000)	1.70	62.0	1 390 867	26 747
24	IBAO (2000)	26.52	0	0	0

[a] Conditions: 30 μmol of catalyst, 1 hour reaction time, 40 bar ethylene, 50 °C, total volume 150 mL in toluene.

It was only upon the addition of greater amounts of MAO (entries 21-23) that appreciable levels of activity were observed. There is a drastic increase in activity from 1000 eq. of MAO to 2000 eq. and then a somewhat smaller increase at 3000 eq. The large amounts of MAO also had virtually no impact on the amount of PE being produced by the reaction. The most unanticipated result was obtained when the activator IBAO (di-isobutylaluminumoxane) was used. In this case the activity of the catalyst was completely switched from an oligomerization catalyst, into a PE producing catalyst via an, as yet, unknown mechanism.[40]

Table 7.6.16 Effect of MAO Activator Equivalents on the α-Olefin Product Distribution of **3**.[a]

Entry	Activator (eq.)	Activity g/g·Cr·h	α-olefin mol %						
			C_4	C_6	C_8	C_{10}	C_{12}	C_{14}	C_{16}
20	MAO (500)	22 433	10.1	41.6	28.4	8.5	5.9	2.9	2.5
21	MAO (1000)	33 650	13.5	38.7	24.4	11.5	6.4	3.2	2.1
22	MAO (2000)	1 211 400	12.3	36.8	22.7	13.2	7.8	4.6	2.7
23	MAO (3000)	1 390 867	16.8	33.2	21.3	12.9	7.8	4.9	3.0

[a] Determined by GC-FID, against standard solutions of authentic α-olefin samples.

Increasing the amount of MAO not only had no significant impact on the amount of PE produced, but also did not impact on the selectivity of the catalyst. As seen in Table 7.6.16 the distribution of α-olefins remains nearly constant throughout all the different

equivalents of MAO. This would then indicate that a large amount of MAO is required to properly activate the catalyst, but that MAO does not directly influence the metal centre after generating the active species.

Since the $Cr^{(III)}$ complex [N-MeTripyrCrCl] (**5**) (Figure 7.6.5) had such a poor activity it was decided to replace the Cl group with a methyl group in order to produce a catalyst which should be better able to initiate the oligomerization process and to evaluate the stability of the $Cr^{(III)}$-C bond. This was attempted via two methods which are detailed in Scheme 7.6.17. The first method involves reacting Complex **5** (left side of Scheme 7.6.17) with a variety of alkylating agents in order to substitute the chloride for an alkyl group.

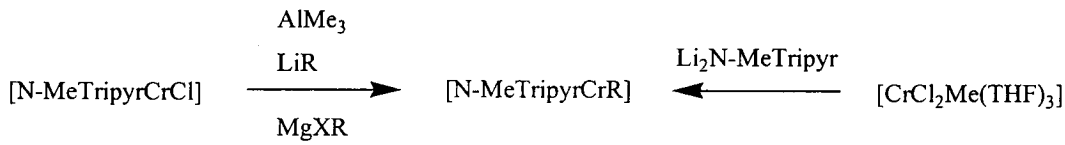

Scheme 7.6.17 Synthetic Routes to [N-MeTripyrR].

The second method involves the reaction of the $Cr^{(III)}$ mono-methyl species[41] with the lithium salt of the ligand (right side Scheme 7.6.17). Although many different alkylating agents were used, they invariably led to dark coloured intractable materials, except in the case of $AlMe_3$ (5 eq). The reaction yielded a small amount of crystalline compound which was found to be the result of ligand leaching (see Figure 7.6.18).

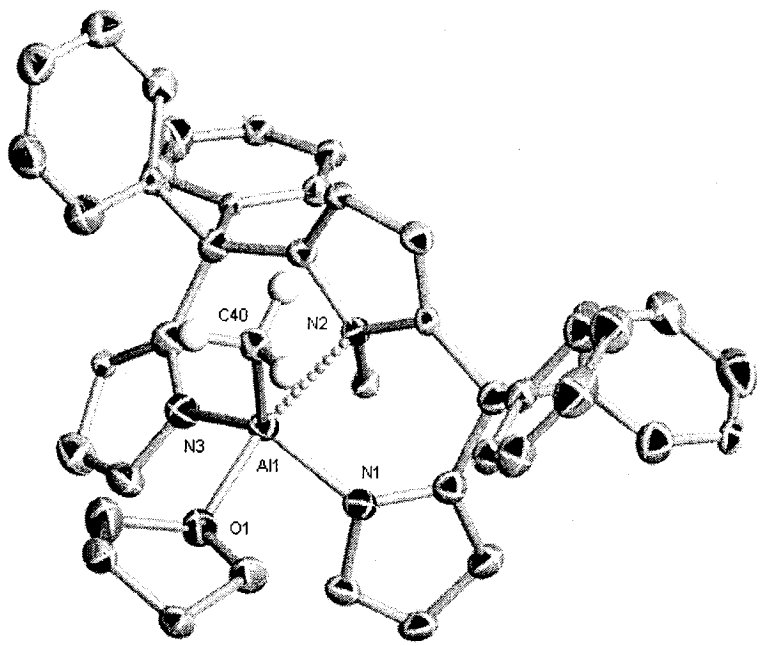

Figure 7.6.18 Crystal Structure of [N-MeTripyrAlMeTHF] (**6**) with 30% Thermal Ellipsoids.

The Al(1) atom exists in a slightly distorted trigonal bipyramidal coordination geometry with the equatorial plane comprised of the two pyrrolide functions and the methyl group [Al(1)–N(1) = 1.891(4), Al(1)–N(3) = 1.895(4), Al(1)–C(40) = 1.951(5) Å, N(1)–Al(1)–N(3) = 113.71(15), N(1)–Al(1)–C(40) = 126.10(19), N(1)–Al(1)–O(1) = 90.46(14)°]. The axial plane is composed of a molecule of THF and the N-Mepyrrole N(2) [Al(1) O(1) = 1.994(3), Al(1)–N(2) = 2.466(3) Å, N(2)–Al(1)–O(1) = 165.99(14)°]. The strong Lewis acidity of the Al atom has caused the N-Me pyrrole group to lose its planarity, adopting a more tetrahedral arrangement to better donate the N(2) lone pair to Al(1) [N-Me group is now 26.97(14)° out of the ring plane]. The formation of this species clearly demonstrates that $AlMe_3$ has the power to remove the ligand from the Cr metal. Since $AlMe_3$ is present in MAO, this could explain the poor behaviour exhibited for the oligomerization reaction. The second synthetic strategy was partly successful in the sense that a trivalent species was isolated in this case (see Figure 7.6.19).

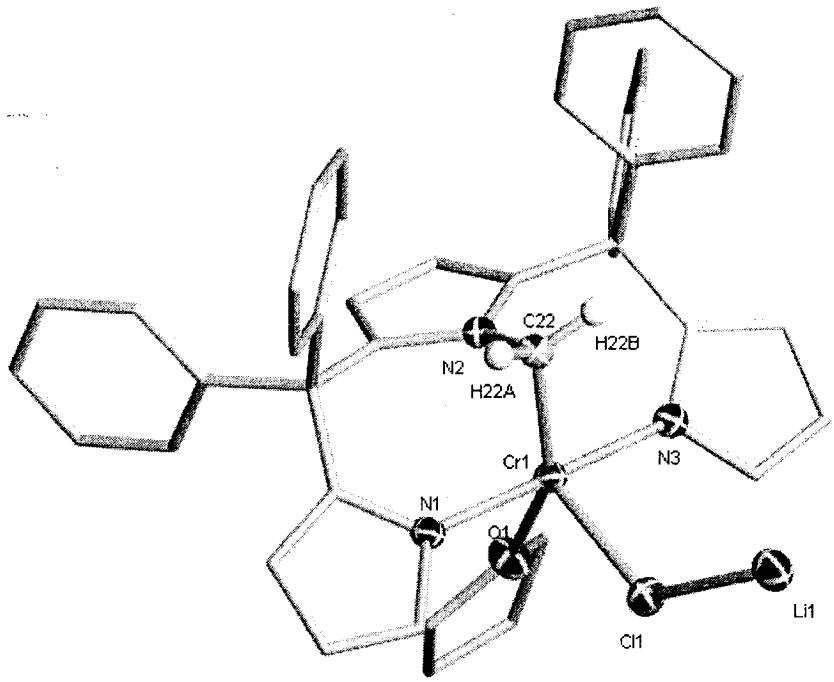

Figure 7.6.19 Crystal Structure of **7** with 30% Thermal Ellipsoids, Li-THF_3 Molecules Omitted for Clarity.

Complex **7** is most likely the result of an attack of the N-Me group by the CH_3 group on the Cr starting material. The structure adopts a trigonal bipyramidal geometry with the equatorial plane defined by the N-CH_2 (C22), a molecule of THF, and Cl(1) [Cr(1)–C(22)

= 2.005(3), Cr(1)–O(1) = 2.195(2), Cr(1)–Cl(1) = 2.3527(11) Å, C(22)–Cr(1)–O(1) = 145.42(9), C(22)–Cr(1)–Cl(1) = 113.76(7), C(22)–Cr(1)–N(1) = 89.61(10)°]. The axial positions are filled by the two pyrrolide moieties which are almost perfectly *trans* to one another [Cr(1)–N(1) = 2.074(2), Cr(1)–N(3) = 2.068(2), N(1)–Cr(1)–N(3) = 178.70(9)°]. Though the trivalent oxidation state was preserved, the N-Me group is now directly σ-bonded to the Cr centre. This type of reactivity tends to indicate that the $Cr^{(III)}$–Me moiety is quite unstable, a fact which is reiterated in the literature.[42] Furthermore, it was observed in the previous structure **6** (see Scheme 7.6.18) that the presence of an Al-Me residue in close proximity to the N-Me pyrrole was incapable of this deprotonation reaction. Taken together these two results offer a reasonable explanation as to why the $Cr^{(III)}$ N-MeTripyr system is such a poor oligomerization catalyst.

The results outlined above are quite encouraging. Not only do they demonstrate that the σ,π-bonding pyrrolides are capable of sustaining oligomerization activity, but they have clearly demonstrated that the $Cr^{(II)}$ oxidation state may be closer to the active species than $Cr^{(III)}$, contrary to the current consensus. In fact, the $Cr^{(II)}$ oxidation state was over six times more active than the analogous $Cr^{(III)}$ complex. The results of the reactions of $Cr^{(III)}$ with $AlMe_3$ may provide some insight as to the reason behind the general lack of selectivity in these systems. It is not difficult to envisage this ligand leaching reaction occurring in the presence of the large excess of MAO which is required for the trimerization process. The reaction of the $Cr^{(III)}$-Me with the ligand system clearly demonstrates that the $Cr^{(III)}$-Me moiety is quite unstable and highly reactive in combination with the pyrrolide ligand system, perhaps leading to the low activity found in the case of the $Cr^{(III)}$ catalyst.

7.7 $Cr^{(II)}$ Imine Based Ligands:

The synthesis of the Cr- amidinate (NCN), amidate (NCO), and NacNac ligand complexes used in this work was carried out via the metathetic reaction between the ligand in the form of either a lithium or potassium salt (see Figure 7.7.1) with $CrCl_2(THF)_2$.

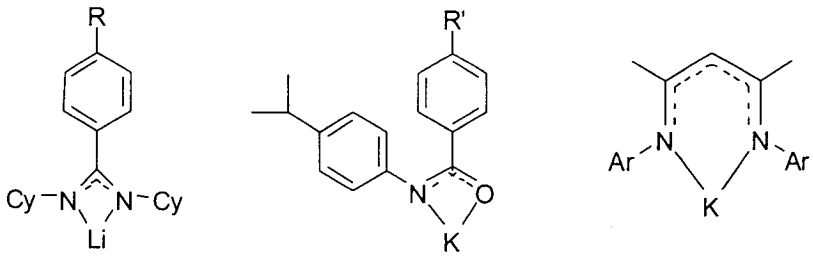

R = H **(8)**
OMe **(9)**
CF_3 **(10)**

R' = H **(11)**
OMe **(12)**
F **(13)**

Ar = 2,5-(*i*-Pr)$_2$Ph **(14)**
Ar = 2,5-(*Me*)$_2$Ph **(15)**

Figure 7.7.1 K or Li Salts of the NCN (**8-10**), NCO (**11-13**) and NacNac (**14, 15**) Ligands Utilized.

The amidinate ligands **8-10** were prepared by reacting dicyclohexylcarbodiimide (DCC) with the appropriate RLi reagents (see Scheme 7.4.3) according to literature methods[34] and were fully characterized by NMR (^{1}H, ^{13}C{^{1}H}, ^{13}C{^{1}H}DEPT, ^{1}H-^{1}H COSY, ^{13}C-^{1}H HMQC) and IR (Nujol). The NMR spectra for ligands **8-10** showed the presence of small amounts of impurities (<3%); however, the compounds were considered sufficiently pure for the subsequent methathesis reactions. The amidate ligands **11-13** were prepared via reaction of the appropriate *para*-substituted benzoyl chloride with *p*-isopropylaniline (see Scheme 7.4.3). Once again, full spectroscopic characterization was satisfactory and in agreement with the protonated formulations reported in Figure 7.4.3. The NMR spectra of the protonated ligands **11-13** showed that they were all pure (>99%) after their aqueous workup and subsequent drying. These ligands also showed an interesting trend in the ^{1}H spectra with respect to the N-H peaks. Due to the progressive deshielding effect from the adjacent phenyl ring which resulted from the different electron donating/withdrawing substituents, the N-H peak progressively shifted downfield, going from 7.88, to 8.08 and 8.57 for **11** (Ph), **12** (*p*-MeO-Ph) and **13** (*p*-F-Ph) respectively. This confirmed that there are indeed pronounced electronic effects due to the different substituents which should influence the Cr center once complexed. The formation of the potassium salt of **11**, was obtained via the *in situ* treatment of the ligand with KH in anhydrous THF prior to the reaction with $CrCl_2(THF)_2$. Unfortunately, the reaction of the ligands **12** and **13** did not readily occur in THF due to insolubility, precluding their further use in this study. If future investigations are to be conducted on

the amidate class of ligands it will be imperative that side chains which confer greater solubility be added. The protonated form of the NacNac ligands **14** and **15** were prepared according to literature procedure[43] and the potassium salt was generated via its reaction with KH in THF, followed by isolation from hexanes. Full characterization indicated the formation of solvent-free KNacNac in pure form (>99%).

The metathetic reactions of the ligands with $CrCl_2(THF)_2$ were carried out in THF at room temperature by using the appropriate ligand/Cr stoichiometric ratios (see Scheme 7.7.2). In spite of repeated attempts, compounds **16-18** proved impossible to crystallize into X-ray diffraction quality form, as they consistently grew as multiple needles/plates regardless of solvent. Therefore, the formulations of these species rely on their analogy with previously reported compounds and on satisfactory values obtained for the magnetic moments and elemental analyses.

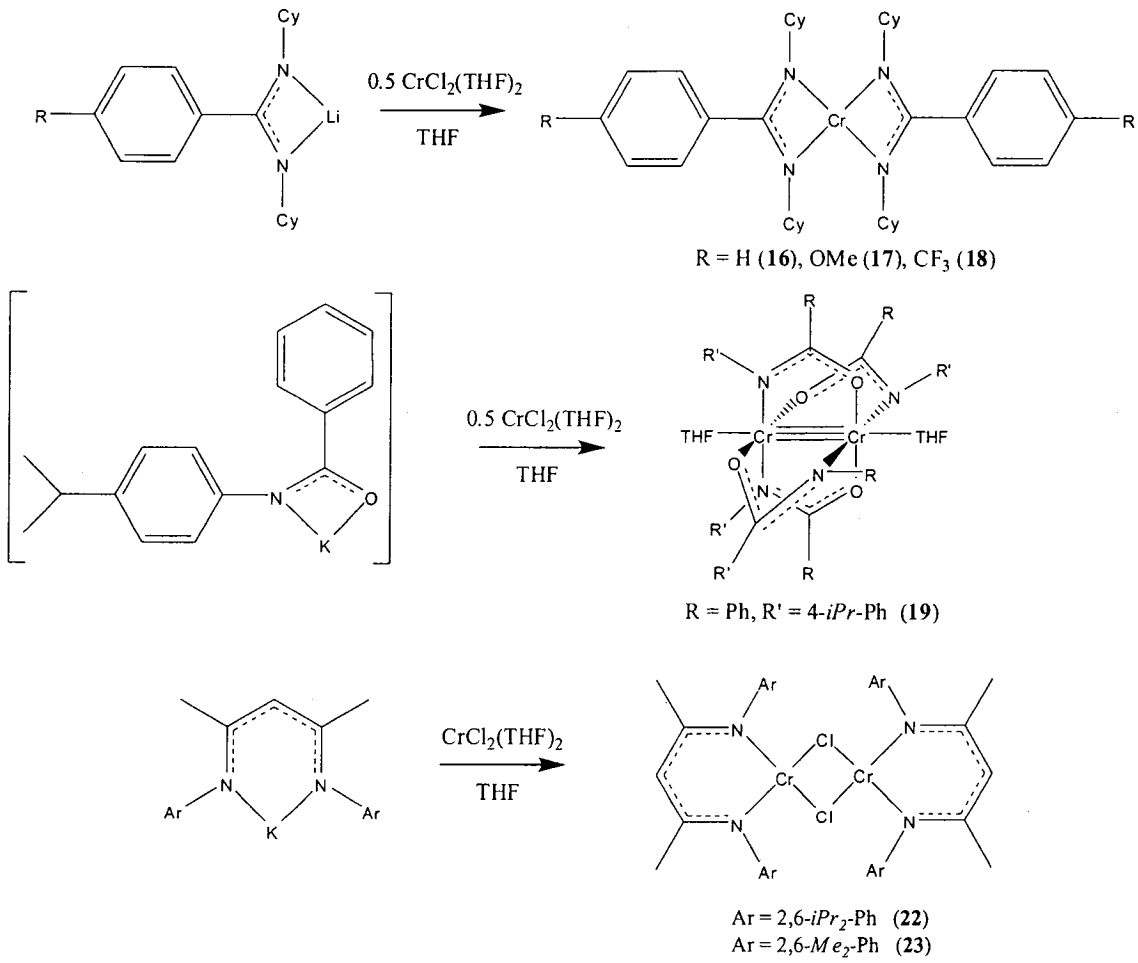

Scheme 7.7.2 Metathetic Routes to $Cr^{(II)}$ NCN, NCO, and NacNac Pre-Catalysts.

There is good reason to believe that the compounds obtained from the syntheses are as depicted in Scheme 7.7.2. The proposed coordination geometries for complexes **16-18** are based on previous work performed by this group[44] and by Winter *et al.*[45] It was reported that modifying the R group on the amidinate carbon has a profound impact on the eventual arrangement of the $Cr^{(II)}$ structure (see Scheme 7.7.3).

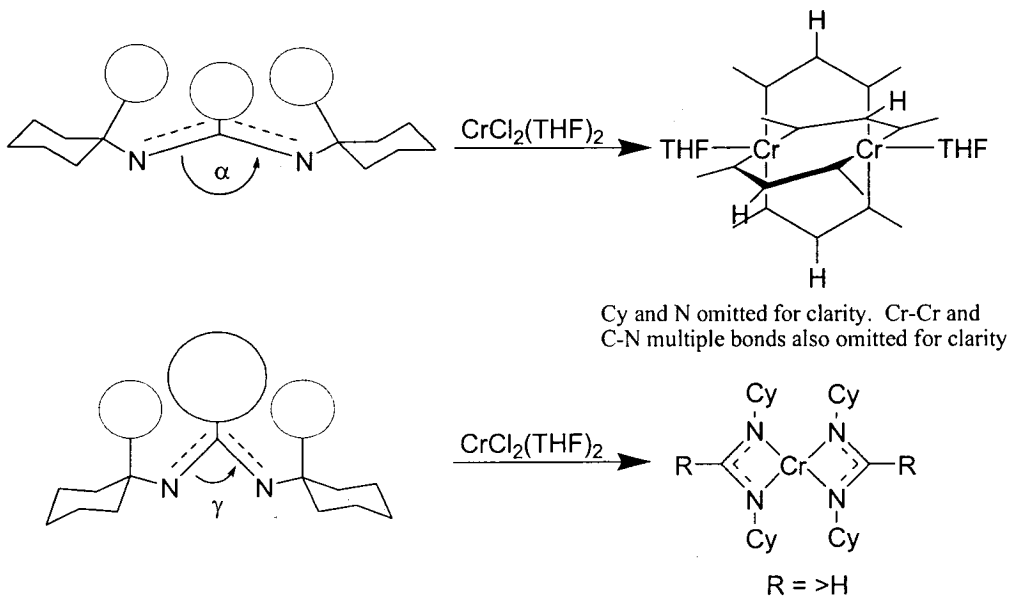

Scheme 7.7.3 Effect of Bite Angle (α vs γ) on $Cr^{(II)}$ Amidinate Complexes.

In essence, it was found that when R = H, the "paddlewheel" possibly quadruply bonded, Cr-Cr complexes are formed (top-right Scheme 7.7.3). However, when R = Me or a larger substituent, only the bis-amidinate monomeric complexes are formed (bottom-right Scheme 7.7.3).[44] It also appears that the amidinate class of ligand only provides 2:1 complexes regardless of the stoichiometric ratio employed in the preparation, as the 1:1 reactions always yielded unreacted $CrCl_2(THF)_2$ along with the 2:1 products. This observation is reinforced by the fact that no 1:1 amidinate $Cr^{(II)}X$ complexes have ever been reported in the literature. The binuclear paddlewheel complexes exhibit extensive metal-metal bonding leading to nearly diamagnetic complexes, or genuinely diamagnetic, depending on the extent of Cr···Cr interaction. The mononuclear configuration, conversely, nearly always affords high-spin, square-planar, complexes with very few low-spin square pyramidal exceptions. Since **16-18** all had magnetic moments ranging

from 4.68–4.84 μ_B, the complexes are quite clearly in the d^4 high-spin electronic configuration of divalent chromium in a square-planar ligand field, further supporting the formulation of the structures in Scheme 7.7.2.

Although reaction of the amidate (NCO) (**11**) with $CrCl_2(THF)_2$ did not produce crystalline material of sufficient quality for an X-ray structure determination, the diamagnetism of the complex permitted elucidation of the structure via NMR. Just as in the case of the published $Cr^{(II)}$ amidinate complexes,[44,45] a paddlewheel structure with short metal-metal contacts and two axial THF molecules was found (**19**).

Current work in our lab on an amidate NCO ligand system (see Figure 7.7.4), similar to the previously discussed **11** (see Figure 7.7.1) has also yielded $Cr^{(II)}$ catalysts for examination.

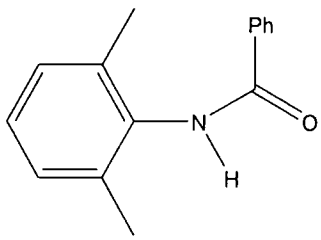

Figure 7.7.4 NCO Ligand for Complexes **20** and **21**.

Complex **20** was characterized by both NMR and X-ray crystallography and was found to adopt the classic paddlewheel configuration with a short Cr···Cr distance (see right side of Figure 7.7.5). Each "spoke" of the paddlewheel is an amidate ligand which is staggered versus the neighbouring ligands so that the steric repulsions between each 2,6-Me_2-Ph is minimized.

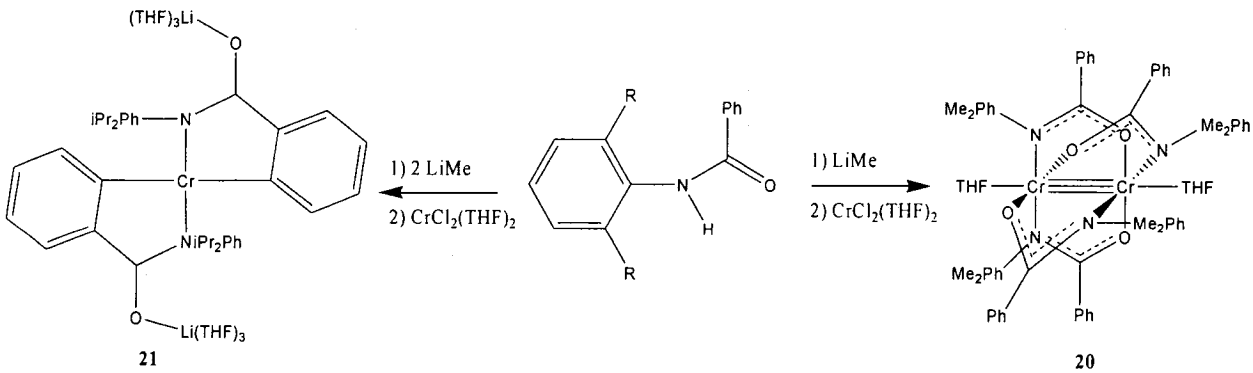

Scheme 7.7.5 Synthesis of NCO Ligand Complexes **20** and **21**.

As this ligand is so structurally similar to **11**, this provides further evidence that the proposed structure (**19**) is most likely correct (see Scheme 7.7.2). The second complex with this ligand (**21**) is an ionic complex in which the *ortho* positions of the backbone phenyl are anionically coordinated to Cr (see left side Scheme 7.7.5). This complex represents a deviation from the normal amidate (NCO) bonding style and was structurally characterized via X-ray crystallography. The metal adopts a distorted square-planar geometry with each amidate nitrogen *trans* to one another, as are the phenyl groups.

The chromium NacNac complex **22** was obtained in excellent yield as X-ray quality crystals (see Figure 7.7.6). Although the cell parameters were slightly different, the structure of **22** was identical to that of a previously published example, though the synthetic routes were different.[46]

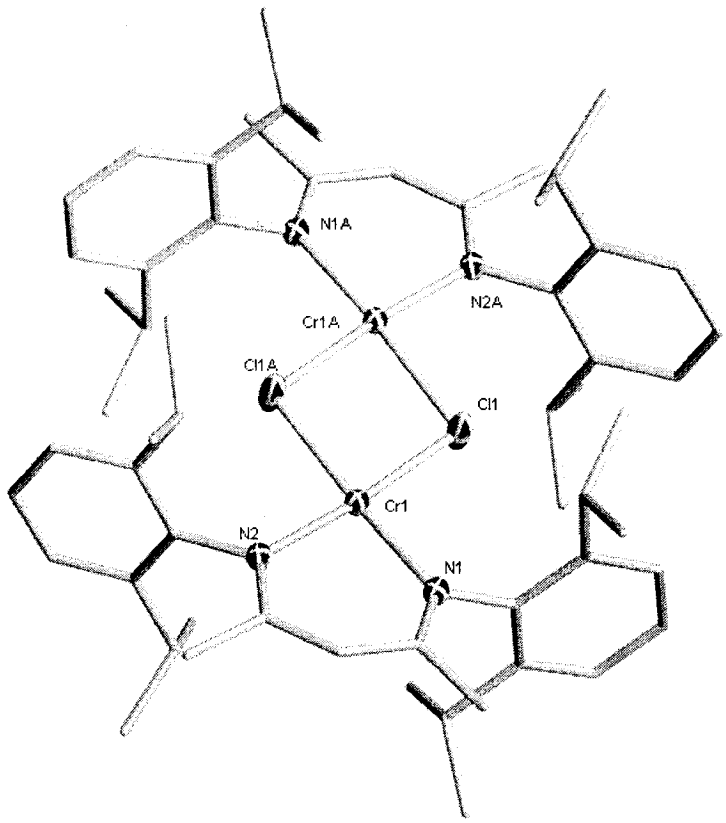

Figure 7.7.6 Crystal Structure of (**22**) with 30% Thermal Ellipsoids.

Complex **22** was formed regardless of the stoichiometric ratio employed (2:1 or 1:1), most likely due to the steric constraints of the bulky 2,6-*i*Pr$_2$-Phenyl groups. The structure is composed of two square-planar Cr centres which are bridged to one another

via two chlorine atoms [Cr(1)–Cl(1) = 2.3796(8), Cr(1)–Cl(1A) = 2.3970(9), Cr(1)–N(1) = 2.047(2), Cr(1)–N(2) = 2.038(2) Å, Cl(1)–Cr(1)–N(1) = 94.90(6), Cl(1)–Cr(1)–Cl(1A) = 81.04(3), Cl(1)–Cr(1)–N(2) = 174.01(6)°]. The long Cr–Cr distance [3.631(8) Å] precludes any direct metal-metal bonding. The 2,6-iPr$_2$-Phenyl groups of each NacNac ligand are slightly skewed in the crystal structure indicating that there is some steric repulsion occurring, a fact which may help to cleave the dimeric structure in solution.

Complex **23** was generated by addition of the potassium salt of the slightly less bulky (2,6-Me$_2$-Ph)NacNac ligand (**15**) with [$CrCl_2(THF)_2$]. X-ray quality crystals were retrieved in a good yield and their analysis shows a very similar structure to **22**, though two molecules of THF are retained in this case (see Scheme 7.7.7).

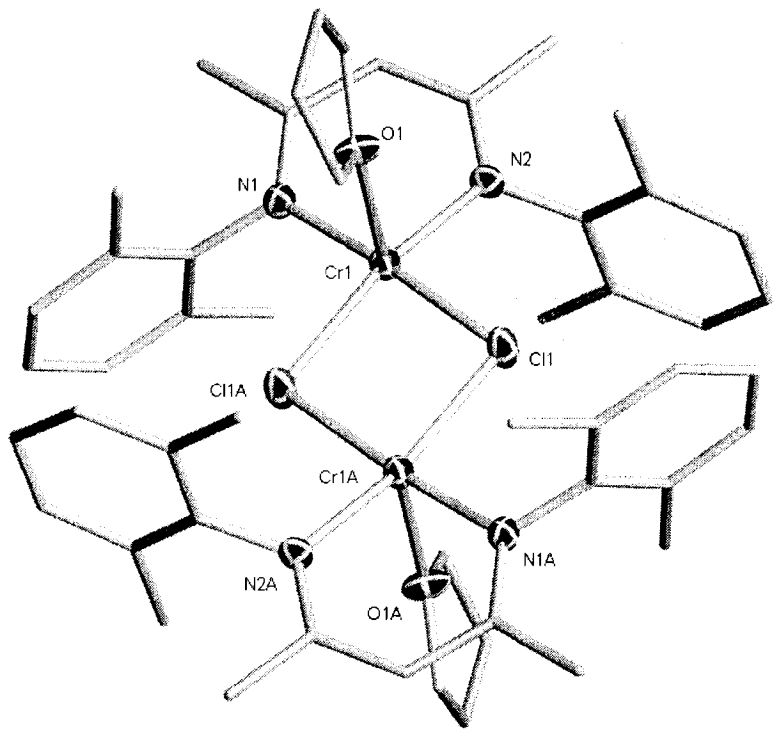

Figure 7.7.7 Crystal Structure of (**23**) with 30% Thermal Ellipsoids.

Each Cr centre exists in a square pyramidal coordination environment with the basal plane defined by the NacNac ligand and the two bridging chlorides [Cr(1)–N(1) = 2.062(5), Cr(1)–N(2) = 2.056(5), Cr(1)–Cl(1) = 2.4168(19), Cr(1)–Cl(1a) = 2.3976(18) Å, N(1)–Cr(1)–N(2) = 89.5(2), N(1)–Cr(1)–Cl(1) = 175.67(15), N(1)–Cr(1)–Cl(1a) = 93.88(15)°]. The axial position of each Cr atom is filled by a coordinated molecule of THF [Cr(1)–O(1) = 2.393(4), O(1)–Cr(1)–Cl(1) = 90.06(12), O(1)–Cr(1)–N(2) =

97.08(12)°]. This additional coordination of THF is most likely due to the slightly less sterically constrained environment around the Cr centre as opposed to the previous case with complex **22**. Similar to **22** the phenyl groups of the ligand are skewed indicating that there is steric interference which may favour a monomeric structure in solution.

With our hypothesis that $Cr^{(II)}$ could possibly create more active oligomerization catalysts than $Cr^{(III)}$ the imine-based catalysts were tested for activity in March of 2006 at the Technical University of Eindhoven. The catalytic testing was broken down into several sections: for the amidinate (NCN) see Figure 7.7.8, for the amidate (NCO) see Figure 7.7.12 and for the NacNac systems see Figure 7.7.17.

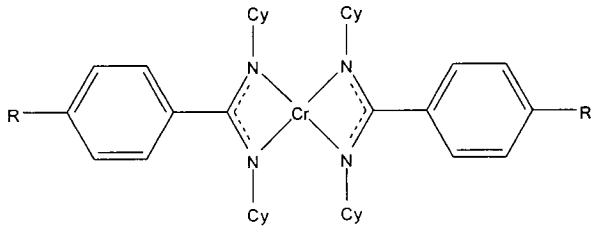

R = H (**16**), OMe (**17**), CF_3 (**18**)

Figure 7.7.8 Amidinate Complexes for Oligomerization Testing.

The amidinate system quickly proved to be exceedingly active; producing large amounts of oligomers (see Table 7.7.9) through a very exothermic reaction. The activities of all three complexes tested put them on par with the previously tested N-MeDipyr and N-MeTripyr $Cr^{(II)}$ complexes, though the amidinates showed a roughly 25% increase in activity.

Table 7.7.9 Amidinate Complexes; Oligomerization Activity.[a]

Entry	Catalyst	Temp (°C)	PE (g)	Alkenes (mL)	Activity g/mol·h	Activity g/g·Cr·h
25	16	50	1.03	61.5	1 379 650	26 532
26	17	50	1.87	68.25	1 531 075	29 444
27	18	50	1.84	71.25	1 598 375	30 738
28	18	5	1.15	61.5	1 379 650	26 532

[a] Conditions: 30 μmol of catalyst, 2000 eq. of MAO activator, 35 bar ethylene, total volume 150 mL in toluene, 1 hour reaction time.

In general, it appears that the activity of the catalysts increased in relation to the electron withdrawing ability of the ligand. The O-Me containing complex (**17**), which is the most electron donating, shows the lowest activity. The Ph derivative (**16**) yields an activity (entry 27) between the two other groups, as expected. The electron-withdrawing CF_3 ligand (**18**) displays the highest activity of the three. This then indicates that a metal centre which is more electron poor is more capable of producing higher activity which in turn is consistent with a "cationic" type of mechanism.

Table 7.7.10 Amidinate Complexes; α-Olefin Product Distribution.[a]

Entry	Catalyst	Temp (°C)	Activity g/g·Cr·h	α-olefin mol %						
				C_4	C_6	C_8	C_{10}	C_{12}	C_{14}	C_{16}
25	16	50	26 532	10.1	35.5	21.8	14.3	9.2	5.5	3.5
26	17	50	29 444	13.5	35.4	21.3	13.3	8.4	4.9	3.0
27	18	50	30 738	13.1	33.1	21.1	13.9	9.2	5.7	3.8
28	18	5	26 532	14.6	53.3	18.2	8.8	3.4	1.3	0.5

[a] Determined by GC-FID, against standard solutions of authentic α-olefin samples.

Just as in the case of the pyrrolide ligand systems, the amidinates only produced a Shulz-Flory distribution of oligomers which was centered at 1-hexene. There appears to be no direct link between the electron donating/withdrawing ability of the ligand system and the selectivity it displays, as all three complexes display near identical selectivities (entries 25-27). When the reaction was carried out at 5 °C (entry 31), a 13% drop in activity was observed (entry 27). This drop in activity is accompanied by a 20% increase in the amount of 1-hexene produced (entries 27 and 28), though, allowing for some thermal control over the products. At 5 °C catalyst **18** produces much less higher α-olefins than the other catalysts. All four polymerizations were performed in a reactor equipped with a thermocouple in order to sample the temperatures within the reactor. In the case of each amidinate ligand an exotherm was observed upon catalyst injection (see Figure 7.7.11).

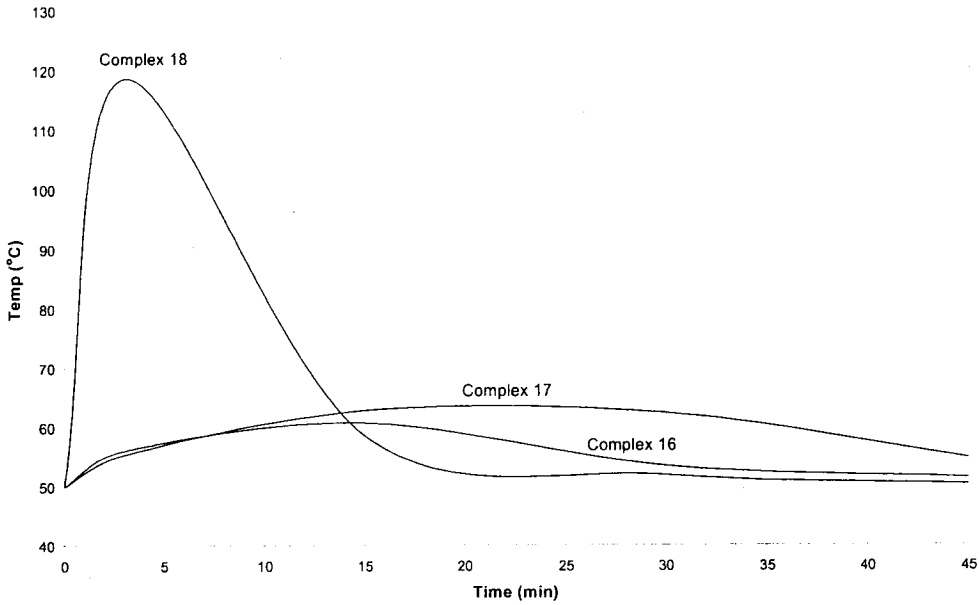

Figure 7.7.11 Exotherms for Entries 25-28.

It should be noted that the most active catalyst **18** exhibited a very large exotherm, reaching 118.7 °C within three minutes of being injected and charged with ethylene. The other two complexes slowly build in temperature until they reach a maximum and begin falling. This most likely indicates that, in the case of **18** (entry 27), there is a massive amount of activity which causes the temperature to rise to a level where the catalyst begins to decompose, at which point the temperature begins to fall. It is also noteworthy that the O-Me ligand (**16**) exhibits the lowest temperature increase, which is in line with its lower overall activity.

The amidate ligand systems (see Scheme 7.7.12) were also tested in thermocouple-equipped reactors for their oligomerization ability.

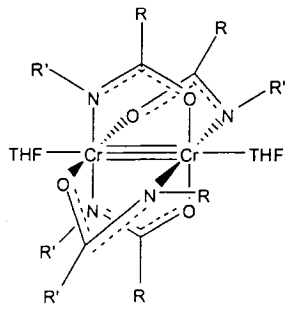

R = Ph, R' = 4-*iPr*-Ph (**19**)
R = Ph, R' = 2,6-Me-Ph (**20**)

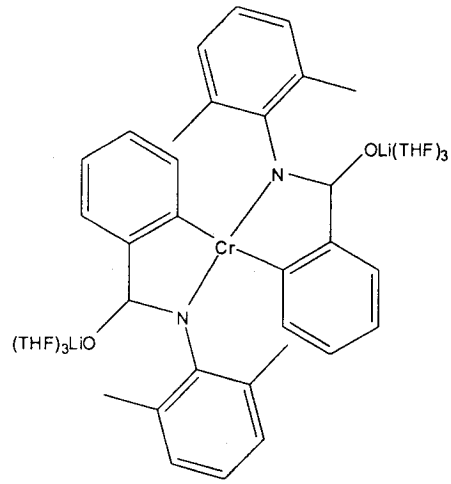

Complex **21**

Figure 7.7.12 Amidate (NCO) Complexes.

All three amidate Cr complexes displayed good catalytic activity for the oligomerization of ethylene (see Table 7.7.13). It appears that there is a steric influence on the activity as complex **19** (entry 29) which contains 2,5-Me_2-Ph groups has a much lower activity than **20** (entry 31) which has only hydrogens in the *ortho* positions.

Table 7.7.13 Amidate Complexes; Oligomerization Activity.[a]

Entry	Catalyst	Temp (°C)	PE (g)	Alkenes (mL)	Activity g/mol·h	Activity g/g·Cr·h
29	19	50	0.26	63.0	1 413 300	27 179
30	19	5	0.29	76.5	1 716 150	33 003
31	20	50	0.24	69.8	2 040 946	39 249
32	20	5	0.67	73.5	2 150 674	41 359
33	21	50	1.901	64.5	1 446 950	27 826

[a] Conditions: 30 μmol of catalyst, 2000 eq. of MAO activator, 35 bar ethylene, total volume 150 mL in toluene, 1 hour reaction time.

The square-planar, *ortho*–metallated analogue of **20** displays a decent level of activity (entry 33), though it is 30% less active than its parent compound (entry 31). It also produces significantly more PE than the other non-metallated amidate ligand systems. When the temperature of the reaction is lowered to 5 °C, the activity for both **19** (entry 30) and **20** (entry 32) increases. This most likely indicates that higher temperatures lead to catalyst decomposition.

Table 7.7.14 Amidate Complexes; α-Olefin Product Distribution.[a]

Entry	Catalyst	Temp (°C)	Activity g/g·Cr·h	α-olefin mol %						
				C_4	C_6	C_8	C_{10}	C_{12}	C_{14}	C_{16}
29	19	50	27 179	6.6	32.1	22.6	15.9	10.9	7.0	4.8
30	19	5	33 003	23.2	46.1	17.2	8.1	3.4	1.3	0.6
31	20	50	39 249	2.1	28.7	26.1	17.9	12.2	7.7	5.2
32	20	5	41 359	18.7	46.0	20.3	8.8	4.0	1.5	0.7
33	21	50	27 826	6.4	31.9	23.8	15.9	10.7	6.9	4.6

[a] Determined by GC-FID, against standard solutions of authentic α-olefin samples.

The higher temperature runs (entries 29, 31, 33) all show a Shulz-Flory distribution of α-olefins, centred at 1-hexene. When the temperature is lowered to 5 °C the catalysts become much more selective for 1-hexene and 1-octene, though they do also produce much more 1-butene. If the trend were to continue at even lower temperatures, it may be possible to develop a system that only produces 1-butene, 1-hexene, and 1-octene. When all three amidate ligand systems were tested at 50 °C extremely large exotherms were observed within the first minutes of catalysis (see Figure 7.7.15).

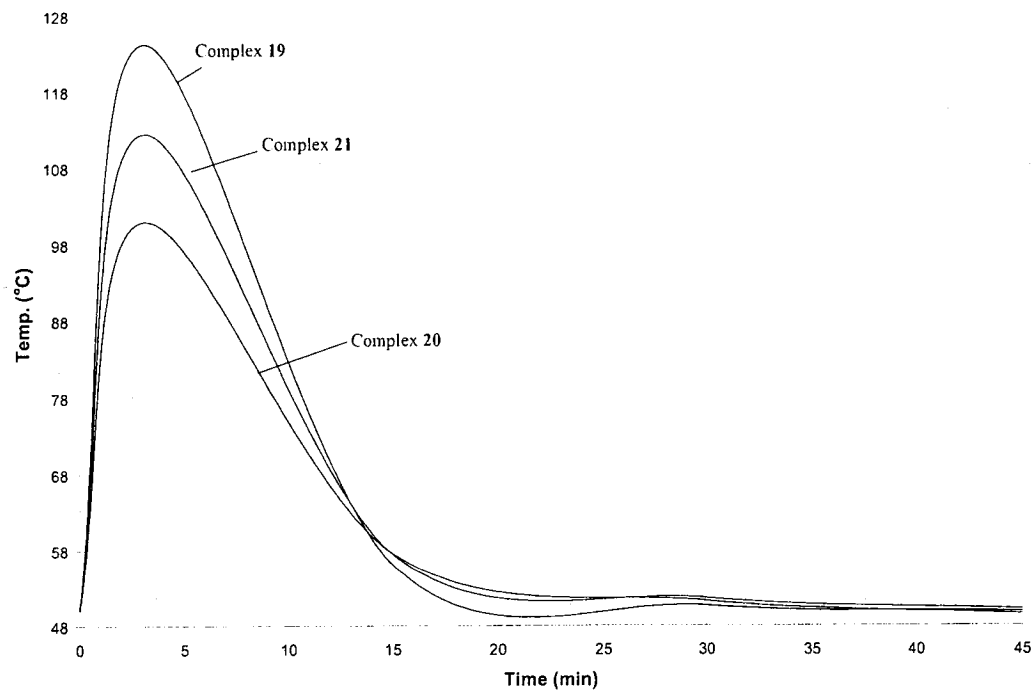

Figure 7.7.15 Exotherms for Entries 29, 31, 33.

As Figure 7.7.15 demonstrates, the reactions almost reach the boiling point of toluene within the first minutes of oligomerization. The temperature then rapidly declines, which most likely indicates that all of the catalytic activity is being performed within the first ten minutes of the run, during this time the catalysts are probably decomposing due to the extreme temperatures. In the case of the 5 °C runs (entries 30, 32) an exotherm is still observed, but it is now much milder (see Figure 7.7.16).

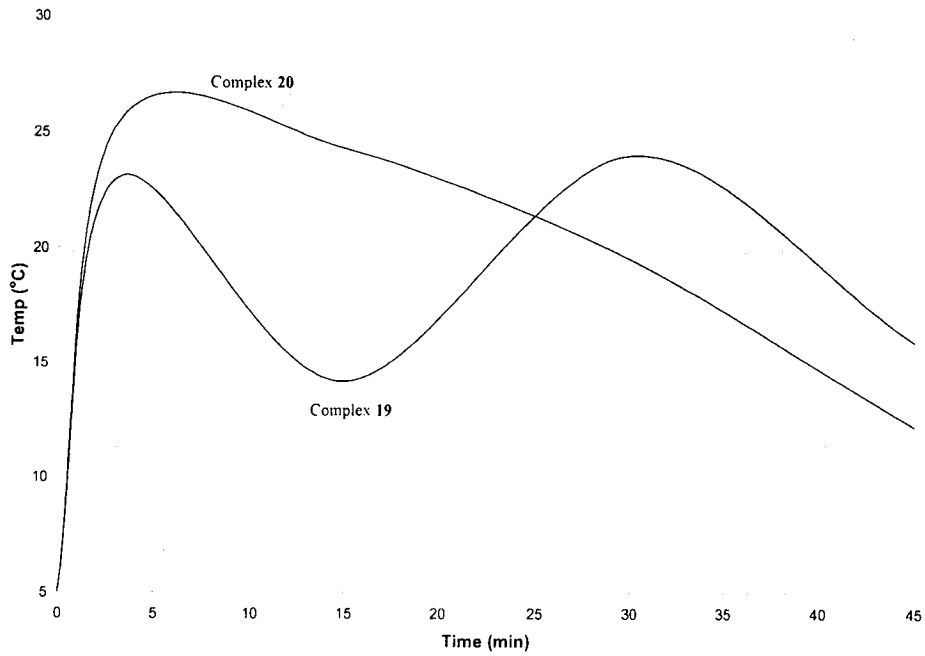

Figure 7.7.16 Exotherms for Entries 30, 32.

Oddly, Complex **20** now displays the larger exotherm, though it is only by a few degrees. It is also observed that in both cases the temperature does not fall to the regulated 5 °C temperature of the reactor. This would indicate that at lower temperatures the catalysts are remaining active for much longer periods of time. Complex **19** also displays a strange, bi-modal exotherm, which could possibly be attributed to an initial exothermic reaction at the metal centre, followed by an induction period, and then the actual catalytic activity.

The final complexes in the imine nitrogen donor ligand series are the NacNac Cr complexes **22** and **23** (see Scheme 7.7.17).

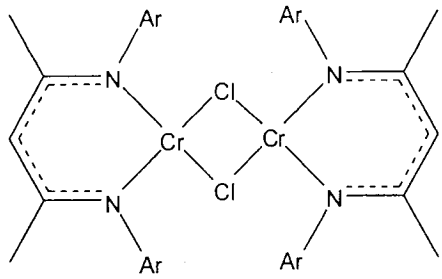

Ar = 2,6-iPr_2-Ph (**22**)
Ar = 2,6-Me_2-Ph (**23**)

Figure 7.7.17 NacNac Cr Complexes **22** and **23**.

It had been previously reported that complex **22** was a poor PE producing catalyst, but no testing was done to detect oligomers.[46] It seemed logical that the poor PE producing ability may be an indication that oligomerization was the more active catalytic pathway; especially given that all previously tested oligomerization catalysts had such poor yields of PE.

Table 7.7.18 NacNac Complexes; Oligomerization Activity.[a]

Entry	Catalyst	Temp (°C)	PE (g)	Alkenes (mL)	Activity g/mol·h	Activity g/g·Cr·h
34	22	50	18.22	1.0	22 433	431
35	23	50	6.03	1.8	40 379	776

[a] Conditions: 30 μmol of catalyst, 2000 eq. of MAO activator, 35 bar ethylene, total volume 150 mL in toluene, 1 hour reaction time.

Table 7.7.18 shows that the NacNac complexes do produce some oligomers, however the amount is extremely low. This low activity was also reflected in the exotherms produced by the catalysts, which never increased above 56 °C. In addition, the systems produce much more PE than any other oligomerization system with the exception of the IBAO N-MeTripyr reaction (see Table 7.7.10), however that system did not produce any oligomers.

Table 7.7.19 NacNac Complexes; α-Olefin Product Distribution.[a]

Entry	Catalyst	Temp (°C)	Activity g/g·Cr·h	α-olefin mol %						
				C_4	C_6	C_8	C_{10}	C_{12}	C_{14}	C_{16}
34	22	50	431	41.0	59.0	0.0	0.0	0.0	0.0	0.0
35	23	50	776	28.2	67.6	4.2	0.0	0.0	0.0	0.0

[a] Determined by GC-FID, against standard solutions of authentic α-olefin samples.

What is very intriguing about catalyst **22** is the selectivity of the oligomers produced. From Table 7.7.19 it is apparent that the catalyst produces only 1-butene and 1-hexene, with no higher olefins detected. This is unprecedented in all of the systems we have examined thus far. It may be an indication that the extremely large steric bulk of the ligand favours the linear PE production mechanism. However, when it does under go the metallacyclic oligomerization mechanism, the steric constraint must be so great that only small ring sizes are accommodated. In order to test this hypothesis the sterically less bulky NacNac complex **23** was synthesized and tested (entry 35). A drastic reduction of PE production was observed along with a concomitant increase in both the oligomerization activity and selectivity for longer chain α-olefins. This result would tend to support the hypothesis that removing some steric crowding about the Cr centre allows space for the trimerization catalytic cycle to occur preferentially over the production of PE. Furthermore, the presence of 1-octene in the case of the less bulky ligand, which is not present when the bulkier analogue is used, would tend to indicate that the steric bulk of the ligand can directly influence the size of the metallacycle which can be accommodated by the catalyst.

In summary, it appears from our work that the $Cr^{(II)}$ oxidation state can provide a very substantial level of oligomerization activity. Unfortunately, this activity is unaccompanied by any selectivity, as Shulz-Flory distributions are inevitably found. Whether this lack of selectivity may be attributed to the oxidation state is debatable however, given that the $Cr^{(III)}$ compound [N-MeTripyrCrCl] (**5**) (see Table 7.6.8) produced the same distribution of oligomers as did it's $Cr^{(II)}$ analogue. This would tend to indicate that the N-donor ligand systems themselves may be inadequate for enforcing selectivity. Furthermore, the ligand leaching and instability of the Cr-Me moiety demonstrated by the N-MeTripyr ligand (see Figures 7.6.18-19) may indicate a further

inability of the nitrogen-based ligand framework to support the selective, active catalyst. The variable temperature testing on both the amidate (NCO), and amidinate (NCN) frameworks demonstrated that, at lower temperatures the oligomerizations did become more selective for 1-hexene. Thus indicating that, perhaps under carefully chosen conditions the nitrogen-based ligand systems could become selective for 1-hexene. The interesting questions inspired by this work lead us to investigate some of the most performing catalyst systems to date in order to better determine if selectivity is oxidation state dependant, or whether it is ligand dependant.

7.8 Sasol SNS/PNP Ligand Systems:

The Sasol/BP PNP and Sasol SNS ligand systems are amongst the best oligomerization catalysts due to their selectivity for 1-octene, and 1-hexene respectively. The activities of these two catalysts are also quite respectable making them industrially relevant. That said, no current work has been published exploring the actual active oxidation state of the catalyst, nor its interaction with alkyaluminum activators (which are present during catalysis). A complete understanding of these two very important factors is required in order to fully comprehend the catalytic mechanism, and to design future catalysts. As such the catalytic behaviour of the two literature systems was critically examined with respect to the metal oxidation state, and the systems reactivity with Al activators.

Recent work in our lab on the reaction of the $Cr^{(III)}$ PNP complex [$PNPCrCl_3$] (PNP = $Ph_2PN(Cy)PPh_2$) with $AlMe_3$ yielded quite an enigma. It was found that after exposure to 10 eq. of $AlMe_3$ the *divalent* complex [$PNP_2Cr(ClAlMe_3)$] [$AlMe_3Cl$]·$(toluene)_{0.25}$ $(hexane)_{0.25}$ (**24**) formed in 48 % yield (see Scheme 7.8.1) .[47]

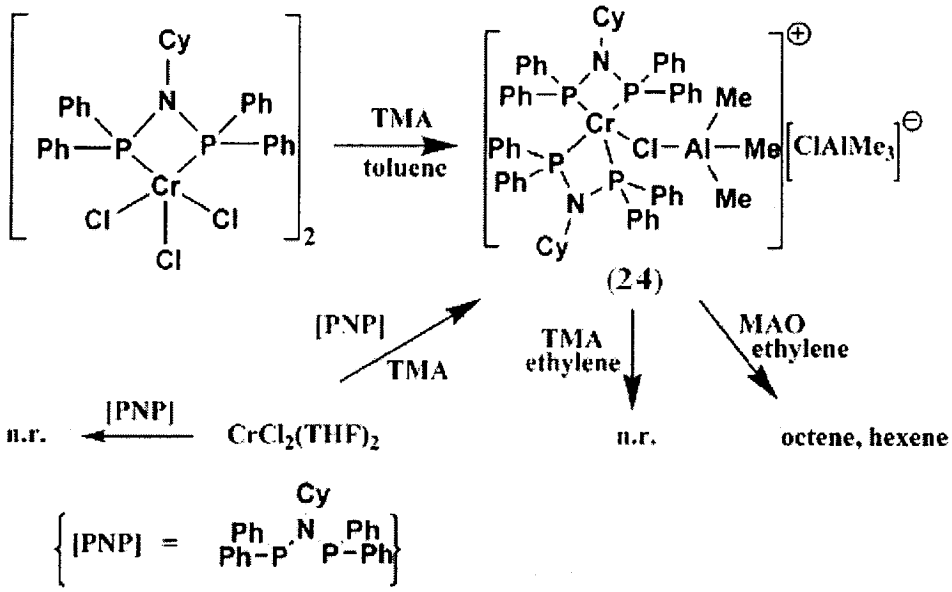

Scheme 7.8.1 Generation of **24** from $Cr^{(III)}$ or $Cr^{(II)}$.[47]

In addition **24** could be prepared by reacting the PNP ligand with $CrCl_2(THF)_2$, but only in the presence of $AlMe_3$. The literature published on the 1-octene selective PNPCr system utilized $Cr^{(III)}$ as the precursor, and reported that this was the oxidation state of the active catalyst.[19] Since we had discovered that $Cr^{(II)}$ catalyzes the oligomerization reaction more efficiently than $Cr^{(III)}$ in the case of the N-MeTripyr ligand system (see Table 7.6.7), Complex **24** was tested to determine the impact of the $Cr^{(II)}$ oxidation state on catalysis (see Table 7.8.2).

Table 7.8.2 PNP Complexes; Oligomerization Results.[a]

Entry	Catalyst	MAO (eq.)	PE (g)	Alkenes (mL)	Activity g/mol·h	Activity g/g·Cr·h
36[b]	[PNPCrCl$_3$]	300	0.5	n/a	n/a	8 050
37	**24**	300	0.16	19.5	437 450	8 413
38	**24**	2000	10.67	66.75	1 497 425	28 797

[a] Conditions: 30 μmol of catalyst, 30 bar ethylene, 65 °C, total volume 150 mL in toluene, 1 hour reaction time. [b] Reported in ref. 19.

As the results in the table indicate, the $Cr^{(II)}$ (entry 37) analogue of the published PNP ligand (entry 36) is active and more importantly, selective, for the oligomerization of ethylene. Furthermore, the catalyst is 10% more selective towards 1-octene production

than the $Cr^{(III)}$ compound (see Table 7.8.3) and does so with no drop in activity compared to the literature value. It also appears that the addition of a large excess of MAO (2000, entry 38) results in a threefold increase in activity.

Table 7.8.3 PNP Complexes; α-Olefin Product Distribution of **24**.[a]

Entry	Catalyst	MAO (eq.)	Activity g/g·Cr·h	α-olefin mol %						
				C_4	C_6	C_8	C_{10}	C_{12}	C_{14}	C_{16}
36[b]	[PNPCrCl$_3$]	300	8 050	-	27.6	59	-	-	-	-
37	**24**	300	8 413	1.1	23.6	71.0	1.5	1.3	0.8	0.8
38	**24**	2000	28 797	9.7	33.1	34.8	10.2	6.2	3.7	2.3

[a] Determined by GC-FID, against standard solutions of authentic α-olefin samples. [b] Reported in ref. 19.

The increase in activity, unfortunately, is concomitant to a decrease in selectivity as the catalyst now produces a Shulz-Flory distribution of α-olefins. The drop in selectivity most likely indicates that the large excess of MAO is disrupting the ligand environment around the Cr centre, resulting in less steric control over the process. These results strongly indicate that, in the case of the PNP ligand, $Cr^{(II)}$ produces a catalyst which is more selective, and more active than $Cr^{(III)}$.[47] This reaction demonstrates that $Cr^{(III)}$ complexes can be readily reduced to $Cr^{(II)}$. Complex **24** is a catalyst precursor since it also requires activation by MAO. The fact that the catalytic results clearly show that the $Cr^{(II)}$ compound produces the same (if not better) activities and selectivities as the $Cr^{(III)}$ parent compound, strongly suggests that the catalytically active species is based on divalent chromium. This observation is in agreement with our results described above on the different nitrogen-based ligand systems, invariably pointing towards divalent chromium as the catalytically active species.

Our results with both the N-MeTripyr and PNP systems lead us to believe that the $Cr^{(II)}$ oxidation state was closer to the actual active catalyst oxidation state, or may even be the true active catalyst. To further probe this working hypothesis, our group has recently embarked on an extensive study on the other Sasol selective catalyst: [SNSCrCl$_3$] SNS = $CySCH_2CH_2NHCH_2CH_2SCy$ (see Scheme 7.8.4).[48,49] This catalytic system as reported by Sasol consists of a simple coordinatively saturated $Cr^{(III)}$ octahedral compound formulated on the basis of its crystal structure. Since no information was

reported about the reaction mechanism, we have applied the same strategy previously used and extensively investigated the reactivity of this catalyst precursor with several Al activators. In addition to exploring the oxidation state of the SNSCr system, the role of the N-H group of the ligand was also examined. It has been claimed that deprotonation of this function occurs during catalysis,[17b] so the presence or absence of the N-H function in an alkylating environment such as that provided by the Al activators is an important issue to be addressed.

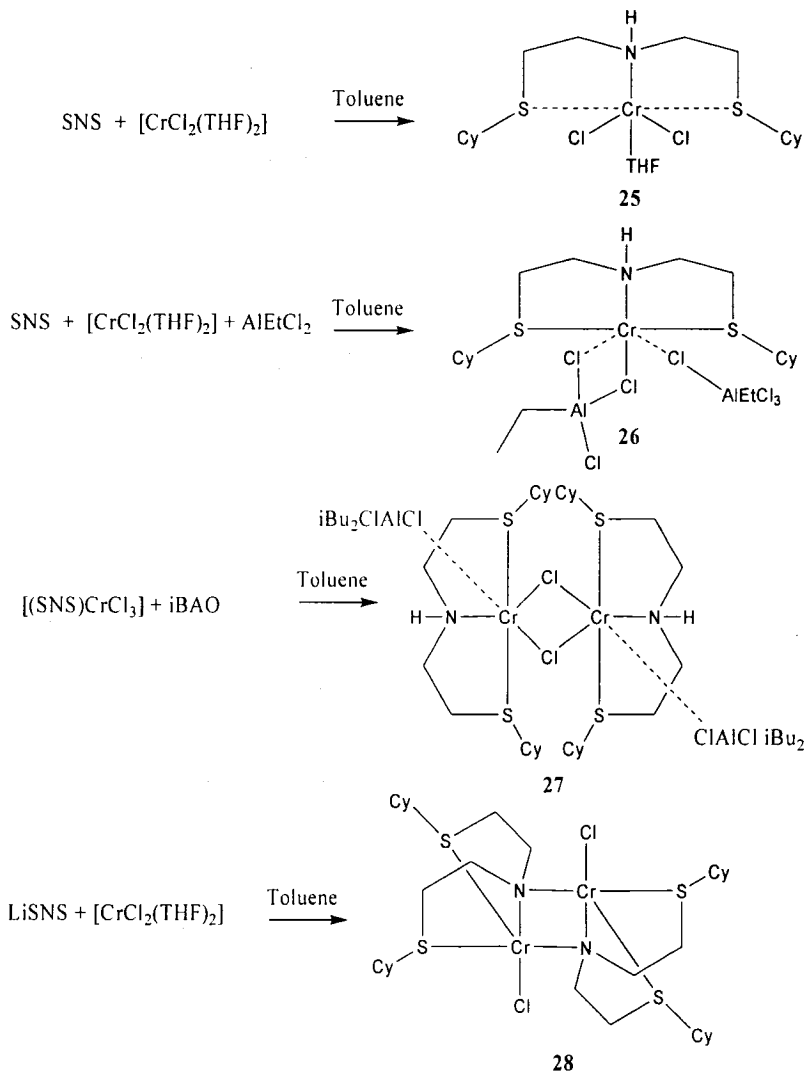

Scheme 7.8.4 Preparation of $Cr^{(II)}$ SNS Complexes **25-28**.

It is known that $Cr^{(II)}$ complexes, having a d^4 electron configuration, commonly adopt a square-planar geometry. However, there does exist the possibility to form octahedral complexes. If strong ligand-field splitting ligands are utilized, low-spin octahedral complexes can result. The other case is a high-spin octahedral geometry which exhibits strong Jahn-Teller distortions.[50] This Jahn-Teller distorted octahedral geometry was observed for complexes **25-27**. One reaction of significant interest was the formation of **27** which formed from the spontaneous reduction of a $Cr^{(III)}$ species in the presence of the alkyl aluminum reagent IBAO. This reaction is very similar to the PNPCr case and reiterates the point that $Cr^{(III)}$ alkyls may be quite unstable. Complex **28** was prepared by reacting the deprotonated SNS ligand with $[CrCl_2(THF)_2]$ in order to test the catalytic activity of an SNS catalyst which has no N-H bond.

A stunning discovery was made when the SNS ligand and $[CrCl_2(THF)_2]$ was reacted with 10 eq. of $AlMe_3$. From the reaction mixture green X-ray quality crystals of a *trivalent* and *cationic* complex $[SNSCrMe(\mu\text{-}Cl)]_2[(AlMe_3)_2(\mu\text{-}Cl)]_2\cdot$(toluene) (**29**) were isolated in moderate yield (see Figure 7.8.5).

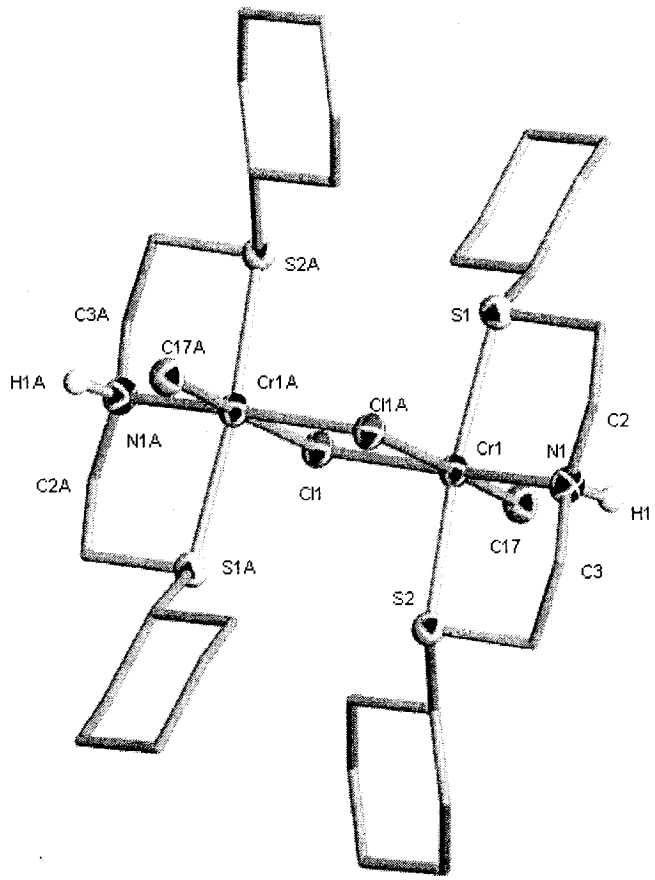

Figure 7.8.5 Crystal Structure of **29** with 30% Thermal Ellipsoids, $[(Me_3Al)_2Cl]$ Anion Omitted for Clarity.

The dicationic dimeric structure $[SNSCrMe(\mu\text{-}Cl)]_2[(AlMe_3)_2(\mu\text{-}Cl)]_2 \cdot$(toluene) (**29**) has an octahedral geometry and contains a terminal methyl group [Cr(1)–C(17) = 2.049(5) Å]. The dimer is bridged by two chlorine atoms which are *cis* to one another and *trans* to the methyl and nitrogen of the SNS ligand [Cr(1)–Cl(1) = 2.339(2), Cr(1)–Cl(1a) = 2.519(2), Cr(1)–N(1) = 2.088(4), Cr(1)–S(1) = 2.445(2), Cr(1)–S(2) = 2.446(2) Å]. The angles about Cr(1) are again quite close to the ideal values for an octahedral geometry with only a slight distortion at the sulphur groups [N(1)–Cr(1)–S(1) = 83.63(13), N(1)–Cr(1)–S(2) = 83.59(13), N(1)–Cr(1)–Cl(1) = 174.09(12), N(1)–Cr(1)–Cl(1a) = 88.61(13), N(1)–Cr(1)–C(17) = 91.8(2)°]. Two $[(Me_3Al)_2(\mu\text{-}Cl)]$ anions balance the charge of the chromium complex and appear to be hydrogen bonding to the N-H groups of the SNS ligand [Cl(6)–H(1) = 2.537(2) Å]. The oxidation of the metal center during the formation of **29** has no straightforward explanation given that an alkylating agent, such as $AlMe_3$, can hardly be regarded as an oxidizing agent. The only possibility of explaining this behaviour is to propose that a disproportionation reaction may account for the re-oxidation of the metal center (see Scheme 7.8.6).

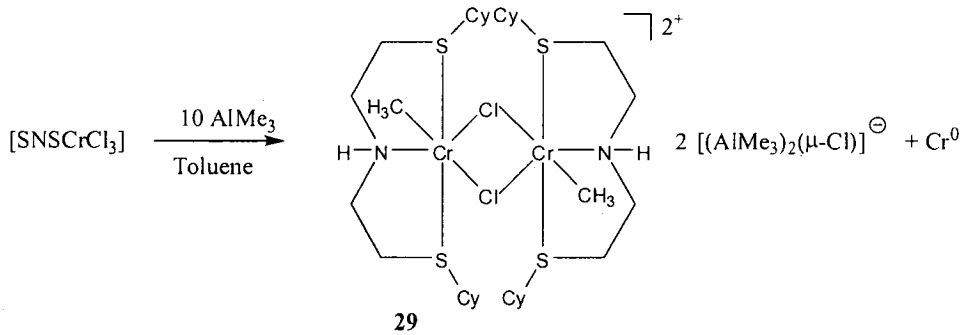

29

Scheme 7.8.6 Proposed Formation of $Cr^{(III)}$ Complex **29**.

This proposal, in turn, implies that a species with a valence lower than two must be generated as a result of the formation of the trivalent **29**. The well-established stability of zero- and mono-valent chromium–arene complexes[51] could well be a driving force for the disproportionation. However, we found no evidence for these species, although we did observe that a substantial amount of metallic chromium was invariably present in these

reaction mixtures as a black, pyrophoric, and insoluble material. The X-ray fluorescence spectrum of this material confirmed the presence of Cr as the only heavy element while both the IR spectrum and combustion analysis showed the absence of organic functions. Furthermore, the EPR spectrum of the crude reaction mixture was found to be identical to that of an analytically pure sample of **29**,[49] thereby conclusively proving that **29** is the only EPR-active species formed during this unusual reaction.

Work in our lab found that the reaction of the trivalent Sasol catalyst precursor [$SNSCrCl_3$] with 4 eq. of $AlMe_3$ (see Scheme 7.8.7) also afforded the trivalent **29**. The fact that the trivalent oxidation state was preserved in this unprecedented cationic organochromium species is in stark contrast with the PNP chemistry (see Scheme 7.8.1) described above.

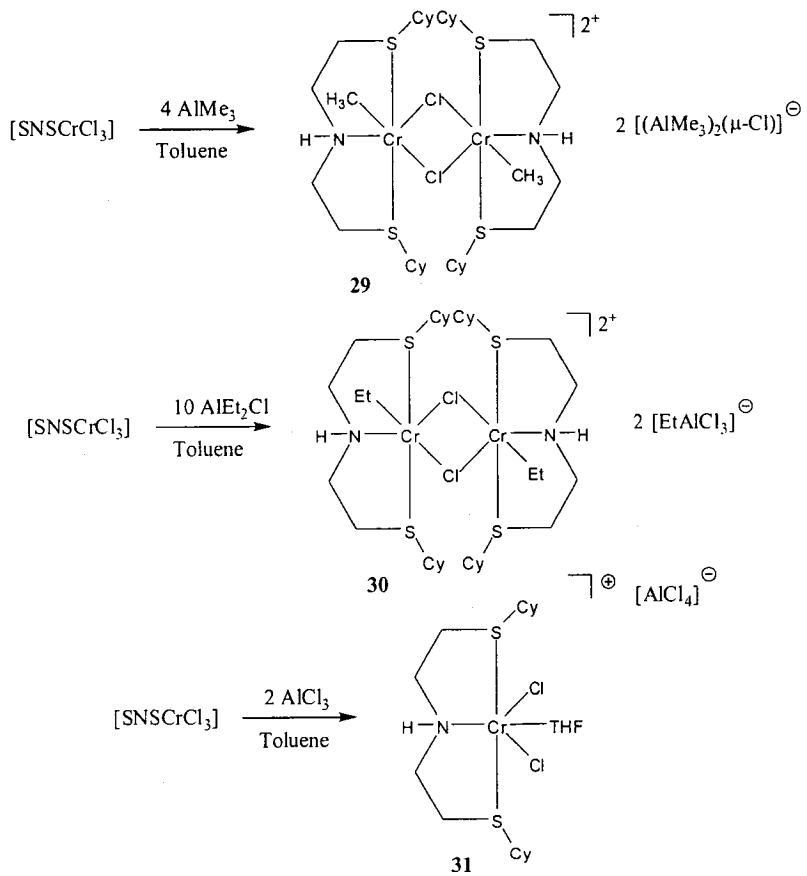

Scheme 7.8.7 Preparation of $Cr^{(III)}$ SNS Complexes **29-31**.

Furthermore, the trivalent oxidation state was also preserved when the ethyl containing alkyl aluminum $AlEt_2Cl$ was used, forming the dicationic Cr-Et containing complex **30**.

The M-Et bond is known to be even more reducing than the M-Me bond (found in **29**), implying that these $Cr^{(III)}$ complexes may have a uniquely stable M-C bond. The final complex, **31**, resulted from the reaction of [$SNSCrCl_3$] with $AlCl_3$ and should provide information as to whether a cationic complex is more performing than the neutral literature system.

As no $Cr^{(II)}$ SNS catalyst systems had been previously reported, they provide an interesting point to begin the analysis of the oligomerization results (see Figure 7.8.8).

[$SNSCrCl_2(THF)$]
25
monomeric

[$SNSCr(\eta^2\text{-}ClAlEtCl_2)(ClAlEtCl_2)$]
26
monomeric

[$SNSCr(\mu\text{-}Cl)(\eta^2\text{-}Cl_2Al^iBu_2)]_2$
27
dimeric

[$(CySCH_2CH_2)_2N)CrCl]_2$
28
dimeric

Figure 7.8.8 $Cr^{(II)}$ SNS Catalysts From Scheme 7.8.4.

All $Cr^{(II)}$ SNS catalysts which were tested produced oligomerization activity, albeit at only ~10% of the activity of the previously discussed nitrogen based ligand systems.

Table 7.8.9 $Cr^{(II)}$ SNS Complexes; Oligomerization Activity.[a]

Entry	Catalyst	MAO (eq.)	PE (g)	Alkenes (mL)	Activity g/mol·h	Activity g/g·Cr·h
39	25	1000	2.58	6.8	151 425	2 912
40	26	1000	0.64	5.3	117 775	2 265
41	27	1000	0.86	6.0	134 600	2 588
42	28	2000	2.2	0.9	22 433	431

[a] Conditions: 30 μmol of catalyst, 35 bar ethylene, 50 °C, total volume 150 mL in toluene, 1 hour reaction time.

The most active system was the aluminum free complex **25** (entry 39) which was 11% more active than the bulky IBAO containing **27** (entry 41), and 29% more active than the $AlEtCl_3$ containing **26** (entry 40). This may indicate that the coordinated anions may be hindering the reactivity, and that the more bulky IBAO containing complex might dissociate more readily. When the SNS ligand is deprotonated (entry 42), the activity

drastically decreased, thus indicating that the N-H moiety may play a crucial role in creating an effective catalyst.

Table 7.8.10 $Cr^{(II)}$ SNS Complexes; α-Olefin Product Distribution.[a]

Entry	Catalyst	MAO (eq.)	Activity g/g·Cr·h	α-olefin mol %						
				C_4	C_6	C_8	C_{10}	C_{12}	C_{14}	C_{16}
39	25	1000	2 912	2.7	97.3	0.0	0.0	0.0	0.0	0.0
40	26	1000	2 265	2.2	96.0	1.1	0.3	0.2	0.1	0.1
41	27	1000	2 588	17.1	68.0	5.8	4.5	2.6	1.3	0.8
42	28	2000	431	14.3	16.0	34.8	19.4	9.1	4.0	2.4

[a] Determined by GC-FID, against standard solutions of authentic α-olefin samples.

Analysis of the oligomers yielded some interesting results. Similar to the published Cr-SNS examples,[17] catalysts **25** and **26** (entries 39 and 40) are extremely selective for 1-hexene, though they also produce small amounts of 1-butene. Curiously, none of the Sasol literature published to date has even acknowledged the presence of 1-butene in the selective systems, although this is most likely attributed to an oversight, or improper testing on their part. Interestingly, it appears that the nature of the Al anion has an impact on the catalyst selectivity as the $AlEtCl_3$ containing **26** produces 1-hexene in 96 % selectivity versus the IBAO containing **27**, which only has 68% selectivity for 1-hexene and also shows the beginnings of a Shulz-Flory distribution of products. It is possible that the differences between entries 40 and 41 could also be attributed to the monomeric and dimeric catalyst structures, respectively. The deprotonation of the SNS ligand not only had a large impact on the activity, but also the selectivity as well (entry 42). The products are now produced in a Shulz-Flory distribution which is centred at 1-octene. These results tend to indicate one of two things: 1) The N-H group is an integral component for the production of a selective catalyst; 2) Strongly bound dimeric structures lead to Shulz-Flory product distributions. The fact that both of the dimeric structures tend to produce a Shulz-Flory distribution would be in agreement with the second point. Unfortunately no other deprotonated SNS systems currently exist with which to compare to, so the first point must remain a conjecture until further evidence

arises. There were basically no temperature deviations during any of the reactions, and hence no information, as all runs remained within 2 °C of the reactor temperature.

Since complexes **26** and **27** were so similar, and yet produced such disparate results in the original testing (see Tables 7.8.9-10), it was decided to further investigate the two systems. It was found that varying the number of equivalents of MAO had a profound impact on the catalyst activities (see Table 7.8.11).

Table 7.8.11 Effect of MAO Concentration on the $Cr^{(II)}$ SNS Complexes **26** and **27**.[a]

Entry	Catalyst	MAO (eq.)	PE (g)	Alkenes (mL)	Activity g/mol·h	Activity g/g·Cr·h
43	26	500	0.80	6	134 600	2 588
44	26	1000	0.64	5.3	117 775	2 265
45	26	2000	1.53	4.5	100 950	1 941
46	27	300	0.70	10.5	235 550	4 530
47	27	500	0.78	8.3	185 075	3 559
48	27	1000	0.86	6.0	134 600	2 588
49	27	2000	1.47	3.8	84 125	1 618

[a] Conditions: 30 µmol of catalyst, 35 bar ethylene, 50 °C, total volume 150 mL in toluene, 1 hour reaction time.

Contrary to the nitrogen donor ligand catalysts, increasing the amount of MAO actually leads to a marked decrease in catalyst performance. Inversely, by reducing the amount of MAO the catalyst performance increases. Furthermore, the amount of MAO also has a large impact on the α-olefin product distribution.

Table 7.8.12 Effect of MAO on the SNS Complexes **26** and **27**; α-Olefin Product Distribution.[a]

Entry	Catalyst	MAO (eq.)	Activity g/g·Cr·h	α-olefin mol %						
				C_4	C_6	C_8	C_{10}	C_{12}	C_{14}	C_{16}
43	26	500	2 588	2.7	92.2	2.6	1.2	0.7	0.4	0.2
44	26	1000	2 265	2.2	96.0	1.1	0.3	0.2	0.1	0.1
45	26	2000	1 941	23.9	54.8	11.2	5.5	2.7	1.2	0.6
46	27	300	4 530	0.8	98.5	0.2	0.2	0.1	0.1	0.1
47	27	500	3 559	1.6	96.6	0.7	0.5	0.3	0.2	0.1
48	27	1000	2 588	17.0	68.0	5.8	4.5	2.6	1.3	0.7
49	27	2000	1 618	26.5	49.7	11.0	6.2	3.7	1.9	1.0

[a] Determined by GC-FID, against standard solutions of authentic α-olefin samples.

At 2000 eq. of MAO both catalysts yield nearly identical, Shulz-Flory product distributions centred at C_6 (entries 45 and 49). When the MAO is reduced to 500 (entry 43) or 300 (entry 46) the catalysts produce 1-hexene in high selectivity. These observations clearly demonstrate that too much activator harshly effects both the activity, and selectivity of the $Cr^{(II)}$ SNS systems. This is most likely due to large amounts of MAO leading to catalyst decomposition, or the creation of other, non-selective catalytic species. Even the most active run (entry 46) did not show any temperature increases during the catalytic run, once again offering no insights into the system.

Concurrent with the $Cr^{(II)}$ SNS runs, a series of $Cr^{(III)}$ SNS catalytic testing was performed on the complexes detailed in Figure 7.8.13.

$[SNSCrCl_2(THF)][AlCl_4]$	$[SNSCrMe(\mu\text{-}Cl)]_2[(Me_3Al)_2(\mu\text{-}Cl)]_2$	$[SNSCrEt(\mu\text{-}Cl)]_2[AlEtCl_3]_2$
31	**29**	**30**
monomeric	dimeric	dimeric

Figure 7.8.13 $Cr^{(III)}$ SNS Catalysts from Scheme 7.8.7.

Upon first inspection it can be seen that the $Cr^{(III)}$ catalysts appear to be up to 6.5 times more active than their $Cr^{(II)}$ counterparts (see Table 7.8.14). However, there appears to be much more fluxionality involved in the $Cr^{(III)}$ systems.

Table 7.8.14 $Cr^{(III)}$ SNS Complexes; Oligomerization Activity.[a]

Entry	Catalyst	MAO (eq.)	PE (g)	Alkenes (mL)	Activity g/mol·h	Activity g/g·Cr·h
50[b]	$[SNSCrCl_3]$	1000	0.08	-	-	5 824
51	31	1000	1.01	32.3	723 475	13 913
52	29	1000	0.82	16.0	358 933	6 903
53	30	1000	0.80	29.3	487 925	12 619

[a] Conditions: 30 μmol of catalyst, 35 bar ethylene, 50 °C, total volume 150 mL in toluene, 1 hour reaction time. [b] Ref. 49.

There appears to be little in the way of a logical explanation for the wide range of catalytic activity. If, for example, the monomeric versus dimeric species are compared (entries 50, 51 vs. 52, 53), both display a higher and lower activity catalyst. Complexes **29** (entry 52) and **30** (entry 53) are nearly identical in structure, differing at only the

terminally bound methyl or ethyl groups, and yet they display distinctly different reactivities. So too can the presence, or absence of an aluminum counter-anion be ruled out as the sole source of the different activities (entry 50 vs. 51-52). Perhaps the nature of the anion plays some role as demonstrated by entries 51-53. Both **30** and **31** display higher activities and both have monomeric anions ($[AlEtCl_3]^-$ and$[AlCl_4]^-$) versus **29** which has a dimeric anion ($[(Me_3Al)_2(\mu\text{-}Cl)]^-$).

Table 7.8.15 $Cr^{(III)}$ SNS Complexes; α-Olefin Product Distribution.[a]

Entry	Catalyst	MAO (eq.)	Activity g/g·Cr·h	α-olefin mol %						
				C_4	C_6	C_8	C_{10}	C_{12}	C_{14}	C_{16}
50[b]	$[SNSCrCl_3]$	1000	5 824	-	>98	-	-	-	-	-
51	31	1000	13 913	0.0	100	0.0	0.0	0.0	0.0	0.0
52	29	1000	6 903	1.9	97.7	0.4	0.1	0.0	0.0	0.0
53	30	1000	9 383	0.6	98.8	0.5	0.1	0.0	0.0	0.0

[a] Determined by GC-FID, against standard solutions of authentic α-olefin samples. [b] Ref. 49.

Even though all four complexes had quite disparate activities, they did share one trait in common. All four compounds are nearly 100 % selective for the production of 1-hexene (see Table 7.8.15). There is virtually no difference between the selectivity for each, indicating that even though something is influencing the overall activity it is not interfering with the selective production of the α-olefins.

In order to try and gain a better understanding into the factors which are effecting the $Cr^{(III)}$ catalysts, complexes **29** and **30** were selected for more extensive testing. Varying the amount of MAO had a large impact on **29**, and to a lesser extent **30** (see Table 7.8.16).

Table 7.8.16 Effect of MAO Concentration on the $Cr^{(III)}$ SNS Complexes **29** and **30**.[a]

Entry	Catalyst	MAO (eq.)	PE (g)	Alkenes (mL)	Activity g/mol·h	Activity g/g·Cr·h
54	29	500	0.41	18.6	417 260	8 024
55	29	1000	0.82	16.0	358 933	6 903
56	29	2000	4.26	3.5	78 517	1 510
57	30	500	0.74	26.3	588 875	11 325
58	30	1000	0.80	29.3	487 925	12 619
59	30	2000	1.64	21.8	656 175	9 383

[a] Conditions: 30 µmol of catalyst, 35 bar ethylene, 50 °C, total volume 150 mL in toluene, 1 hour reaction time.

In both cases, as the number of equivalents of MAO is decreased, there is a concomitant increase in activity. An eightfold increase in activity is observed between 500 and 2000 eq. in the case of complex **29** (entry 54 and 56). Whereas only a 17 % increase in activity is observed for catalyst **30** (entry 57 and 59). The decrease in activity occurs concurrently with an increase in PE production, hinting that perhaps some of the catalyst is being converted from an oligomerization catalyst to a PE producing catalyst.

Table 7.8.17 Effect of MAO on the SNS Complexes **29** and **30**; α-Olefin Product Distribution.[a]

Entry	Catalyst	MAO (eq.)	Activity g/g·Cr·h	α-olefin mol %						
				C_4	C_6	C_8	C_{10}	C_{12}	C_{14}	C_{16}
54	29	500	8 024	1.6	98.2	0.2	0.0	0.0	0.0	0.0
55	29	1000	6 903	1.9	97.7	0.4	0.1	0.0	0.0	0.0
56	29	2000	1 510	24.4	38.9	19.6	9.4	4.6	2.0	1.1
57	30	500	11 325	0.1	99.4	0.5	0.0	0.0	0.0	0.0
58	30	1000	12 619	0.6	98.8	0.5	0.1	0.0	0.0	0.0
59	30	2000	9 383	0.6	98.8	0.5	0.1	0.0	0.0	0.0

[a] Determined by GC-FID, against standard solutions of authentic α-olefin samples.

In the case of **29** the drop in activity was accompanied by a switch in selectivity towards a Shulz-Flory distribution of products centred at 1-hexene. On the other hand, catalyst **30** did not seem to be effected by the increased concentration of MAO as it continued to produce 1-hexene almost exclusively. This extreme dichotomy between two catalysts which are almost identical structurally remains a perplexing mystery, and is currently being studied by our group.

Overall it has been demonstrated that in the case of the SNS ligand the $Cr^{(III)}$ oxidation state produces both a more active and more selective catalyst. This can be seen by comparing the most active $Cr^{(II)}$ and $Cr^{(III)}$ catalysts (see Table 7.8.18).

Table 7.8.18 Comparison of $Cr^{(II)}$ **27** and $Cr^{(III)}$ **30**; Activity and α-Olefin Product Distribution.[a]

Ox State	Entry	Catalyst	MAO (eq.)	Activity g/g·Cr·h	α-olefin mol %						
					C_4	C_6	C_8	C_{10}	C_{12}	C_{14}	C_{16}
$Cr^{(II)}$	46	27	300	4 530	0.8	98.5	0.2	0.2	0.1	0.1	0.1
	47	27	500	3 559	1.6	96.6	0.7	0.5	0.3	0.2	0.1
	48	27	1000	2 588	17.0	68.0	5.8	4.5	2.6	1.3	0.7
	49	27	2000	1 618	26.5	49.7	11.0	6.2	3.7	1.9	1.0
$Cr^{(III)}$	57	30	500	11 325	0.1	99.4	0.5	0.0	0.0	0.0	0.0
	58	30	1000	12 619	0.6	98.8	0.5	0.1	0.0	0.0	0.0
	59	30	2000	9 383	0.6	98.8	0.5	0.1	0.0	0.0	0.0

[a] Determined by GC-FID, against standard solutions of authentic α-olefin samples.

The $Cr^{(II)}$ catalyst (**27**) approaches half of the activity of the $Cr^{(III)}$ catalyst at lower loading of MAO (300 eq. entry 46) and shows almost the same overall selectivity for 1-hexene. The $Cr^{(II)}$ catalyst is much more sensitive to the presence of excess activator, however, as can be seen by the rapid loss of selectivity towards a Shulz-Flory distribution at higher loadings of MAO. The $Cr^{(III)}$ catalyst appears much more resistant towards this loss in selectivity.

It is difficult to rationalize the active oxidation state for the oligomerization process. In the case of the PNP ligand (see Table 7.8.3) it seems quite clear that the $Cr^{(III)}$ catalyst is reduced in the presence of the aluminum activator, and that the $Cr^{(II)}$ analogue produces the same activity and selectivity as the parent $Cr^{(III)}$ compound. In the case of the SNS ligand, the same reduction of a $Cr^{(III)}$ to a $Cr^{(II)}$ complex was observed in the case of the aluminum activator IBAO (Complex **27** Scheme 7.8.4). This complex produced lower activities and selectivities than the parent $Cr^{(III)}$ compound, though it did approach the parent compound results at a very low loading of MAO (Table 7.8.12). Our working hypothesis that all $Cr^{(III)}$ compounds spontaneously reduce to the $Cr^{(II)}$ oxidation state was thrown into disarray upon the discovery that the $Cr^{(II)}$ complex **29** was actually oxidized to a $Cr^{(III)}$ alkyl in the presence of $AlMe_3$ (see Scheme 7.8.6). This serves to further confuse the situation, and currently there is no solid explanation as to which oxidation state is better, or how readily they interconvert. That said, in general, for the SNS ligand system the $Cr^{(III)}$ oxidation state does appear to generate better catalysts based on several criteria: 1) The $SNSCr^{(III)}$ catalysts are generally 3-12 times more active than their $Cr^{(II)}$

analogues; 2) The selectivity of the $Cr^{(III)}$ catalysts are generally for 1-hexene only; 3) The $Cr^{(III)}$ catalysts appear more tolerant to an excess of Al activator and only begin to show loss of selectivity at very high loading (~2000 eq. MAO).

7.9 Conclusions:

This project has been successful in a number of areas. Firstly, it was conclusively demonstrated that the Cr complexes of the hemi-labile ligands (N-MeDipyr and N-MeTripyr) produced in Chapter 2 are capable of oligomerizing ethylene (see Table 7.6.7). Though not selective, these catalysts can be optimized further to produce better yields of the desired products. Another fascinating ability exhibited by the N-MeTripyr complex is its ability to switch between oligomerization and polymerization depending on the nature of the activator. The ability of alkyaluminums to cause ligand leaching as well as the instability of the Cr-Me moiety were also demonstrated using the N-MeTripyr ligand system.

The amidinate (NCN) catalysts yielded excellent activities (see Table 7.7.10). More importantly, by varying the electron donating/withdrawing ability of the ligand, it was demonstrated that electron-withdrawing ligands produce much higher activities.

The amidate (NCO) catalysts proved to be the most active out of all those tested, although producing only Shulz-Flory product distributions. These catalysts displayed the effects of steric crowding on the overall activity, as the catalyst without *ortho* substituents yielded a higher activity while maintaining the same selectivity as the *ortho* substituted catalyst (see Table 7.7.14).

Although the NacNac ligand displayed the lowest activity out of all the nitrogen based ligands and produced the most polymer, it did have one unique feature. The oligomers it produced were exclusively 1-butene and 1-hexene (see Table 7.7.19). Given the ease of changing the substituents on the NacNac ligand it should be quite easy to remove some steric bulk to observe if the yield of oligomers increases.

Our investigations into the PNP ligand framework rather conclusively demonstrated that the $Cr^{(II)}$ oxidation state results from the spontaneous reduction of the parent [$PNPCrCl_3$] in the presence of the alkyl aluminum $AlMe_3$. Furthermore, the $Cr^{(II)}$

analogue exhibited a slightly higher activity and improved selectivity. These results lead us to the conclusion that the $Cr^{(II)}$ oxidation state was more closely related to the active catalyst in the case of the PNP ligand system.

Vice versa, the SNS complexes are perhaps the most difficult to assess as there were no clear-cut trends. On the whole $Cr^{(III)}$ does appear to produce a more active and selective catalyst, however, when the $Cr^{(II)}$ complexes were reacted at low-loadings of MAO their activities and selectivity neared that of the $Cr^{(III)}$ analogues (see Table 7.8.18). The identity of the oxidation state of the catalyst will most likely remain unclear for some time, especially given that we have found that the SNS complexes can be both oxidized and reduced in the presence of alkylaluminums. The isolation of several cationic $Cr^{(III)}$-alkyl complexes has given us cause to consider that perhaps the SNS ligand is capable of stabilizing this reactive moiety, perhaps to such an extent as to allow the +3 oxidation state to form an active catalyst. Another, as yet unsolved mystery is the reason why all of the nitrogen based ligand systems yielded catalysts which provided a Shulz-Flory distribution of oligomers only, while the PNP and SNS systems are capable of selective catalysis. The most straight-forward answer is that the 2^{nd} row atoms P, and S, are somehow influencing the catalyst centre, making it selective. Another intriguing possibility is the geometry of the metal. In all of the nitrogen/oxygen donor cases the complexes were either square-planar or paddlewheel (low-spin octahedral). However, all of the $Cr^{(II)}$ SNS catalysts exhibited the very odd, Jahn-Teller distorted octahedral structure. There is the possibility that this type of geometry bestows a unique electronic and steric environment upon the metal, and perhaps this could lead to the selectivity which is observed. Whether this Jahn-Teller distortion is a function of the ligand framework, or is created by the nature of the sulphur atoms remains yet to be determined. Current work is under way to synthesize a S,N ligand which should only bond in a square-planar manner to test this hypothesis.

On the whole we have failed to conclusively identify the oxidation state of the active Cr catalyst involved in the oligomerization process. We have, however, conclusively proven that the $Cr^{(II)}$ oxidation state can quite likely form active catalysts, which has been a largely ignored possibility in the literature. It would seem that the process may, in fact, be mediated by the nature of the ligand about the Cr centre. In the

case of the σ,π –bonding pyrrolides, and the PNP ligand the $Cr^{(II)}$ oxidation state yielded much better catalysis in terms of both selectivity and activity. However, given the results of the SNS chemistry we can not discount the possibility that $Cr^{(II)}$ is being oxidized to an active $Cr^{(III)}$ species. Furthermore, these results may indicate that selectivity is governed solely by the nature of the ligand attached to the metal and is independent of the oxidation state, be it +2, +3 or some as yet undetermined valency.

7.10 X-Ray Crystallography Section:

The full crystallographic data, including bond lengths and angles may be found in Appendix 7. The abbreviated crystallographic data for the structures contained within this chapter are as presented in Tables 7.10.1 to 7.10.4.

Table 7.10.1 Crystal Data and Structure Analysis Results for Complexes **1-3**.

	1	**2**	**3**
Formula	$C_{50.25}H_{51}CrN_4O_{1.625}$	$C_{47}H_{47}CrN_3O_2$	$C_{54.50}H_{52}CrN_5O_{1.38}$
FW	788.98	737.89	851.01
space group	Monoclinic, ***P2(1)/n***	Triclinic, ***P1***	Orthorhombic, ***Cmc2(1)***
a (Å)	9.340(2)	8.969(1)	18.080(4)
b (Å)	12.030(3)	12.744(7)	17.140(4)
c (Å)	38.232(9)	17.005(5)	16.732(4)
α (deg)	90	89.466(4)	90
β (deg)	93.339(6)	85.866(5)	90
γ (deg)	90	88.870(7)	90
V ($Å^3$)	4288.3(18)	3987.1(18)	5185(2)
Z	4	2	4
radiation (Kα, Å)	0.71073	0.71073	0.71073
T (K)	203(2)	203(2)	209(2)
D_{calcd} (g cm^{-3})	1.157	1.134	1.090
μ_{calcd} (mm^{-1})	0.305	0.311	0.261
F_{000}	1576	1511	1796
R, R_w [2 a]	0.0961, 0.2209	0.1251, 0.2439	0.0518, 0.1185
GoF	1.033	1.085	1.012

[a] $R = \Sigma||Fo| - |Fc||/\Sigma|F|$. $Rw = [\Sigma(|Fo| - |Fc|)^2/\Sigma wFo^2]^{1/2}$.

Table 7.10.2 Crystal Data and Structure Analysis Results for Complexes **4-6**.

	4	**5**	**6**
Formula	$C_{51}H_{55}ClCrLiN_3O_3$	$C_{39}H_{31}ClCrN_3$	$C_{46.10}H_{44.40}AlN_3O$
FW	852.37	629.12	683.43
space group	Orthorhombic, ***Pnma***	Monoclinic, ***P2(1)/c***	Triclinic, ***P-1***
a (Å)	18.88(10)	8.594(10)	13.013(7)
b (Å)	22.13(12)	15.904(19)	13.057(7)
c (Å)	11.15(6)	23.14(3)	13.186(7)
α (deg)	90	90	87.737(9)
β (deg)	90	99.04(2)	62.129(7)
γ (deg)	90	90	72.480(8)
V (Å^3)	4658(44)	3124(6)	1879.3(17)
Z	4	4	2
radiation (Kα, Å)	0.71073	0.71073	0.71073
T (K)	211(2)	210(2)	208(2)
D_{calcd} (g cm^{-3})	1.215	1.338	1.208
μ_{calcd} (mm^{-1})	0.347	0.485	0.093
F_{000}	1800	1308	726
R, R_w[2 a]	0.0633, 0.1279	0.0592, 0.1055	0.0649, 0.1804
GoF	1.039	1.054	1.049

[a] $R = \Sigma||Fo| - |Fc||/\Sigma|F|$. $Rw = [\Sigma(|Fo| - |Fc|)^2/\Sigma wFo^2]^{1/2}$.

Table 7.10.3 Crystal Data and Structure Analysis Results for Complexes **7**, **22-23**.

	7	**22**	**23**
Formula	$C_{55}H_{62}ClCrLiN_3O_4$	$C_{29}H_{41}ClCrN_2$	$C_{25}H_{33}ClCrN_2O$
FW	923.47	505.09	464.98
space group	Monoclinic, ***P2(1)/c***	Monoclinic, ***P2(1)/n***	Monoclinic, ***P2(1)/n***
a (Å)	15.099(7)	9.2086(17)	12.982(3)
b (Å)	17.935(8)	14.392(3)	12.726(3)
c (Å)	19.398(9)	21.035(4)	15.123(3)
α (deg)	90	90	90
β (deg)	109.114(7)	91.812(4)	97.535(5)
γ (deg)	90	90	90
V (Å^3)	4963(4)	2786.5(9)	2477.0(10)
Z	4	4	4
radiation (Kα, Å)	0.71073	0.71073	0.71073
T (K)	209(2)	198(2)	202(2)
D_{calcd} (g cm^{-3})	1.236	1.204	1.247
μ_{calcd} (mm^{-1})	0.332	0.525	0.587
F_{000}	1956	1080	984
R, R_w[2 a]	0.0537, 0.1159	0.0449, 0.1083	0.0625, 0.1485
GoF	1.004	1.040	1.003

[a] $R = \Sigma||Fo| - |Fc||/\Sigma|F|$. $Rw = [\Sigma(|Fo| - |Fc|)^2/\Sigma wFo^2]^{1/2}$.

Table 7.10.4 Crystal Data and Structure Analysis Results for Complex **29**.

	29
Formula	$C_{29.85}H_{59.55}Al_2Cl_{2.15}CrNS_2$
FW	678.83
space group	Monoclinic, ***P2(1)/c***
a (Å)	13.782(12)
b (Å)	12.776(11)
c (Å)	21.606(19)
α (deg)	90
β (deg)	96.037(16)
γ (deg)	90
V (Å^3)	3783(6)
Z	4
radiation (Kα, Å)	0.71073
T (K)	208(2)
D_{calcd} (g cm^{-3})	1.192
μ_{calcd} (mm^{-1})	0.630
F_{000}	1457
R, R_w [2 a]	0.0734, 0.1659
GoF	1.042

[a] $R = \Sigma||Fo| - |Fc||/\Sigma|F|$. $Rw = [\Sigma(|Fo| - |Fc|)^2/\Sigma wFo^2]^{1/2}$.

7.11 Experimental Section:

All reactions were carried out under a dry nitrogen or argon atmosphere. Solvents were dried using an aluminum oxide solvent purification system. The Aluminum activators, i-BAO (Aldrich), $AlMe_3$ (Strem), $AlEt_3$ (Strem) and MAO (Chemtura) were used as received. The amidinate **8-10**,[34] amidate **11-13**,[35] and NacNac **14,15**[37] ligands were prepared according to literature methods, using starting materials supplied by Aldrich and used without further purification. The full experimental details for the SNS[48,49] and PNP[47] ligand synthesis and complex formation are detailed in our recent publications. The full experimental details for **8-11** have also been recently published by our group.[40] N-MeDipyr, and N-MeTripyr were prepared as detailed in chapter 2. Infrared spectra were recorded on an ABB Bomem FTIR instrument from Nujol mulls prepared in a drybox. Samples for magnetic susceptibility were pre-weighed inside a drybox equipped with an analytical balance and measured on a Johnson Matthey

Magnetic Susceptibility balance. NMR were collected on an INOVA Varian 300 or 500 MHz instrument in $CDCl_3$ unless otherwise stated. The oligomer reaction mixtures were analyzed using a CP 9000 gas chromatograph (GC) fitted with a 30 m X 0.32 mm i.d. capillary CP volamine column, with an FID detector. Elemental analysis was carried out with a Perkin-Elmer 2400 CHN analyzer. Data for X-ray crystal structure determination were obtained with a Bruker diffractometer equipped with a 1K Smart CCD area detector.

Polymerization Details: Polymerizations were carried out in a steel 250 mL Büchi reactor equipped with a mechanical stirrer and temperature controller, which had been dried in a 150 °C oven for a minimum of five hours prior to each run. The reactor was then placed under vacuum for 30 mins, after which it was flushed in three cycles of argon/vacuum. The toluene/MAO mixture was then injected and the reactor was allowed to stir for several minutes at the desired reaction temperature. The catalyst was then injected as a solution in toluene under a flow of argon gas, after which the reactor was charged with the appropriate pressure of ethylene. After the reaction time had expired the reactor was rapidly cooled to 5 °C in order to minimize the loss of 1-butene and an EtOH/HCl solution was injected in order to quench the reaction. The reaction mixture was then removed and stirred with a large excess of EtOH/HCl for several minutes. The toluene fraction was then removed and any PE was filtered. The reaction mixture was then analyzed by NMR to determine the production of oligomers, after which it was analyzed by GC to determine the selectivity of oligomers. The PE portion was stirred in HCl/H_2O for ~30 mins and then dried overnight under vacuum at 60 °C.

Ligand Preparation:

Synthesis of $[(C_6H_5)$-C-$(NCy)_2]$Li (8): A solution of dicyclohexylcarbodiimide (DCC) (4.25 g, 20.6 mmol) in hexane (30 mL) was added dropwise to PhLi (13.1 mL, 2.1 M in O^nBu_2, 27.5 mmol) in hexanes (20 mL) at room temperature. The reaction was slightly exothermic. After 18 hours of stirring, the reaction mixture was refluxed for 1 hour. The

precipitate was isolated by glass frit filtration and washed with cold hexanes (2 x 50 mL). The beige solid was subsequently dried *in vacuo*. The yield was 42% (2.5 g, 8.7 mmol).

^{1}H NMR (500 MHz, THF-d_8) δ = 0.88-1.55 (m, 20H), 2.51 (m, 2H), 7.01 (d, 2H, J = 7.5 Hz), 7.15 (t, 1H, J = 7.0 Hz), 7.24 (dd, 2H, J = 7.0, 7.5 Hz). IR (KBr, Nujol, cm^{-1}): 1641, 1362, 1347, 1260, 1063, 1027, 986, 916, 888, 778, 703, 610.

Synthesis of [*p*-MeO(C_6H_4)-C-($NCy)_2$]Li (9): BuLi (8.44 mL, 2.7 M in hexane, 22.8 mmol) was added dropwise to a stirred solution of *p*-MeO(C_6H_4)Br (2.85 mL, 22.8 mmol) in hexane (30 mL) at room temperature. After 12 hours of stirring, the white precipitate was washed with cold hexane (2 x 10 mL). Hexane (30 mL) was then added to the white solid, then DCC (4.70 g, 22.8 mmol) hexane (30 mL) was added dropwise at room temperature. The reaction was slightly exothermic. Once the solution cooled, the white suspension was refluxed for 2 hours. After cooling, the white precipitate was isolated by glass frit filtration and washed with cold hexane (2 x 50 mL). The white crystalline solid was subsequently dried *in vacuo*. The yield was 55% (4.05 g, 12.5 mmol).

^{1}H NMR (500 MHz, THF-d_8) δ = 0.88-1.56 (m, 20H), 2.54 (m, 2H), 3.77 (s, 3H), 6.84 (d, 2H, J = 8.0 Hz), 6.93 (d, 2H, J = 8.0 Hz).

^{13}C NMR (500 MHz, THF-d_8) δ = 158.99, 134.11, 128.82, 113.72, 112.47, 57.63, 55.18, 38.38, 27.12, 27.02.

IR (KBr, Nujol, cm^{-1}): 1605, 1508, 1489, 1410, 1357, 1343, 1234, 1175, 1062, 1025, 1017, 985, 901, 886, 843, 614.

Synthesis of [*p*-F_3C(C_6H_4)-C-($NCy)_2$]Li (10): BuLi (7.48 mL, 2.7 M in hexane, 20.2 mmol) was added dropwise to a stirred solution of *p*-F_3C(C_6H_4)Br (2.79 mL, 20.2 mmol) in Et_2O (30 mL) at -78°C (dry ice/acetone bath). The solution was allowed to warm to room temperature and was stirred for 18 hours. The solvent was evaporated and the solid

dissolved in hexane (30 mL). To this solution was added dropwise a solution DCC (3.47 g, 16.8 mmol) in hexane (30 mL) at room temperature. The reaction was slightly exothermic. The brown/orange solution was stirred for 12 hours, then refluxed for 1 hour. After cooling, the beige precipitate was isolated by glass frit filtration and washed with hexane (50 mL). The solid was subsequently dried *in vacuo*. The yield was 23% (1.4 g, 3.9 mmol).

^{1}H NMR (500 MHz, THF-d_8) δ = 0.82-1.79 (m, 20H), 2.29 (m, 2H), 7.09-7.87 (m, 4H).

^{13}C NMR (500 MHz, THF-d_8) δ = 129.92, 128.63, 125.26, 59.98, 57.56, 38.64, 34.71, 33.59, 32.63, 27.36, 27.21, 27.17, 26.97, 26.55.

IR (KBr, Nujol, cm^{-1}): 1641, 1617, 1599, 1449, 1405, 1365, 1326, 1292, 1261, 1240, 1163, 1129, 1107, 1066, 1021, 986, 890, 851.

Synthesis of [$(C_6H_5)C(O)NH(C_6H_4p$-$^{i}Pr)$] (11): To a solution of benzoyl chloride (9.7 mL, 83.5 mmol) in dichloromethane (160 mL) was added dropwise *p*-^{i}propylaniline (11.88 mL, 83.5 mmol) at room temperature. The reaction was mildly exothermic and a precipitate was seen to form immediately. The solution was allowed to cool to room temperature, then Et_3N (17 mL) was added. The precipitate solubilized initially, but reformed after approximately 15 minutes. The reaction mixture was stirred at room temperature until completion was detected by TLC (3:2 hexane:ethyl acetate). The organic phase was washed with water (3 x 250 mL), then dried over $MgSO_4$. The solvent was removed *in vacuo* to yield a peach/beige coloured solid. The yield was 84% (16.7 g, 70.1 mmol).

^{1}H NMR (500 MHz, $CDCl_3$) δ = 1.23 (d, 6H, *J* = 7.0 Hz), 2.88 (septet, 1H, *J* = 7.0 Hz), 7.18 (d, 2H, *J* = 8.5 Hz), 7.54 (d, 2H, *J* = 8.0 Hz), 7.38-7.83 (m, 5H), 8.08 (s br., 1H).

^{13}C NMR (500 MHz, $CDCl_3$) δ = 166.05, 145.42, 135.81, 135.21, 131.82, 128.82, 127.24, 127.07, 120.70, 33.79, 24.21.

EI-MS: *m/z* = 239 [M^+], 224 [M^+ - CH_3], 105 [M^+ - $N(H)C_6H_4(CH(CH_3)_2)$], 77 [M^+ - $C(O)NC_6H_4(CH(CH_3)_2)$]. IR (NaCl, Nujol, cm^{-1}): 3299, 1648, 1595, 1578, 1530, 1515, 1414, 1318, 1265, 1053, 1025, 902, 830, 715, 695.

Synthesis of [*p*-MeO(C_6H_5)C(O)NH(C_6H_4p-^{i}Pr)] (12): To a solution of *p*-methoxybenzoyl chloride (14.24 g, 83.5 mmol) in dichloromethane (160 mL) was added dropwise *p*-^{i}propylaniline (11.88 mL, 83.5 mmol) at room temperature. The reaction was mildly exothermic and a precipitate was immediately formed. Once the solution cooled, Et_3N (17 mL) was added. The reaction mixture was stirred at room temperature until completion was determined by TLC (3:2 hexane:ethyl acetate). The organic phase was washed with water (5 x 250 mL), then dried over $MgSO_4$. The solvent was removed *in vacuo* to yield a peach/beige coloured solid. The yield was 87% (19.6 g, 72.6 mmol).

^{1}H NMR (500 MHz, $CDCl_3$) δ = 1.24 (d, 6H, *J* = 7.0 Hz), 2.89 (septet, 1H, *J* = 7.0 Hz), 3.85 (s, 3H), 6.93 (d, 2H, *J* = 9.0 Hz), 7.20 (d, 2H, *J* = 8.0 Hz), 7.54 (d, 2H, *J* = 8.0 Hz), 7.82 (d, 2H, *J* = 8.5 Hz), 7.88 (s br., 1H).

^{13}C NMR (500 MHz, $CDCl_3$) δ = 165.45, 162.53, 145.23, 135.98, 129.09, 127.43, 127.10, 120.57, 114.07, 55.63, 33.81, 24.24.

EI-MS: *m/z* = 269 [M^+], 135 [M^+ - $NC_6H_4(CH(CH_3)_2)$]. IR (NaCl, Nujol, cm^{-1}): 3326, 1643, 1607, 1521, 1502, 1319, 1310, 1251, 1241, 1179, 1026, 840, 827, 762.

Synthesis of [*p*-F_3C(C_6H_5)C(O)NH(C_6H_4p-^{i}Pr)] (13): To a solution of *p*-trifluoromethylbenzoyl chloride (10 mL, 83.5 mmol) in dichloromethane (160 mL) was added dropwise *p*-^{i}propylaniline (11.88 mL, 83.5 mmol) at room temperature. The reaction was mildly exothermic and a precipitate was immediately formed. The solution was allowed to cool to room temperature, then Et_3N (17 mL) was added. The reaction mixture was stirred at room temperature until completion was detected by TLC (3:2 hexane:ethyl acetate). The organic phase was washed water (9 x 250 mL) however, a

white emulsion did not solubilize in either the organic or aqueous phases. The white emulsion was allowed to dry. The organic phase was dried with $MgSO_4$ and capped in a flask with a septum for 4 to 5 days. Clear crystalline needles suitable for X-ray crystallography formed in the flask.

^{1}H NMR (500 MHz, CD_3CN) at 65°C of the crystalline product; δ = 1.26 (d, 6H, J = 7.0 Hz), 2.93 (septet, 1H, J = 6.8 Hz), 7.21-7.99 (m, 8H), 8.57 (s br., 1H).

^{13}C NMR (500 MHz, CD_3CN) δ = 131.66, 131.59, 128.27, 122.60, 117.03, 116.85, 35.07, 24.94, 17.00.

EI-MS: *m/z* = 257 [M^+], 242 [M^+ - CH_3], 123 [M^+ - $NC_6H_4(CH(CH_3)_2)$], 95 [M^+ - $C(O)NC_6H_4(CH(CH_3)_2)$]. IR (NaCl, Nujol, cm^{-1}): 3346, 3068, 3048, 1910, 1651, 1598, 1525, 1501, 1416, 1364, 1321, 1298, 1223, 942, 902, 851, 828, 759.

Synthesis of [K-2,6-iPr$_2$Ph-NacNac] (14): NacNac[36] [(ArNC(Me)CHC(Me)NHAr); Ar = 2,6-*i*Pr$_2$C$_6$H$_3$] (2 g, 4.78 mmol) was dissolved in THF (10 mL), then KH (0.230 g, 5.7 mmol) was added. The suspension was stirred overnight and the solution slowly turned from colourless to a yellow solution. After stirring, the solution was dried *in vacuo* and hexanes (20 mL) was added. The yellow hexanes solution was then centrifuged to remove insoluble materials. The yellow solution was then evaporated to dryness and left under vacuum for 6 hours at 60°C. The product was isolated as a yellow solid. The yield was 96% (2.1 g, 4.6 mmol).

^{1}H NMR (500 MHz, C_6D_6) δ = 1.11 (d, 12H, J = 7.0 Hz), 1.29 (d, 12H, J = 7.0 Hz), 1.91 (s, 6H), 3.38 (septet, 4H, J = 7.0 Hz), 4.84 (s, 1H), 7.06 (t, 1H, J = 7.5 Hz), 7.18 (d, 2H, J = 7.5 Hz).

^{13}C NMR (500 MHz, C_6D_6) δ = 160.75, 151.21, 140.00, 123.97, 121.67, 91.52, 28.06, 24.89, 24.27, 24.03.

IR (NaCl, Nujol, cm^{-1}): 2361, 1623, 1595, 1558, 1514, 1419, 1363, 1322, 1255, 1221, 1165, 1018, 922, 795, 786, 761, 665, 610.

Synthesis of [K-2,6-Me_2Ph-NacNac] (15): NacNac[36] [(ArNC(Me)CHC(Me)NHAr); Ar = 2,6-$Me_2C_6H_3$] (2 g, 6.53 mmol) was dissolved in THF (10 mL), then KH (0.314 g, 7.8 mmol) was added. The suspension was stirred overnight and the solution slowly turned from colourless to a yellow solution. After stirring, the solution was dried *in vacuo* and Et_2O (20 mL) was added. The yellow Et_2O solution was then centrifuged to remove insoluble materials. The yellow solution was then evaporated to dryness and left under vacuum for 6 hours at 60°C. The product was isolated as a yellow solid. The yield was 91% (2.05 g, 5.9 mmol).

^1H NMR (500 MHz, C_6D_6) δ = 1.61 (s, 12 H), 1.94 (s, 6H), 4.84 (s, 1H), 7.08 (t, 1H, J = 7.5 Hz), 7.17 (d, 2H, J = 7.5 Hz).

^{13}C NMR (500 MHz, C_6D_6) δ = 161.65, 150.14, 141.11, 121.37, 120.37, 90.52, 27.76, 24.99.

IR (NaCl, Nujol, cm^{-1}): 2362, 1624, 1591, 1552, 1522, 1409, 1355, 1322, 1262, 1220, 1161, 1018, 914, 792, 782, 752, 666, 601.

Preparation of Cr complexes:

Synthesis of [CrL_2; L =[(C_6H_5)-C-$(NCy)_2$]$^-$] (16): A mixture of $CrCl_2(THF)_2$ (0.216 g, 0.81 mmol) and [(C_6H_5)-C-$(NCy)_2$]Li (0.471 g, 1.62 mmol) in THF (15 mL) was stirred at room temperature for 18 hours resulting in a green/brown solution. After centrifugation and decantation, the solvent was removed *in vacuo* and the residue was extracted with hexane. The concentrated hexane solution was stored at -35°C for one day. Dark green needle-like microcrystals, of insufficient quality for X-ray crystallography, were obtained (0.312 g ,0.50 mmol, 62.3% Yield).

IR (KBr, Nujol, cm^{-1}): 1363 (m), 1343 (m), 1092 (s), 1056 (s), 986 (s), 911 (w), 887 (m), 776 (s), 701 (m), 660 (m).

Elemental Analysis calcd (Found) for $CrC_{38}H_{54}N_4$: C 73.75 (74.15), H 8.80 (8.62), N 9.05 (9.22). $\mu_{eff} = 4.62\ \mu_B$.

Synthesis of [CrL_2; L = [*p*-MeO(C_6H_4)-C-($NCy)_2$]$^-$] (17): A mixture of $CrCl_2(THF)_2$ (0.197 g, 0.74 mmol) and [*p*-MeO(C_6H_4)-C-($NCy)_2$]Li (0.472 g, 1.47 mmol) in THF (15 mL) was stirred at room temperature for 18 hours resulting in a dark green solution. After centrifugation and decantation, the solvent was removed *in vacuo* and the residue was extracted with hexane. The concentrated hexane solution was stored at -35°C for one day. Pale green solid was obtained upon cooling (0.327 g, 0.48 mmol, 65.1% Yield).

IR (KBr, Nujol, cm^{-1}): 1609 (s), 1576 (m), 1364 (m), 1345 (m), 1292 (m), 1246 (s), 1227 (s), 1173 (m), 1034 (s), 989 (s), 888 (m), 835 (m), 811 (w), 629 (m).

Elemental Analysis calcd (Found) for $CrC_{40}H_{58}N_4O_2$: C 70.76 (70.58), H 8.61 (8.41), N 8.25 (8.51). $\mu_{eff} = 4.83\ \mu_B$.

Synthesis of [CrL_2; L = [*p*-F_3C(C_6H_4)-C-($NCy)_2$]$^-$] (18): A mixture of $CrCl_2(THF)_2$ (0.177 g, 0.66 mmol) and [*p*-F_3C(C_6H_4)-C-($NCy)_2$]Li (0.476 g, 1.33 mmol) in THF (15 mL) was stirred at room temperature for 18 hours resulting in a dark green solution. After centrifugation and decantation, the solvent was removed *in vacuo* and the residue was extracted with hexane. The concentrated hexane solution was stored at -35°C for one day. Brown needle-like microcrystals, of insufficient quality for X-ray crystallography, were obtained (0.245 g, 0.32 mmol, 48.9% Yield).

IR (KBr, Nujol, cm^{-1}): 1493 (s), 1322 (m), 1260 (s), 1222 (s), 1167 (m), 1129 (m), 1064 (w), 1047 (s), 1021 (m), 848 (m), 610 (m).

Elemental Analysis calcd (Found) for $CrC_{40}H_{52}N_4F_6$: C 63.65 (63.27), H 6.94 (6.77), N 7.42 (7.36). $\mu_{eff} = 4.74\ \mu_B$.

Synthesis of [2,6-iPr$_2$-NacNacCr(μ-Cl)]$_2$ (22): A mixture of $CrCl_2(THF)_2$ (0.232 g, 0.87 mmol) and [K-2,6-iPr$_2$-NacNac] (0.396 g, 0.87 mmol) in THF (10 mL) was stirred at room temperature for 18 hours resulting in a dark green solution. After centrifugation and decantation, the solvent was removed *in vacuo* and the residue was extracted with 2 mL of hexanes. The concentrated hexane solution was stored at -35°C for one day. Dark green single crystals, suitable for X-ray crystallography, were obtained (0.391 g, 0.77 mmol, 89.1% Yield).

IR (KBr, Nujol, cm^{-1}): 1539 (s), 1526 (m), 1505 (m), 1437 (w), 1311 (m), 1253 (s), 1173 (m), 1054 (w), 1029 (m), 935 (w), 854 (m), 794 (s), 758 (w).

Elemental Analysis calcd (Found) for $Cr_2Cl_2C_{58}H_{82}N_4$: C 68.96 (69.08), H 8.18 (8.11), N 5.55 (5.39). $\mu_{eff} = 2.42\ \mu_B$.

Synthesis of [2,6-Me$_2$-NacNacCr(μ-Cl)]$_2$ (23): A mixture of $CrCl_2(THF)_2$ (0.250 g, 0.94 mmol) and [K-2,6-Me$_2$-NacNac] (0.325 g, 0.94 mmol) in THF (10 mL) was stirred at room temperature for 18 hours resulting in a dark green solution. After centrifugation and decantation, the solvent was removed *in vacuo* and the residue was extracted with 2 mL of hexanes. The concentrated hexane solution was stored at -35°C for one day. Dark green single crystals, suitable for X-ray crystallography, were obtained (0.315 g, 0.68 mmol, 72.3% Yield).

IR (KBr, Nujol, cm^{-1}): 1544 (s), 1519 (m), 1513 (m), 1422 (w), 1309 (m), 1255 (s), 1164 (m), 1063 (w), 1028 (m), 935 (w), 847 (m), 802 (s), 766 (w).

Elemental Analysis calcd (Found) for $Cr_2Cl_2C_{50}H_{66}N_4$: C 69.90 (69.78), H 7.74 (7.61), N 6.52 (6.55). $\mu_{eff} = 2.59\ \mu_B$.

Synthesis of [(N-MeDipyr)$_2$Cr(THF)] (7): N-MeDipyr (0.320 g, 1.02 mmol) was dissolved in 15 mL of THF and KH (1.05 eq, 0.043 g, 1.08 mmol) was added while stirring, bubbles immediately formed in the solution. After stirring for 4 hours the solution was added to a suspension of $CrCl_2(THF)_2$ (1eq, 0.274 g, 1.02 mmol) in 10 mL of THF. The suspension slowly dissolved yielding a light blue solution from which precipitate slowly evolved. The THF solution was dried *in vacuo* and fresh THF (5 mL) was added. The solution was then cooled to -35 °C and stored for 4 days after which time 0.531 g of pale blue plate crystals of X-ray quality formed (0.67 mmol, 66.0% Yield).

IR (KBr, Nujol, cm^{-1}): 1604 (s), 1218 (m), 1153 (m), 1043 (m), 751 (s), 692 (s), 632 (s).

Elemental Analysis calcd (Found) for $CrC_{50.25}H_{51}N_4O_{1.625}$: C 76.50 (76.55), H 6.52 (6.62), N 7.10 (7.52). $\mu_{eff} = 4.52\ \mu_B$.

7.12 References:

1) Weissermal, K.; Arpe, J.-J. *Industrial Organic Chemistry: Important Raw Materials and Intermediates*, Verlag Chemie, New York, 1978.
2) Flory, P. J. *J. Am. Chem. Soc.* **1940**, *62*, 1561. b) Schulz. G. V. Z. *Phys. Chem. Abt. B.* **1939**, *43*, 25. c) Schulz, G. V. Z. *Phys. Chem. Abt. B.* **1935**, *30*, 379.
3) Thomas, J. M.; Thomas, W. J. *Principals and Practice of Heterogeneous Catalysis* VCH: Weindheim, **1997**.
4) Manyik, R. M.; Walker, W. E.; Wilson, T. P. US Pat. 3 300 458 (Union Carbide Corporation), **1967**.
5) Manyik, R. M.; Walker, W. E.; Wilson, T. P. *J. Catal.* **1977**, *47*, 197.
6) Dixon, J. T.; Green, M. J.; Hess, F. M.; Morgan, D. H. *J. Organomet. Chem.* **2004**, *689*, 3641.
7) Reagan, W. K. EU Pat. 0 417 477 (Phillips Petroleum Company), **1991**.
8) Freeman, J. W.; Buster, J. L.; Knudsen, R. D. US Pat. 5 856 257 (Philips Petroleum Company), **1999**.
9) Araki, Y.; Nakamura, H.; Nanba, Y.; Okanu, T. US Pat. 5 856 612 (Mitsubishi Chemical Company), **1994**.
10) Aoyama, T.; Mimura, H.; Yamamoto, T.; Oguri, M.; Koie, Y. Jap. Pat. 09 176 299 (Tosoh Corporation), **1997**.
11) Mimura, H.; Aoyama, T.; Yamamoto, T.; Oguri, M.; Koie, Y. Jap. Pat 09 268 133 (Tosoh Corporation), **1997**.
12) Yang, Y.; Kim, H.; Lee, J.; Paik, H.; Jang, H. G. *Appl. Cat. A* **2002**, *193*, 29.
13) Britovsek, G. J. P.; Gibson, V. C.; Wass, D. F. *Angew. Chem. Int. Ed.* **1999**, *38*, 428. b) Theopold, K. H. *Eur. J. Inorg. Chem.* **1998**, 15.

14) Mahomed, H.; Bollmann, A.; Dixon, J.; Gokul, V.; Griesel, L.; Grove, C.; Hess, F.; Maumela, H.; Pepler, L. *Appl. Cata. A* **2003**, *255*, 355. b) Grove, J. J. C.; Mahomed, H. A.; Griesel, L. WO Pat. 03/004158 (Sasol Technology), **2002**.
15) Deckers, P. J. W.; Hessen, B.; Teuben, J. H. *Organometallics* **2002**, *21*, 5122. b) Decker, P. J. W.; Hessen, B. WO Pat. 02/066404 (Stichting Dutch Polymer Institute), **2002**. c) Decker, P. J. W.; Hessen, B. WO Pat 02/066405 (Stichting Dutch Polymer Institute), **2002**. d) Deckers, P. J. W.; Hessen, B.; Teuben, J. H. *Angew. Chem. Int. Ed.* **2001**, *40*, 2516.
16) Hagen, H.; Kretschmer, W. P.; van Buren, F. R.; Hessen, B.; van Oeffelen, D. A. *J. Mol. Catal. A* **2006**, *248*, 237.
17) McGuinness, D. S.; Wasserscheid, P.; Keim, W.; Morgan, D. H.; Dixon, J. T.; Bollmann, A.; Maumela, H.; Hess, F. M.; Englert, U. *J. Am. Chem. Soc.* **2003**, *125*, 5272. b) McGuinness, D. S.; Wasserscheid, P.; Morgan, D. H.; Dixon, J. T. *Organometallics* **2005**, *24*, 552.
18) Carter, A.; Cohen, S. A.; Cooley, N. A.; Murphy, A.; Scutt, J.; Wass, D. F. *Chem. Commun.* **2002**, 858.
19) Bollmann, A.; Blann, K.; Dixon, J. T.; Hess, F. M.; Killian, E.; Maumela, H.; McGuinness, D. S.; Morgan, D. H.; Neveling, A.; Otto, S.; Overett, M.; Slawin, A. M. Z.; Wasserscheid, P.; Kuhlmann, S. *J. Am. Chem. Soc.* **2004**, *126*, 14712. b) Overett, M. J.; Blann, K.; Bollmann, A.; Dixon, J. T.; Hess, F.; Killian, E.; Maumela, H.; Morgan, D. H.; Neveling, A.; Otto, S. *Chem. Commun.* **2005**, 622.
20) Regan, W. K.; Freeman, J. W.; Conroy, B. K.; Pettijohn, T. M.; Benham, E. A. US Pat. 5 451 645 (Phillips Petroleum Company), **1995**. b) Santi, R.; Romano, A. M.; Grande, M.; Sommazzi, A.; Masi, F.; Proto, A. WO Pat. 01/68572 (Enichem S. P. A.), **2001**.
21) Regan, W. K.; Freeman, J. W.; Conroy, B. K.; Pettijohn, T. M.; Benham, E. A. US Pat. 5 451 645 (Phillips Petroleum Company), **1995**. b) Sugimura, K.; Nitabara, T. S.; Fujita, T. Jap. Pat. (Mitsui Chemical Incorporated), **1998**.
22) Winter, M. J. In *Comprehensive Organometallic Chemistry II*; Wilkinson, G., Ed.; Pergamon Press: Oxford, U.K., **1995**. b) Kirtley, S. W. In *Comprehensive Organometallic Chemistry*; Wilkinson, G., Ed.; Pergamon Press: Oxford, U.K., **1978**.
23) Emrich, R.; Heinemann, O.; Jolly, P. W.; Kruger, C.; Verhovnik, G. P. J. *Organometallics* **1997**, *16*, 1511.
24) van Rensburg, W. J.; Grove, C.; Steynberg, J. P.; Stark, K. B.; Huyser, J. J.; Steynberg, P. J *Organometallics* **2004**, *23*, 1207. b) Yu, Z.-X.; Houk, K. N. *Angew. Chem. Int. Ed.* **2003**, *42*, 808.
25) Blok, A. N. J.; Budzelaar, P. H. M.; Gal, A. W. *Organometallics* **2003**, *22*, 2564.
26) Yu, Z.-X.; Houk, K. N. *Angew. Chem. Int. Ed.* **2003**, *42*, 808. b) Blok, A. N. J.; Budzelaar, P. H. M.; Gal, A. W. *Organometallics* **2003**, *22*, 2564.
27) Mimura, H.; Oguri, M.; Yamamoto, T.; Murakita, H.; Okada, H.; Yoshida, T. US Pat. 6 337 297 (Tosoh Corporation), **2002**. b) Mimura, H.; Oguri, M.; Yamamoto, T.; Okada, H.; Osamu, Y. Jap. Pat. 2001002724 (Tosoh Corporation), **2001**. c) Mimura, H.; Oguri, M.; Okada, H.; Yoshida, T. Jap. Pat. 2000176291 (Tosoh Corporation), **2000**. d) Oguri, M.; Mimura, H.; Okada, H.; Yoshida, T. Jap. Pat. 2000202299 (Tosoh Corporation), **2000**.

28) Fang, Y.; Liu, Y.; Ke, Y.; Guo, C.; Zhu, N.; Mi, X.; Ma, Z.; Hu, Y. *J. Appl. Catal. A* **2002**, *193*, 33. b) Kohn, R. D.; Haufe, M.; Mihan, S.; Lilge, D. *Chem. Commun.* **2000**, 1927.
29) van Rensburg, W. J.; Grove, C.; Steynberg, K. B.; Stark, K. B.; Huyser, J. J.; Steynberg, K. B. *Organometallics* **2004**, *23*, 1207. b) Morgan, D. H.; Schwikkard, S. L.; Dixon, J. T.; Nair, J. J.; Hunter, R. *Adv. Synth. Catal.* **2003**, *345*, 939. c) Theopold, K. H. *Eur. J. Inorg. Chem.* **1998**, 15.
30) Meijboom, N.; Schaverien, C. J.; Orpen, A. G. *Organometallics*, **1990**, *9*, 774.
31) Agapie, T.; Schofer, S. J.; Labinger, J. A.; Bercaw, J. E. *J. Am. Chem. Soc.* **2004**, *126*, 1304. b) Tomov, A. K.; Chirinos, J. J.; Jones, D. J.; Long, R. J.; Gibson, V. C. *J. Am. Chem. Soc.* **2005**, *127*, 10166.
32) Kohn, R. D.; Haufe, M.; Mihan, S.; Lilge, D. *Chem. Commun.* **2000**, 1927.
33) Andes, C.; Harkins, S. B.; Murtuza, S.; Oyler, K.; Sen, A. *J. Am. Chem. Soc.* **2001**, *123*, 7423. b) Santi, R.; Romano, A. M.; Grande, M.; Sommazzi, A.; Masi, F.; Proto, A. WO Pat. 01/68572 (Enichem S. P. A.), **2001**.
34) Hao, S.; Gambarotta, S.; Bensimon, C.; Edema, J. J. H. *Inorganica Chimica Acta.* **1993**, *213*, 65. b) Harder, S.; Boersma, J.; Brandsma, L. *Organometallics.* **1990**, *9*, 515. c) Jiabi, C.; Guixin, L.; Weihua, X.; Xianglin, J.; S. Meicheng; Youqi, T. *J. Organomet. Chem.* **1985**, *286*, 66. d) Eapen, K. C.; Tamborski, C. *J. Fluorine Chem.* **1980**, *15*, 241. e) Pornet, J.; Miginiac, L. *Bull. Soc. Chimi. Fra.* **1974**, *5-6*, 997.
35) Ockey, D. A.; Dotson, J. L.; Struble, M. E.; Stults, J. T.; Bourell, J. H.; Clark, K. R.; Gadek, T. R. *Bioorg. Med. Chem.* **2004**, *12*, 37.
36) V.C. Gibson; C. Newton; C. Redshaw; G.A. Solan; A.J.P. White; D.J. Williams. *Eur. J. Inorg. Chem.* **2001**, 1895-1903.
37) McGeachin, S. G. *Can. J. Chem.* **1968**, *46*, 1903. b) Parks, J. E.; R.H. Holm, *Inorg. Chem.* **1968**, *7*, 1408.
38) Tonzetich, Z. J.; Jiang, A. J.; Schrock, R. R.; Mueller, P. *Organometallics* **2006**, *25*, 4725. b) Eckert, N. A.; Vaddadi, S.; Stoian, S.; Lachicotte, R. J.; Cundari, T. R.; Holland, P. L. *Angew. Chem. Int. Ed.* **2006**, *45*, 6868.
39) Holleman, A. F.; Wiberg, E. *Inorganic Chemistry* Academic Press: New York, **2001**.
40) Crewdson, P.; Gambarotta, S.; Djoman, M.-C.; Korobkov, I.; Duchateau, R. *Organometallics* **2005,** *24,* 5214.
41) Kauffmann, T.; Moeller, T.; Rennefeld, H.; Welke, S.; Wieschollek, R. *Angew. Chem.* **1985**, *97*, 351.
42) Sugiyama, H.; Aharonian, G.; Gambarotta, S.; Yap, G. P. A.; Budzelaar, P. H. M. *J. Am. Chem. Soc.* **2002**, *124*, 12268. b) Reardon, D.; Aharonian, G.; Gambarotta, S.; Yap, G. P. A. *Organometallics* **2002**, *21*, 786. c) Kooistra, M.; Knijnenburg, Q.; Smits, J. M. M.; Horton, A. D.; Budzelaar, P. H. M.; Gal, A. W. *Angew. Chem. Int. Ed.* **2001**, *40*, 4719. d) Gibson, V. C.; Humphries, M. J.; Tellmann, K. P.; Wass, D. F.; White, A. J. P.; Williams, D. J. *Chem. Commun.* **2001**, 2252.
43) Feldman, J.; McLain, S. J.; Parthasarathy, A.; Marshall, W. J.; Calabrese, J. C.; Arthur, S. D. *Organometallics* **1997**, *16*, 1514.
44) Hao, S.; Gambarotta, S.; Bensimon, C.; Edema, J. J. H. *Inorganica Chimica Acta.* **1993**, *213*, 65.
45) Sadique, A. R.; Heeg, M. J.; Winter, C. H. *J. Am. Chem. Soc.* **2003**, *125*, 7774.

46) V.C. Gibson; C. Newton; C. Redshaw; G.A. Solan; A.J.P. White; D.J. Williams. *Eur. J. Inorg. Chem.* **2001**, 1895-1903.
47) Jabri, A.; Crewdson, P.; Gambarotta, S.; Korobkov, I.; Duchateau, R. *Organometallics* **2006**, *25*, 715.
48) Jabri, A.; Temple, C.; Crewdson, P.; Gambarotta, S.; Korobkov, I.; Duchateau, R. *J. Am. Chem. Soc.* **2006**, *128*, 9238.
49) Temple, C.; Jabri, J.; Crewdson, P.; Gambarotta, S.; Korobkov, I.; Duchateau, R. *Angew. Chem. Int. Ed.* **2006**, *45*, 7050.
50) Cotton, F. A.; Wilkinson, G. *Advanced Inorganic Chemistry* John Wiley & Sons: Toronto, **1988**.
51) Calderazzo, F.; Englert, U.; Pampaloni, G.; Volpe, M. *J. Organomet. Chem.* **2005**, 690, 3321. b) Kohn, R.; Smith, D.; Mahon, M. F.; Prinz, M.; Mihan, S.; Kociok-Kohn, G. *J. Organomet. Chem.* **2003**, 683, 200.

Chapter

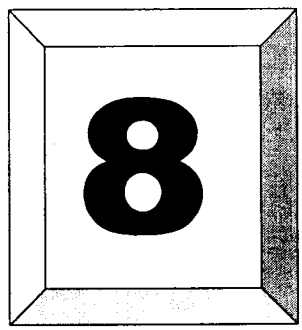

Conclusions and Future Research Aims

Though each of the projects presented within this thesis successfully reached logical conclusions, there is still much room left for further exploration and refinement. Perhaps the best example of this is the hemi-labile bonding ligands prepared in chapter 2. In the short time they have been available in our lab they have already been used to generate low-valent Th,[1] and Ti[2] complexes as well as supporting ethylene trimerization and polymerization.[3] The major limitation of the hemi-labile ligand systems is their generally poor solubilities. More work will be required in order to create compounds that contain highly soluble side-groups. The most intriguing modification of the ligand system, however, would be to close the N-MeTripyrrolide ligand in order to create a macrocycle (see Scheme 8.1).

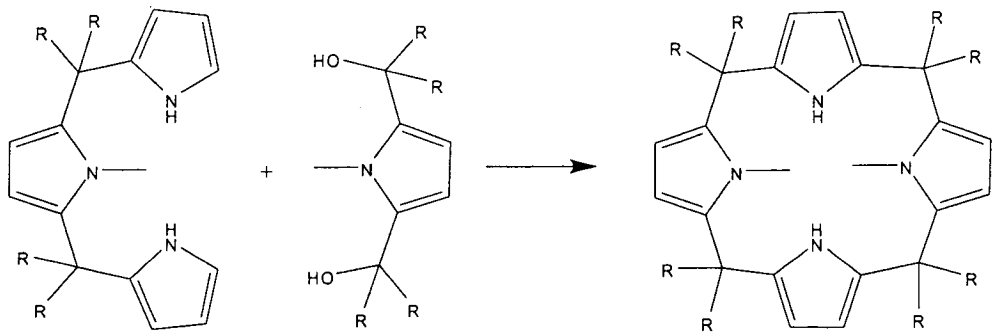

Scheme 8.1 Proposed Macrocycle Formation.

The most likely route to accomplishing this task would be to combine the N-MeTripyr ligand and its alcohol analogue. This condensation reaction would most likely be catalyzed by the addition of a weak acid or via addition of the strong Lewis acid BF_3. This new class of ligand would combine the robust nature of the porphyrinogen[4] ligand with the hemi-lability of the N-Me pyrrole groups and should serve to stabilize a plethora of highly-reactive low-valent metals.

The Mn alkyl complexes synthesized in chapter 3 served as highly valuable starting materials for the synthesis of various Mn complexes in the following chapters. The only compound missing from the series $[Mn(CH_2SiMe_3)_n]$ (n= 0-3) is the mono-alkylated analogue $[MnCl(CH_2SiMe_3)]$. This compound would serve as an excellent reagent for ligand metathesis reactions, while at the same time leaving the chloride ligand as a site for further chemical transformation. As such, developing this material could be useful for future research. In addition, the pentameric carboxylate structure should be explored in future research as it should readily serve as an anchor for building up larger macromolecules via metathesis reactions with its terminal alkyl groups (see Figure 8.2).

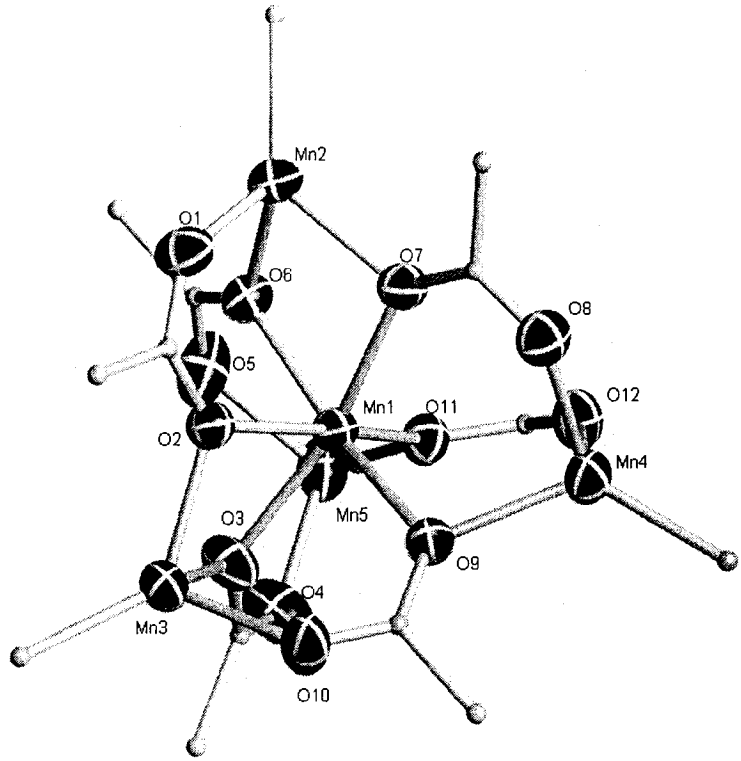

Figure 8.2 Simplified Structure of Pentameric Mn Cluster.

The majority of the model complexes synthesized to mimic the OEC in chapter 4, unfortunately, proved to be incompatible with water. However, the recent aqueous based chemistry of the tartrate ligand in combination with $[Mn(OAc)_2]$ and $KMnO_4$ has yielded the encouraging evolution of O_2 from the mixture. This major breakthrough must now be fully evaluated in order to determine how efficient the liberation of O_2 from water is. Furthermore, the eventual coupling of this reaction with a non chemical-based oxidizing agent would be our long term goal. A group that successfully coupled this reaction with solar energy would largely solve our world's energy problems, providing an imperative incentive for us to continue this line of research.

The unprecedented ability of $Mn^{(II)}$ to catalyze the co-polymerization of CO_2 with epoxide was demonstrated in chapter 5. Our findings that the process led to a very broad distribution of molecular weights in the resulting polymer were at first very confusing. The subsequent investigation of discrete Mn complexes quickly revealed that both ligand leaching and radical reduction of the Mn were likely responsible for the large PDI's observed. Given the relatively low activity of the catalysts, and their very poor control

over the molecular weight, it is not likely that $Mn^{(II)}$ complexes will be investigated in the future. However, since the recent publication of Inoue[5] has revealed that $Mn^{(III)}$ can serve to catalyze the process it would be very interesting to explore some of our novel hemi-labile ligands in conjunction with $Mn^{(III)}$ for this process.

Exploring the ability of the well-known Brookhart-Gibson ligand to support low-valent Mn complexes led us to two major findings. We found that the radical coupling behaviour of the ligand was present whenever an alkyl group was attached to a Mn atom. And secondly, a formally mono-valent [(BisImine)MnCl(THF)] complex (see Figure 8.3) was found.

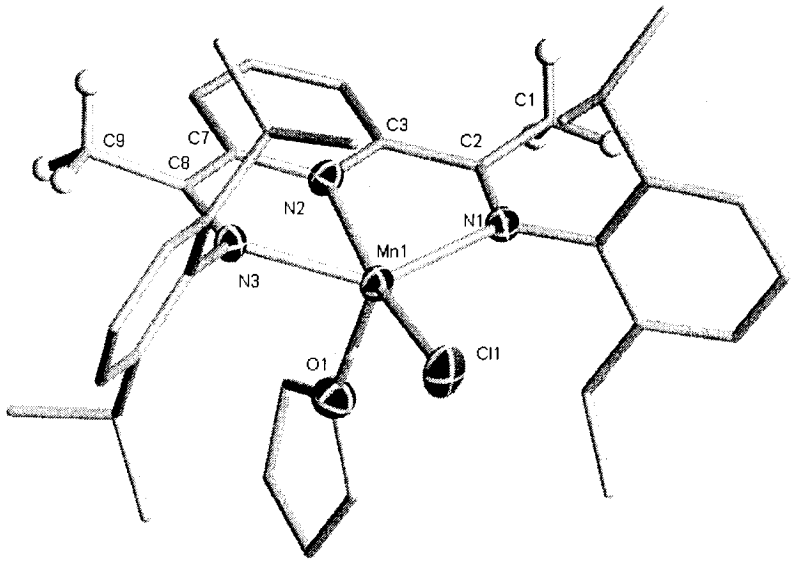

Figure 8.3 Structure of formally $Mn^{(I)}$ [(BisImine)MnCl(THF)].

The aim of further research will be to discover whether this structure is truly in the mono-valent state, or is actually $Mn^{(II)}$ with a radical residing on the ligand. Generating formally zero-valent complexes using the NaH synthetic route is also an intriguing proposition to explore in the future.

Chapter 7 detailed our investigations into the fascinating Cr catalyzed selective ethylene trimerization (and tetramerization) reaction. Use of the hemi-labile ligands developed in chapter 2 in conjunction with both $Cr^{(II)}$ and $Cr^{(III)}$ led to active oligomerization catalysts, though without 1-hexene selectivity. Furthermore, it was found that changing the activator from the normal MAO to IBAO led to a change in catalyst productivity, yielding PE instead.[3] Though our investigations attempted to

identify which oxidation state bestowed catalyst selectivity, we were unable to conclusively identify either $Cr^{(II)}$ or $Cr^{(III)}$ as being the selective oxidation state. To further confuse the issue it was found that both oxidation states were susceptible to oxidation and reduction reactions that occurred in the presence of activators which could conceivably interconvert the two oxidation states. On the whole it appears that catalyst selectivity may be ligand dependant only, precluding the need to use either valent metal specifically. Further investigations of this system are ongoing in our lab with the goal of modifying the SNS ligand system in order to fully understand how selectivity is bestowed upon this remarkable and sometimes confusing catalytic system.

Overall this thesis has helped advance the state of the art for both Mn and Cr chemistry in both basic and practical terms. In addition the novel hemi-labile ligand systems should help stimulate further research in the chemistry community due to their published ability to support a variety of chemical processes. This now draws to a close my doctoral thesis, I sincerely hope that you have found it to be both concise and informative.

References:

1) Arunachalampillai, A.; Crewdson, P.; Korobkov, I.; Gambarotta, S. *Organometallics* **2006**, *25*, 3856.
2) Nikiforov, G. B.; Crewdson, P.; Gambarotta, S.; Korobkov, I.; Budzelaar, P. H. M. *J. Am. Chem. Soc.* **2007**, *26*, 48.
3) Crewdson, P.; Gambarotta, S.; Djoman, M.-C.; Korobkov, I.; Duchateau, R. Organometallics **2005**, 24, 5214.
4) Jubb, J.; Gambarotta, S. *J. Am. Chem. Soc.* **1994**, *116*, 4477.
5) Sugimoto, H.; Ohshima, H.; Inoue, S. *J. Polym. Sci. Part A: Polym. Chem.* **2003**, *41*, 3549.

APPENDIX 2

X-Ray Crystallography:

Complex **1** consists of a dimer of two N-MePyrrolides, each bridged to the other by a lithium atom. Each pyrrolide ring is slightly skewed and forms a 3-centered 2-electron bond (C(4) –Li(1A) = 2.202(6), C(4) –Li(1) = 2.239(6) Å, Li(1)–C(4)–Li(1A) = 67.9(2)°). The coordination sphere of each Li is completed by two molecules of THF. The electrons of the pyrrolide rings appear to be delocalized (C(4)–C(3) = 1.388(5), C(3)–C(2) = 1.408(5), C(2)–C(1) = 1.351(5), C(1)–N(1) = 1.373(4), N(1)–C(4) = 1.395(4) Å).

Complex **2** crystallized as the monomeric solvent free molecule depicted. The C(6)–O(1) = 1.444(2) Å distance corresponds to a single C-O bond, and makes chemical sense as C(6) is tetrahedral.

Complex **3** also crystallized as the monomeric solvent free molecule depicted. The only notable feature of the structure is that the N-Me pyrrole appears to be slightly less delocalized than the un-methylated pyrrole: C(6)–N(2) = 1.389(4), N(2)–C(9) = 1.368(3), C(9)–C(8) = 1.370(3), C(8)–C(7) = 1.402(4), C(7)–C(6) = 1.380(3) Å vs. C(1)–N(1) = 1.361(3), N(1)–C(4) = 1.378(3), C(4)–C(3) = 1.369(3), C(3)–C(2) = 1.424(4), C(2)–C(1) = 1.363(4) Å.

Complex **4** crystallized as the monomeric solvent free molecule depicted. Other than hydrogen bonding between adjacent diol units (H(1)–O(2)' = 2.105 (6) Å) there are no structurally abnormal features to describe.

Complex **5** co-crystallized with ¾ of a molecule of CH_2Cl_2. All bond distances and geometries are as chemically expected.

Complex **6** crystallized as the monomeric solvent free molecule depicted. The C(6)–O(1) = 1.449(8) Å distance corresponds to a single C-O bond, and makes chemical sense as C(6) is tetrahedral.

Complex **7** as the monomeric solvent free molecule depicted. All bond distances and geometries are as chemically expected.

For the complete Crystallographic data please see the attached data CD.

APPENDIX 3

X-Ray Structures:

The full crystallographic packages for Complex **2** has been previously published, and will not be listed herein.[1] Since the geometries of the different structures were discussed in the body of chapter 3, only the full Crystallographic data will be listed here:

1. Crewdson, P.; Gambarotta, S.; Yap, G. P. A.; Thompson, L. K. *Inorg. Chem.* **2003**, *42,* 8579.

For the complete Crystallographic data please see the attached data CD.

APPENDIX 4

X-Ray Structures:

The full crystallographic packages for Complexes **3**, and **4** have been previously published, and will not be listed herein.[1] Since the geometries of the different structures were discussed in the body of chapter 7, only the full Crystallographic data will be listed here:

1. Crewdson, P.; Gambarotta, S.; Yap, G. P. A.; Thompson, L. K. *Inorg. Chem.* **2003**, *42,* 8579.

For the complete Crystallographic data please see the attached data CD.

APPENDIX 5

% Carbonate Linkage Calculation: The ^{1}H NMR is diagnostic for determining ether, and carbonate linkages.[1] The cyclohexyl methine proton appears at 4.6 ppm for polycarbonate and 3.3 ppm for polyether linkages. Integrating the relative intensities yields the % carbonate (See Figure 1).

$$\% \text{ carbonate} = \frac{\text{carbonate H}}{(\text{carbonate H} + \text{ether H})}$$

Figure 1. Typical NMR with polyether and polycarbonate methine signals integrated.

TOF Calculation: The TOF (TurnOver Frequency) represents the mols of CHO utilized per mol of catalyst per hour. The figure is calculated taking into consideration the % carbonate linkages. The mass of the end-groups of the polymer chains are negligible and therefore aren't considered in the calculation.

In order to determine the mass of CHO in the polymer:

$$\% \text{ CHO}_{\text{incorporated}} = \frac{98.14 \text{ g/mol}}{(98.14 + 44.011 \text{ (\% carbonate)})}$$

$$\text{TOF} = \frac{\text{(polymer g) (\% CHO}_{\text{incorporated}})}{(98.14 \text{ g/mol}) (3.0\text{X}10^{-4} \text{ mol catalyst}) (\text{h})}$$

References:

1) Vitanova, D. V.; Hampel, F.; Hultzsch, K. C. *J. Organomet. Chem.* **2005**, *690*, 5182.

X-Ray Crystallography:

Since the geometries of the different structures was discussed in the body of chapter 4, only the full Crystallographic data will be listed here:

For the complete Crystallographic data please see the attached data CD.

APPENDIX 6

X-Ray Structures:

The full crystallographic packages for Complex **4** has been previously published, and will not be listed herein.[1] Since the geometries of the different structures were discussed in the body of chapter 6, only the full Crystallographic data will be listed here:

1. Sugiyama, H.; Aharonian, G.; Gambarotta, S.; Yap, G. P. A.; Budzelaar, P. H. M. *J. Am. Chem. Soc.* **2002**, *124*, 12 268.

For the complete Crystallographic data please see the attached data CD.

APPENDIX 7

Oligomeration Activity:

Activity was calculated by integrating the methylene ^{1}H NMR signals of the alkenes versus the known volume of of toluene (150 mL) and assuming the identity of the oligomeric signal was 1-hexene. As such, the reported activity values are not exact values, as the selectivities of all other olefins should be accounted for in order to yield the true activity. For the scope of this study the slight differences in activities were not enough to warrant the more exact calculations. The following Figure represents a typical NMR, and the resulting yield of oligomers.

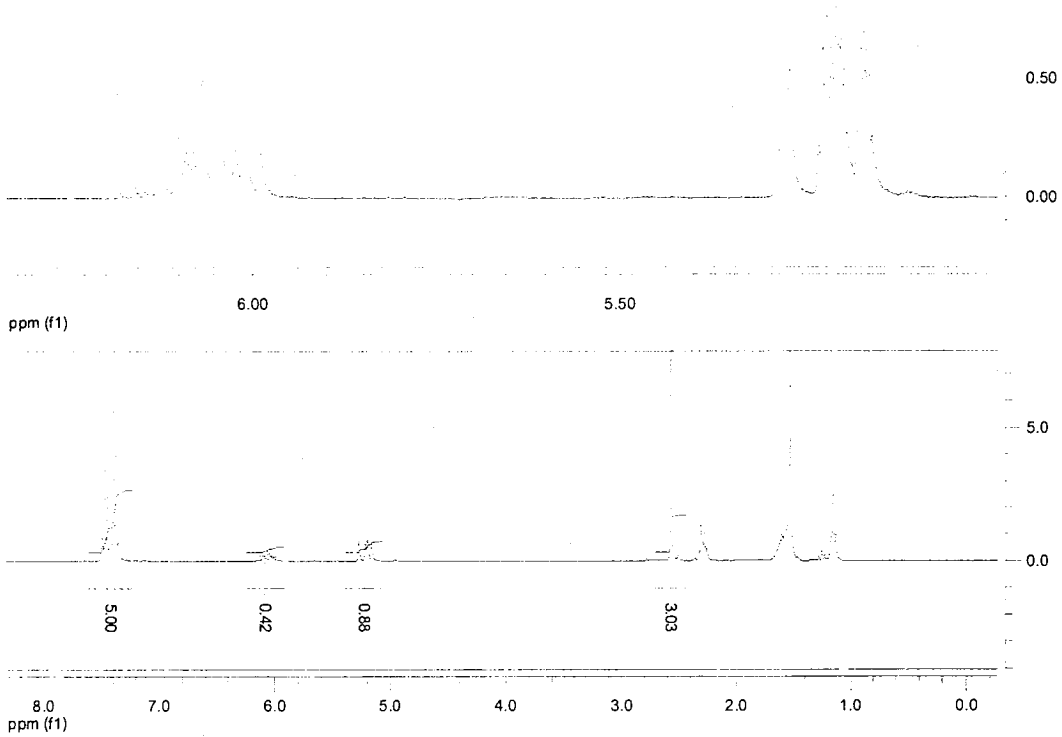

Oligomerization Selectivity:

A stock solution was prepared in order to properly calibrate the GC in order to quantify the different oligomers:

Stock Solution 2006:

30 μL	1-hexene	=	8.0561×10^{-2} M
30 μL	1-octene	=	6.3720×10^{-2} M
30 μL	1-decene	=	5.2827×10^{-2} M
30 μL	1-dodecene	=	4.5033×10^{-2} M
2880 μL	toluene		

The stock solution was then used to prepare a number of standard with a total volume of 1 mL and a differing amount of stock solution:

Standard Dilutions:

2 μL, 5 μL, 10 μL, 20 μL, 50 μL, 100 μL, 200 μL, 500 μL, 700 μL, 1000 μL

The standard solutions were then injected into the GC and the area of the peaks was used to prepare calibration curves:

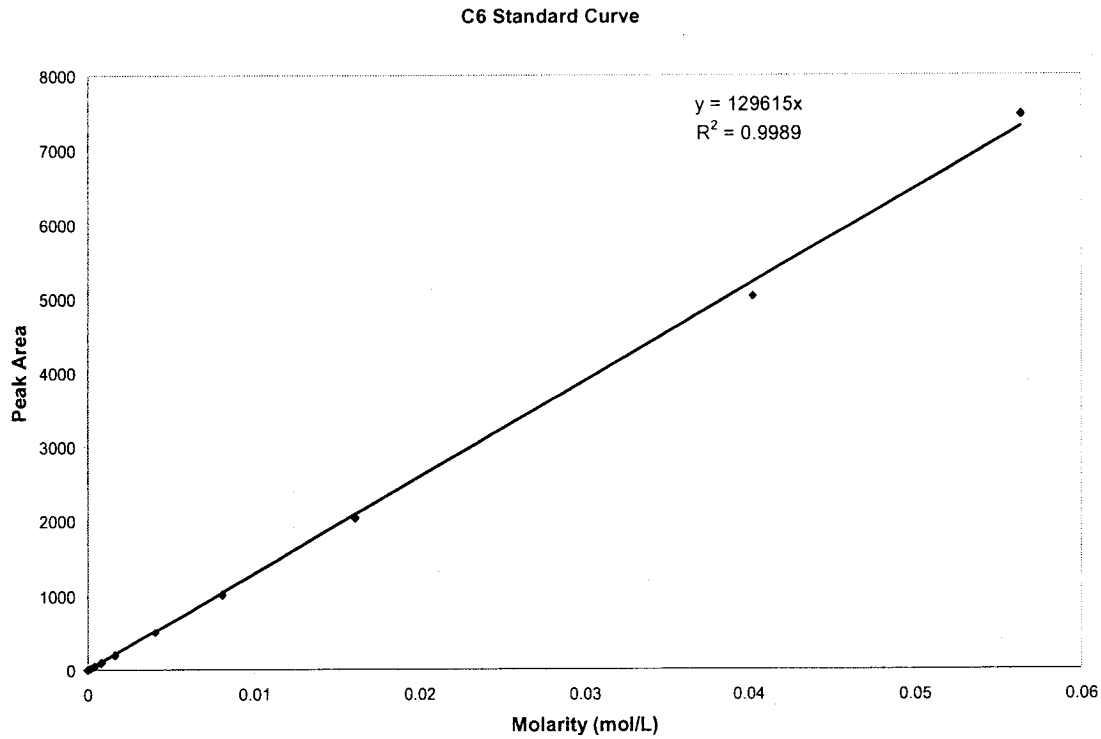

C8 Standard Curve

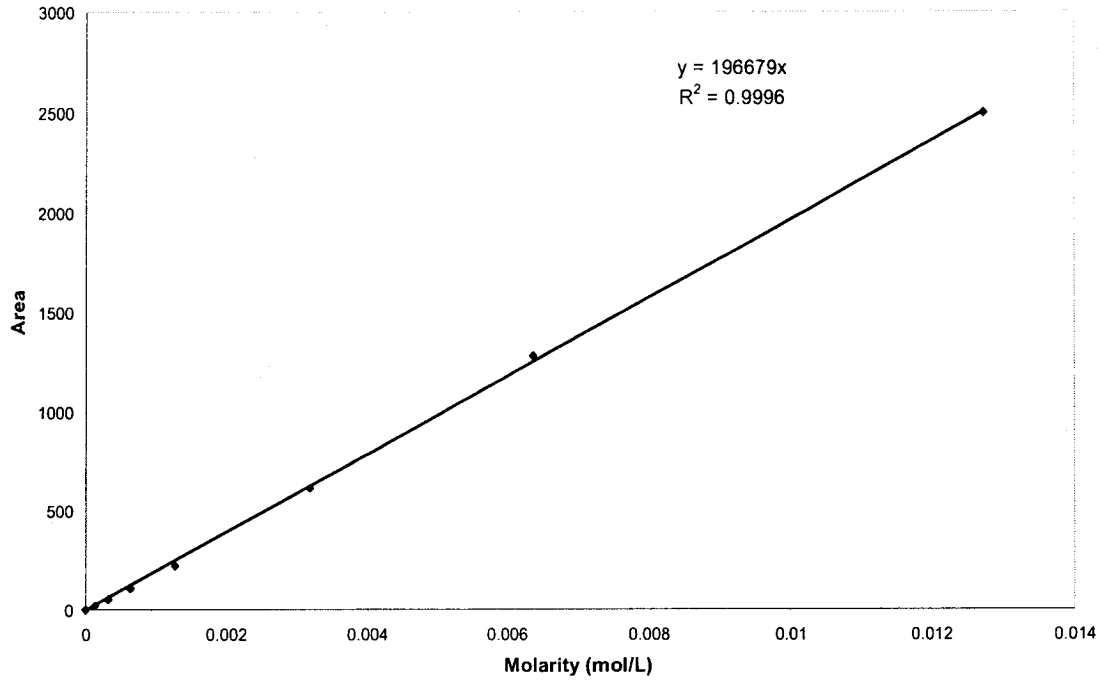

C10 Standard Curve

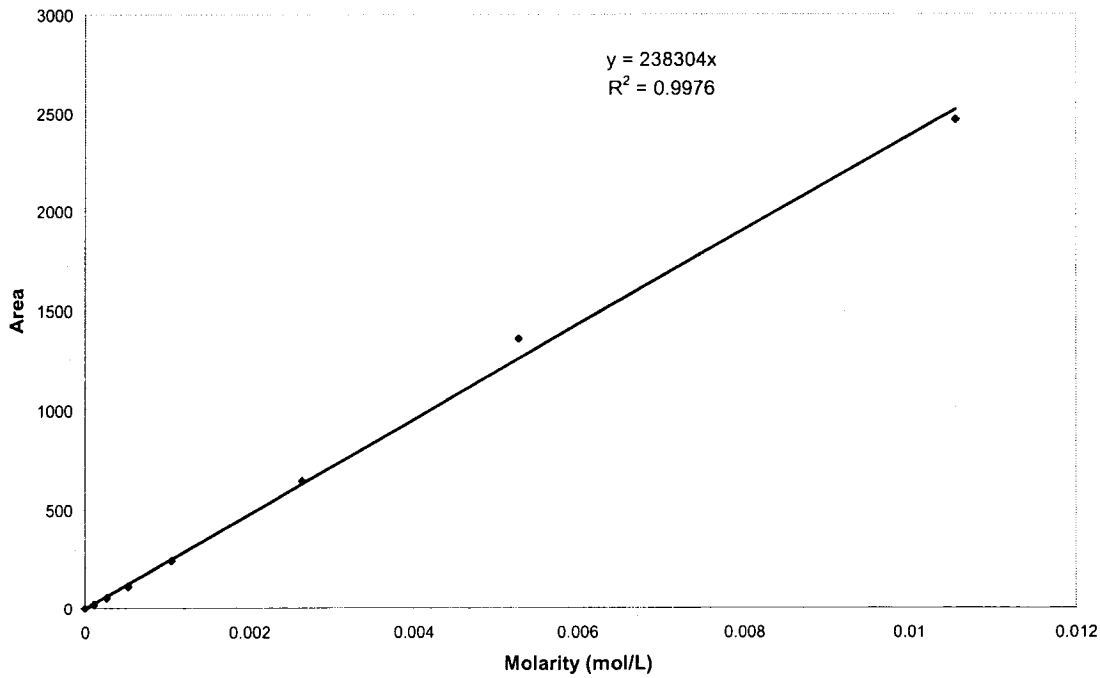

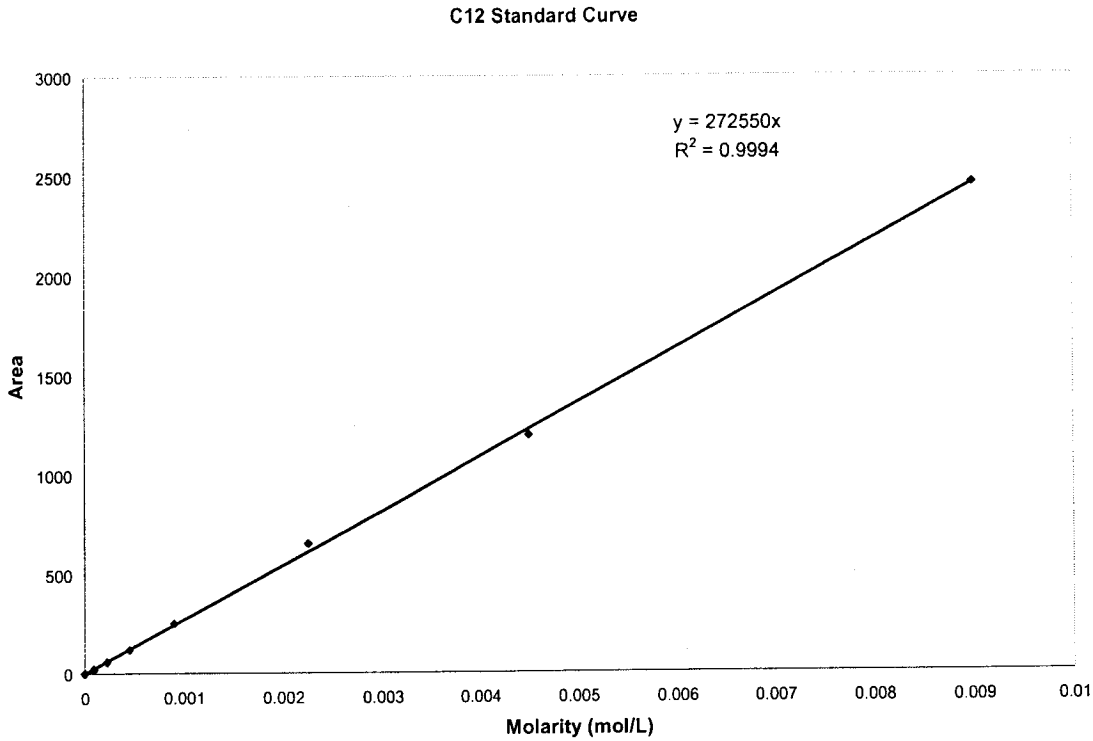

Since it was not possible to obtain samples for the quantification of the 1-butene, 1-tetradecene, and 1-hexadecene the values were extrapolated and interpolated from the standard curves of the other samples.

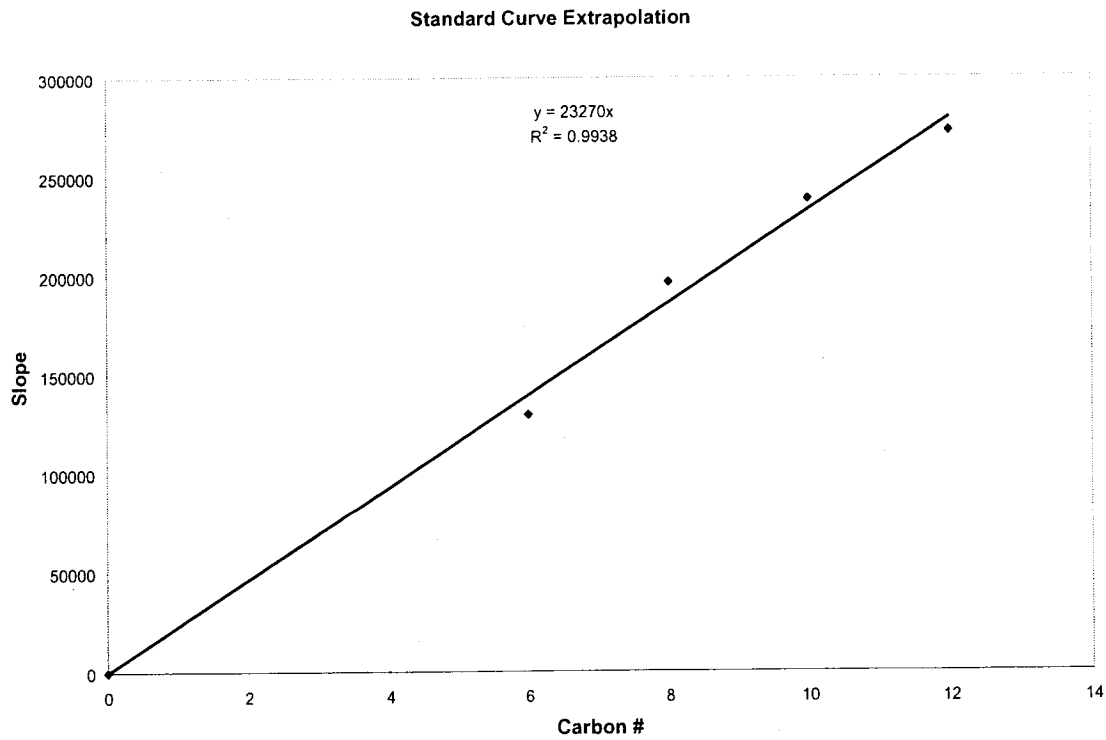

The equations of the lines from the different standard curves were then used in order to quantify the oligomers produced from the catalysis according to the following formulae:

1-butene: Peak Area / 93 080 area/M
1-hexene: Peak Area / 129 615 area/M
1-octene: Peak Area / 196 679 area/M
1-decene: Peak Area / 238 304 area/M
1-dodecene: Peak Area / 272 550 area/M
1-tetradecene: Peak Area / 325 780 area/M
1-hexadecene: Peak Area / 372 320 area/M

The mol % values were then determined by the following formula (1-hexene shown as an example):

mol % = (1-hexene M / Sum of all oligomers M) X 100 %

X-Ray Structures:

Since the geometries of the different structures were discussed in the body of chapter 5, only the full Crystallographic data will be listed here:

For the complete Crystallographic data please see the attached data CD.